

Abstract

Title of Dissertation: Intramolecular Carbon-Nitrogen Reductive Elimination from Isolated Monohydrocarbyl Palladium(IV) Complexes Prepared Using H₂O₂ as Terminal Oxidant

Elikplim Abada, Doctor of Philosophy, 2017

Dissertation directed by: Professor Andrei N. Vedernikov,
Department of Chemistry and Biochemistry
University of Maryland, College Park

Carbon-nitrogen coupling is achieved traditionally by coupling of aryl halides and amines through a Pd(0)/Pd(II) catalytic cycle (Buchwald-Hartwig amination). A newer, more atom-economical approach to the synthesis of amines is based on oxidative C-H amination. Recent studies of C-H amination propose the involvement of Pd(II)/Pd(IV) catalytic cycle through a C-H activation step.

This work seeks to develop new stoichiometric and catalytic ways of forming C-N bonds through a Pd(II)/Pd(IV) cycle using H₂O₂ as terminal oxidant. In this effort, di-2-pyridylketone(dpk) ligated palladacycles were synthesized, oxidized with H₂O₂, and the reductive elimination of the high oxidation state Pd(IV, d⁶) containing species monitored. *N*-R-2-aminobiphenyl – derived substrates with electron donating groups (R = H, Me, Et) readily form carbazoles at room temperature without formation of appreciable amounts of intermediates. The use of electron withdrawing group (R = COCH₃, COCF₃, SO₂CH₃, SO₂CF₃) slows down the reaction for intermediates to be

observed and isolated. Mechanistic studies of the first ever C(sp²)-N reductive elimination from an isolated Pd(IV, d⁶) intermediate was observed to be accelerated in the presence of acids. Reductive elimination is proposed to occur from a 6-coordinate Pd(IV, d⁶) center.

The dpk ligated Pd(IV, d⁶) palladacycles derived from 4-X-substituted *N*-SO₂CF₃-2-*tert*-butylaniline (X = H, Br, I), reductively eliminate the corresponding C(sp³)-N coupled products, 5-X-substituted indolines in high yield only in the presence of halohalic acids (HCl, HBr and HI). This confirms the importance of a proton source and a nucleophilic anion for this process to take place. Reductive elimination is proposed to occur through several competing pathways based on the fractional order of reaction with respect to [Br⁻] in solution.

Catalytic heterocyclization reaction was achieved using H₂O₂ with *N*-acetyl-2-aminobiphenyl to form *N*-acetylcarbazole with yields dependent on temperature and rate of addition of H₂O₂.

INTRAMOLECULAR CARBON-NITROGEN COUPLING FROM ISOLATED
MONOHYDROCARBYL PALLADIUM(IV) COMPLEXES PREPARED USING
H₂O₂ AS TERMINAL OXIDANT

by

Elikplim Abada

Dissertation submitted to the Faculty of the Graduate School of the
University of Maryland, College Park, in partial fulfillment
of the requirements for the degree of
Doctor of Philosophy
2017

Advisory Committee:

Professor Andrei N. Vedernikov, (Chair)
Professor Philip DeShong
Professor Lawrence R. Sita
Professor Daniel E. Falvey
Professor Nam S. Wang

© Copyright by
Elikplim Abada
2017

This thesis is dedicated to nothing.

Acknowledgements

I would like to thank my Advisor, Professor Andrei N. Vedernikov for agreeing to take me into his lab when no one else would. I appreciate his patience, guidance, honesty, invaluable advice, and the opportunity to grow as a scientist.

I want to thank my committee members Prof. Philip DeShong, Prof. Lawrence Sita, and Prof. Daniel Falvey. All of you were my lecturer at a point in time, and your classes formed the basis of my graduate chemistry education. Even though I was not your 'ideal' student, you were excellent in your knowledge, insights, and delivery.

Thanks to Dr. Nam Sun Wang for graciously agreeing to serve as Dean's Representative on my thesis committee.

Next are Dr. Patrick K. Arthur, Dr. Kwaku Dayie and Dr. Herman Sintim for facilitating my coming to the University of Maryland, College Park. I will always be indebted to you.

I would also like to thank Dr. Yiu-Fai Lam, Dr. Yinde Wang and Dr. Peter Zavalij for NMR and XRD experiments. You guys were fantastic.

To my lab mates Shrin, Dave, Daoyong, Xiaohang, Courtney, David, Daniel, Anna, Fan, Jiaheng and Vinny, sorry for the huge mess in my hood all the time. Thanks for your tolerance and making the lab a fun place to work.

Lastly, I will like to thank my family and close friends, especially Naa Adei for being my backbone.

Table of Contents

Dedication	i
Acknowledgements	iii
Table of Contents	iv
List of Schemes	xi
List of Figures.....	xvii
List of Abbreviations	xxv

Chapter 1: Pd(II)/Pd(IV) couple mediated C-H functionalization and common oxidants used.....	1
1.1 C-H Activation at Transition metal centers.....	1
1.1.1 C-H Activation at Pd(II) centers.....	3
1.1.2 C-H Activation at Pd(IV) centers	4
1.2 Buchwald-Hartwig Amination	6
1.2.1 Oxidative Addition to Pd(0)	8
1.2.2 Reductive Elimination from Pd(II).....	9
1.3 Intermediacy of high oxidation state Pd(III)/Pd(IV) in C-H functionalization.....	9
1.3.1 Some selected reagents for oxidation of Pd(II) to Pd(IV)	10
1.3.1.1 Iodine(III) based reagents	10
1.3.1.2 N-Halosuccinimides as oxidant	13
1.3.1.3 Peroxide Oxidants	14
1.3.1.4 Dioxygen as a Terminal Oxidant	15
1.3.1.5 Electrophilic Fluorinating Reagents	15
1.3.2 Pd(III)-mediated reactions.....	17
1.4 Dpk-enabled C-Pd bond functionalization with hydrogen peroxide....	19
1.5 Our goal and approach	21

Chapter 2. Synthesis of κ^2-C,N-2'-(N-R-amino)biphenyl-2-yl Pd(II) complexes with electron donating groups R=H, Et, Me and their oxidation with H₂O₂	23
2.1 Introduction and Background.....	23
2.2 Synthesis of Palladacycles, 30-33	25
2.3 Oxidation of acetate-bridged palladacycle, 32, with H₂O₂ in CD₃CN ..	26
2.5 Preparation of dpk-ligated palladacycles, 35-38	27
2.6 Reactivity of palladacycle 35 towards H₂O₂ in various solvents.....	28
2.6.1 D ₂ O.....	28
2.6.2 AcOD.....	29
2.6.3 MeOD.....	31
2.7 Reactivity of 37 towards H₂O₂ in MeOD.....	33
2.8 Reactivity of 38 in MeOD	35
2.9 Reactivity of 36 in MeOD	36
2.10 Conclusion.....	38
2.11 Experimental.....	40
Chapter 3. Synthesis and Reactivity of κ^2-C,N-2'-(N-R-amido)biphenyl-2-yl Pd(II) complexes with electron withdrawing groups R = COCH₃,COCF₃, SO₂CH₃, SO₂CF₃	48
3.1 Introduction and Background.....	48
3.2 Preparation of dpk – ligated palladacycles 50, 51, 61 and 66 bearing an electron-withdrawing group at the amide nitrogen atom	50
3.3 Characterization and reactivity of the N-acetyl Pd(II) complex, 50(MeOH)	51
3.3.1 Structural characterization of 50(MeOH).....	51
3.3.2 Reactivity of 50 towards H ₂ O ₂ in different solvents.	52
3.3.2.1 MeOD.....	52

3.3.2.2 <i>AcOD</i>	55
3.3.2.3 <i>CD₃CN</i>	56
3.3.2.4 <i>THF</i>	60
3.4 Characterization and reactivity of the N-trifluoroacetyl Pd(II) complex, 51(MeOH)	62
3.4.1 Characterization of the N-trifluoroacetyl Pd(II) complex, 51(MeOH)	62
3.4.2 Reactivity of 51(MeOH) towards H ₂ O ₂ in different solvents.....	63
3.4.2.1 <i>MeOD</i>	63
3.4.2.2 <i>CD₃CN</i>	64
3.4.2.3 <i>THF</i>	66
3.4.2.4 <i>AcOD</i>	68
3.4.3 Isolation and reactivity of N-trifluoroacetyl Pd(IV) complex, 59	71
3.4 Characterization and reactivity of the N-methanesulfonyl Pd(II) complex, 61(MeOH)	73
3.4.1 Characterization of the N-methanesulfonyl Pd(II) complex 61(MeOH)	73
3.4.2 Reactivity of 61(MeOH) towards H ₂ O ₂ in different solvents.....	74
3.4.2.1 <i>MeOD</i>	74
3.4.2.2 <i>AcOD</i>	75
3.4.2.3 <i>THF</i>	77
3.4.2.4 <i>CH₃CN</i>	82
3.5 Isolation and characterization of the methanesulfonyl Pd(IV) amido aryl complex 63.....	83
3.6 Characterization and reactivity of the N-trifluoromethanesulfonyl Pd(II) complex 66·MeCN	84
3.6.1 Characterization of the N-trifluoromethanesulfonyl Pd(II) complex 66·MeCN	84
3.6.2 Reactivity of 66·MeCN towards H ₂ O ₂ in different solvents.....	86
3.6.2.1 <i>AcOD</i>	86
3.6.2.2 <i>MeOD</i>	88
3.6.2.3 <i>THF</i>	88

3.6.2.4 CD_3CN	91
3.7 Synthesis of the N-trifluoromethanesulfonyl Pd(IV) amido aryl complex 68.....	93
3.8 Conclusions	94
3.9 Experimental.....	96
Chapter 4: Reactivity of κ^2-C,N-2'-(N-R-amido)biphenyl-2-yl Pd(IV) complexes	109
4.1 Introduction	109
4.2 Characterization and reactivity of N-methanesulfonylamido Pd(IV) complex, 63	110
4.2.1 H/D exchange of 63	110
4.2.2 C(sp ²)-N Reductive elimination of 63	111
4.3 Characterization and reactivity of N-trifluoromethanesulfonylamido Pd(IV) complex 68.....	114
4.3.1 H/D exchange	114
4.3.2 C(sp ²)-N Reductive elimination of 68.MeCN in CD_3CN at 105 °C .	116
4.3.3 Reactivity of 68.MeCN in THF- <i>d</i> ₈	118
4.3.4 Reactivity of 68.MeCN in MeOD	119
4.3.5 Reactivity of 68.MeCN in AcOD	121
4.3.6 Reactivity of 69.AcOH in CD_3CN	126
4.3.7 Reactivity of 68 in the presence of different acids	126
4.3.7.1 $HClO_4$	126
4.3.7.2 CF_3SO_3H	126
4.3.7.3 H_2SO_4	127
4.3.7.5 CH_3SO_3H	128
4.3.7.6 TFA	130
4.3.7.7 HBr and HCl	131
4.3.8 Reaction of 68 in CD_3CN with different equivalents of HBf_4	133

4.3.8.1 With 1 equivalent of HBF ₄ to form N-trifluoromethanesulfonamido Pd(IV)(MeCN), 75 (BF ₄).....	133
4.3.8.2 With 1.3 equivalents HBF ₄	138
4.3.9 Lability of CD ₃ CN ligand in 75 (BF ₄)	140
4.3.9.1 Addition of CF ₃ COONa to a solution of 75 (BF ₄).....	140
4.3.9.2 Addition of CF ₃ SO ₃ Na to a solution of 75 (BF ₄)	142
4.3.10 Reactivity of 68 in CD ₂ Cl ₂ with 1 eq of HBF ₄	143
4.3.11 Proposed mechanism for C-N bond elimination of 68 in MeCN containing HBF ₄ additives	145
4.4 Conclusion.....	147
4.5 Experimental.....	148

Chapter 5. Synthesis and Reactivity of κ^2 -C,N-2'-(2',2'-dimethylethanediy)-

N-R-anilido Pd(II) Complexes with Electron Withdrawing Group

R=SO₂CF₃ 150

5.1 Introduction and Background..... 150

5.2 Preparation, characterization, and oxidation of dpk-supported amido alkyl Pd(II) complex, **81..... 151**

5.2.1 Preparation and characterization of N-(2-*tert*butylphenyl)trifluoromethanesulfo- namidePd(II)(dpk), **81** 151

5.2.2 Oxidation of **81** with H₂O₂ to form **84** 153

5.3 Reactivity of **84 in different solvents 156**

5.3.1 Acetonitrile 157

5.3.2 Acetone 157

5.3.3 Methanol 158

5.3.4 Toluene 158

5.3.5 Dichloromethane 158

5.3.6 Acetic acid 159

5.3.7 DMSO..... 159

5.4 Reactivity of **84 with different additives 159**

5.4.1 Pyridine.....	159
5.4.2 Pyridine-TFA.....	160
5.4.3 Trifluoroacetic acid (TFA)	160
5.4.4 Acetic acid	161
5.4.5 Brookhart's acid	161
5.4.6 Hydrochloric acid	162
5.4.7 Hydrobromic acid.....	164
5.4.8 Hydroiodic acid	165
5.4.9 Addition of salts KBr and LiCl	166
5.4.10 TFA/KBr.....	166
5.4.11 Tosyl Chloride	166
5.4.12 KOH(aq).....	167
5.5 Kinetics	168
5.5.1 Reaction with 2 equivalents of HBr(aq).....	168
5.5.2 Reversibility of protonation.....	169
5.5.3 Possible mechanisms of the C-N coupling of 84 in the presence of HBr	171
5.5.4 Initial rates	173
5.5.5 Pathway 1 - direct C(sp ³)-N reductive elimination from a Pd(IV) complex	175
5.5.6 Pathway 2c –S _N 2 attack at CH ₂ fragment of Pd(IV)	176
5.5.7 Pathway 3 – dissociation of the amido donor atom.....	176
5.6 Characterization and reactivity of a bromo-substituted analog of amido alkyl Pd(IV) complex 84	179
5.7 Characterization and reactivity of an iodo-substituted analog of amido alkyl Pd(IV) complex 84	181
5.8 Conclusion.....	182
5.9 Experimental.....	184

Chapter 6. Palladium-Catalyzed Oxidative C-H Amination with H₂O₂ as Oxidant.....	198
6.1 Introduction	198
6.2 Results and Discussion	199
6.3 Conclusions	203
Chapter 7: Conclusion and Future Directions	204
Appendices.....	207
References	258

List of Schemes

Scheme 1.1 Electrophilic aromatic substitution mechanism for C-H activation at a Pd center with indolines. (L) _n is PPh ₃	3
Scheme 1.2 Concerted cyclometallation-deprotonation (CDM) mechanism of C-H activation.....	4
Scheme 1.3 C-H Activation at a Pd(IV) d ⁶ metal center by Sanford	5
Scheme 1.4 Proposed catalytic route involving C-H activation at a Pd(IV) and a Pd(II) metal centers through a dual catalytic pathway.	5
Scheme 1.5 General scheme for the Buchwald-Hartwig amination reaction	7
Scheme 1.6 Proposed mechanism for the Buchwald-Hartwig amination reaction	7
Scheme 1.7 Proposed mechanism for oxidative addition of phenyl iodide to Pd(PPh ₃) ₂	8
Scheme 1.8 Proposed mechanism for the acetoxylation of 2-phenylpyridine with PhI(OAc) ₂ as oxidant and Pd(OAc) ₂ as a catalyst.	11
Scheme 1.9 Stoichiometric acetoxylation of benzo[h]quinoline with PhI(OAc) ₂ as the terminal oxidant.	11
Scheme 1.10 Proposed mechanisms for the formation of 11 from 9	12
Scheme 1.11 Proposed ionic mechanism for the formation of 11 from 9 as proposed by the Sanford group.....	13
Scheme 1.12 Chlorination of 2-phenylpyridine with N-chlorosuccinimide as terminal oxidant through a Pd(IV) intermediate.	14

Scheme 1.13 C-O and C-X (X=Cl, Br) reductive elimination from a Pd(IV) center with H ₂ O ₂ as terminal oxidant	14
Scheme 1.14 Acetoxylation of 8-methylquinoline substrates with O ₂ as terminal oxidant as reported by Vedernikov.....	15
Scheme 1.15 Proposed transformations of 15 into different products based on additives and reaction conditions.	16
Scheme 1.16 Transformation of 16 into different products 17 or 18 based on the identity of the cation bound to tosylate by the Sanford group	16
Scheme 1.17 C-N reductive elimination from Pd(IV) alkyl complex, 19 , as reported by Sanford.....	17
Scheme 1.18 C-Cl reductive elimination from isolated dimeric Pd(III) as reported by Ritter	18
Scheme 1.19 Proposed mechanisms for the formation of C-Cl product 23 from the isolated dimeric Pd(III) precursor, 21	19
Scheme 1.20 Proposed mechanism for the dpk enabled oxidation of a monohydrocarbyl Pd(II) center with H ₂ O ₂ to form the corresponding Pd(IV).....	20
Scheme 1.21 Proposed mechanism for the oxidative C-H amination with H ₂ O ₂ as terminal oxidant.....	21
Scheme 2.1 Proposed mechanism for the reaction of N-acyl-2-aminobiphenyl substrates with Pd(OAc) ₂ catalyst and Cu(OAc) ₂ /O ₂ as oxidant to give the corresponding N-acetylcarbazoles as reported by Gaunt.	23
Scheme 2.2 Proposed mechanism for the Pd(OAc) ₂ catalyzed oxidative C-H amination with PhI(OAc) ₂ as terminal oxidant as proposed by Gaunt.....	24
Scheme 2.3 Synthesis of acetate-bridged palladacycles 30 - 33	25

Scheme 2.4 Reactivity of 32 with 3 equivalents of H ₂ O ₂ to form 34	26
Scheme 2.5 Preparation of dpk-ligated Pd complexes 35 - 38	27
Scheme 2.6 Reversible addition of MeOH across the C=O bond of 35 – 38	28
Scheme 2.7 Oxidation of 35 with H ₂ O ₂ in AcOH to produce 40 via intermediate 39 at 22 °C.....	29
Scheme 2.8 Oxidation of 35 with H ₂ O ₂ in CD ₃ OD to produce 40 at 22 °C.	31
Scheme 2.9 Proposed neutral Pd(IV) intermediate formed by deprotonation of the ammine group by OAc ⁻	33
Scheme 2.10 Reactivity of 37 with 3 equivalents of H ₂ O ₂ in MeOD.	34
Scheme 2.11 Reactivity of 38 in MeOD with 3 equivalents of H ₂ O ₂ to give 43	35
Scheme 2.12 Reactivity of 36 in MeOD with 3 equivalents of H ₂ O ₂ to give 45	36
Scheme 3.1 Dependence of rate of reductive elimination on the presence of electron donating or electron withdrawing groups at the amide nitrogen atom at a Pd(II) center, as reported by Hartwig.	48
Scheme 3.2 Preparation of dpk ligated palladacycles 50 , 51 , 61 and 66	50
Scheme 3.3 Reactivity of 50 toward H ₂ O ₂ in MeOD to form 55 at 5 °C.	52
Scheme 3.4 Reactivity of 50 toward H ₂ O ₂ in AcOD to form 55 at 22 °C.....	55
Scheme 3.5 Reactivity of 50 toward H ₂ O ₂ in CD ₃ CN to form 53 and 55 at 22 °C.	57
Scheme 3.6 Reactivity of 50 toward H ₂ O ₂ in THF-d ₈ to form 55 at 22 °C.	60
Scheme 3.7 Reactivity of 51 towards H ₂ O ₂ in MeOD at 22 °C.....	63

Scheme 3.8 Reactivity of 51 toward H ₂ O ₂ in CD ₃ CN at 22 °C.....	65
Scheme 3.9 Reactivity of 51 toward H ₂ O ₂ to form 58 in THF-d ₈	66
Scheme 3.10 Proposed reaction of 51 with H ₂ O ₂ in AcOD to form intermediates 57 , 59 and the carbazole 58	69
Scheme 3.11 Reactivity of 61 toward H ₂ O ₂ to form 64 in MeOD.	74
Scheme 3.12 Reactivity of 61 toward H ₂ O ₂ in AcOD to form the carbazole 64	76
Scheme 3.13 Reactivity of 61 toward H ₂ O ₂ in THF-d ₈ to form the intermediates 62 , 63 and the carbazole 64	78
Scheme 3.14 The interconversion between the endo and exo isomers of 62	78
Scheme 3.15 Reactivity of 61 toward H ₂ O ₂ in CD ₃ CN to form 63 at 22 °C.....	82
Scheme 3.16 Reactivity of 66 toward H ₂ O ₂ to form 70 in AcOD.	86
Scheme 3.17 Reactivity of 66 toward H ₂ O ₂ in THF-d ₈ to form 70	89
Scheme 3.18 Reactivity of 66 toward H ₂ O ₂ to form 68 in CD ₃ CN.....	91
Scheme 4.1 Reactivity of a TpNi(IV) complex to form 3,3'-dimethylindoline as reported by Sanford.	110
Scheme 4.2 The H/D exchange of 63 with D ₂ O.....	110
Scheme 4.3 Reductive elimination of 63 to form 64 in MeOD at 22 °C.....	112
Scheme 4.4 H/D exchange reaction involving 68 and D ₂ O.....	114
Scheme 4.5 Reactivity of 68 at 105 °C in CD ₃ CN.	117
Scheme 4.6 Reactivity of 68 in THF-d ₈	118

Scheme 4.7 Reactivity of 68 in MeOD at 22 °C.....	119
Scheme 4.8 Reactivity of 68 to form 69 and 70 in AcOD at 22 °C.....	121
Scheme 4.9 Reactivity of 69 in DMSO to form 70 at room temperature.....	125
Scheme 4.10 Proposed reactivity of 68 in CD ₃ CN with 3 equiv of MeSO ₃ H to form 72 and 70 at 22 °C.....	129
Scheme 4.11 Proposed reactivity of 68 in CD ₃ CN with 3 equiv of CF ₃ COOH to form 73 and 70 at 22 °C.....	130
Scheme 4.12 Proposed reactivity of 68 in CD ₃ CN with 3 equiv of HCl or HBr at 22 °C.	132
Scheme 4.13 Reactivity of 68 with 1 equiv of HBF ₄ in CD ₃ CN to form 75 at 22 °C....	134
Scheme 4.14 Reactivity of 75 with CF ₃ COONa to form 78 at 22 °C.....	140
Scheme 4.15 Plausible reaction routes for 68 with 1 equiv of HBF ₄ in CD ₂ Cl ₂ at 22 °C.	143
Scheme 4.16 Proposed reaction scheme for the C-N reductive elimination from 68 in the presence of 1 equivalent of HBF ₄ in CD ₃ CN to form 70 at 22 °C.....	145
Scheme 5.1 Direct synthesis of substituted N-acylindolines from corresponding substituted N-acyl-2-tertbutylanilides as reported by Glorius.....	151
Scheme 5.2 Synthesis of dpk ligated 2-tertbutylaniline palladacycles 81-83	152
Scheme 5.3 Synthesis of 84	153
Scheme 5.4 Reductive elimination from 84 to form 86 and/or 89 (R = H).....	156

Scheme 5.5 Reactivity of 84 in the presence of HCl to form a rapidly equilibrating mixture of 84 and a derived aqua complex 85 which undergoes reductive elimination to produce 86 and 89	162
Scheme 5.6 Reactivity of 84 in the presence of KOH to give 89 as the sole organic product.	167
Scheme 5.7 Reaction of 84 with 2 equivalents of HBr at 22 °C.....	168
Scheme 5.8 Reversibility of protonation of 84 with in DMSO at 22 °C	169
Scheme 5.9 Proposed mechanisms for the formation of 86 from 84	175
Scheme 5.10 Independent synthesis of 86 from 90	177
Scheme 5.11 Synthesis of complex 91	179
Scheme 5.12 Reactivity of 91 to form 93 with 2 equivalents of HBr in DMSO-d ₆	180
Scheme 5.13 Synthesis of 92 from 80	181
Scheme 5.14 Reactivity of 92 to form 94 with 2 equivalents of HBr in DMSO-d ₆	182
Scheme 6.1 Screening of substrates towards reactivity with H ₂ O ₂	200
Scheme 6.2 Screening of ligands for catalytic C-H amination with 46	200
Scheme 6.3 Catalytic C-H amination with 46 to form 54 with Li-(Me-dpms) as ligand.	202
Scheme 7.1 Trends for the reactivity of dpk ligated Pd(II) 2-aminobiphenyl substrates towards H ₂ O ₂	204

List of Figures

Figure 2.1 ^1H NMR spectrum of the mixture of 35 and H_2O_2 to form 40 in AcOD at 22 $^\circ\text{C}$	30
Figure 2.2 ^1H NMR spectrum of a mixture of 35 and H_2O_2 to form 40 in MeOD at 22 $^\circ\text{C}$	32
Figure 2.3 ^1H NMR spectrum of the reaction mixture of 38 and H_2O_2 to form 43 in MeOD at 22 $^\circ\text{C}$	36
Figure 2.4 Reactivity of 36 in MeOD with 3 equivalents of H_2O_2 to give 45	37
Figure 2.5 ^1H NMR spectra of the reaction mixture containing 36 and H_2O_2 in MeOD at 22 $^\circ\text{C}$	38
Figure 3.1 Electronic effects on the rate of reductive elimination of C-N bond from an isolated Pd(II) complex as reported by Buchwald.....	49
Figure 3.2 X-ray crystal structure of 50(MeOD) showing the addition of MeOD across the ketone group of 50	51
Figure 3.3 Monitoring of 50(MeOH) in MeOD with 3 equivalents of H_2O_2 to give 55 at 22 $^\circ\text{C}$	53
Figure 3.4 Monitoring of 50(MeOH) in MeOD with 3 equivalents of H_2O_2 to give 55 at 5 $^\circ\text{C}$	54
Figure 3.5 ^1H NMR of 52 in CD_3CN showing the signal of the proton of its peroxyketal fragment at 14.78 ppm.	57
Figure 3.6 ^1H NMR monitoring of the reaction of 50 with H_2O_2 in CD_3CN to form 55 ..	59
Figure 3.7 First order plot for the elimination from 53 to form 55	60

Figure 3.8 ^1H NMR spectrum of a mixture of 49 with H_2O_2 in THF-d_8 showing peroxyketal proton signal at 14.81 ppm.....	61
Figure 3.9 ^1H NMR spectroscopy monitoring of the reactivity of 51(MeOH) in MeOD at $22\text{ }^\circ\text{C}$	64
Figure 3.10 ^1H NMR spectroscopy monitoring of the reactivity of 51 in CD_3CN at $22\text{ }^\circ\text{C}$	66
Figure 3.11 ^1H NMR spectroscopy monitoring of the reactivity of 51 in THF-d_8 at $22\text{ }^\circ\text{C}$	68
Figure 3.12 A profile of the reaction of 51 (blue diamonds) with 3 equiv H_2O_2 in AcOD to form intermediates 57 , 59 and the carbazole 58 , based on ^1H NMR monitoring at $22\text{ }^\circ\text{C}$	69
Figure 3.13 ^1H NMR monitoring of the reaction of 51 with H_2O_2 in AcOD at $22\text{ }^\circ\text{C}$	70
Figure 3.14 ^1H NMR spectrum in DMSO-d_6 of a mixture containing 59 and 60 as the major component, before (below) and after addition of two drops of D_2O (above).	72
Figure 3.15 ^{19}F NMR spectrum of a mixture containing 59 as the major component in DMSO-d_6	73
Figure 3.16 ^1H NMR monitoring of the reaction of 61 with H_2O_2 in MeOD at $22\text{ }^\circ\text{C}$	75
Figure 3.17 ^1H NMR monitoring of the reaction of 61 with 3 equiv H_2O_2 in AcOD at $22\text{ }^\circ\text{C}$	77
Figure 3.18 ^1H NMR spectra of 61 (below) and 62 (above) in THF-d_8	79
Figure 3.19 ORTEP plot of complex 62 with the endo-orientation of the OOH group....	79

Figure 3.20 ¹ H NMR spectrum of the Pd(II) hydroperoxo ketal complex 62 (bottom) and its mixture with the Pd(IV) hydroxo derivative 63 and the carbazole 64 (top) after 24 hours in THF-d ₈ at 22 °C.....	81
Figure 3.21 ¹ H NMR spectrum of 61(MeOH) in CD ₃ CN (bottom), 30 minutes after adding H ₂ O ₂ (middle) and 60 minutes after addition of H ₂ O ₂ (top).....	83
Figure 3.22 ¹ H NMR spectrum in DMSO-d ₆ of the Pd(IV) amido aryl complex 63 containing <5% of the dpk hydroperoxoketal – derived Pd(II) complex 62 as a major impurity.	84
Figure 3.23 X-ray crystal structure of 66·MeCN (the solvent of crystallization is not shown).....	85
Figure 3.24 Oxidation of 65 with 3 eq of H ₂ O ₂ in AcOD at 22 °C.....	87
Figure 3.25 ¹ H NMR spectrum of a 5:1 mixture of endo- and exo-isomers of 67 in THF-d ₈ with arrows showing the peroxyketal signals at 11.03 ppm and 10.59 ppm.	89
Figure 3.26 ¹ H NMR monitoring of the reaction of 66 with H ₂ O ₂ in THF-d ₈ at 22 °C.	90
Figure 3.27 ¹ H NMR spectrum showing the conversion of 67 into 68 DMSO-d ₆	91
Figure 3.28 A detailed picture of the downfield region of ¹ H NMR spectrum showing the conversion of 67 to 68 in DMSO-d ₆	92
Figure 3.29 Plot of ln([67] ₀ /[67]) vs time in DMSO-d ₆	92
Figure 3.30 X-ray crystal structure of 68	93
Figure 4.1 ¹ H NMR spectra of 63 in DMSO-d ₆ before (bottom) and after addition of D ₂ O (top).....	111
Figure 4.2 A plot of ln([63] ₀ /[63]) vs time for 63 in MeOD at 22 °C.....	112

Figure 4.3 The DFT-calculated Gibbs energy profile for the C-N reductive elimination of 63 in MeOH.	113
Figure 4.4 ¹ H NMR spectra of 68·MeCN in DMSO-d ₆ before (bottom) and after addition of D ₂ O (top).	116
Figure 4.5 ¹ H NMR spectra of complex 68 (bottom) after heating for 14 hours at 60 °C and 105 °C (top).	117
Figure 4.6 ¹ H NMR spectra of complex 68 containing a more soluble impurity of 66 and some 67 in THF-d ₈ after 5 minutes upon dissolution (bottom) and after 46 hours (top)	118
Figure 4.7 ¹⁹ F NMR spectrum in MeOD of 68 containing impurities of 67 and 66 . The arrow points to the peak for 70 which was formed only in 3.6% yield after 95 h.....	120
Figure 4.8 ¹ H NMR spectral monitoring of 68 in AcOD for 51 hours..	122
Figure 4.9 Comparison of ¹ H NMR spectra of 68 observed in the direct oxidation of 66 with H ₂ O ₂ in AcOD (bottom) and isolated 68 dissolved in AcOD (top).....	123
Figure 4.10 ¹ H NMR spectrum of 68·MeCN (bottom) and 69·AcOH (top) in DMSO-d ₆ . The aromatic region is expanded for clarity. The apical ligand OAc could be observed at 1.71 ppm for 69·AcOH	124
Figure 4.11 ¹ H NMR spectrum of 69·AcOH in DMSO-d ₆ after 5 minutes (bottom), 48 hours (middle) and nine days (top).	125
Figure 4.12 ¹ H NMR spectrum of 68 ; 5 minutes after adding 3 equivalents of HBF ₄ and 15 minutes after addition.	128
Figure 4.13 Plot of ln([68] ₀ /[68]) vs time with 3 equivalent of MeSO ₃ H in CD ₃ CN.....	129
Figure 4.14 Plot of ln([68] ₀ /[68]) vs time with 3 equivalent of TFA in CD ₃ CN	131

Figure 4.15 ^1H NMR spectrum of 68 ; 5 minutes after adding 3 equivalents of HBr, 60 minutes after addition and 72 h after addition..	132
Figure 4.16 ^1H NMR spectrum of 68 ; 5 minutes after adding 3 equivalents of HCl, 60 minutes after addition and 72 h after addition.	133
Figure 4.17 ^1H NMR spectrum of 68 + 1 equivalent HBF_4 upon mixing and after 24 hours.	135
Figure 4.18 Plot of $\ln([\mathbf{75}]_0/[\mathbf{75}])$ vs time/min in CD_3CN at $22\text{ }^\circ\text{C}$.	135
Figure 4.19 Mass spectrum of 68 in CH_3CN + 1 equivalent of HBF_4 . The peak at $m/z=605.90$ is assigned to a formally 5-coordinate Pd(IV) species 74 and the peak at $m/z= 646.99$ is attributed to 75 .	136
Figure 4.20 ^1H NMR spectrum of 75 in CD_2Cl_2 .	137
Figure 4.21 First order kinetic plot for the reductive elimination of 75 isolated as a BF_4 salts in CD_2Cl_2 .	138
Figure 4.22 Plot of $\ln([\text{Pd(IV)}]_0/[\text{Pd(IV)}])$ vs. time/min for 68 with 1.3 equivalent of HBF_4 in CD_3CN at $22\text{ }^\circ\text{C}$.	139
Figure 4.23 Plot of $[1/A]/\text{mol}^{-1}\text{L}^{-1}$ vs. time /min for 68 with 1.3 equivalents of HBF_4 in CD_3CN at $22\text{ }^\circ\text{C}$.	139
Figure 4.24 Exchange reaction of 75 with CF_3COONa .	141
Figure 4.25 Comparison of the ^1H NMR spectrum of 73 (bottom) and 69 (top) in DMSO-d_6 at $22\text{ }^\circ\text{C}$.	141
Figure 4.26 First order kinetic plot for the exchange reaction of the CH_3CN ligand in 75 with trifluoroacetate ion to form 73 in CD_3CN .	142

Figure 4.27 Plot of $\ln([\text{Pd(IV)}]_0/[\text{Pd(IV)}])$ vs time/min for 68 with 1 equivalent of HBF_4 in CD_2Cl_2 at 22°C	144
Figure 4.28 The Gibbs energy profile for the C-N reductive elimination of $\mathbf{75^+}, \text{BF}_4^-$ in CH_2Cl_2	146
Figure 5.1 X-ray crystal structure of 81 ·MeCN (the solvent of crystallization is not shown).....	152
Figure 5.2 X-ray crystal structure of 84 ·MeCN (the solvent of crystallization and trifluoromethylsulfonyl groups are not shown for clarity).	154
Figure 5.3 ^1H NMR spectrum of the $\text{CH}_2\text{Pd(IV)}$ fragment of 84 in different solvents: CD_2Cl_2 (bottom), MeOD (middle) and DMSO-d_6 (top).....	156
Figure 5.4 Reactivity of 84 with 2 equivalents of HCl.	163
Figure 5.5 Reactivity of 84 with 2 equivalents of HBr	165
Figure 5.6 X-ray crystal structure of 87	168
Figure 5.7 The kinetic profile of the reaction between 84 and 2 equivalents of HBr to form the indoline 86 (grey triangle) and Pd(dpk)Br_2 , 87	169
Figure 5.9 Reversibility of protonation of 84 in DMSO-d_6	170
Figure 5.10 Addition of different equivalents of Brookhart's Acid to 84 in DMSO-d_6 at 22°C	172
Figure 5.11 Plot of Chemical shift versus equivalents of acid added for figure 5.10 above.	172
Figure 5.12 Structures of Brookhart's acid as our source of H^+ and tetra-n-butylammonium bromide as our source of Br^-	173

Figure 5.13 The reaction Gibbs energy profile corresponding to the most kinetically favorable C(sp³)-N coupling mechanism of the amido alkyl Pd(IV) complex **84** in the presence of HBr in DMSO solution..... 178

Figure 7.1 Trend for reductive elimination from substituted dpk-ligated Pd(IV) alkyl N-anilido complexes. 205

List of Tables

Table 5.1 Solubility of 84 •MeCN in different common solvents.	155
Table 5.2. Initial rates of reaction involving 84 , H ⁺ and Br ⁻	173
Table 6.1. Effect of the ligand on the yield of N-acetylcarbazole (Scheme 6.2). Reaction conditions: 46 (30 mg, 0.14 mmol), Pd(OAc) ₂ (10 mol%), Ligand (10 mol%), solvent(0.6 mL), 6 equivalents of 30 % H ₂ O ₂ added at the beginning of reaction, 23 °C, 24 h. Yield (%) of 54 determined by ¹ H NMR spectroscopy with dioxane as an internal standard.	201
Table 6.2. Effect of the reaction conditions on the yield of N-acetylcarbazole Reactants loading: 46 (30 mg, 0.14 mmol), Pd(OAc) ₂ (10 mol%), Ligand (10 mol%), solvent(0.6 mL), 0.5 equivalent of H ₂ O ₂ added each time. Yield (%) of 54 determined by ¹ H NMR spectroscopy with dioxane as internal standard	202

List of Abbreviations

Tf	trifluoromethanesulfonyl
d	days
equiv	equivalents
h	hours
min	minutes
s	seconds
mL	milliliters
Me	Methyl
Et	Ethyl
<i>J</i>	¹ H- ¹ H coupling
THF	tetrahydrofuran
TFA	trifluoroacetic acid
AcOH	acetic acid
MeCN	acetonitrile
g	gram
C-H	carbon-hydrogen bond

Chapter 1: Pd(II)/Pd(IV) couple mediated C-H functionalization and common oxidants used

1.1 C-H Activation at Transition metal centers

Carbon-hydrogen bonds are common in most simple natural occurring organic molecules (e.g., Natural gas and oil), this makes them a readily available source of feedstock for the syntheses of complex molecules which contain carbon-oxygen, carbon-halogen, carbon-nitrogen, carbon-sulfur, and carbon-carbon bonds.¹ Traditional methods available for the formation of carbon-carbon and carbon-heteroatom bonds rely on pre-functionalized starting materials for both reactivity and selectivity. However, the constraint for installing a functional group prior to the desired C-O, C-X, C-N, C-S, or C-C bond adds unwanted and costly chemical steps to the overall construction of a molecule.² As such, by-passing this issue will not only improve atom economy but also increase the overall efficiency. Current research is involved in the search for mild and selective processes for the syntheses of products for pharmaceuticals, natural products, agrochemicals, polymers, advanced materials, feedstock commodity chemicals and other value-added commercial products. The use of transition metal catalyzed processes represents essential tools for the construction of C-C and C-heteroatom bonds. Procedures which involve direct C-H functionalization will improve atom economy, increase the efficiency of a multistep reaction sequence and render these transformations more favorable.³

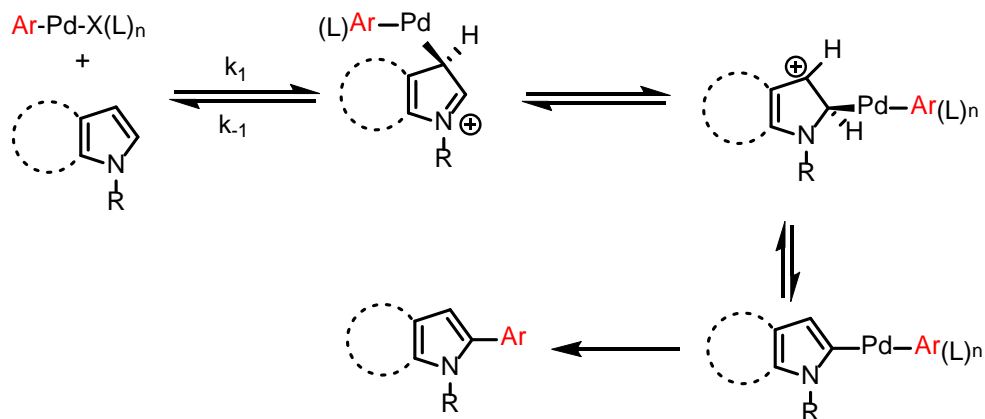
Palladium complexes are particularly attractive catalysts for such transformations for several reasons.⁴ First, ligand-directed C-H functionalization at palladium centers can be employed in the formation of different types of bonds, including carbon-oxygen, carbon-halogen, carbon-nitrogen, carbon-sulfur, and carbon-carbon linkages. Just a few other catalysts allow such wide-ranging

bond constructions, and this versatility is largely the result of two key features: (i) the compatibility of many Pd(II) catalysts with various oxidants (functionalizing agents), and (ii) the ability to preferentially functionalize cyclopalladated intermediates. Second, palladium participates in cyclometalation with a wide variety of directing groups and, unlike many other transition metals, readily promotes C-H activation at both sp^2 and sp^3 C-H sites. Finally, majority of Pd-catalyzed directed C-H functionalization reactions can be performed in the presence of ambient air and moisture, making them practical for applications in organic synthesis.⁵

Two major challenges limit direct C-H bond functionalization reactions. The first challenge is the inert nature of most carbon-hydrogen bonds; which comprises of a low bond polarity (a value of 0.35 on the Pauling electronegativity scale), high bond strength (between 85-105 kcal/mol) and also a relatively high pKa (~43 for benzene). This makes C-H bonds very unreactive towards both heterolytic and homolytic cleavage.⁶ A number of studies have addressed the first challenge by confirming that transition metals can activate C-H bond. C-H activation processes are generally divided into two extreme mechanisms: oxidative addition and σ -bond metathesis.⁷ Oxidative addition consists of two steps: coordination of the σ (C-H) bond after generation of a vacant site and actual cleavage of the C-H bond. This transformation is most commonly observed for low-valent electron-rich metals with d^8 configuration (e.g. Ir^I, Pt^{II}) that allow easy access to an oxidized d^6 configuration accommodating two extra ligands.^{8, 9} When no d electrons are available in the metal, an oxidative transformation is not possible and the C-H activation proceeds through a σ -bond metathesis pathway.^{10, 11} Essential to such a transformation are the absence of an intermediate and the concerted bond-breaking and bond-making processes.^{12, 13} For transition metal fragments with d^4 to d^8 configurations, a σ -bond metathesis transformation is in principle possible, with the additional potential formation of a stable σ -adduct before and after the actual metathesis.⁶

1.1.1 C-H Activation at Pd(II) centers

With respect to Pd, two major reaction mechanisms for C-H activation have been touted: electrophilic aromatic substitution (S_{EAr}) with electron-rich, π -nucleophilic heteroarenes and concerted cyclometallation-deprotonation (CMD) with simple and electron-deficient benzenes.¹⁴

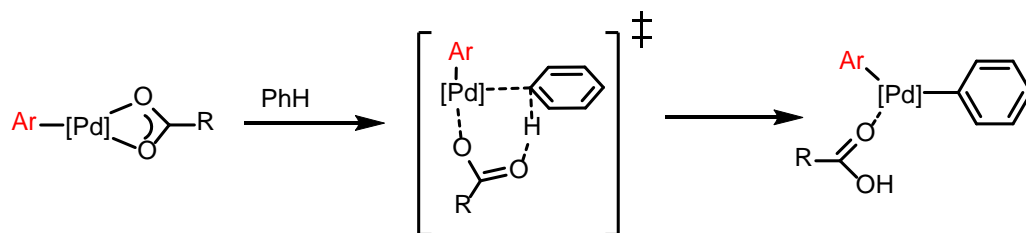


Scheme 1.1 Electrophilic aromatic substitution mechanism for C-H activation at a Pd center with indolines. (L)_n is PPh₃

To probe the S_{EAr} mechanism, Sames¹⁵ and coworkers looked at the C-2 arylation of indolines (Scheme 1.1). Kinetic plots indicated a first order reaction with respect to both substrate and catalyst. A high secondary isotope effect of 1.6 was observed for the 3-position where arylation was not observed. Also, a Hammett plot revealed a negative ρ -value, which indicated a positive charge accumulating at the 3-position of indole and affording a strong support for the electrophilic palladation mechanism.

While working on direct arylation of electron deficient benzene groups, Fagnou¹⁶ and coworkers observed that the reactivity was dependent on the acidity of the hydrogen involved in the C-H

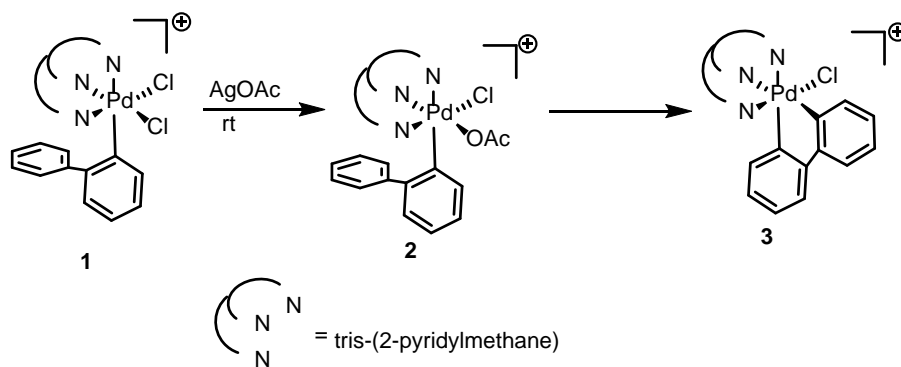
activation step. Based on a combination of experimental data and computational studies for Pd(OAc)₂ as a catalyst in these arylation reactions with electron poor substrates, a concerted cyclometallation-deprotonation (CMD) mechanism was proposed (Scheme 1.2).^{14, 17-19} This mechanism explains the dependency of the reaction yield on the basicity of the acetate ion.



Scheme 1.2 Concerted cyclometallation-deprotonation (CMD) mechanism of C-H activation.

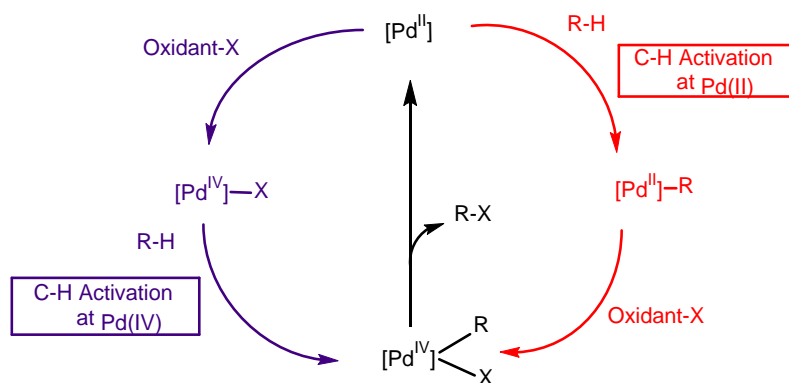
1.1.2 C-H Activation at Pd(IV) centers

Recently, the C-H activation at a Pd(IV) center was proposed by the Sanford group.²⁰ To study the mechanism of the proposed C-H activation at Pd(IV), **1** was synthesized, and it was only observed to undergo C-Cl reductive elimination even upon heating to 90 °C. Exchanging one of the Cl ligands with OAc formed **2**, resulting in facile C-H activation even at room temperature to form **3**. It was suggested that C-H activation at the high oxidation state Pd(IV) occurred through a concerted cyclometallation-deprotonation (CMD) mechanism similar to C-H activation at Pd(II).²¹⁻²⁴



Scheme 1.3 C-H Activation at a Pd(IV) d^6 metal center by Sanford

The successful C-H activation at a Pd(IV) center shows a dual catalytic cycle for Pd-catalyzed C-H functionalization is feasible. A dual catalytic pathway will include, oxidation of Pd(II) to Pd(IV), C-H bond activation at Pd(IV), and reductive elimination to release the product and regenerate the Pd(II) catalyst. And/or C-H activation at Pd(II), oxidation of Pd(II) to Pd(IV) and its subsequent reductive elimination to release the catalyst. Both of these mechanisms will be at play (Scheme 1.4).²⁰

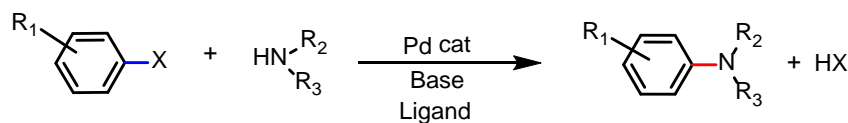


Scheme 1.4 Proposed catalytic route involving C-H activation at a Pd(IV) and a Pd(II) metal centers through a dual catalytic pathway.

1.2 Buchwald-Hartwig Amination

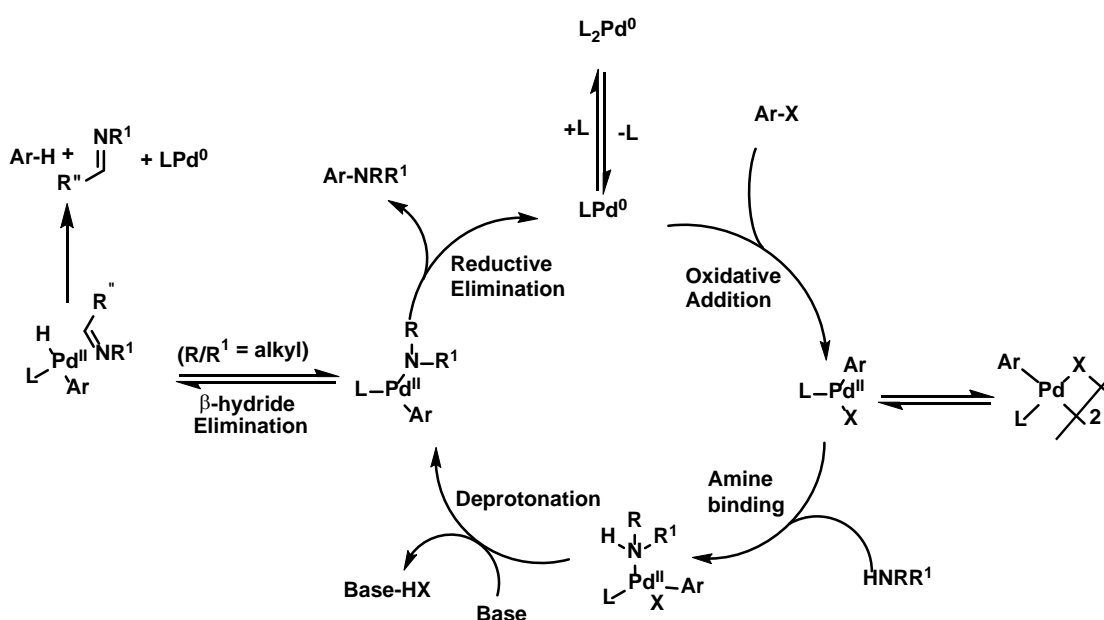
Previously, carbon-nitrogen bonds were generally synthesized through electrophilic aromatic substitution, reductive amination, Gabriel's synthesis, Curtius re-arrangement, Schmidt reaction or Ullman coupling and other methods.²⁵ Ullman coupling which was discovered over a century ago, involves the use of stoichiometric amounts of copper salts, and was the most common method for C-N coupling even though the exact mechanism was poorly understood. While working on different alternatives to the Ullman coupling reaction, Migita and coworkers developed the first C-N bond formation from Pd(0) using organotin reagents (similar to Stille coupling).²⁶ This method was not useful synthetically because of the toxicity which arises from using tin reagents. After the discovery of the Suzuki-Miyaura coupling²⁷ to form carbon-carbon bonds, similar methods were developed independently by Buchwald²⁸ and Hartwig²⁹ to form carbon-nitrogen bonds.

The Buchwald-Hartwig amination involves the formation of carbon-nitrogen bonds via the Palladium-catalyzed cross coupling of amines with aryl halides or pseudohalides (scheme 1.5). Catalysts responsible for Buchwald-Hartwig aminations have been significantly improved upon over several generations which help in increasing the substrate scope and performing the reactions under milder conditions.^{30, 31} Aryl and alkyl C-N bonds are very common in pharmaceuticals and natural products, making the Buchwald-Hartwig C-N coupling reactions very useful in synthetic organic chemistry.³²



X = Cl, Br, I, OTf
 R₁, R₂, R₃ = H, Alkyl, Aryl

Scheme 1.5 General scheme for the Buchwald-Hartwig amination reaction



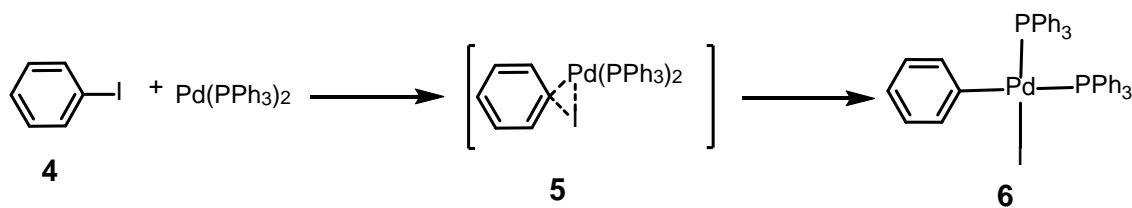
Scheme 1.6 Proposed mechanism for the Buchwald-Hartwig amination reaction

The Buchwald-Hartwig amination reaction mechanism have been proposed to go through steps similar to the corresponding Suzuki coupling reactions as shown in Scheme 1.6.³¹ These include (i) oxidative addition of the aryl halide to a Pd(0) species, (ii) the binding of the amine to the oxidative addition Pd(II) complex (iii) deprotonation of the amine by a base (iv) C-N reductive elimination from Pd(II) complex to form Pd(0) (scheme 1.22). An unwanted β -hydride elimination competing

pathway is also usually observed with substrates containing β -hydrogens. Different people have worked on elucidating the mechanism of the different steps of the Buchwald-Hartwig amination.

1.2.1 Oxidative Addition to Pd(0)

Oxidative addition which is usually proposed as the rate determining step for most coupling reactions has been studied by Fitton in detail. The trend $\text{PhI} > \text{PhBr} > \text{PhCl}$ was observed by for the oxidative addition of halides to the Pd(0) precursor $\text{Pd}(\text{PPh}_3)$. Ph-I was observed to react with $\text{Pd}(\text{PPh}_3)_4$ at room temperature to form $\text{PdIPh}(\text{PPh}_3)_2$ and Ph-Br reacted at $80\text{ }^\circ\text{C}$, but the corresponding Ph-Cl did not react even at $135\text{ }^\circ\text{C}$. This indicates that, the strength of the C-X bond was vital in these type of transformations.³³ Further studies by Pflüger and Amatore in solvents with different polarities (THF and toluene) showed that the activation parameters are similar in both solvents, suggesting that, oxidative addition proceeds via a neutral concerted, three-centered intermediate as shown in Scheme 1.7.³⁴



Scheme 1.7 Proposed mechanism for oxidative addition of phenyl iodide to $\text{Pd}(\text{PPh}_3)_2$

1.2.2 Reductive Elimination from Pd(II)

Reductive elimination has been proposed as the product forming step in the cycle of most coupling reactions. Studies have shown that reductive eliminations to form the C-N bond in arylamines are faster from complexes with more electron-rich amido ligands than from complexes with more electron-poor amido ligands.³⁵ Also, it was demonstrated that complexes with the ligands in *cis* position reacted faster than the *trans* isomer and prior isomerization of the *trans* complex to *cis* was required before the reductive elimination occurred.³⁶ In addition to that, complexes containing more sterically hindered ligands tend to undergo faster C-N reductive elimination than complexes with less hindered ancillary ligands.³²

1.3 Intermediacy of high oxidation state Pd(III)/Pd(IV) in C-H functionalization

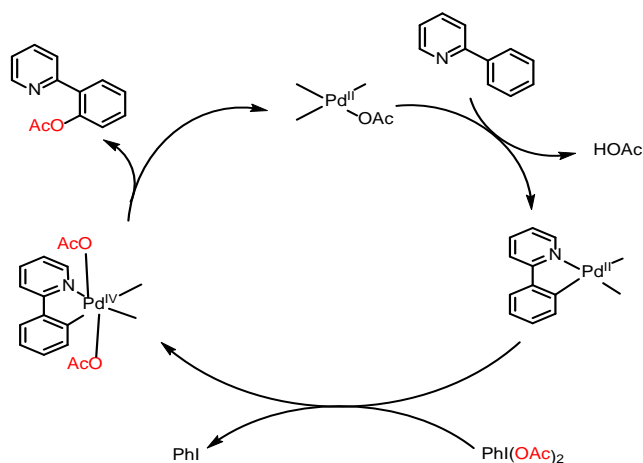
Until recently, the Pd(II)/Pd(IV) hydrocarbyl cycles had received little attention even though it had been implicated in a lot of reactions.³⁷ This was partly due to the inability to isolate and characterize well-defined Pd(IV) complexes which were presumed to be intermediates in different Pd-catalyzed reactions. Different oxidants have been shown to oxidize hydrocarbyl Pd(II) intermediates effectively to their corresponding Pd(IV) forms which can subsequently undergo reductive eliminations to form C-C and C-X bonds.³⁸ The Pd(II)/Pd(IV) route has eliminated the formation of Pd black through mostly beta-hydride elimination mechanism, which usually occurs through a Pd(0)/Pd(II) catalytic cycle. Also, since Pd(IV) is already a high oxidation state for the

metal, it is easier to undergo reductive elimination compared to the corresponding Pd(II) which is deemed to be more electron rich center. Therefore, no fine tuning of the ligand is necessary to enhance reductive elimination as it occurs with Pd(II).³⁸

1.3.1 Some selected reagents for oxidation of Pd(II) to Pd(IV)

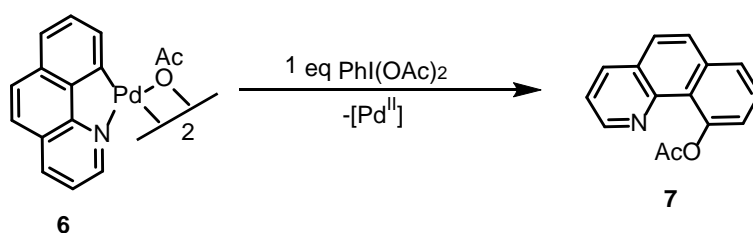
1.3.1.1 Iodine(III) based reagents

Even though Uson³⁹ and co-workers synthesized the very first Pd(IV) compounds containing a Pd-C bond in 1975, hypervalent iodine based reagents had been used as oxidizing agents for a lot of other reactions including oxidation of alcohols and carbonyl compounds.⁴⁰ The first palladium catalyzed acetoxylation of C(sp²)-H bonds using PhI(OAc)₂ as oxidant was reported by Crabtree where the intermediacy of a Pd(IV) species was proposed.⁴¹ Sanford optimized the acetoxylation of C(sp²)-H bonds with PhI(OAc)₂ and performed detailed mechanistic studies on this reaction. The different steps of this cycle as shown in scheme 1.8 involves: (i) ligand-directed C-H activation to form a cyclopalladated intermediate, (ii) two-electron oxidation of the palladacycle to generate a Pd(IV) species, and, finally, (iii) C-O bond-forming reductive elimination to release the product.⁴²



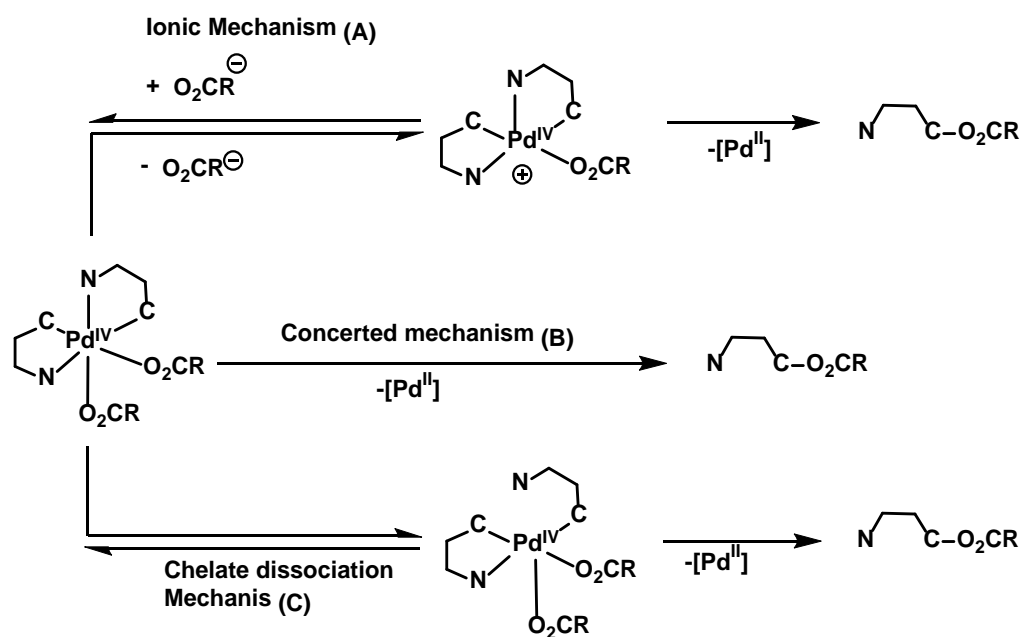
Scheme 1.8 Proposed mechanism for the acetoxylation of 2-phenylpyridine with $\text{PhI}(\text{OAc})_2$ as oxidant and $\text{Pd}(\text{OAc})_2$ as a catalyst.

Upon changing the substrates to benzo[*h*]quinoline, the rates of reaction were observed to be comparable using either $\text{Pd}(\text{OAc})_2$ or the independently synthesized catalyst **6**. Also, **6** was observed to undergo stoichiometric transformation to form **7** which confirms the intermediacy of **6** in the formation of **7**.



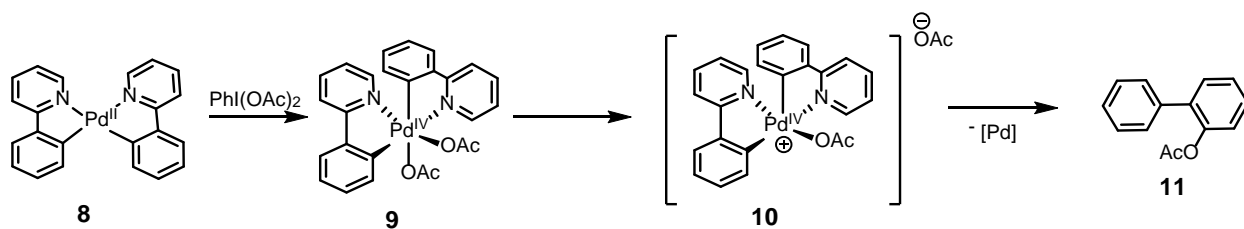
Scheme 1.9 Stoichiometric acetoxylation of benzo[*h*]quinoline with $\text{PhI}(\text{OAc})_2$ as the terminal oxidant.

To probe the mechanism of reductive elimination, **9** was synthesized and monitored under different conditions (Scheme 1.10). Three different mechanisms were proposed for reductive elimination from complexes **9** (scheme 1.11): the ionic mechanism (A), concerted mechanism (B) and chelate dissociation mechanism (C). The ionic mechanism involves dissociation of a carboxylate ligand, followed by reductive elimination from a 5-coordinate Pd(IV) intermediate. The concerted mechanism involves direct reductive elimination from a 6-coordinate octahedral complex. The chelate dissociation mechanism involves an initial dissociation of the chelate followed by reductive elimination from the resulting 5-coordinate Pd(IV) intermediate formed.⁴³



Scheme 1.10 Proposed mechanisms for the formation of **11** from **9**

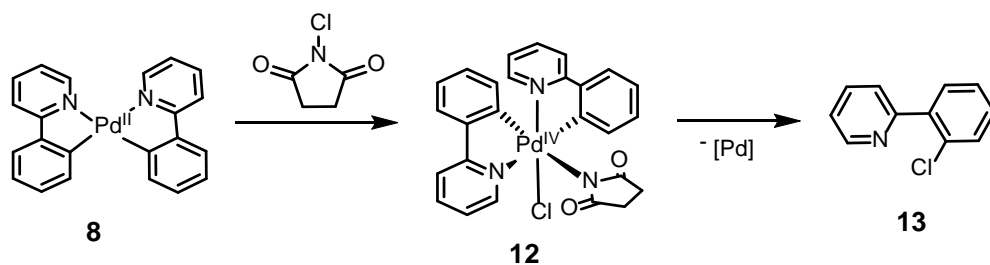
Kinetic experiments with **9** showed that the reductive elimination proceeds through a dissociation of an acetate ligand followed by reductive elimination from a 5-coordinate intermediate (Pathway A). The rapid exchange of bound and free carboxylate ligands was observed, which indicates that the dissociation of the carboxylate ligand from Pd(IV) is possible.^{44, 45}



Scheme 1.11 Proposed ionic mechanism for the formation of **11** from **9** as proposed by the Sanford group.

1.3.1.2 *N*-Halosuccinimides as oxidant

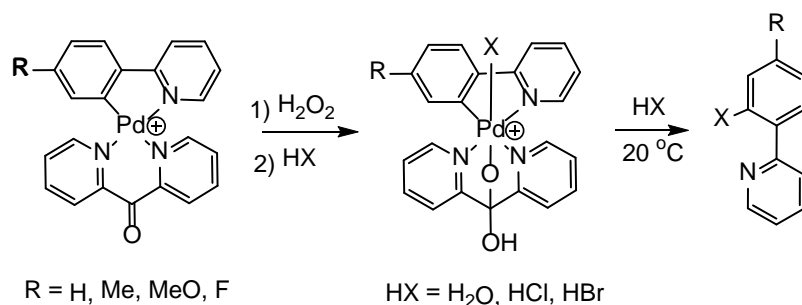
The Sanford group, explored the corresponding C-X (X = Cl, Br) reductive elimination from an isolated Pd(IV) using *N*-halosuccinimide (NCS) as a representative oxidant. In the model studies, complex **8** was synthesized and oxidation with NCS formed the Pd(IV) oxidative addition product **12** which could be observed by ¹H NMR spectroscopy and isolated. When **12** warmed at 80 °C it was observed to undergo C-Cl bond-forming reductive elimination to form **13** in high yield confirming a C-Cl bond-forming reductive elimination from Pd(IV).⁴⁶



Scheme 1.12 Chlorination of 2-phenylpyridine with N-chlorosuccinimide as terminal oxidant through a Pd(IV) intermediate.

1.3.1.3 Peroxide Oxidants

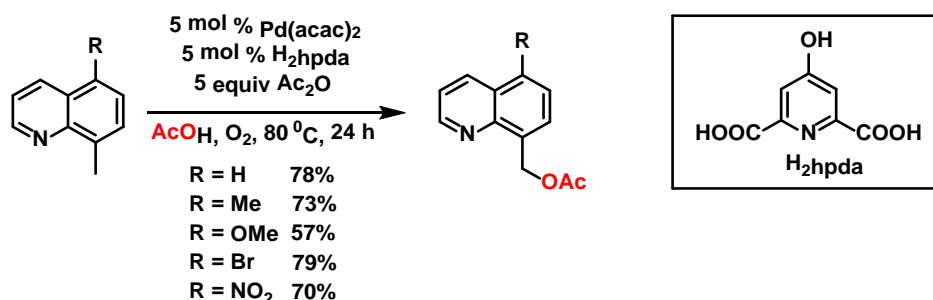
Peroxide oxidants are better substitutes to much more expensive iodine-based reagents for Pd-catalyzed ligand-directed C-H oxygenation. The Pd-catalyzed oxygenation of C-H bonds has been realized using peroxides such as Oxone, $\text{K}_2\text{S}_2\text{O}_8$ and tertbutylperoxyacetate.⁴⁷ In addition to that, the Vedernikov group reported the oxidation of monohydrocarbyl Pd(II) substrates with H_2O_2 to form the corresponding mono-hydrocarbyl Pd(IV) analogs. These Pd(IV) species stabilized by one or two facially chelating ligands such as one derived from a hydrated di-(2-pyridyl)ketone (dpk) were observed to undergo C-X (X=Cl, Br) and C-O reductive eliminations in D_2O or other solvents.⁴⁸



Scheme 1.13 C-O and C-X (X=Cl, Br) reductive elimination from a Pd(IV) center with H_2O_2 as terminal oxidant

1.3.1.4 Dioxygen as a Terminal Oxidant

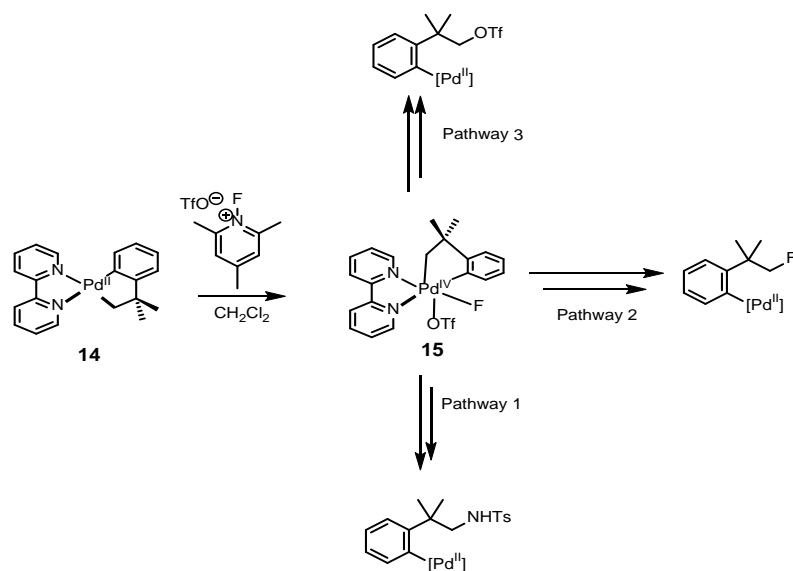
The use of O₂ as an oxidant for catalytic oxygenation of 8-methylquinoline-derived substrates with Pd(acac)₂ as the catalyst and 2,6-pyridinedicarboxylate as ligand (H₂hpda) in AcOH as solvent was reported by the Vedernikov group.⁴⁹ It is an exciting development because O₂ is readily available and inexpensive, and will serve as the best oxidant for this type of transformations. After the initial report by Vedernikov, there arose questions about whether O₂ can be used to produce high oxidation state palladium intermediates. Subsequent works by Mirica group showed that aerobic oxidation of Pd(II) dimethyl complexes is possible when *fac*-chelating such as N,N',N''-trimethyl-1,4,7-triazacyclononane (Me₃tacn) are used.⁵⁰



Scheme 1.14 Acetoxylation of 8-methylquinoline substrates with O₂ as terminal oxidant as reported by Vedernikov.

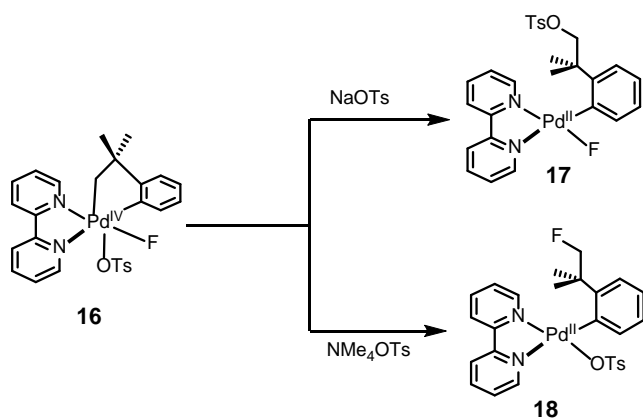
1.3.1.5 Electrophilic Fluorinating Reagents

The use of electrophilic fluorinating agents to oxidize Pd(II) to Pd(IV) and isolation of Pd(IV) fluorides was reported by the Sanford^{22,51} and Ritter⁵² groups. One of the isolated Pd(IV) fluorides, which was observed to undergo C(sp³)-N reductive elimination is shown in scheme 1.15 (Pathway 1).



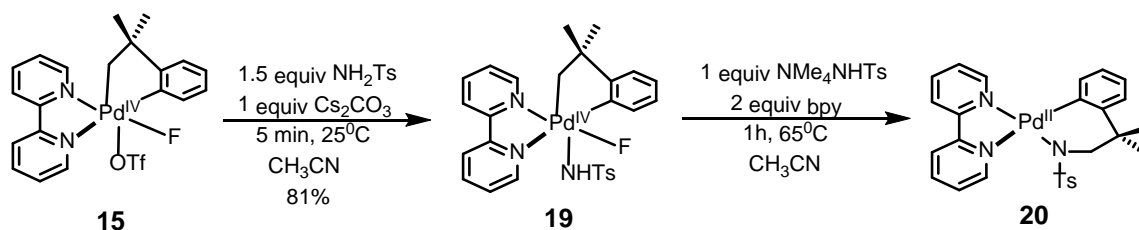
Scheme 1.15 Proposed transformations of **15** into different products based on additives and reaction conditions.

Interestingly, **15** was also observed to give a product selectivity which is dependent on the type of cation used for the tosylate anion. Changing the nitrate/tosylate source from NaOR to NBu₄OR under otherwise identical conditions resulted in a dramatic shift in the product distribution.⁵³



Scheme 1.16 Transformation of **16** into different products **17** or **18** based on the identity of the cation bound to tosylate by the Sanford group

To study C-N reductive elimination from Pd(IV), NH_2SO_2 -*p*-tolyl (NH_2Ts) was added to **15** afford **19** (scheme 1.17) Upon warming, the C-N reductively eliminated product **20** was observed in high yield.⁵⁴



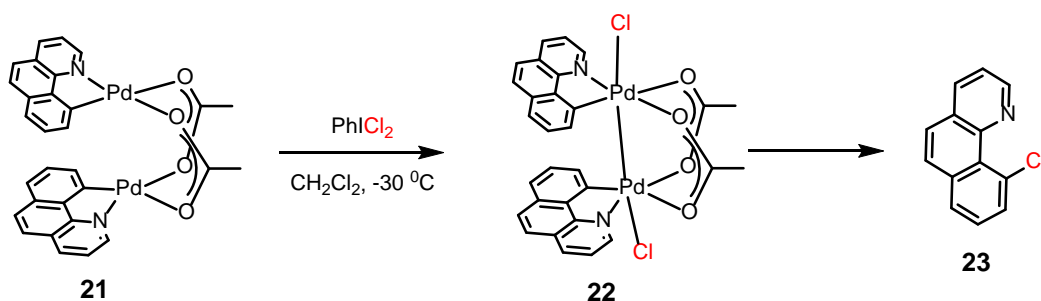
Scheme 1.17 C-N reductive elimination from Pd(IV) alkyl complex, **19**, as reported by Sanford.

To probe the reaction mechanism, kinetic studies were conducted to determine the rate dependence on each species. The reaction exhibited clean kinetics with a first-order dependence on substrate and zero order dependence on nucleophile. This rules out a pathway involving a direct $\text{S}_{\text{N}}2$ reaction between TsNH^- and **19**, since this should show first-order kinetics in both **19** and the nucleophile confirming an $\text{S}_{\text{N}}2$ -like reductive elimination from a five coordinate Pd(IV) intermediate.⁵⁴ Subsequent computational studies showed a concerted inner sphere C-N bond formation that proceeds via a 5-membered transition state from an O-bound sulfonamide intermediate.⁵⁵

1.3.2 Pd(III)-mediated reactions.

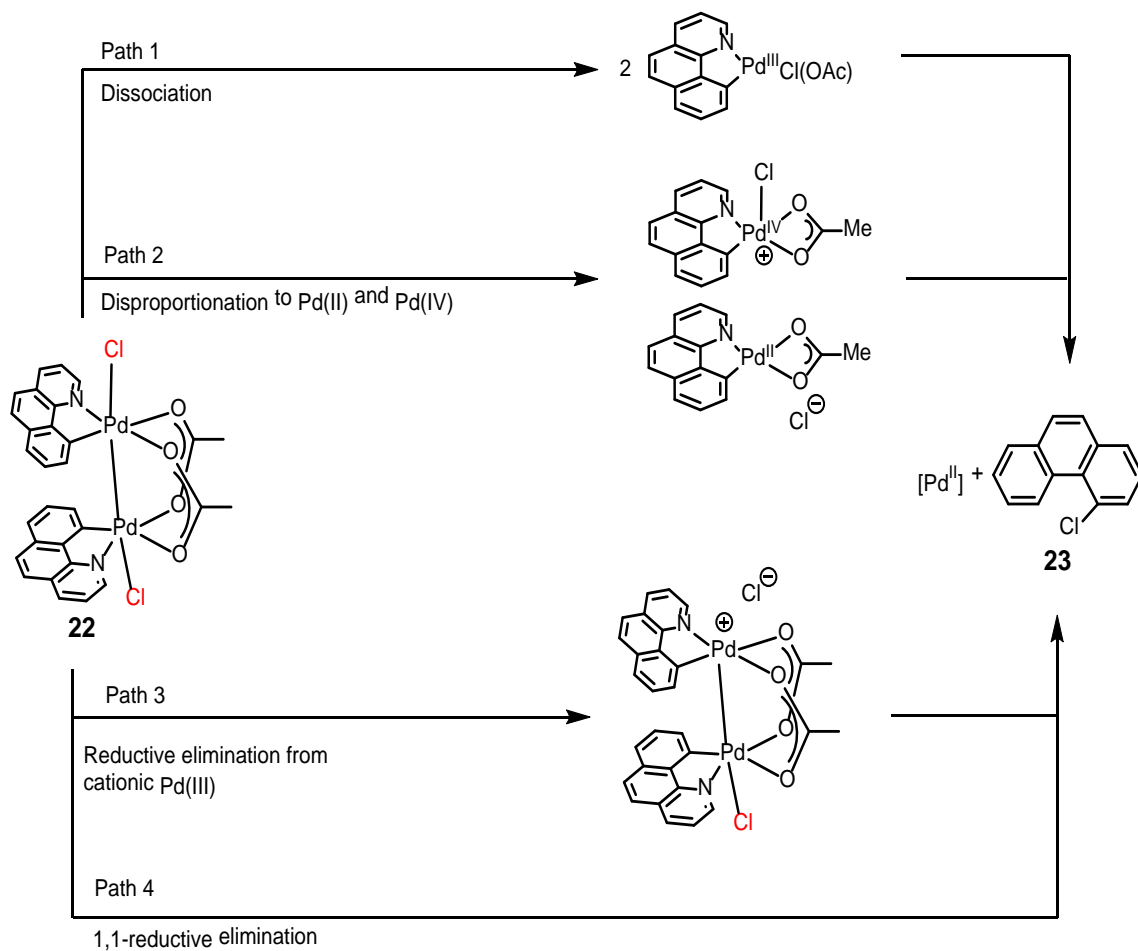
Pd(II) usually undergoes a facile two-electron oxidation to Pd(IV), but Ritter and co-workers reported the first isolated Pd(III)-dimeric complex **22**. Complex **21** was observed to undergo a

single electron oxidation at each Pd center to form **22** which could be isolated and characterized (d^8 to d^7) as shown in scheme 1.18. A d^7 electronic configuration is expected to result in a metal–metal single bond.⁵⁶



Scheme 1.18 C-Cl reductive elimination from isolated dimeric Pd(III) as reported by Ritter

Even though reductive elimination from **22** to form **23** was observed, the exact mechanism was not apparent since there are many possible pathways for this to take place. The first pathway proposed was rate-determining dissociation of **22** into two Pd(III) monomers followed by fast reductive elimination from Pd(III) or by pre-equilibrium dissociation of **22** into two monomers with a rate-determining reductive elimination from a monomeric Pd(III) complex. This pathway was ruled out by kinetic experiments (scheme 1.20).⁵⁷ Kinetic experiments also ruled out disproportionation of **22** into one Pd(II) and one Pd(IV) complex followed by reductive elimination from Pd(IV) (Pathway 2). Kinetic measurements also excluded rate-determining dissociation of chloride or acetate followed by fast reductive elimination from a cationic bimetallic Pd(III) complex (Path 3). The results of the kinetic experiments and DFT calculations were consistent with a concerted, bimetallic 1,1-reductive elimination from **22** (Path 4).⁵⁸

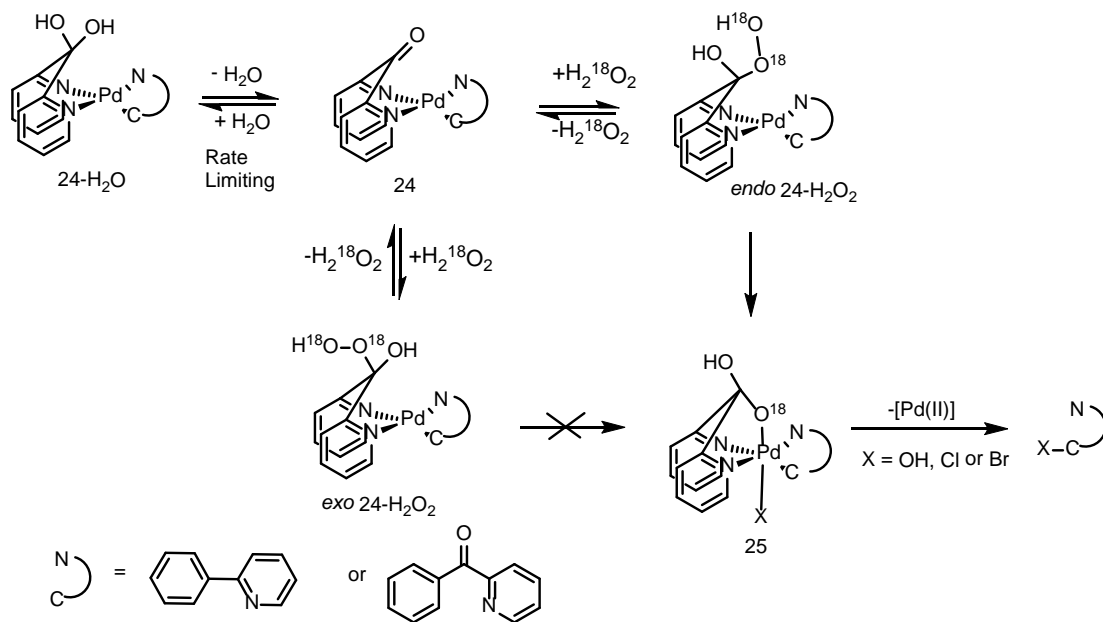


Scheme 1.19 Proposed mechanisms for the formation of C-Cl product **23** from the isolated dimeric Pd(III) precursor, **21**.

1.4 Dpk-enabled C-Pd bond functionalization with hydrogen peroxide

The use of dpk as a ligand to enable oxidation of Pd(II) to Pd(IV) was studied in detail by Oloo from our group. Kinetic studies showed dehydration of **24-H₂O** to form **24** was rate limiting, which

then undergoes nucleophilic attack by H_2O_2 across the $\text{C}=\text{O}$ bond of dpk to give *endo* **24-H₂O₂**(endo-isomer) or *exo* **24-H₂O₂**(exo-isomer) as shown in scheme 1.20.

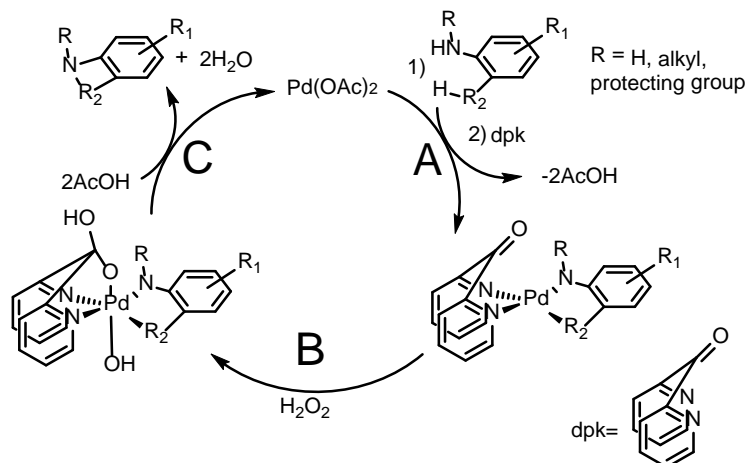


Scheme 1.20 Proposed mechanism for the dpk enabled oxidation of a monohydrocarbyl Pd(II) center with H_2O_2 to form the corresponding Pd(IV)

Exo 24-H₂O₂ cannot form **25** because the hydroperoxy group is far away from the Pd center. *Endo 24-H₂O₂* has the hydroperoxy group in close proximity to the Pd center and forms the corresponding Pd(IV), **25**, through an intramolecular reaction. Isotopic labelling studies showed the incorporation of only one of the ^{18}O in $\text{H}_2^{18}\text{O}_2$ into **25** which is consistent with nucleophilic attack at the α -oxygen of the hydroperoxy group in *endo 22-H₂O₂* by the Pd(II) center. **25** undergoes reductive elimination to give the corresponding C-O reductive elimination product at elevated temperatures. **25** can also undergo ligand exchange in the presence of HCl or HBr and

subsequent reductive elimination to give the corresponding C-Cl and C-Br reductive elimination products.

1.5 Our goal and approach



Scheme 1.21 Proposed mechanism for the oxidative C-H amination with H_2O_2 as terminal oxidant

Previously, Oloo and Vedernikov have demonstrated the ability of the di(2-pyridyl)ketone (dpk) and some di(2-pyridine)methanesulfonate (dpms) family ligands coordinated to various Pd(II) monohydrocarbyls to enable an efficient functionalization of their Pd^{II}-C(sp²) bonds using H_2O_2 as oxidant.⁵⁹ The reactions proceeded via intermediacy of rare Pd(IV) monohydrocarbyl complexes, some of which could be isolated and fully characterized. Reductive elimination of the isolated Pd(IV) complexes to produce functionalized products with C-O, C-Cl, C-Br or C-I bonds could also be characterized in detail in a number of cases. Some of these reactions could be made catalytic in Pd with H_2O_2 serving as the oxidant.⁴⁸ At the same time, previous attempts of Oloo to

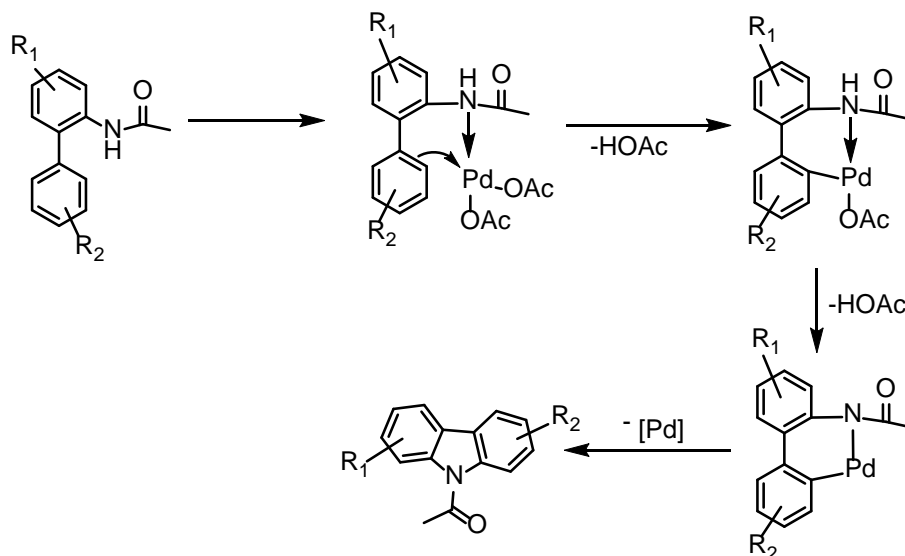
prepare amido aryl Pd(IV) compounds and observe their C-N reductive elimination were not successful.

In this work, we wanted to extend the previously developed approach to ligand-enabled functionalization of Pd^{II}-C(sp²) as well as Pd^{II}-C(sp³) bonds using H₂O₂ as oxidant towards the C-N bond forming processes. Our goals included i) preparation of various dpk – ligated palladacyclic hydrocarbyl amido Pd(II) complexes, ii) their transformation to the corresponding Pd(IV) amido hydrocarbyls, iii) detailed characterization of the resulting Pd(IV) species, including their C-N reductive elimination reactivity and iv) development of a catalytic oxidative C-H amination with H₂O₂ as the oxidant (scheme 1.24). Our choice of substrates includes N-substituted-2-aminobiphenyls which, according to Scheme 1.21, are expected to form N-substituted carbazoles, the products of C(sp²)-N coupling at the Pd(IV) center and N-substituted-2-*tert*-butylanilines which are expected to form N-substituted indolines, the products of oxidative C(sp³)-N coupling.

Different groups have used other oxidants to perform oxidative amination of C(sp²)-H or C(sp³)-H bonds. Most of these oxidants are relatively expensive and generate waste which need to be removed and treated after the reaction is over. Conversely, the cost of 1 mol of 30% aqueous H₂O₂ is only 2 cents and the only waste product expected is H₂O which is environmentally benign. As such H₂O₂ will be a ‘greener’ and more atom-economical oxidizing reagent and may apply to a large scale synthesis. The disadvantages of using H₂O₂ include its ability to decompose with time and/or at elevated temperatures. Also, H₂O₂ may become explosive at very high concentrations. Therefore, only low concentrations of H₂O₂ will be used in our reactions (Step B).

Chapter 2. Synthesis of κ^2 -C,N-2'-(N-R-amino)biphenyl-2-yl Pd(II) complexes with electron donating groups R=H, Et, Me and their oxidation with H₂O₂

2.1 Introduction and Background

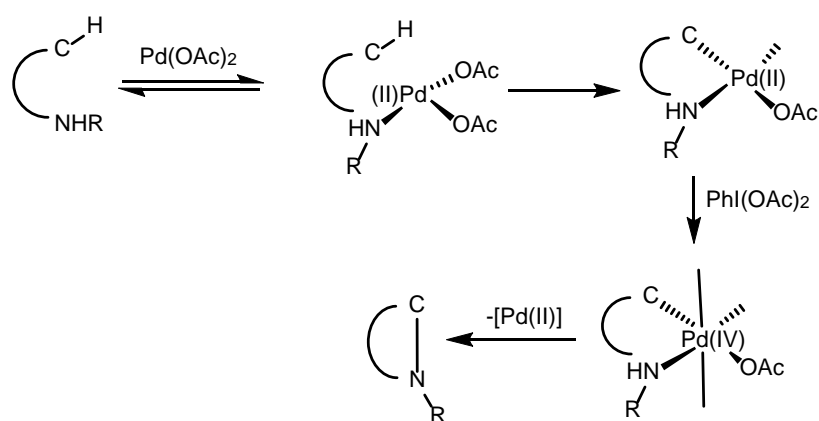


Scheme 2.1 Proposed mechanism for the reaction of N-acyl-2-aminobiphenyl substrates with Pd(OAc)₂ catalyst and Cu(OAc)₂/O₂ as oxidant to give the corresponding N-acetylcarbazoles as reported by Gaunt.

In 2005, Buchwald reported the Pd-catalyzed synthesis of N-acetyl substituted carbazoles with Cu(OAc)₂/O₂ as the terminal oxidant. This was the first reported synthesis of carbazoles through a direct oxidative C-H amination. A Pd(0)/Pd(II) mechanism was proposed, similar to the Buchwald-Hartwig amination reaction, with the amido group serving as a directing group (Scheme 2.1). This mechanism includes: (i) pre-association of the amide moiety of the N-acyl-2-

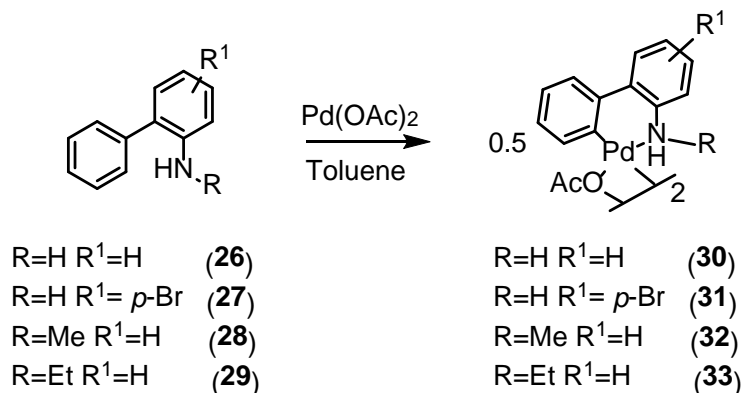
aminobiphenyl with Pd(OAc)₂ which facilitates the *ortho*-palladation process with concomitant release of an acetic acid, (ii) The formation of the six-membered palladacycle and (iii) subsequent reductive elimination leading to formation of the C-N coupled product and Pd(0) compounds. The Pd(0) species is re-oxidized to Pd(II) by Cu(OAc)₂.⁶⁰ The resulting Cu(I) species may be then oxidized by O₂ to form Cu(OAc)₂.

Based on the elegant work by the Buchwald group, the Gaunt group reasoned that reductive elimination from a high oxidation state Pd(IV) center would more readily facilitate C-N bond formation.⁶¹ To realize this process, an amine bearing an electron-donating group should coordinate strongly to a Pd(II) center, resulting in a complex that could then undergo cyclopalladation. Next, oxidation of the Pd(II) complex to a Pd(IV) species would expedite C-N bond formation (Scheme 2.2). A series of N-benzyl substituted carbazoles were synthesized by using Pd(OAc)₂ as catalyst and PhI(OAc)₂ as the oxidant from the corresponding 2-aminobiphenyl precursors.⁶²



Scheme 2.2 Proposed mechanism for the Pd(OAc)₂ catalyzed oxidative C-H amination with PhI(OAc)₂ as terminal oxidant as proposed by Gaunt.

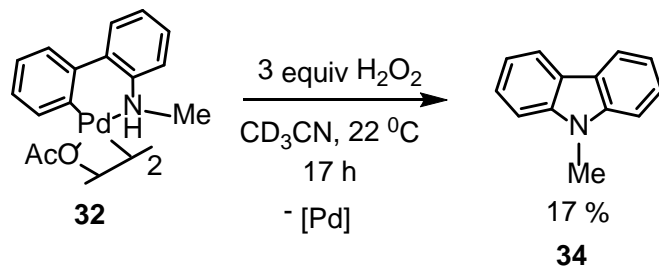
2.2 Synthesis of Palladacycles, 30-33



Scheme 2.3 Synthesis of acetate-bridged palladacycles 30 - 33

Based on the work done Gaunt, we decided to begin our work with 2-aminobiphenyl substrates **26** – **29**: attach them to Pd and oxidize the corresponding palladacycles with H₂O₂ to form the corresponding carbazoles. Substrates **26-29** were combined with 0.9 equivalents of Pd(OAc)₂ in toluene and the resulting solutions were stirred for 24 h - 96 h at r.t. Resulting acetate-bridged palladacycles **30-33** (Scheme 2.3) were isolated in over 90 % yields as pink or gray solids. These complexes are expected to be dinuclear acetate-bridged complexes by analogy with numerous known examples.⁶³ Complexes **30-33** are not soluble in common solvents such as MeOH, AcOH, THF and Acetone, except **32** which dissolves in CD₃CN. Compounds **30-33** were used in subsequent transformations without additional purification. Notably, various not-whole number of toluene molecules was typically found in elemental analyses of similar compounds.⁶⁴ ¹H NMR spectrum of **32** showed a single species in solution with a peak at 1.83 ppm which was indicative of a bridging acetate ligand compared to the non-bridging acetate ligand which normally shows up at about 2.00 ppm.⁵⁹ A broad peak at 11.48 ppm integrating for 1H was observed in the ¹H NMR spectrum indicative of an NH signal.

2.3 Oxidation of acetate-bridged palladacycle, **32**, with H₂O₂ in CD₃CN



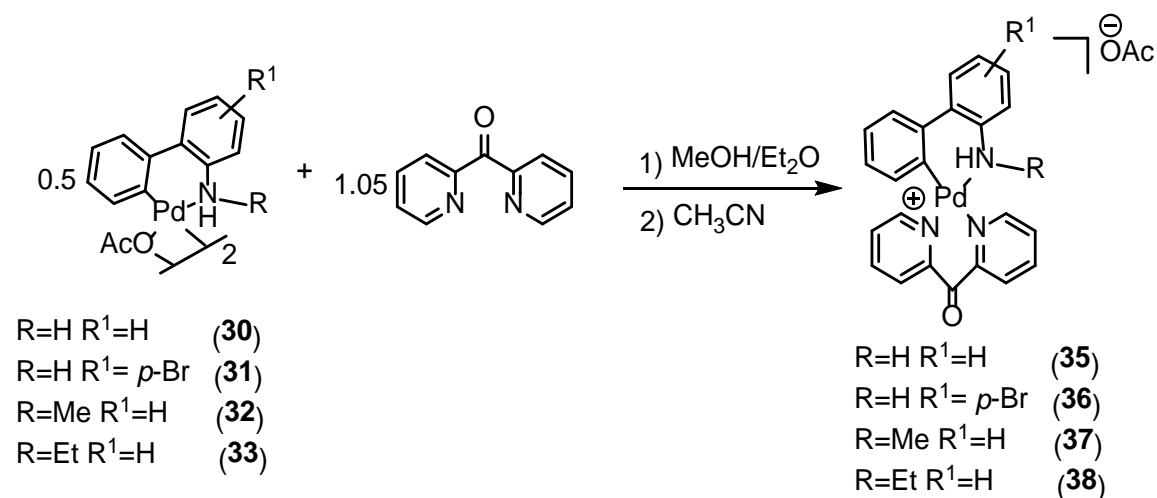
Scheme 2.4 Reactivity of **32** with 3 equivalents of H₂O₂ to form **34**

We used **31** as a representative OAc-bridged pallada(II)cycle to characterize their reactivity toward H₂O₂ (Scheme 2.4). In a typical experiment **32** was combined with 3 equivalents of H₂O₂ in CD₃CN and the reaction was monitored by ¹H NMR spectroscopy. Upon addition of 3 equiv of H₂O₂, the light brown solution instantly turned dark brown. In 15 min ¹H NMR spectrum analysis of the resulting solution showed 13 % conversion of the original starting material and formation of N-methylcarbazole, **34**, in 7% yield. There were some tiny broad peaks which could not be assigned to either **32** or **34**. After 5 hours, the yield of **34** increased to 15 % with the conversion of **32** of 22%. After 17 h the yield of **34** was 17% with no change in the conversion of **32**. The addition of extra 3 equiv of H₂O₂ did not lead to any change in yield of **34** by ¹H NMR spectroscopy, and no visual change was observed.

These experiments indicate that H₂O₂ can be engaged in Pd(II)-C bond functionalization of acetato-bridged pallada(II)cycle **32** albeit with very low yield and conversion. Based on previous work by Oloo and Vedernikov, we expected that by producing the dpk complexes **35-38** derived from the palladacycles **30-33** (Scheme 2.5) their reactivity toward H₂O₂ could be

enhanced, the corresponding carbazoles could be produced in high yield. Moreover, the ability of the hydrated dpk ligand to stabilize the anticipated Pd(IV) hydrocarbyl intermediates could make it possible to observe and, possibly, isolate the Pd(IV) species involved in the reaction.

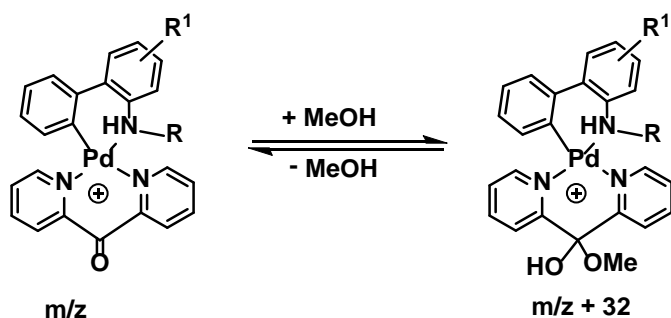
2.5 Preparation of dpk-ligated palladacycles, 35-38



Scheme 2.5 Preparation of dpk-ligated Pd complexes 35 - 38

Complexes **34** – **37** were prepared by a combination of the acetate-bridged palladacycle **30-33** with 1.05 equivalent of the dpk ligand in an appropriate solvent. Some of the complexes **35-38** crystallized out of reaction mixtures prepared in CH₃CN/CH₂Cl₂ solvent; some were precipitated upon addition of Et₂O. The identity of the complexes was confirmed by NMR spectroscopy and ESI(+)/MS. The complexes were shown by ¹³C NMR spectroscopy in MeOD to show a peak between 95 - 100 ppm which is indicative of hemiketal carbon atom resulting from the addition of a methanol molecule across the ketone group of the dpk fragment (Scheme 2.6). The presence of

OAc⁻ counterion was confirmed by ¹H NMR spectroscopy as a signal observed at about 2.00 ppm. The ESI(+)/MS of the complexes in MeOH showed signals derived from both the dpk complexes **35-38** and from their MeOH adducts having about 32 units greater mass/charge ratio. At the same time, their elemental analyses were not ideal even after repeated recrystallizations, presumably, because of the partial loss of acetic acid resulting from deprotonation of the hydrated dpk ligand OH group by the acetate.⁴⁸ That change could also be observed in ¹H NMR spectra.



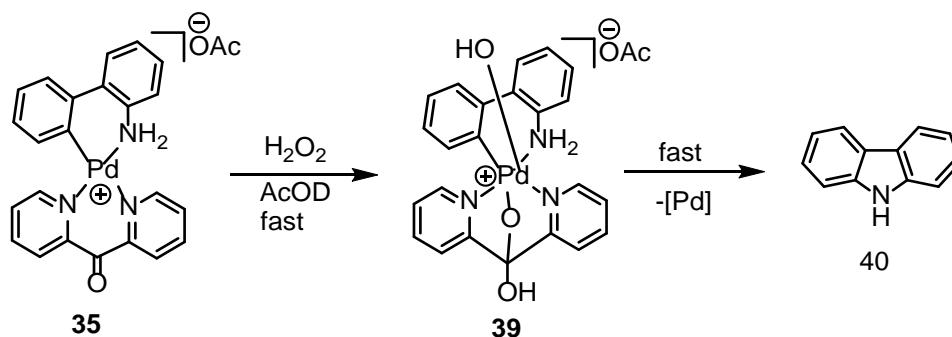
Scheme 2.6 Reversible addition of MeOH across the C=O bond of **35** – **38**

2.6 Reactivity of palladacycle **35** towards H₂O₂ in various solvents

2.6.1 D₂O

Complex **35** is sparingly soluble in D₂O to form a light-yellow solution. **35** was dissolved in D₂O and 3 equiv of H₂O₂ was added leading to the formation of a deep yellow solution which was monitored by ¹H NMR spectroscopy. A broadening of the signals in the ¹H NMR spectrum was observed after about 3 h. As a result, no reaction intermediates could be reliably detected. The solution was then heated at 60 °C for 48 h resulting in a turbid mixture, possibly, containing water-insoluble reaction products. About 61% of the starting material remained unchanged.

2.6.2 AcOD



Scheme 2.7 Oxidation of **35** with H_2O_2 in AcOH to produce **40** via intermediate **39** at 22 °C.

Since products of the reaction of **35** and H_2O_2 appeared to be insoluble in D_2O , we changed the solvent to AcOD. **35** was dissolved in AcOD and combined with 5 eq of H_2O_2 which turned the light yellow solution to orange. ^1H NMR analysis of the resulting solution just after 10 min showed the formation of carbazole in 76 % yield together with 4 different intermediates which were observed in small quantities (Scheme 2.7, Fig. 2.1). One of these intermediates can be viewed as the Pd(IV) complex **39** which is the expected Pd(IV) intermediate which reductively eliminates **35** (Scheme 2.7). This assumption is based on observations which are described later in the chapter. The yield of carbazole increased to 86% after 60 minutes, and after 48 hours, the yield of carbazole was 94%. A small amount (<5%) of a different product was present whose identity could not be determined.

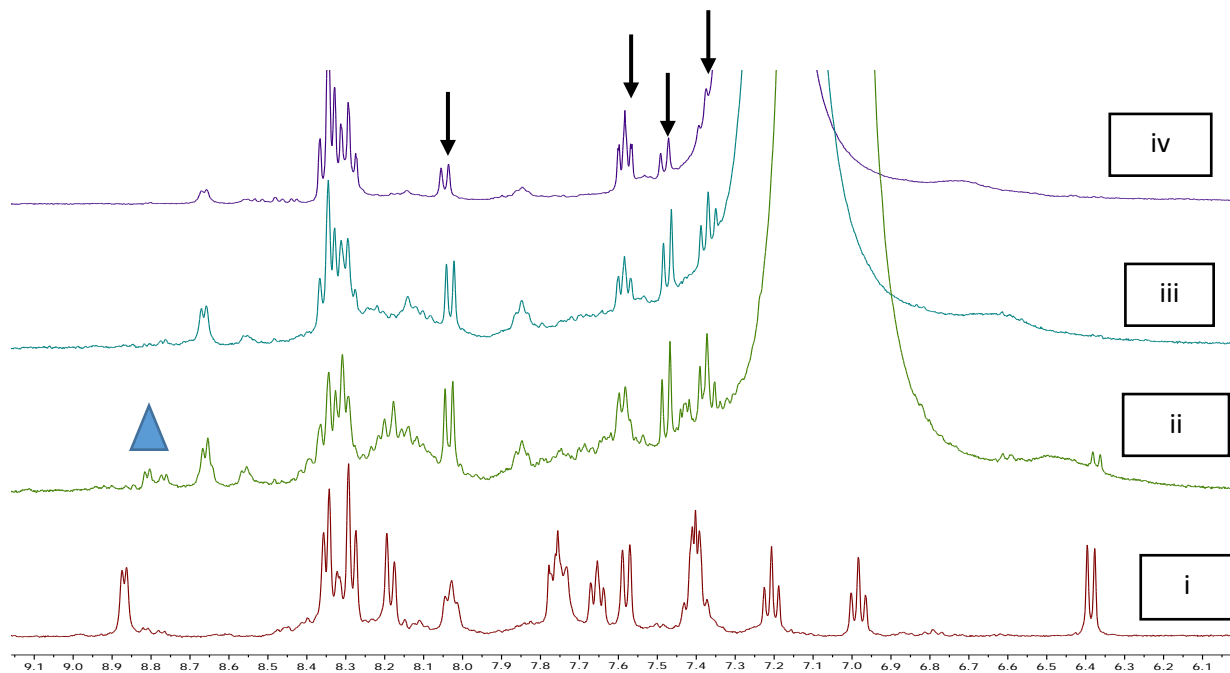
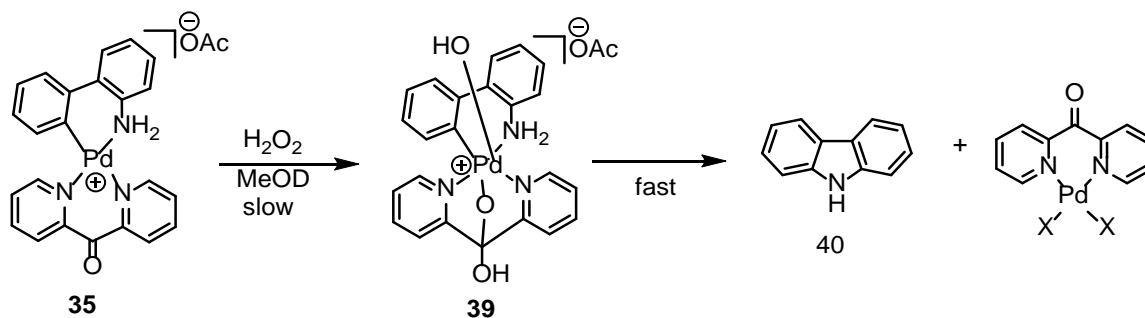


Figure 2.1 ^1H NMR spectrum of the mixture of **35** and H_2O_2 to form **40** in AcOD at $22\text{ }^\circ\text{C}$. Arrows show **40** in solution and blue triangles show intermediates in small concentrations which were assigned to **39** (i) **35** in solution before addition of H_2O_2 , (ii) 5 minutes after addition of H_2O_2 , (iii) 60 minutes after addition of H_2O_2 , (iv) 24 hours after addition of H_2O_2

A decrease in the amount of H_2O_2 to 1.5 equ did not noticeably affect the rate of the reaction. ^1H NMR analysis of the resulting solution 10 min after addition of 1.5 equivalents of H_2O_2 showed the formation of carbazole in 68% yield together with 4 different intermediates which were observed in small quantities in a total of about 28%. The yield of carbazole increased to 81% after 60 minutes, and when the solution was observed after 48 hours, the yield of carbazole was 95%. Since the rate of product formation was not dramatically different between 5 equivalents and 1.5 equivalents of H_2O_2 , it infers that, most likely, the addition of H_2O_2 across the $\text{C}=\text{O}$ bond of the dpk fragment was not rate limiting, consistent with previous observations by Oloo.⁵⁹

2.6.3 MeOD



Scheme 2.8 Oxidation of **35** with H_2O_2 in CD_3OD to produce **40** at $22\text{ }^\circ\text{C}$.

Since no appreciable amount of intermediates was observed in previous cases, we ran the same reaction in MeOD as a solvent which has a sufficiently low freezing point to allow for a low temperature reaction monitoring (Scheme 2.8, Fig. 2.2). **35** was dissolved in MeOD and combined with 5 eq of H_2O_2 which turned the light-yellow solution to deep yellow. ^1H NMR spectral analysis of the resulting solution just after 5 min showed the formation of carbazole in 12% yield together with no appreciable amount of any intermediates. The yield of carbazole increased to 45% after 60 minutes, and when the solution was observed after 13 hours, a turbid mixture had formed with the yield of carbazole increased to 92%. No signals of the dpk ligand were observed in solution after 13 h; in turn, the solid dissolved in $\text{DMSO-}d_6$ showed the presence of a Pd(dpk) fragment in it. No intermediates were observed upon varying the concentration of H_2O_2 , changing the counter ion from OAc^- to BF_4^- , and performing the reactions at $-5\text{ }^\circ\text{C}$.

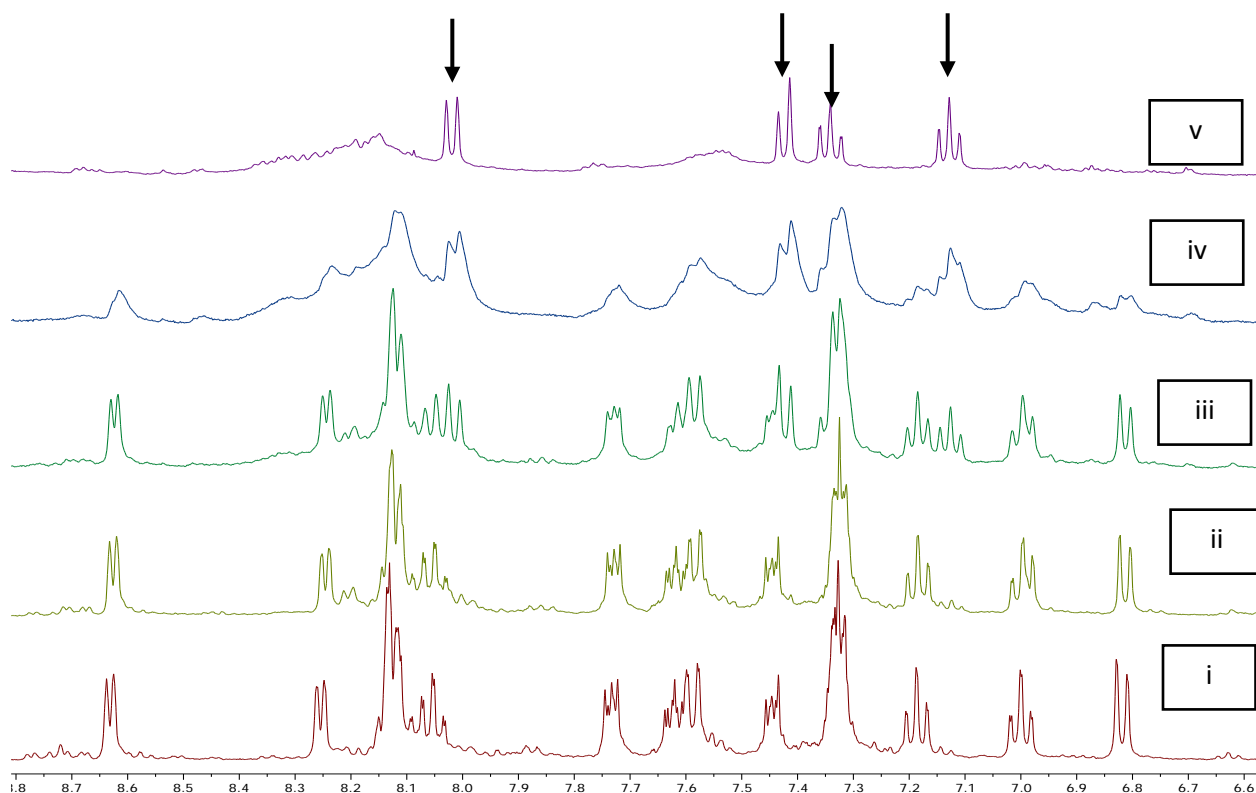
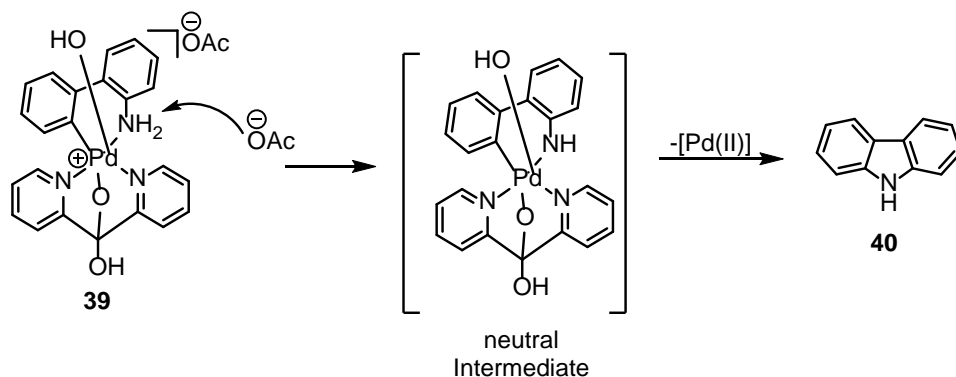


Figure 2.2 ^1H NMR spectrum of a mixture of **35** and H_2O_2 to form **40** in MeOD at $22\text{ }^\circ\text{C}$. Arrows show **40** in solution. (i) **35** in solution before addition of H_2O_2 , (ii) 5 minutes after addition of H_2O_2 , (iii) 60 minutes after addition of H_2O_2 , (iv) 120 minutes after addition of H_2O_2 (v) 13 hours after addition of H_2O_2

In summary, the reaction of **35** with H_2O_2 was much faster in AcOD, as compared to MeOD. Decreasing the reaction temperature and changing counter ion could not help noticeably increase the fraction of the reaction intermediates in these experiments.

We postulate a reaction mechanism where the carbazole reductive elimination from Pd(IV) aryl intermediates is fast, as compared to the Pd(II)-Pd(IV) oxidation, so making it impossible to observe any Pd(IV) intermediates. We also propose formation of a neutral Pd(IV) intermediate

having a deprotonated ammine ligand which may additionally enhance nucleophilicity of the nitrogen atom and the rate of the reductive elimination to form **40** (Scheme 2.9).



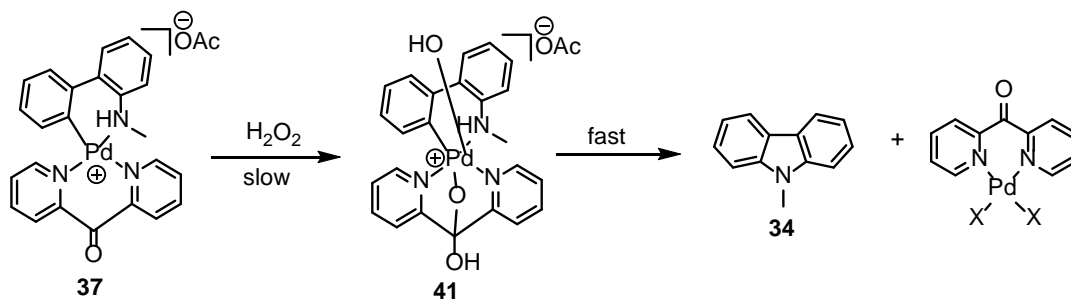
Scheme 2.9 Proposed neutral Pd(IV) intermediate formed by deprotonation of the ammine group by OAc^- .

2.7 Reactivity of **37** towards H_2O_2 in MeOD

Since no Pd(IV) intermediates were observed with **35** as a substrate we decided to modify the structure of the 2-aminobiphenyl – derived pallada(II)cycle **35** and prepare its N-methyl- and N-ethyl-2-aminobiphenyl analogs. Our assumption was that since the Pd(IV) intermediate would be very electron poor d^6 metal center, electron donating groups might help stabilize it.⁶⁵ Preparation of the corresponding dpk complexes **37** and **38** was achieved as shown previously in Scheme 2.5.

37 was dissolved in MeOD and combined with 5 eq of H_2O_2 which turned the light-yellow solution to deep yellow, similar to the oxidation of **35** in MeOD with H_2O_2 . ^1H NMR

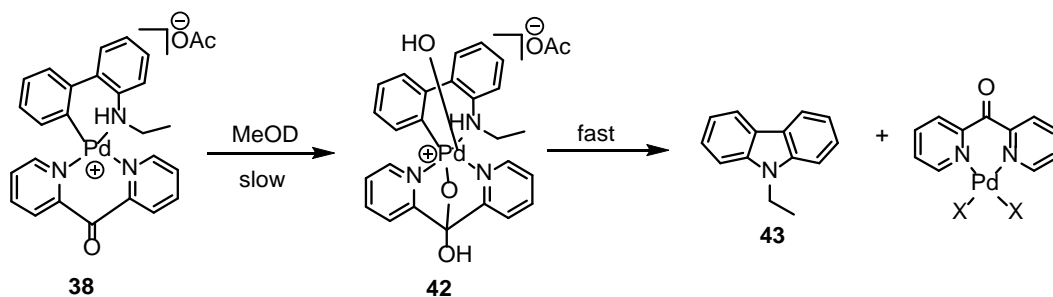
analysis of the resulting solution after about 15 min showed the formation of N-methylcarbazole, **34**, in 18% yield with no appreciable amount of other intermediates. The yield of **34** increased to 52% after 60 minutes.



Scheme 2.10 Reactivity of **37** with 3 equivalents of H_2O_2 in MeOD.

After 21 h the mixture turned turbid and the yield of **34** had increased to 91%. No signals of the Pd(dpk) fragment were observed in solution after 21 h. In turn, the solid formed was collected and dissolved in DMSO to show the presence of the Pd(dpk) fragment. We postulate a reaction mechanism similar to that for the oxidation of **35** where the C-N reductive elimination of the resulting Pd(IV) intermediate is very fast thereby making it difficult to observe any Pd(IV) intermediates involved.

2.8 Reactivity of **38** in MeOD



Scheme 2.11 Reactivity of **38** in MeOD with 3 equivalents of H₂O₂ to give **43**.

Complex **38** was dissolved in MeOD and combined with 3 equivalents of H₂O₂ which turned the light yellow solution to deep yellow. ¹H NMR spectral analysis of the resulting solution just after 5 min showed the formation of the carbazole **43** in 3% yield; no appreciable amount of intermediates were observed (Scheme 2.11, Fig. 2.3). After 15 h a turbid mixture was produced with the yield of carbazole increasing to 94 %. The solid isolated from the mixture and dissolved in DMSO showed the presence of the Pd(dpk) fragment in it. No Pd(IV) intermediates were observed in solution. There was no qualitative trend observed in the formation of N-R-carbazoles upon using different neutral and electron donating R groups (R = H, Me, Et)

Since no Pd(IV) intermediates were observed in reactions of H₂O₂ with electron-rich pallada(II)cycles containing Me and Et donor groups at the Pd-coordinated nitrogen atom, we next explored oxidation of electron-poorer substrates. In this vein, complex **36** was synthesized which bore a Br group para to the NH₂ group of the 2-aminobiphenyl fragment.

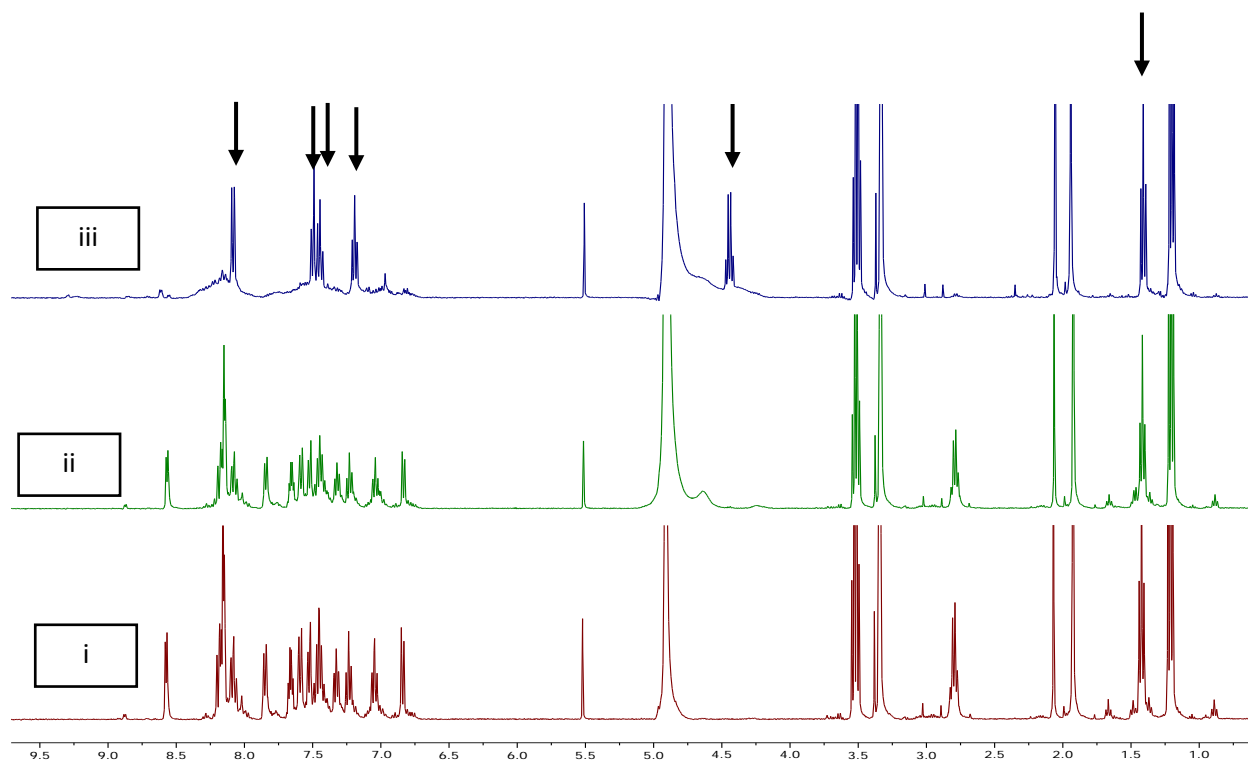
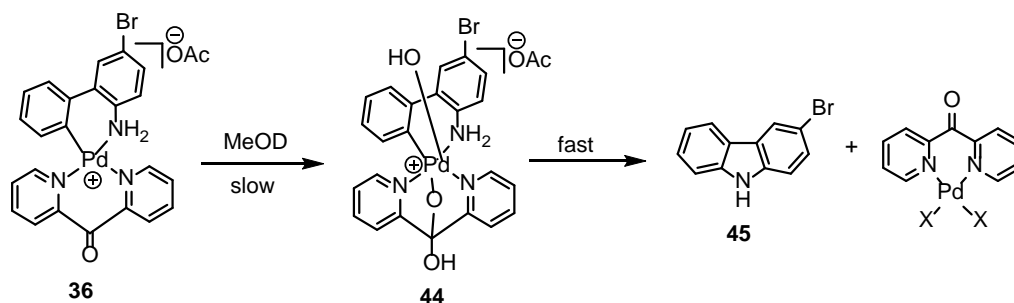


Figure 2.3 ^1H NMR spectrum of the reaction mixture of **38** and H_2O_2 to form **43** in MeOD at 22°C . Arrows show **43** in solution. (i) **38** in solution before addition of H_2O_2 , (ii) 5 minutes after addition of H_2O_2 (iii) 15 hours after addition of H_2O_2 . Structures are on p. 35 Scheme 2.11.

2.9 Reactivity of **36** in MeOD



Scheme 2.12 Reactivity of **36** in MeOD with 3 equivalents of H_2O_2 to give **45**.

Complex **36** was dissolved in MeOD and combined with 3 equiv of H₂O₂ which turned the light brown solution to deep brown. ¹H NMR spectral analysis of the resulting solution just after 5 min showed a less than 5% conversion of the **36** (Scheme 2.12, Fig. 2.5). The product was observed to form gradually, and a small fraction of less than 3% intermediate was observed which persisted in solution but disappeared after the reaction was over. All attempts to increase the fraction of the intermediate by changing the counterion to BF₄⁻, decreasing the equivalents of H₂O₂ added or performing the reaction at 0 °C were unsuccessful.

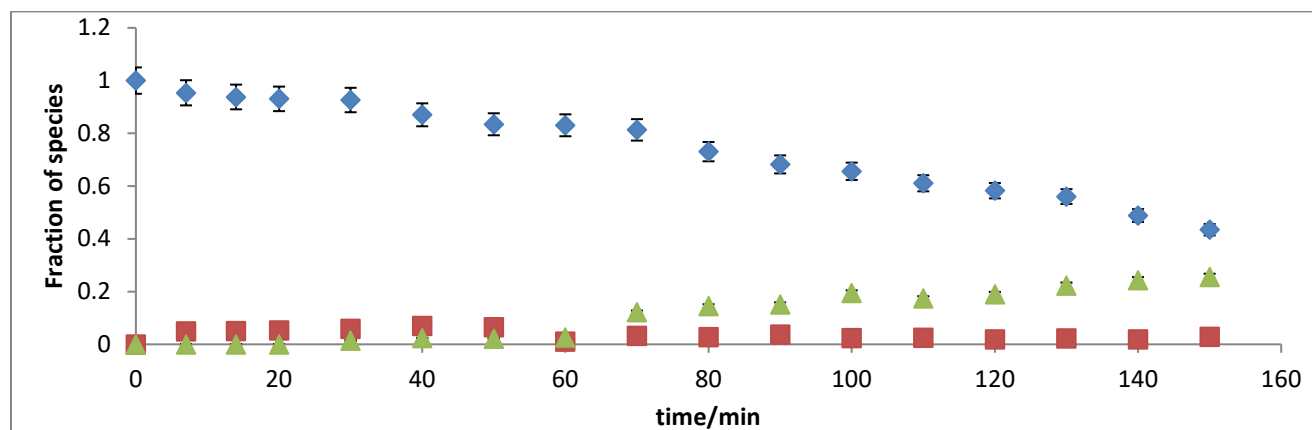


Figure 2.4. Reactivity of **36** in MeOD with 3 equivalents of H₂O₂ to give **45**. Blue diamonds is **36**, green triangles is **45** and red squares is the proposed intermediate **44**. Structures are on p. 36 Scheme 2.12.

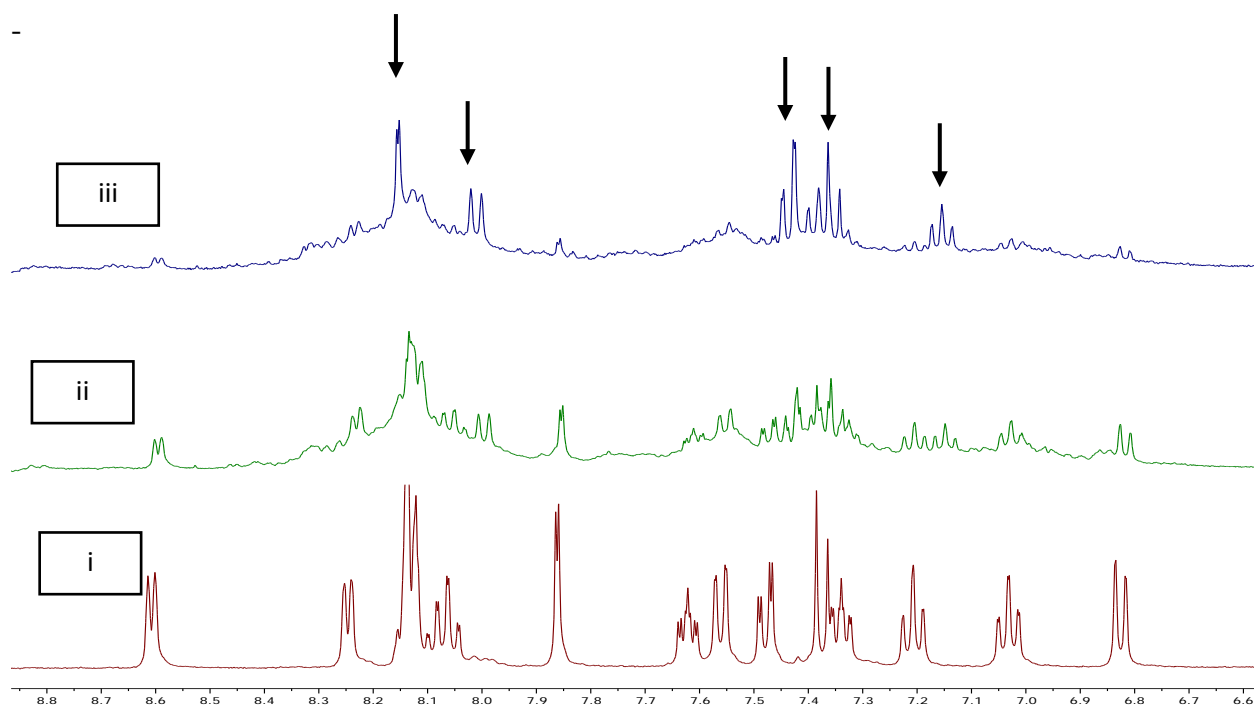


Figure 2.5 ^1H NMR spectra of the reaction mixture containing **36** and H_2O_2 in MeOD at $22\text{ }^\circ\text{C}$. Arrows show dissolved **45**. (i) **36** in solution before addition of H_2O_2 , (ii) 60 minutes after addition of H_2O_2 (iii) 6 hours after addition of H_2O_2 .

2.10 Conclusion

In summary, we synthesized a number of new 2-aminobiphenyl – derived pallada(II)cycles supported by dpk ligand, **36-38**, bearing a substituent at the amine nitrogen ($\text{R} = \text{H}, \text{Me}, \text{Et}$) or in the aniline fragment (*para*-Br). Their reactivity toward H_2O_2 was explored and, in the case of **36**, compared to that of their dpk-free precursors. It has been demonstrated that, as opposed to dpk-free palladacycles, all the dpk complexes undergo a clean oxidation and C-N oxidative coupling

in 90-95% yield at 22 °C in 12 h or less. Therefore, we have shown, for the first time, that the use of tripod *fac*-chelating ligands such as hydrated dpk enhances the rate and selectivity of Pd-mediated oxidative C-N coupling, allowing to use the environmentally friendly oxidant H₂O₂ in these reactions. This effect is, presumably, due to some stabilization provided by dpk of the Pd(IV) center in the transient amido aryl Pd(IV) species. The presence of electron donating groups (R = Me, Et) on the amine nitrogen of the 2-aminobiphenyl fragment did not lead to any dramatic changes in the rate of oxidation and reductive elimination compared to the parent compound (R = H). Placing a modestly electron-withdrawing group (4-Br) on the aniline fragment slowed down the oxidation reaction but only modestly. It also appears that, consistent with Buchwald's observations of the oxidative C-N coupling of his Pd(II) amido aryl complexes,⁶⁶ the oxidative C-N coupling at the Pd(IV) center is not slowed down by electron-donating substituents at the nitrogen atom involved in the coupling. Hence, it may be reasonable to explore the effect of electron-withdrawing substituents at the amine (or amido) nitrogen atom with an expectation to observe and/or isolate the corresponding less reactive Pd(IV) amido aryl intermediates.

Among solvents used, MeOH, AcOH, and H₂O, the first might be the best for potential observation of Pd(IV) intermediates in the reaction of dpk-supported pallada(II)cycles with H₂O₂ at 22 °C. The oxidative C-N coupling is too fast in AcOD, whereas poor solubility of reaction products precludes reliable ¹H NMR reaction monitoring in D₂O. Running the reactions in MeOH would allow one to avoid both issues. Finally, it is worth noting that there was no effect on the reactivity by changing the counter ion from AcO⁻ to BF₄⁻.

2.11 Experimental

All manipulations were carried out under ambient conditions unless otherwise stated. Solvents were obtained from Acros or Aldrich and used directly without further purification. All NMR solvents were purchased from Cambridge Isotopes Inc. and were used as received. ^1H , ^{13}C and ^{19}F NMR spectra were recorded on Varian-Inova (400 MHz, 100.58 MHz and 376.31 MHz, respectively) and Bruker-DRX (500 MHz, 125.72 MHz and 470.38 MHz, respectively) instruments internally referenced to residual solvent resonances. High-resolution mass spectra were recorded at Center for Mass Spectrometry, UMCP using a JEOL AcuTOF-CS instrument. All reagents for which synthesis is not reported are commercially available from Alfa-Aesar, Acros, Sigma-Aldrich, TCI and Pressure Chemical and used as received. Elemental analysis was carried out by Columbia Analytical Services, Tucson, Az. All oxidation reactions were carried out with 30% (w/v) H_2O_2 standardized with oxalic acid and stored in the refrigerator at 5 $^\circ\text{C}$. ^1H NMR yields were calculated with 1,4-dioxane as an internal standard.

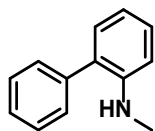
4-bromo-2-aminobiphenyl (27):



1.0 g (6.0 mmol) of *N*-acetyl-2-aminobiphenyl was dissolved in 20 mL of acetic acid and placed in an ice bath. 0.15 mL (6.0 mmol) of bromine was dissolved in 10 mL of dried chloroform. The chloroform solution was added dropwise to the acetic acid mixture with stirring. The mixture was allowed to warm to room temperature and then stirred overnight. After the reaction was complete, the solvent was removed in vacuo and the mixture was partitioned between ethyl acetate and water

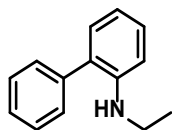
(1:1) mixture. Solvent was removed from the ethyl acetate layer and the residue dissolved in 15 mL of ethanol. 0.5 mL of concentrated HCl is added to the ethanol solution and refluxed overnight. The solution is quenched with 10mL of water and ethyl acetate (2 x 10 mL) is added to extract the organic layer. The organic layer was washed with sodium bicarbonate solution, then brine and dried over Na₂SO₄. Separation of the mixture on a silica gel column using hexane:ethyl acetate 70:30 gave 1.3 g (90%) of the target compound as a light purple tar-like liquid. ¹H NMR (400 MHz, CDCl₃) δ 7.52 – 7.35 (m, 5H), 7.28 – 7.23 (m, 2H), 6.67 (d, *J* = 9.2 Hz, 1H), 3.78 (s, 2H).

Synthesis of N-methyl-2-aminobiphenyl (28):



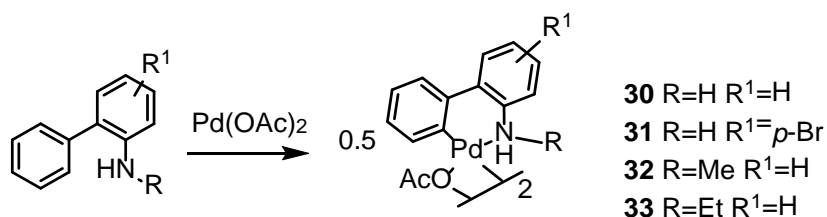
1.0 g (6.0 mmol) of 2-aminobiphenyl was dissolved in anhydrous THF in the glove box. 0.15 g (6.0 mmol) of NaH and 0.37 mL of MeI was added, and the resulting solution stirred for 5 days. The color of the solution turned brownish pink. After 5 days, THF was removed on a rotavap and the residue dissolved in dichloromethane. Washing of the resulting solution with brine (2 x 30 mL) and drying with anhydrous Na₂SO₄ resulted in the formation of the target compound in 0.91 g (84%) after removal of the solvent on a rotavap. ¹H NMR (400 MHz, Chloroform-*d*) δ 7.52 – 7.41 (m, 4H), 7.45 – 7.33 (m, 1H), 7.36 – 7.22 (m, 1H), 7.12 (dd, *J* = 7.4, 1.7 Hz, 1H), 6.81 (td, *J* = 7.4, 1.2 Hz, 1H), 6.73 (dd, *J* = 8.1, 1.2 Hz, 1H), 2.83 (s, 3H).

Synthesis of N-ethyl-2-aminobiphenyl (29)



N-ethyl-2-aminobiphenyl was synthesized by reduction of N-acetyl-2-aminobiphenyl. 1.0 g of **46** was dissolved in 15 mL of THF. 0.35 g of NaBH₄ was added to 0.58 g of I₂ in 10 mL THF. The NaBH₄-I₂ mixture was added dropwise to the solution of **46** at 0 °C. The mixture was monitored by TLC until the spot of the starting material disappeared. The solvent was removed on a rotavap. The residue was worked up by adding water and DCM 15 mL each. The water layer was extracted with 10 mL DCM. The combined organic layer was washed with brine and dried with anhydrous Na₂CO₃. Removal of solvent on a rotavap gave 0.79 g (85%) of the target product. ¹H NMR (400 MHz, Chloroform-*d*) δ 7.54 – 7.33 (m, 6H), 7.28 (s, 1H), 7.27 (ddd, *J* = 8.2, 7.3, 1.6 Hz, 1H), 7.12 (dd, *J* = 7.4, 1.7 Hz, 1H), 6.79 (q, *J* = 9.0, 8.2 Hz, 2H), 3.17 (q, *J* = 7.1 Hz, 2H), 1.19 (t, *J* = 7.1 Hz, 3H).

General procedure for the synthesis of 2-aminobiphenyl – derived pallada(II)cycle **30-33**



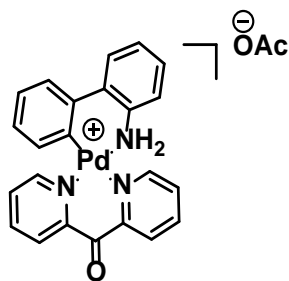
These were synthesized according to literature. 0.50g of Pd(OAc)₂ was weighed and combined in 20mL of toluene to form a suspension. 1.1 equivalent of the corresponding 2-aminobiphenyl substrate was added to the suspension and stirred for 96 h at room temperature and a precipitate forms which is filtered. The precipitate is washed with about 5 mL of cold Et₂O and dried under

vacuum to give the target compound. These compounds were used in subsequent steps without any characterizations. Attempts to get elemental analyses for these compounds were not successful.

General procedure for the synthesis of 2-aminobiphenylPddpk substrates 35-38

0.50 g of **30-33** was stirred in 10mL of MeOH for about 10 min. 1.0 equivalent of dpk ligand was dissolved in 1.0 mL of CH₂Cl₂. The dpk solution in CH₂Cl₂ was added dropwise to the methanol solution of **30-33**. After stirring for about 10 min, the solution became clear and stirring was continued for about 4 hours. The resulting solution was concentrated on a rotavap to about 1.0 mL. Et₂O (or CH₂Cl₂ for only **31**) was added dropwise precipitate started to form. More Et₂O or CH₂Cl₂ was added until precipitation was complete. The resulting precipitate was filtered and washed with cold Et₂O or CH₂Cl₂ and dried under vacuum to give the target compound.

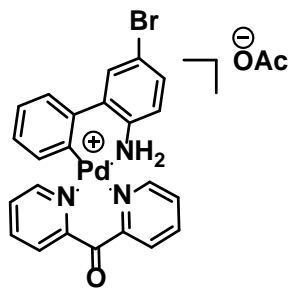
2-aminobiphenylPddpk(OAc). (35):



Yellowish orange solid, (65% yield): ¹H NMR (400 MHz, Methanol-*d*₄) δ 8.63 (d, *J* = 5.3 Hz, 1H), 8.25 (d, *J* = 5.5 Hz, 1H), 8.17 – 7.96 (m, 4H), 7.78 – 7.69 (m, 1H), 7.60 (ddd, *J* = 12.1, 7.3, 3.3 Hz, 2H), 7.48 – 7.42 (m, 1H), 7.32 (dq, *J* = 5.4, 3.4, 2.6 Hz, 3H), 7.18 (t, *J* = 7.4 Hz, 1H), 7.00 (td, *J* = 7.4, 1.6 Hz, 1H), 6.82 (d, *J* = 7.6 Hz, 1H), 1.88 (s, 3H). ¹³C NMR (MeOD) δ: 99.0, 119.2, 123.3, 123.5, 124.8, 125.6, 125.7, 125.8, 125.9, 126.1, 127.6, 127.9, 128.3, 125.4, 137.2, 137.6,

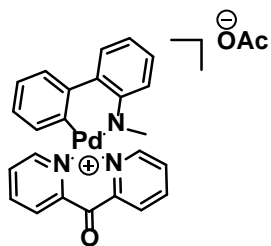
138.2, 139.9, 140.1, 140.2, 141.6, 150.4, 151.1, 154.6, 157.3, 158.1 Esi/MS. Found/Calculated:
457.95/458.04

4-bromo-2-aminobiphenylPdppk(36) :



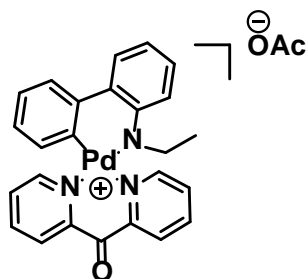
Brown solid, (87% yield): ^1H NMR (400 MHz, methanol- d_4) δ 8.61 (d, $J = 5.1$ Hz, 1H), 8.28 – 8.20 (m, 1H), 8.18 – 8.03 (m, 4H), 7.86 (d, $J = 2.2$ Hz, 1H), 7.62 (ddd, $J = 7.1, 5.1, 2.2$ Hz, 1H), 7.56 (dd, $J = 7.7, 1.5$ Hz, 1H), 7.48 (dd, $J = 8.3, 2.2$ Hz, 1H), 7.42 – 7.30 (m, 2H), 7.21 (td, $J = 7.4, 1.3$ Hz, 1H), 7.03 (td, $J = 7.4, 1.5$ Hz, 1H), 6.82 (dd, $J = 7.7, 1.2$ Hz, 1H), 1.88 (s, 3H). ^{13}C NMR (126 MHz, MeOD) δ 177.14, 156.18, 155.38, 152.64, 149.17, 148.44, 140.36, 138.14, 135.42, 135.17, 129.01, 128.45, 126.22, 123.69, 122.83, 116.41, 97.06, 21.30. Esi/MS. Found/Calculated: 535.89/535.96 Anal. Found / Calculated for $\text{C}_{23}\text{H}_{17}\text{BrN}_3\text{OPd.OAc.MeOH}$: C : 48.86/49.66, H : 4.05/3.85, N : 6.63 /6.68

N-methyl-2-aminobiphenylPddpk(37) :



Yellowish orange solid, (70% yield): ¹H NMR (400 MHz, Methanol-*d*₄) δ 8.57 (d, *J* = 5.3 Hz, 1H), 8.23 (dd, *J* = 5.6, 1.5 Hz, 1H), 8.20 – 8.05 (m, 5H), 7.85 (d, *J* = 7.3 Hz, 1H), 7.65 (ddd, *J* = 7.7, 2.4, 2.0 Hz, 1H), 7.60 (dd, *J* = 7.7, 1.4 Hz, 1H), 7.53 – 7.40 (m, 3H), 7.35 (ddd, *J* = 7.2, 5.3, 1.5 Hz, 1H), 7.27 – 7.19 (m, 1H), 7.02 (td, *J* = 7.5, 1.4 Hz, 1H), 6.75 (dd, *J* = 7.7, 1.1 Hz, 1H), 2.70 (s, 3H), 1.92 (s, 3H). ¹³C NMR (126 MHz, MeOD) δ 178.68, 157.74, 157.01, 154.33, 154.14, 153.72, 151.98, 149.97, 149.87, 148.60, 142.04, 140.24, 139.83, 139.73, 137.19, 137.01, 136.32, 136.08, 128.99, 127.85, 127.75, 127.40, 127.35, 127.12, 126.68, 125.84, 125.61, 125.29, 125.22, 125.05, 124.92, 124.85, 124.62, 123.20, 123.15, 123.04, 122.96, 119.24, 114.42, 98.64, 65.42, 43.21, 22.86, 14.01 Esi/MS. Found/Calculated: 471.98/472.06

N-ethyl-2-aminobiphenylPddpk(38)

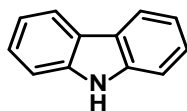


Yellowish orange solid, (54% yield): ^1H NMR (400 MHz, Methanol- d_4) δ 8.60 – 8.53 (m, 1H), 8.21 – 8.04 (m, 5H), 7.84 (dd, $J = 7.3, 1.9$ Hz, 1H), 7.65 (td, $J = 5.1, 3.6$ Hz, 1H), 7.58 (dd, $J = 7.7, 1.5$ Hz, 1H), 7.52 (dd, $J = 7.2, 1.8$ Hz, 1H), 7.49 – 7.38 (m, 2H), 7.32 (ddd, $J = 7.4, 5.6, 1.5$ Hz, 1H), 7.23 (td, $J = 7.4, 1.2$ Hz, 1H), 7.04 (td, $J = 7.4, 1.5$ Hz, 1H), 6.83 (dd, $J = 7.6, 1.2$ Hz, 1H), 2.79 (q, $J = 6.7$ Hz, 2H), 1.91 (s, 3H), 1.41 (t, $J = 7.1$ Hz, 3H). ^{13}C NMR (126 MHz, MeOD) δ 178.71, 157.40, 157.22, 154.30, 152.26, 149.85, 141.26, 140.36, 139.86, 139.76, 137.29, 135.93, 128.95, 127.90, 127.50, 127.12, 125.70, 125.25, 125.16, 124.59, 123.70, 122.76, 119.90, 98.48, 65.45, 50.91, , 23.10, 14.20, 14.04. Esi/MS. Found/Calculated: 486.01/486.08

General procedure for oxidation of dpk ligated 2-aminobiphenyl substrates(35-38)

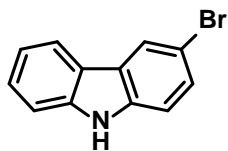
10 mg of the dpk ligated palladacycle was dissolved in 0.60 mL of solvent. 3 eq of H_2O_2 was added to the solution. The solution was then monitored by ^1H NMR until no further change was observed or only peaks corresponding to the product were observed. All solutions were monitored at 22 $^\circ\text{C}$ unless otherwise stated. Isolation was by removing solvent on a rotavap, stirring the residue in CH_2Cl_2 and passing the solution through silica gel to adsorb any Pd-containing species. All reductively eliminated products were compared to literature data.

Carbazole(40):



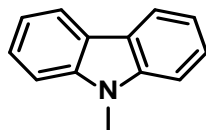
^1H NMR (400 MHz, methanol- d_4) δ 8.03 (d, $J = 7.8$ Hz, 2H), 7.47 – 7.40 (m, 2H), 7.35 (ddd, $J = 8.2, 7.1, 1.2$ Hz, 2H), 7.14 (ddd, $J = 8.0, 7.0, 1.1$ Hz, 2H).

3-bromocarbazole(45):



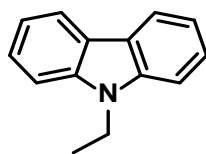
^1H NMR (400 MHz, Chloroform-*d*) δ 8.19 (d, $J = 1.9$ Hz, 1H), 8.11 (s, 1H), 8.03 (d, $J = 7.8$ Hz, 1H), 7.50 (dd, $J = 8.5, 1.9$ Hz, 1H), 7.44 (dd, $J = 3.7, 1.4$ Hz, 2H), 7.32 (d, $J = 8.6$ Hz, 1H), 7.25 – 7.23 (m, 1H).

N-methylcarbazole(34):



^1H NMR (400 MHz, Chloroform-*d*) δ 8.11 (d, $J = 7.7$ Hz, 2H), 7.49 (ddd, $J = 8.2, 7.0, 1.2$ Hz, 2H), 7.43 – 7.39 (m, 2H), 7.25 – 7.20 (m, 2H), 3.87 (s, 3H).

N-ethylcarbazole(43):

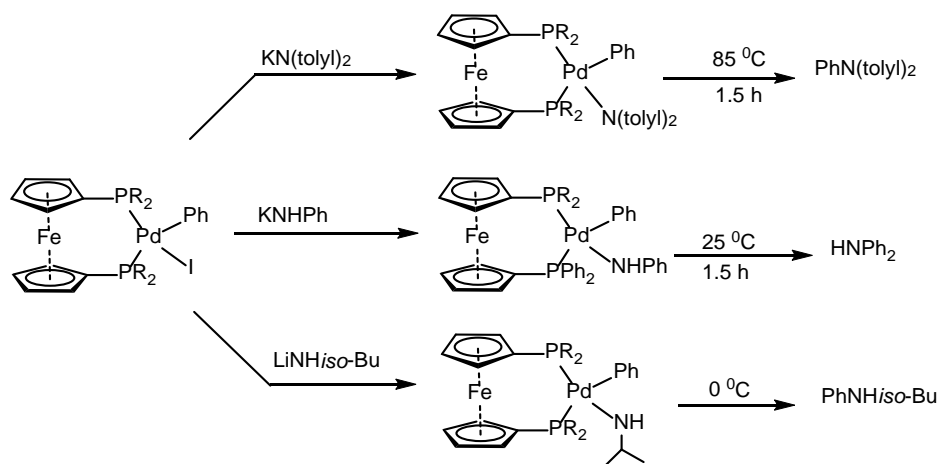


^1H NMR (400 MHz, Methanol-*d*₄) δ 8.05 (dt, $J = 7.8, 1.0$ Hz, 2H), 7.48 – 7.37 (m, 2H), 7.16 (ddd, $J = 8.0, 6.1, 2.0$ Hz, 2H), 4.34 (q, $J = 7.2$ Hz, 2H), 1.33 (t, $J = 7.2$ Hz, 3H).

Chapter 3. Synthesis and Reactivity of κ^2 -C,N-2'-(N-R-amido)biphenyl-2-yl Pd(II) complexes with electron withdrawing groups R = COCH₃, COCF₃, SO₂CH₃, SO₂CF₃

3.1 Introduction and Background

Even though complexes **35** -**38** were observed to undergo an oxidative C-N coupling to form corresponding carbazoles in high yield, no appreciable amount of reaction intermediates were observed. Previous work by Hartwig³⁵ and a recent work by Buchwald⁶⁶ had shown that reductive eliminations from Pd(II) to form the C-N bond was faster from complexes with more electron-rich amido ligands than from complexes with more electron-poor amido ligands. These data were first revealed by the studies of 1,1'-bis(diphenylphosphino)ferrocene (DPPF)-ligated aryl palladium amido complexes summarized in Scheme 3.1.^{32, 35, 67}



Scheme 3.1 Dependence of rate of reductive elimination on the presence of electron donating or electron withdrawing groups at the amide nitrogen atom at a Pd(II) center, as reported by Hartwig.

The diarylamido Pd(II) complexes underwent reductive elimination at elevated temperatures over the course of 1-2 h. The analogous anilide complex underwent reductive elimination at room temperature over a similar time period, and the alkylamide underwent reductive elimination at room temperature over a similar time period, and the alkylamide underwent reductive elimination at 0 °C over this time.⁶⁸ Also, the Buchwald group reported a similar trend while working with different palladium precursors and substrates.⁶⁶ Interestingly, it was also observed that electron donating groups on the aryl ligand slowed down the rate of reductive elimination so as electron withdrawing groups on the aryl amido fragment (Figure 3.1).

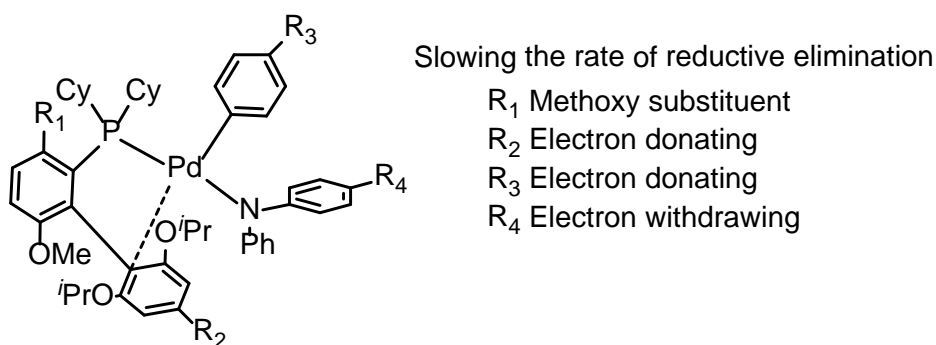
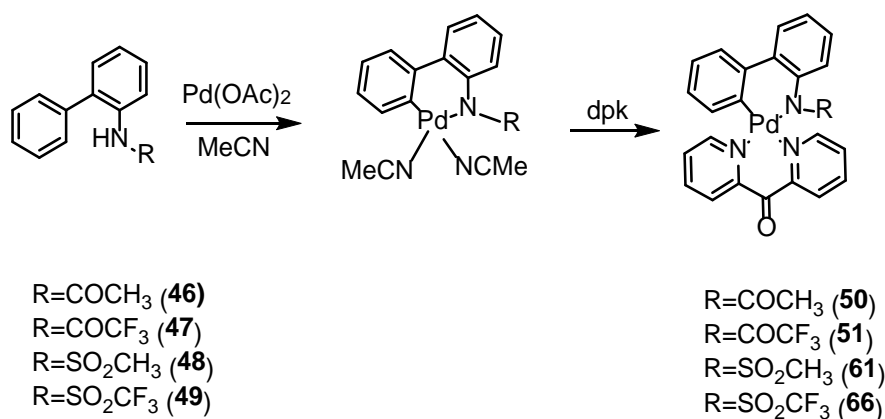


Figure 3.1 Electronic effects on the rate of reductive elimination of C-N bond from an isolated Pd(II) complex as reported by Buchwald.

Based on the work by Hartwig and Buchwald, we decided to explore the effect of electron withdrawing groups on the C-N reductive elimination reaction from Pd(IV) centers and see if there will be any similarities with C-N reductive elimination from analogous Pd(II) center. To this end, we needed, at least, to observe or, ideally, isolate the corresponding amido aryl Pd(IV) intermediates. The key question here was whether these electron-poorer Pd(IV) amido complexes could still be produced at a reasonably fast rate by oxidation of their Pd(II) precursors with H₂O₂.

3.2 Preparation of dpk – ligated palladacycles **50**, **51**, **61** and **66** bearing an electron-withdrawing group at the amide nitrogen atom

The dpk supported palladacycles **50**, **51**, **61** and **66** bearing at the amide nitrogen atom an electron-withdrawing group, Ac, CF₃CO, SO₂Me and SO₂CF₃, respectively, were prepared by a one-pot synthesis from their corresponding 2-(N-R-amino)biphenyl precursors (Scheme 3.2). A 2-(N-R-amino)biphenyl **46-49** was combined with 0.9 equivalents of Pd(OAc)₂ in CH₃CN, and the resulting solution refluxed at 70 °C for between 2 to 12 hours until formation Pd black became apparent. This solution was filtered through Celite and 0.9 equivalents of dpk added and stirred at room temperature for about 4h. The resulting solution was concentrated and combined with Et₂O, or MeOH to afford the target compounds **50**, **51**, **61** or **66** in good yields as yellow or off white precipitates. Their identity was confirmed by NMR spectroscopy and their purity confirmed by elemental analyses.



Scheme 3.2 Preparation of dpk ligated palladacycles **50**, **51**, **61** and **66**

3.3 Characterization and reactivity of the N-acetyl Pd(II) complex, **50**(MeOH)

3.3.1 Structural characterization of **50**(MeOH)

We started our studies with (κ^2 -*C,N*-2'-(N-acetylamido)biphenyl-2-yl) palladium(II) complex **50** which was isolated as a yellow solid in a form of its MeOH adduct **50**(MeOH). As expected,⁵⁹ the compound was shown by ¹³C NMR spectroscopy to exist in MeOD solution predominantly in the form of an adduct with methanol added across the dpk ligand carbonyl group. There was a peak at about 95 ppm in its ¹³C NMR spectra characteristic of the ketal carbon whereas the signal of the dpk carbonyl group at about 195 ppm was missing. The connectivity of **50** was not obvious since amides may bond to a metal center via either oxygen or nitrogen atom. To confirm the proposed structure of **50**(MeOH), X-ray quality crystals were grown from a cold solution of **50** in methanol. The crystal structure demonstrated the presence of an anionic nitrogen rather than oxygen atom bonded to the Pd(II) center as well as the presence of the hemiketal fragment in the product that can be designated as **50**(MeOH). No signals were observed in the ESI(+)/MS spectrum of methanolic solutions of **50**, so confirming that the compound is charge-neutral.

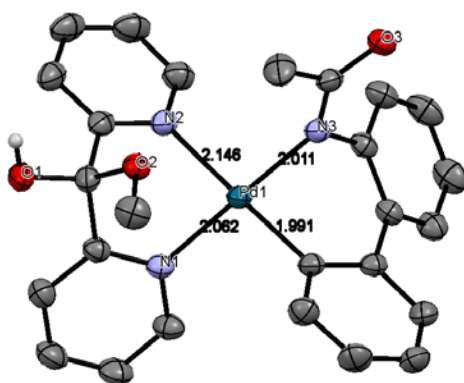
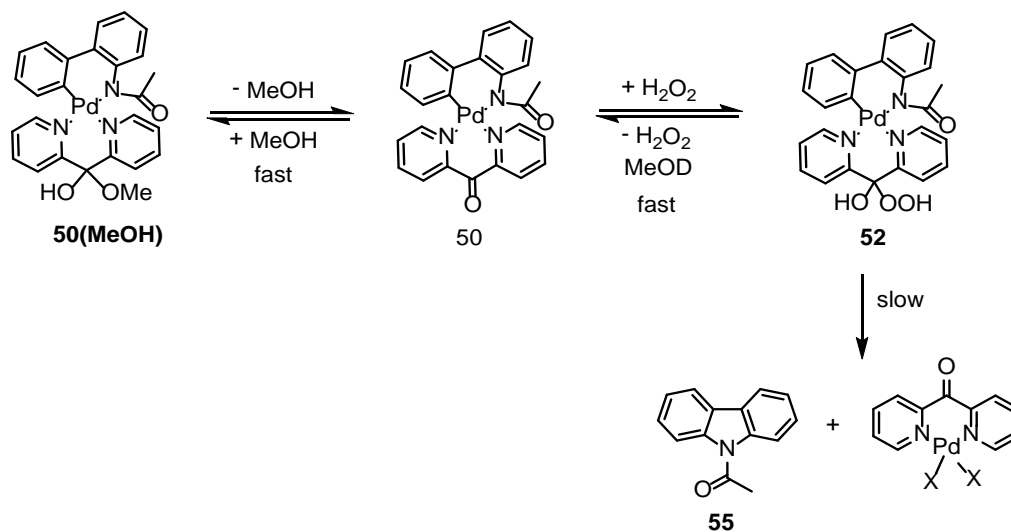


Figure 3.2 X-ray crystal structure of **50**(MeOD) showing the addition of MeOD across the ketone group of **50**.

The X-ray diffraction shows the square planar geometry around the palladium center which is typical for a Pd(II) d^8 center. The dpk fragment is coordinated to Pd in the κ^2 - N,N mode which allows the hemiketal **50(MeOH)** to exist in equilibrium with the corresponding ketone form **50** in solutions. The latter can add H_2O_2 across the carbonyl $C=O$ bond to form a hydroperoxoketal **52** (Scheme 3.3) that can be involved in the Pd(II)-to-Pd(IV) oxidation.⁵⁹ In the solid **50(MeOH)** the Pd1-N2 bond *trans*- to the aryl is elongated (2.146(2) Å) relative to the Pd1-N1 (2.062(2) Å) bond and shows stronger *trans*-influence of the phenyl group in comparison to the amido fragment of the Pd-bound 2'-amidobiphenyl-2-yl ligand. Also, the Pd-aryl bond, Pd1-C41, is shorter, 1.991(2) Å, as compared to the Pd-amide bond, Pd1-N3, 2.011(2) Å.

3.3.2 Reactivity of **50** towards H_2O_2 in different solvents.

3.3.2.1 MeOD



Scheme 3.3. Reactivity of **50** toward H_2O_2 in MeOD to form **55** at 5 °C.

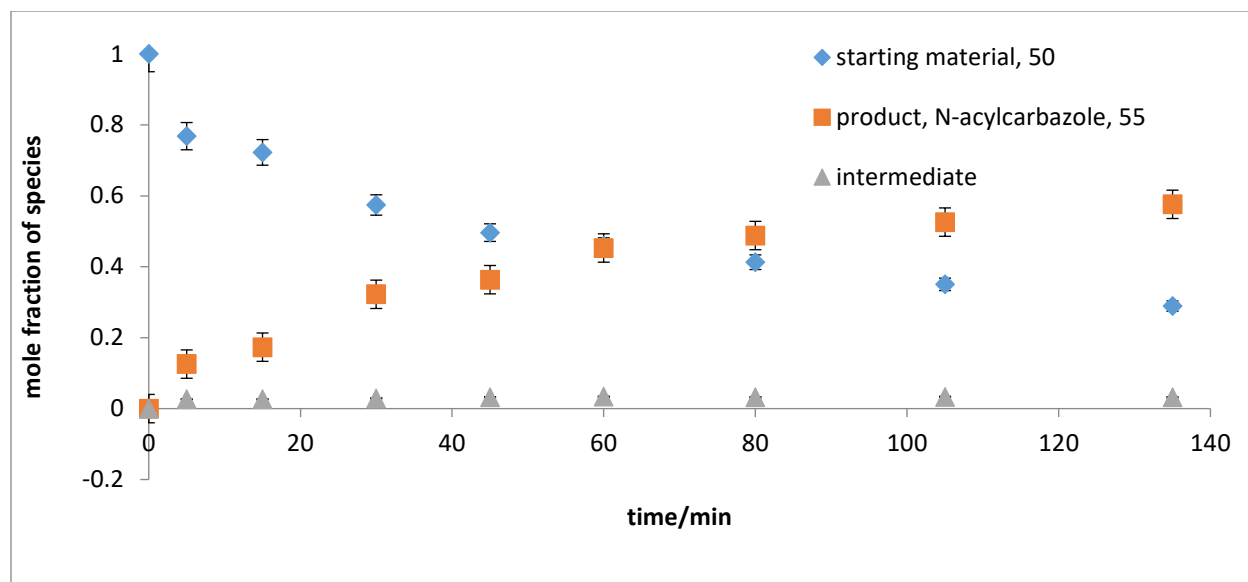


Figure 3.3 Monitoring of **50(MeOH)** in MeOD with 3 equivalents of H₂O₂ to give **55** at 22 °C.

When complex **50(MeOH)** was treated with 3 equivalents of H₂O₂ in methanol solution and monitored by ¹H NMR at room temperature, three sets of signals were observed. First were the signals belonging to the starting material which disappeared gradually with a half-life of about 45 min. Second were the signals belonging to a reaction intermediate which were relatively constant throughout the reaction but eventually disappeared when the reaction was complete. Third were the signals belonging to the N-acetylcarbazole whose concentration increased gradually until reaction was over. Also, the reaction product, N-acetylcarbazole, was found not to be bound to Pd(II); the addition of 3 equivalents of pyridine-*d*₅ did not lead to a change in the ¹H NMR spectrum.

Attempts were made to determine the identity of the intermediate. The *ortho*-pyridyl ¹H NMR signals of dpk-derived species were used as “NMR-handles” to recognize some key dpk derivatives in our chemistry. These signals are typically most downfield shifted and well resolved

in our systems.⁵⁹ A mixture of **50**(MeOH) with 10 eq of H₂O₂ in MeOH was monitored at 5 °C by ¹H NMR spectroscopy. There was an initial spike in the fraction of the intermediate to about 30% and the corresponding initial drop in the amount of starting material to about 70%, but both concentrations did not change much after monitoring for 170 min. When the solution was allowed to warm to room temperature, the carbazole **55** was observed in 87% yield after 120 minutes. This was the first time an intermediate was observed in high concentration in our system. The high concentration of the intermediate observed showed that the formation of this intermediate was fast even at low temperatures. The *ortho*-pyridyl ¹H NMR signals corresponding to this intermediate were upfield shifted (8.60 ppm) compared to the starting material (8.69 ppm). This made us assign these signals to the peroxyketal **52** resulting from the addition of H₂O₂ across the C=O bond of **50**. The corresponding *ortho*-pyridyl signals of an anticipated Pd(IV) intermediate were expected to be more downfield shifted compared to the starting material since the Pd(IV) center is more electron poor than a Pd(II) center.⁵⁹

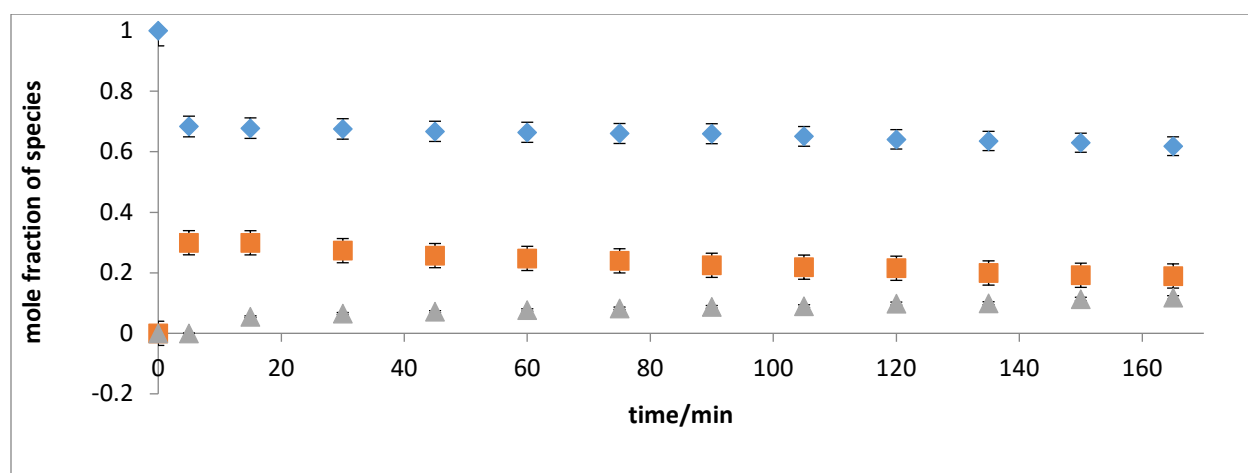
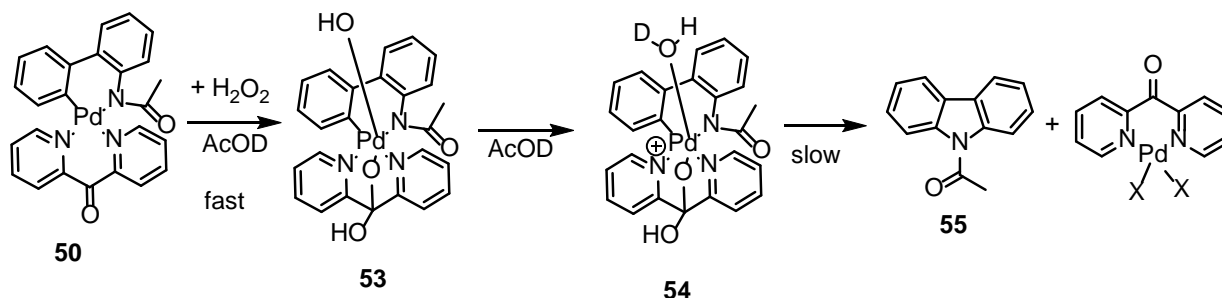


Figure 3.4 Monitoring of **50**(MeOH) in MeOD with 3 equivalents of H₂O₂ to give **55** at 5 °C. Blue diamonds is **50**(MeOH), orange squares is **52**, and gray triangles is **55**.

If our assignments are correct, these observations suggest that the rate of Pd(II)-to-Pd(IV) oxidation is strongly affected (slowed down) by the temperature and that the C-N coupling of the expected Pd(IV) intermediate is still much faster than the Pd(II)-to-Pd(IV) oxidation step. To be able to observe Pd(IV) intermediates we need to make the oxidation step faster than the C-N coupling of the Pd(IV) species. A possible way to accelerate the rate of the oxidation step is by using more powerful H₂O₂ and solvent-derived peroxy species such as AcOOH:



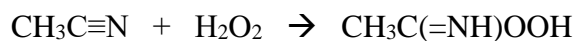
3.3.2.2 AcOD



Scheme 3.4 Reactivity of **50** toward H₂O₂ in AcOD to form **55** at 22 °C. In the absence of MeOH solvent the adduct **50(MeOH)** is expected to dissociate readily into its components, MeOH and **50**.⁵⁹

When a yellow solution of complex **50(MeOH)** in AcOD was treated with 3 equivalents of H₂O₂, and monitored by ¹H NMR at room temperature, broadening of signals was observed

with subsequent formation of the C-N coupled product **55** in 84% yield by ^1H NMR after 60 minutes with the formation of a dark brown colored solution. Decreasing the equivalents of H_2O_2 from 5 to 1.5 did not lead to a change in the reaction rate. Attempts were not made to repeat the reaction at lower temperatures since AcOD freezes at about $16\text{ }^\circ\text{C}$. The increase in the rate of formation of the carbazole **55** in AcOD suggests that the rate of Pd(II)-to-Pd(IV) oxidation is strongly accelerated in this solvent and, possibly, involves peroxyacetic acid, a more powerful oxidizing agent, as compared to H_2O_2 . At the same time, the rate of the C-N reductive elimination step of the Pd(IV) complex **53** may also be affected by AcOH. That might involve formation of an electron-poorer and, hence, more reactive cationic Pd(IV) aqua complex **54**. Hence, the use of less acidic solvents might allow us to observe Pd(IV) amido hydrocarbyl species. In particular, MeCN can also, similar to AcOH, produce strongly oxidizing peroxy imino acetic acid:



At the same time, MeCN should not be affecting dramatically stability of Pd(IV) amido hydrocarbyls.

3.3.2.3 CD_3CN

When a yellow solution of complex **50**(MeOH) in CD_3CN was treated with 3 equivalents of H_2O_2 , and monitored by ^1H NMR at room temperature, one new major species was observed in solution produced immediately after mixing (Scheme 3.5). This species was assigned to the **52** due to the presence of the strongly downfield shifted signal at 14.78 ppm (Fig. 3.5) due to the peroxyketal fragment of the **52**.

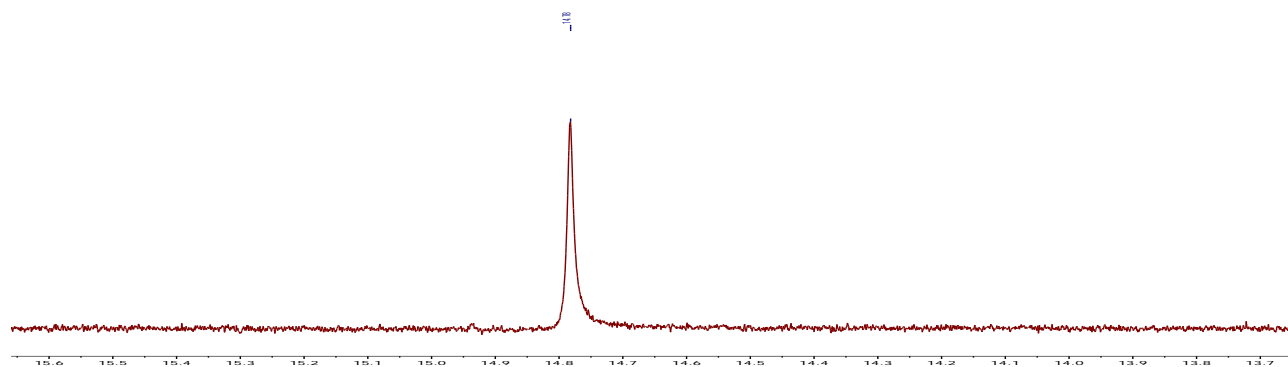
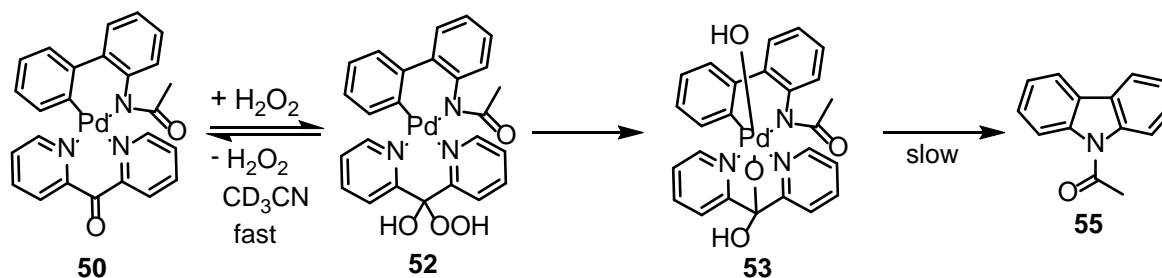


Figure 3.5 ^1H NMR of **52** in CD_3CN showing the signal of the proton of its peroxyketal fragment at 14.78 ppm.

After 15 minutes upon mixing, **52** was observed to fully convert to a new major species **53** (Scheme 3.5).



Scheme 3.5 Reactivity of **50** toward H_2O_2 in CD_3CN to form **53** and **55** at 22°C .

This new species was assigned to the corresponding Pd(IV) amido aryl complex since the signals of its *ortho*-pyridyl hydrogen atoms were much more downfield shifted compared to the starting material. Complex **53** was observed to *slowly* produce the carbazole **55** with a half-life of (182 ± 6) minutes. The latter was observed in 93% yield after 24 h along with a Pd(dpk)-derived compound which crystallized out of solution to give a yellowish-brown precipitate. The precipitate

was isolated and dissolved in DMSO-*d*₆. An ¹H NMR analysis of the resulting solution showed the presence of a dpk – derived species and the absence of **55** which confirms that **55** was not bound to Pd. This was the first time a high concentration of intermediates were observed in our system at room temperature with their possible assignment as a Pd(II) hydroperoxoketal derivative **52** and its isomeric Pd(IV) amido aryl complex **53**. Our attempts to crystallize proposed intermediates, **52** and **53** at low temperatures were not successful. **52** showed one set of signals in the ¹H NMR spectrum with the peroxyketal fragment at 14.78 ppm and an upfield shift in the most downfield *ortho*-pyridyl signal from 8.86 ppm to 8.58 ppm. **53** also showed a single set of signals in the ¹H NMR spectrum with a downfield shift of the most downfield shifted *ortho*-pyridyl signal from 8.86 ppm to 9.12 ppm (Figure 3.6). The use of HBF₄ additives which could help crystallize **53** as a derived salt led instead to faster rates of elimination of **55**. This effect was similar to what we observed when reaction of **50** and H₂O₂ was set up in AcOD solutions. Excited by the ability to observe hypothetical Pd(IV) intermediates in high concentration in MeCN and educated by unsuccessful attempts to isolate them we were led to believe that the success at isolating these intermediates may be highly dependent on the choice of a non-acidic solvent and the R group on the nitrogen atom of the 2-aminobiphenyl fragment.

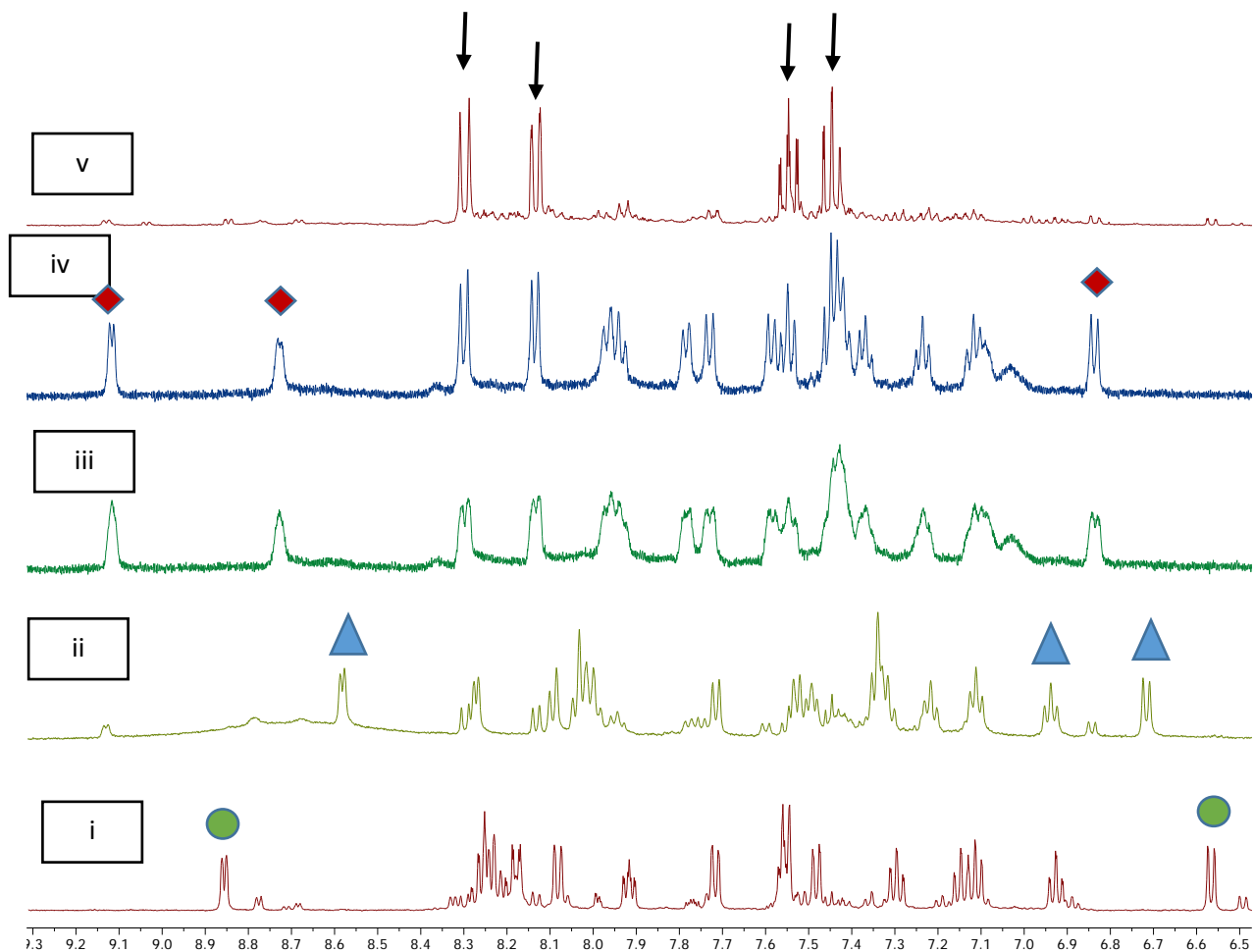


Figure 3.6 ^1H NMR monitoring of the reaction of **50** with H_2O_2 in CD_3CN to form **55**. Green circles show **50**, arrows show **55**, blue triangles show **52** and red diamonds show **53** in solution (i) **50** in solution before addition of H_2O_2 , (ii) 15 minutes after addition (iii) 45 minutes after addition (iv) 3 hours after addition (v) 14 hours after addition.

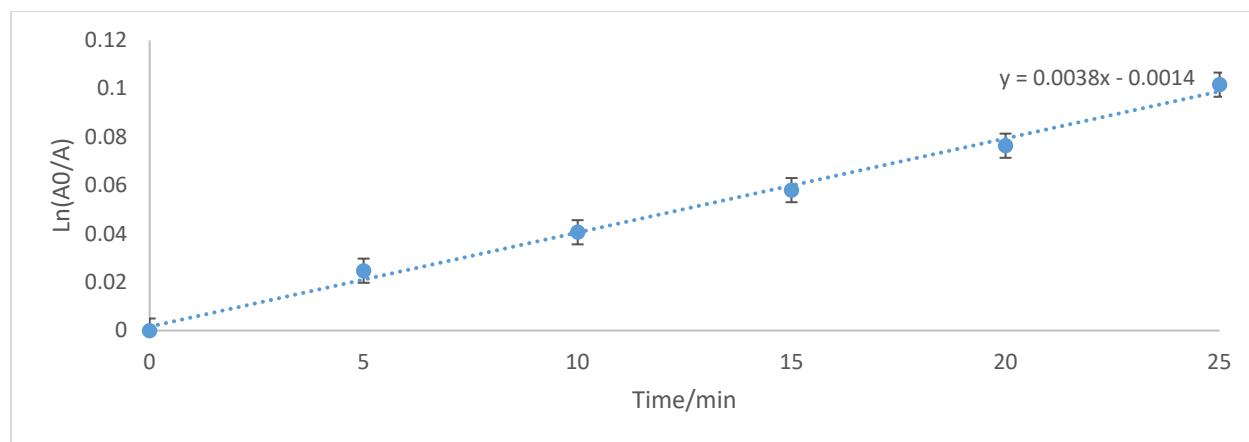
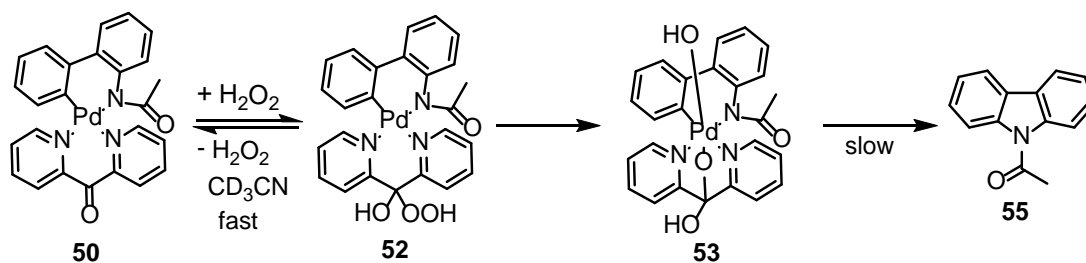


Figure 3.7 First order plot for the elimination from **53** to form **55**; the first order rate constant is $(3.8 \pm 0.2) \times 10^{-3} \text{ min}^{-1}$ in MeCN at 22 °C.

3.3.2.4 THF



Scheme 3.6 Reactivity of **50** toward H_2O_2 in $\text{THF-}d_8$ to form **55** at 22 °C.

When **50**(MeOH) was dissolved in $\text{THF-}d_8$, 3 different species were observed in the yellow solution formed in its ^1H NMR spectrum which could be assigned to the methanol adduct **50**(MeOH), its isomer with an opposite configuration of the ketal carbon and **50**. No change in the ^1H NMR spectrum was observed after letting the solution stand for 2 hours. When a yellow

C-N coupling are not very much different in their rates so not allowing for a clean observation of the Pd(IV) species. In turn, in MeCN solution, according to ^1H NMR spectroscopy, the reaction of **50** with H_2O_2 produces consecutively two major intermediates assignable as a Pd(II) hydroperoxoketal derivative and its isomeric Pd(IV) amido aryl complex. The latter can cleanly produce the corresponding C-N coupled product, the carbazole **55**. Our attempts to isolate these intermediates in a pure form were not successful. At the same time, the successful observation of the Pd(IV) amido aryl complex **53** is, most likely, a result of the presence of an electron-withdrawing group at the nitrogen atom of the Pd-coordinated amido ligand. This conclusion led us to a decision to synthesize and explore other amido aryl Pd(II) complexes containing electron withdrawing groups at the amido nitrogen atom, such as trifluoroacetyl in Pd(II) complex **51**.

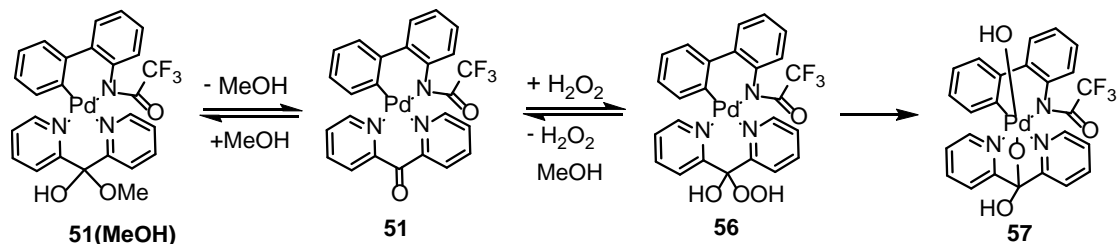
3.4 Characterization and reactivity of the N-trifluoroacetyl Pd(II) complex, **51(MeOH)**

3.4.1 Characterization of the N-trifluoroacetyl Pd(II) complex, **51(MeOH)**

51(MeOH) was isolated from methanolic solutions and shown by ^1H NMR spectroscopy to contain one mol of MeOH per mol of **51** which is presumably added across the dpk fragment C=O bond, similar to **50**(MeOH). The purity of **51**(MeOH) was confirmed by elemental analysis. No signals were observed in the ESI(+)/MS spectrum of methanolic solutions of **51**(MeOH) so confirming the target compound as being neutral. In AcOD solutions, according to ^{13}C NMR spectroscopy, this compound dissociates completely into free MeOH and the “keto form” **51**. Such solutions exhibit no peak at about 95 ppm in ^{13}C NMR spectra characteristic of the dpk-derived ketal carbon whereas the signal of the dpk carbonyl group at about 195 ppm is present.

3.4.2 Reactivity of **51**(MeOH) towards H₂O₂ in different solvents.

3.4.2.1 MeOD



Scheme 3.7 Reactivity of **51** towards H₂O₂ in MeOD at 22 °C.

The off-white **51**(MeOH) dissolves in MeOD readily to form a yellow solution. ¹H NMR analysis of this solution showed two species in a ratio of about 19:1; the minor species being presumably complex **51**, by analogy with similar systems studied previously by Oloo (Scheme 3.7).⁵⁹ When a yellow solution of **51**(MeOH) in MeOD was treated with 5 equivalents of H₂O₂ and monitored by ¹H NMR at room temperature, no new species was observed in solution until about 4 hours when two downfield shifted ortho-pyridyl signals appeared (9.19 ppm and 9.69 ppm) corresponding to a plausible Pd(IV) intermediate, **57**, formed in 23% yield (Fig. 3.9). After 24 h, no peaks which could be assigned to the corresponding carbazole **58** were detected. Upon allowing the solution to stand for seven days, no products of reductive elimination were observed. Our attempts to isolate intermediate **57** were not successful.

The Sanford group observed C(sp³)-N reductive elimination at 60 °C which may be due to the relatively high energy barrier needed for this to happen.⁵⁴ Similarly, we also tried raising the temperature to see if this could increase the rate of reductive elimination. A new experiment was set up and after 16 hours the solution was heated at 70 °C for 4 hours. No carbazole **58** was observed by ¹⁹F NMR after heating; dark brownish decomposition products including Pd black on

the walls of the Young tube were observed. This result may be associated with the ability of MeOH to reduce Pd compounds under harsh conditions to the metal.

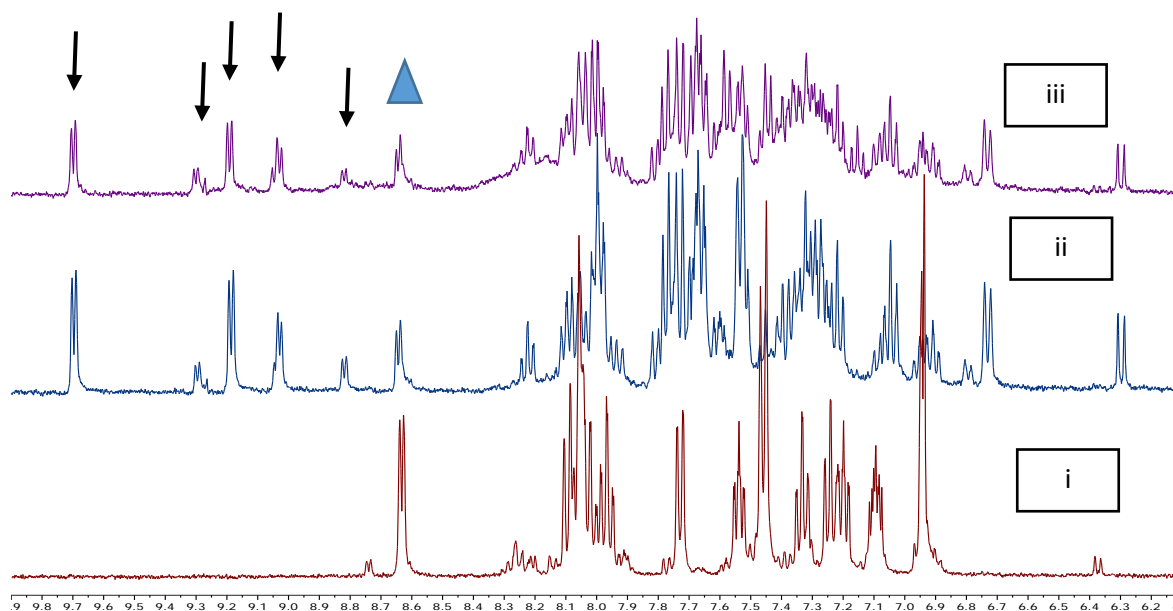


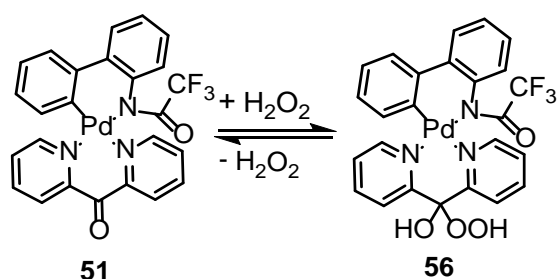
Figure 3.9 ^1H NMR spectroscopy monitoring of the reactivity of **51(MeOH)** in MeOD at 22 $^\circ\text{C}$. Arrows show intermediates observed in solution which was attributed to both **56** and **57**, and blue triangle shows **51**. (i) **51** in solution before addition of H_2O_2 , (ii) 12 hours after addition (iii) 12 hours after addition and warming at 70 $^\circ\text{C}$ for 4 hours.

3.4.2.2 CD_3CN

51(MeOH) dissolves in CD_3CN to give yellow solutions. A yellow solution of complex **51** in CD_3CN was combined with 3 equivalents of H_2O_2 at room temperature. According to ^1H NMR spectroscopy, a new major species was immediately formed in the mixture, along with some small quality of the starting material **51**. This species was hypothesized to be the hydroperoxoketal **56** due to the presence of the strongly downfield shifted signal at 13.57 ppm assigned to the proton of the hydroperoxyketal OOH fragment of **56**. Notably, **56** was observed to quickly convert to

another species in the course of 30 minutes (Fig. 3.10). This new species persisted for about 8 hours as the major product in solution but our attempts to crystallize it were not successful.

Interestingly, according to ^1H NMR of the dark brown solution formed after 24 hours, **51** was observed to reform as the major product, apparently, with O_2 evolution, whereas no carbazole **58** was detected. These results suggest that both species observed in solution could be isomeric hydroperoxoketals, with the OOH group positioned *exo*- or *endo*- with respect to the metal chelate ring (Scheme 3.8). This assumption is based on the consideration that the corresponding Pd(IV) complex **57** could not be reduced to **51** in CD_3CN solvent, which is known to be not a good reducing agent. In addition to the signals of the starting material **51**, after 24h two *ortho*-pyridyl peaks of equal intensity were observed at 9.14 ppm and 9.35 ppm (4% yield). This product may correspond to the Pd(IV) amido aryl complex **57**. As in the case of MeOH as a solvent, after warming up the reaction mixture at 60°C for 3 hours no clean formation of the carbazole **58** was observed by ^{19}F NMR, which may be because of a low content of **57** in the mixture.



Scheme 3.8 Reactivity of **51** toward H_2O_2 in CD_3CN at 22°C .

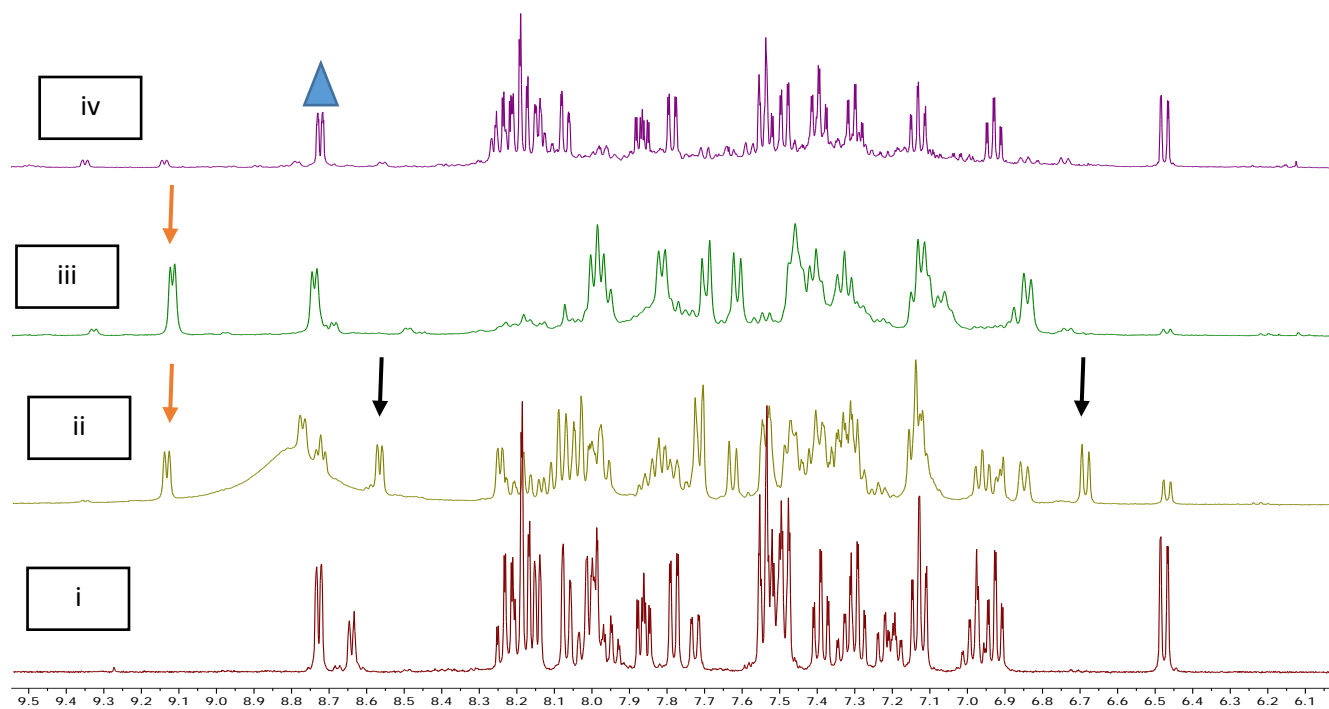
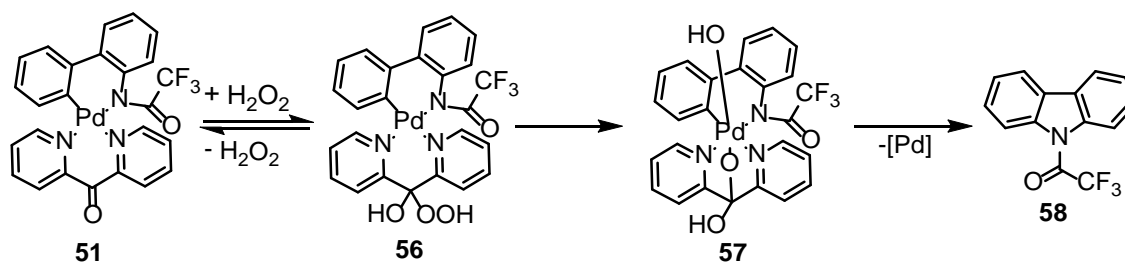


Figure 3.10 ^1H NMR spectroscopy monitoring of the reactivity of **51** in CD_3CN at $22\text{ }^\circ\text{C}$. Black arrows show endo-isomer of **56**, orange arrows show exo isomers of **56** observed in solution and blue triangle shows **51**. (i) **51** in solution before addition of H_2O_2 , (ii) 15 minutes after addition (iii) 60 minutes after addition (iv) 13 hours after addition.

3.4.2.3 THF



Scheme 3.9 Reactivity of **51** toward H_2O_2 to form **58** in $\text{THF-}d_8$

A picture similar to what was observed in CD₃CN solutions was also seen in THF. Complex **51** dissolves in THF-*d*₈ to give yellow solutions. When a yellow solution of complex **51** in CD₃CN was treated with 3 equivalents of H₂O₂ and monitored by ¹H NMR spectroscopy at room temperature, a new major species was observed. This species was assigned to the **56** (Scheme 3.9) due to the presence of a strongly downfield shifted signal at 13.68 ppm of the peroxyketal OOH fragment. Complex **56** persisted for about 8 hours as the major product in solution (Fig. 3.11). After 24 hours, according to ¹H and ¹⁹F NMR of the dark yellow solution formed, **51** was observed to reform in a high yield. A new species was also detected which was presumed to be Pd(IV), **57**, based on the presence of more downfield shifted signals of pyridyls' *ortho*-hydrogen atoms (9.25 ppm and 9.31 ppm), as compared to the starting material (8.80 ppm). Warming up of the solution to 60 °C resulted in the formation of the carbazole **58** in 18% yield by ¹⁹F NMR spectroscopy.

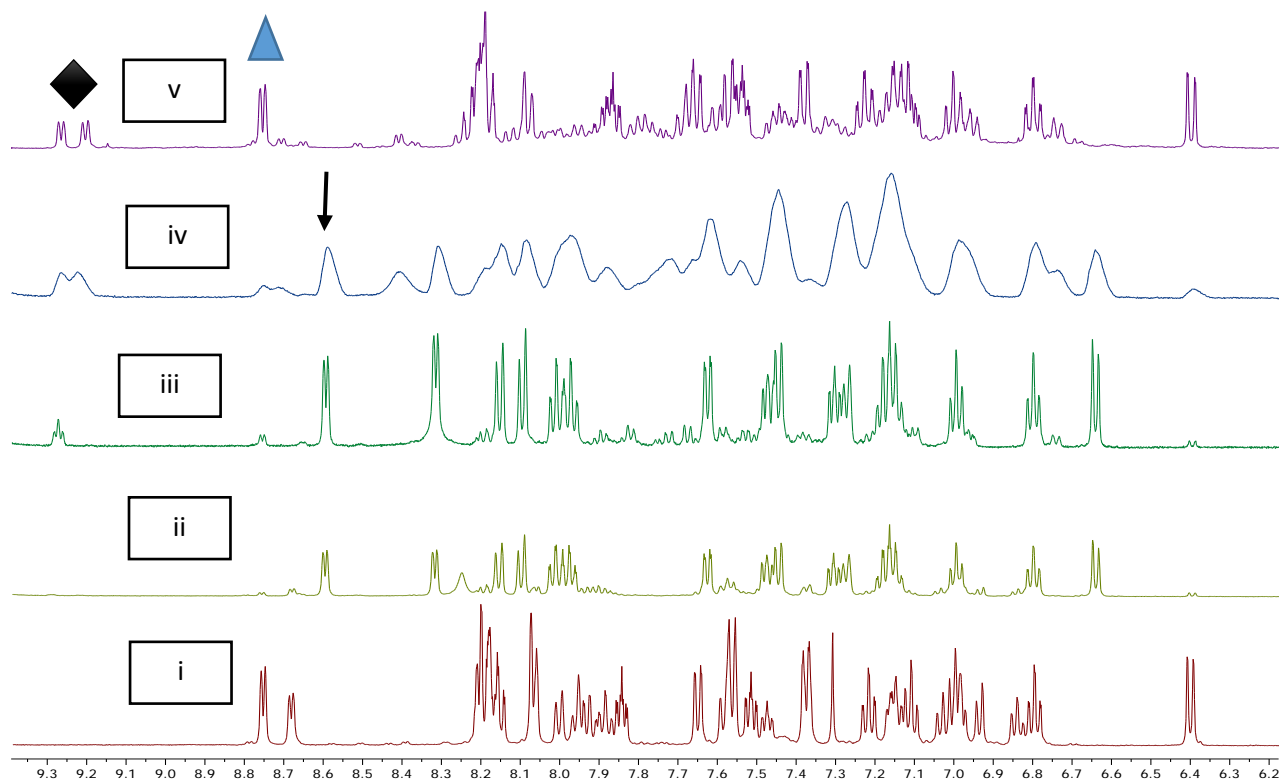
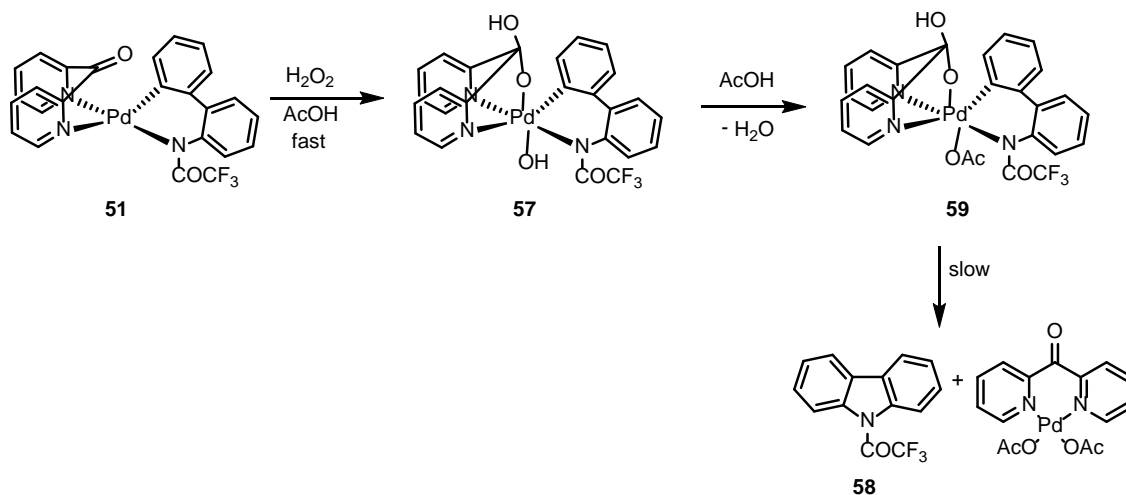


Figure 3.11 ^1H NMR spectroscopy monitoring of the reactivity of **51** in $\text{THF-}d_8$ at $22\text{ }^\circ\text{C}$. Arrows show **56**, black diamond shows peaks presumed to be **57** and blue triangle shows **51**. (i) **51** and **51-H₂O** in solution before addition of H_2O_2 , (ii) 15 minutes after addition (iii) 60 minutes after addition (iv) 500 minutes after addition (v) 24 hours after addition.

3.4.2.4 *AcOD*

Complex **51** dissolves in *AcOD* after 15 minutes on a rotator to form a clear yellow solution. After 50 min upon addition of 3 equivalents of H_2O_2 almost all of the starting material disappears to form two intermediates, **57** and **59** (Scheme 3.10, Fig. 3.12). The former was observed to form

faster than **59** (the **57** : **59** ratio is 2:1 after 10 min) but after 60 minutes both intermediates were present in about equal amounts (Fig. 3.13). This ratio remained constant for 16 h.



Scheme 3.10 Proposed reaction of **51** with H_2O_2 in AcOD to form intermediates **57**, **59** and the carbazole **58**.

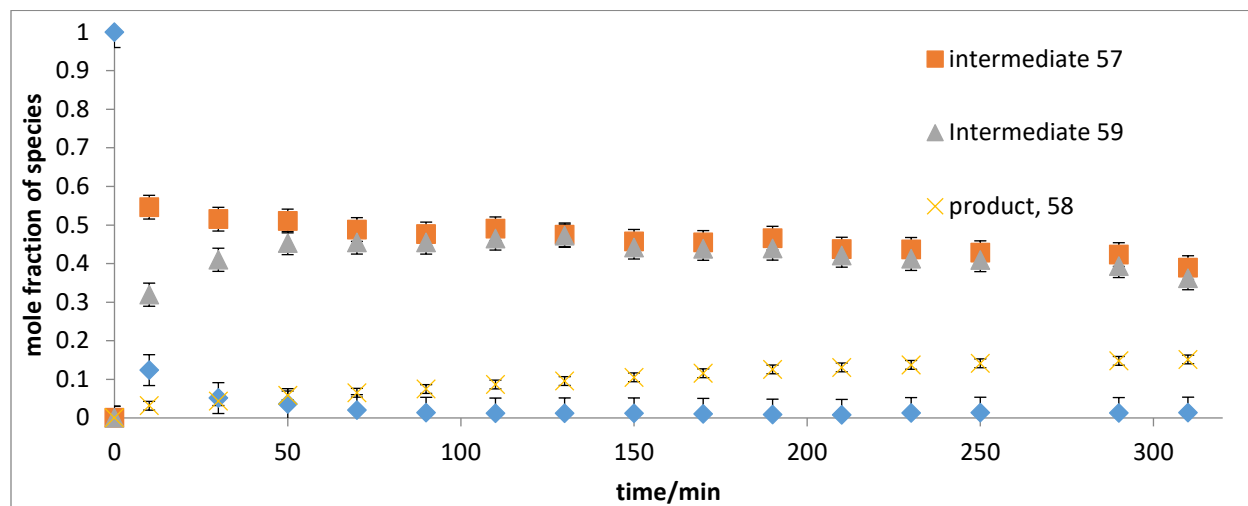


Figure 3.12 A profile of the reaction of **51** (blue diamonds) with 3 equiv H_2O_2 in AcOD to form intermediates **57**, **59** and the carbazole **58**, based on ^1H NMR monitoring at 22°C .

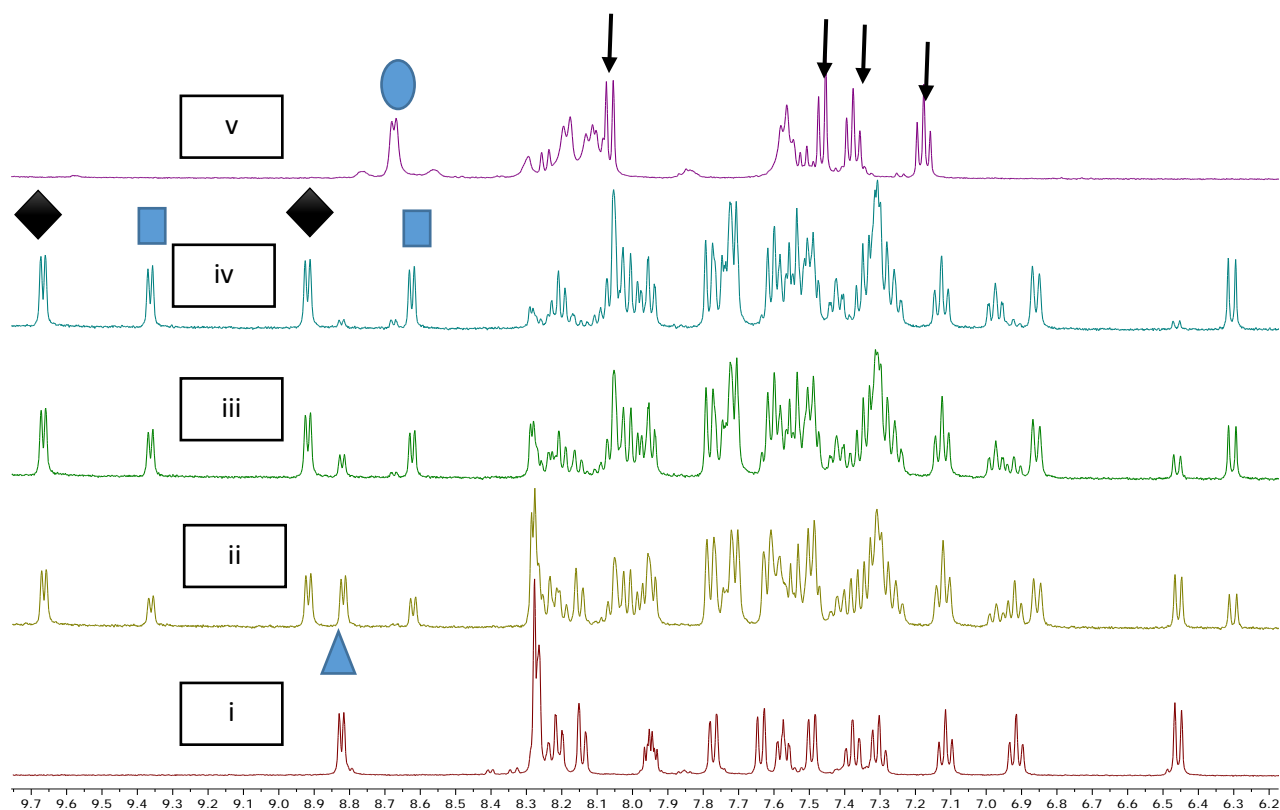


Figure 3.13 ^1H NMR monitoring of the reaction of **51** with H_2O_2 in AcOD at $22\text{ }^\circ\text{C}$. Arrows show **58**, black diamond shows **57**, blue squares show **59** and blue triangle shows **51**. (i) **51** in solution before addition of H_2O_2 , (ii) 10 minutes after addition (iii) 30 minutes after addition (iv) 50 minutes after addition (v) 50 minutes after addition and warming at $60\text{ }^\circ\text{C}$ for 3 hours.

The tentative assignment of both **57** and **59** as Pd(IV) complexes was based on the position of the most downfield-shifted signals of their *ortho*-pyridyl hydrogen atoms (9.67 ppm and 9.37 ppm), much more downfield as compared to the starting material (8.82 ppm).

We hypothesize that the intermediate **57** is a Pd(IV) hydroxo complex which forms upon attack by the Pd at the corresponding peroxyketal O-O bond. Complex **59** may be viewed as a

derived Pd(IV) acetoxo complex. The mixture of **57** and **59** in AcOD produces slowly the carbazole **58**; this reaction is accelerated at 60 °C.

Notably, the carbazole formation is rate limiting in AcOH, as opposed to the reaction of **51** with H₂O₂ in other solvents, MeOD, CD₃CN and THF, where the Pd(II)-to-Pd(IV) oxidation was rate limiting. This shows the dramatic effect of solvent on our reaction. It is likely that AcOD enhances the electrophilicity of the derived peroxoketal OOH group leading to a more facile attack at it by the Pd(II) center.

3.4.3 Isolation and reactivity of N-trifluoroacetyl Pd(IV) complex, **59**

From our observations illustrated in Fig. 3.13 it follows that the highest fraction of intermediates **57** and **59** is observed after about 50 minutes. We, therefore, attempted isolation of **57** and **59** after 50 minutes of reaction at 22 °C. The solvent was removed under vacuum and the resulting brown solid was washed with H₂O to remove any remaining H₂O₂ and AcOH. The solid is insoluble in H₂O and toluene, slightly soluble in MeOH, CH₃CN, acetone and THF and perfectly soluble in DMSO. Complex **57** did not survive the isolation, presumably, due to an extended exchange of the OAc for OH ligand.

An ¹H NMR spectrum of the so-produced solid in DMSO-*d*₆ showed the presence of two species in a ratio of 6:1 (Fig. 3.14). This ratio was also observed using ¹⁹F NMR which showed two fluorine-containing species with the signals at -69.66 ppm and -70.91 ppm in a ratio of 6:1 (Fig. 3.15). A molecule of AcOH was observed to crystallize with the precipitate which was observed at 1.91 ppm. Two CH₃ group signal were also observed at 2.01 ppm and 1.36 ppm in a ratio of 6:1 for the major and minor species, respectively. The major signal was attributed to **59**

while the other signal which is more upfield shifted might be attributed to **60**, an isomeric acetate (see C-N reductive elimination reactivity below).

The addition of two drops of D₂O to the above mixture of **59** and **60** in DMSO-*d*₆ leads to the disappearance of the peaks at 8.62 ppm and 8.82 ppm which could be attributed to the OH group of the hydrated dpk ligand of the major and minor components, respectively. No change in the high field region from 0 ppm to 5 ppm was observed. Since the signal of the Pd(IV)(OH) ligand in **57** would be present in this range, we concluded that **57** was not in the mixture.

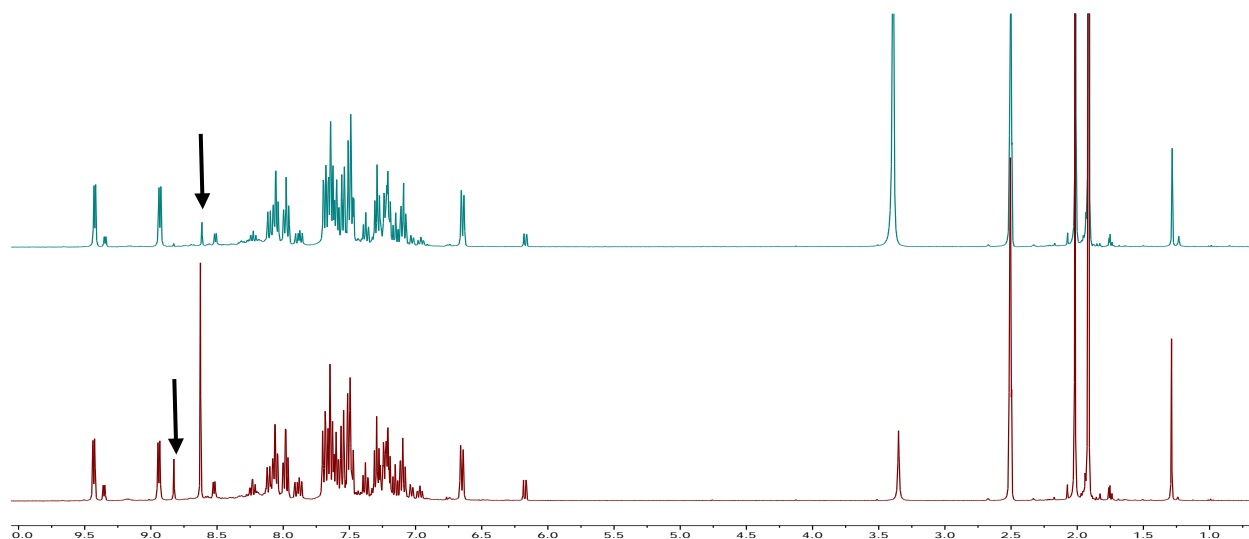


Figure 3.14 ¹H NMR spectrum in DMSO-*d*₆ of a mixture containing **59** and **60** as the major component, before (below) and after addition of two drops of D₂O (above). Arrows show the peaks affected.

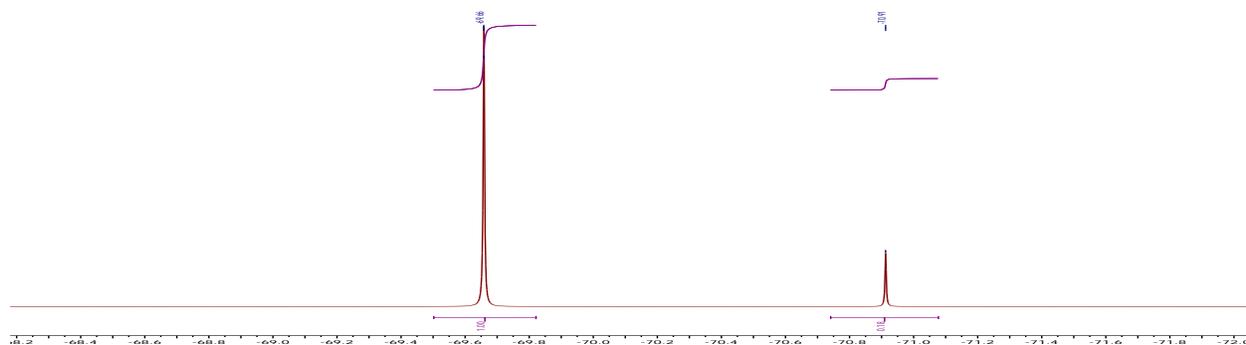


Figure 3.15 ^{19}F NMR spectrum of a mixture containing **59** as the major component in $\text{DMSO-}d_6$.

No change in ^1H NMR spectra of mixtures of **59** and **60** in $\text{DMSO-}d_6$ was observed after 2 hours at $22\text{ }^\circ\text{C}$, but after warming the solution to $60\text{ }^\circ\text{C}$ for 30 minutes, there was a complete conversion of both components to the target carbazole **58** in 95% yield together with $(\text{dpk})\text{Pd}(\text{OAc})_2$. Hence, both Pd(II)-to-Pd(IV) oxidation and C-N coupling of the latter are severely slowed down by the electron withdrawing $\text{CF}_3\text{CO-}$ group. The use of less electron withdrawing methanesulfonyl group may lead to more reactive yet isolable amido aryl Pd(IV) complexes.

3.4 Characterization and reactivity of the N-methanesulfonyl Pd(II) complex, **61(MeOH)**

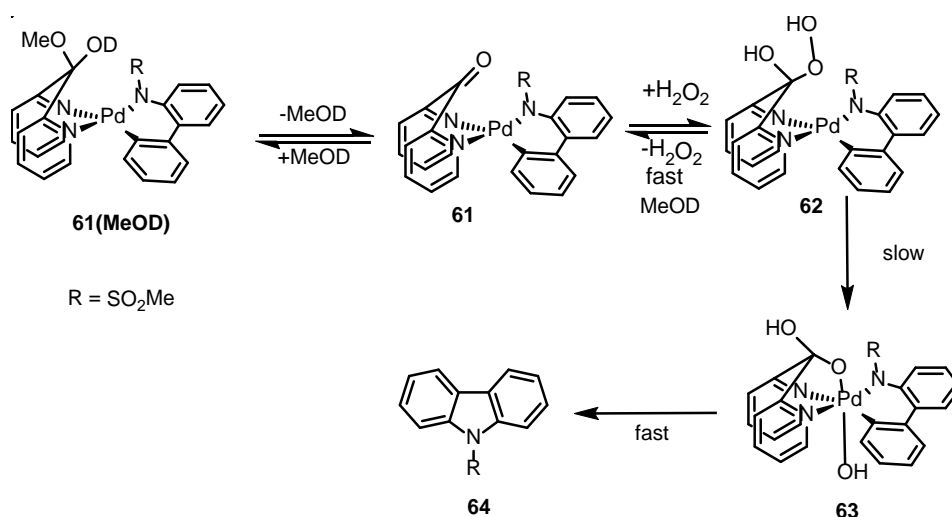
3.4.1 Characterization of the N-methanesulfonyl Pd(II) complex **61(MeOH)**

The title compound was isolated from methanolic solutions and its composition as **61(MeOH)** was confirmed by ^1H NMR spectroscopy and elemental analysis. The MeOH molecule is most likely added across the C=O group of **61**, similar to **51(MeOH)**. In AcOD solutions the title compound exist predominantly in the keto form **61** as it was shown by ^{13}C NMR spectroscopy.

In particular, there was no peak at about 95 ppm in its ^{13}C NMR spectra characteristic of the ketal carbon whereas the signal of the dpk carbonyl group at about 195 ppm was observed. No signals were observed in the ESI(+)/MS spectra of methanolic solutions of **61** so confirming the target compound as being neutral.

3.4.2 Reactivity of **61**(MeOH) towards H_2O_2 in different solvents

3.4.2.1 MeOD (Scheme 3.11)



Scheme 3.11 Reactivity of **61** toward H_2O_2 to form **64** in MeOD.

Two sets of signals corresponding to two species in a ratio of 1:1.7 were observed for **61**(MeOH) in MeOD (Fig. 3.16). These were attributed to two isomeric methanol adducts. The addition of 3 equiv of H_2O_2 to the yellow solution of **61**(MeOH) in MeOD showed a gradual formation of an orange solution. ^1H NMR spectral analyses of the resulting solution showed the

gradual disappearance of **61**(MeOH) (the component with the *ortho*-pyridine hydrogen atom signal at 9.13 ppm disappeared at a faster rate) and formation of two new species with the *ortho*-pyridine hydrogen atom signals at 9.07 and 8.92 ppm, upfield shifted compared to signals for **61**, after about 30 min. These two new species were attributed to two isomers of **62** with the -OOH group positioned *endo*- or *exo*- with respect to the metal chelate ring. Complexes **62** and **61** disappeared at about the same rate to form the carbazole **64** (88% yield, 6 h by ^1H NMR). Since no new intermediates were observed by ^1H NMR spectroscopy, transformation of **62** to form **63** was rate limiting.

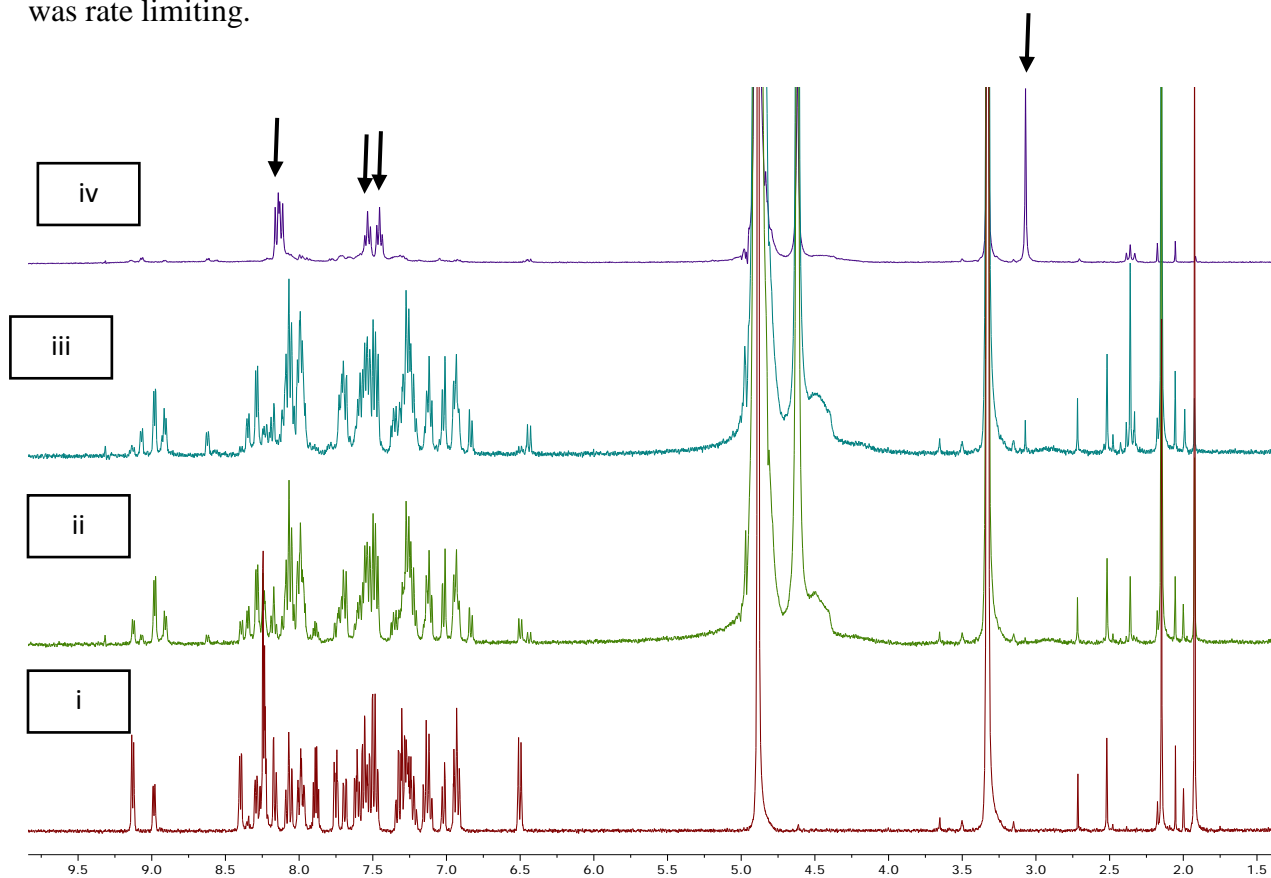
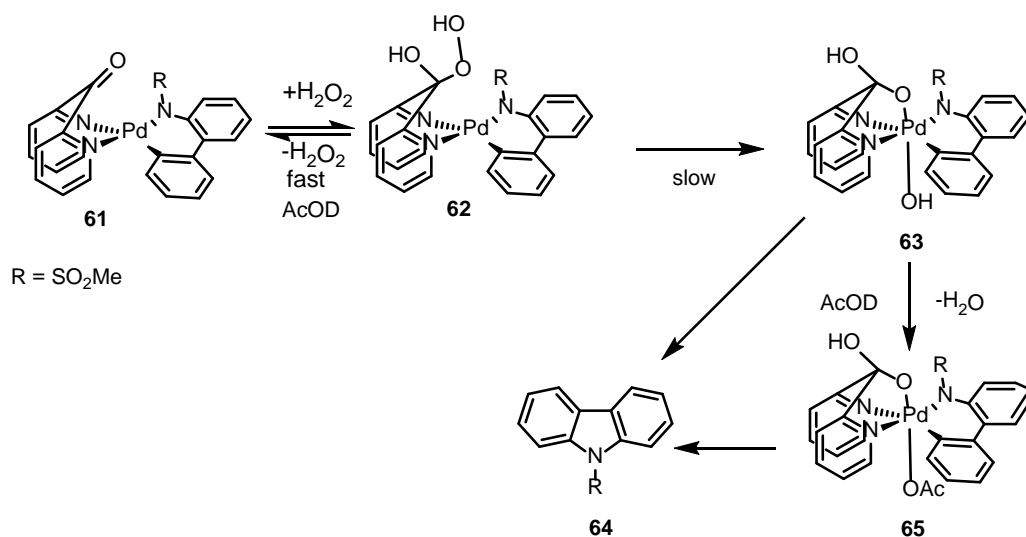


Figure 3.16 ^1H NMR monitoring of the reaction of **61** with H_2O_2 in MeOD at $22\text{ }^\circ\text{C}$. Arrows show the carbazole **64** (i) **61**(MeOH) in solution before addition of H_2O_2 , (ii) 5 minutes after addition (iii) 45 minutes after addition (iv) 6 hours

3.4.2.2 AcOD (Scheme 3.12)

Only one set of signals was observed in the ^1H NMR spectrum of **61**(MeOH) in AcOD which was assigned to **61**, similar to previous observations.⁵⁹ In 5 min upon mixing of 3 equivalents of H_2O_2 and a solution of **61** in AcOD the carbazole **64** formed in 87 % yield (Fig. 3.17). ^1H NMR spectral analysis of the resulting mixture showed the presence of two minor species in solution in a total combined yield of less than 8%. The two minor species were assigned as Pd(IV) complexes **63** and **65**. As it is typical for Pd(IV) dpk – supported complexes, the signals of their *ortho*-pyridine hydrogen atoms were more downfield shifted (9.41 ppm and 9.32 ppm) as compared to the starting material (9.23 ppm). Finally, the yield of the carbazole increased to 97% after 30 min. Since no peroxoketal **62** was detected in the system, our observations imply that the oxidation step was fast and the C-N coupling was rate determining.



Scheme 3.12 Reactivity of **61** toward H_2O_2 in AcOD to form the carbazole **64**.

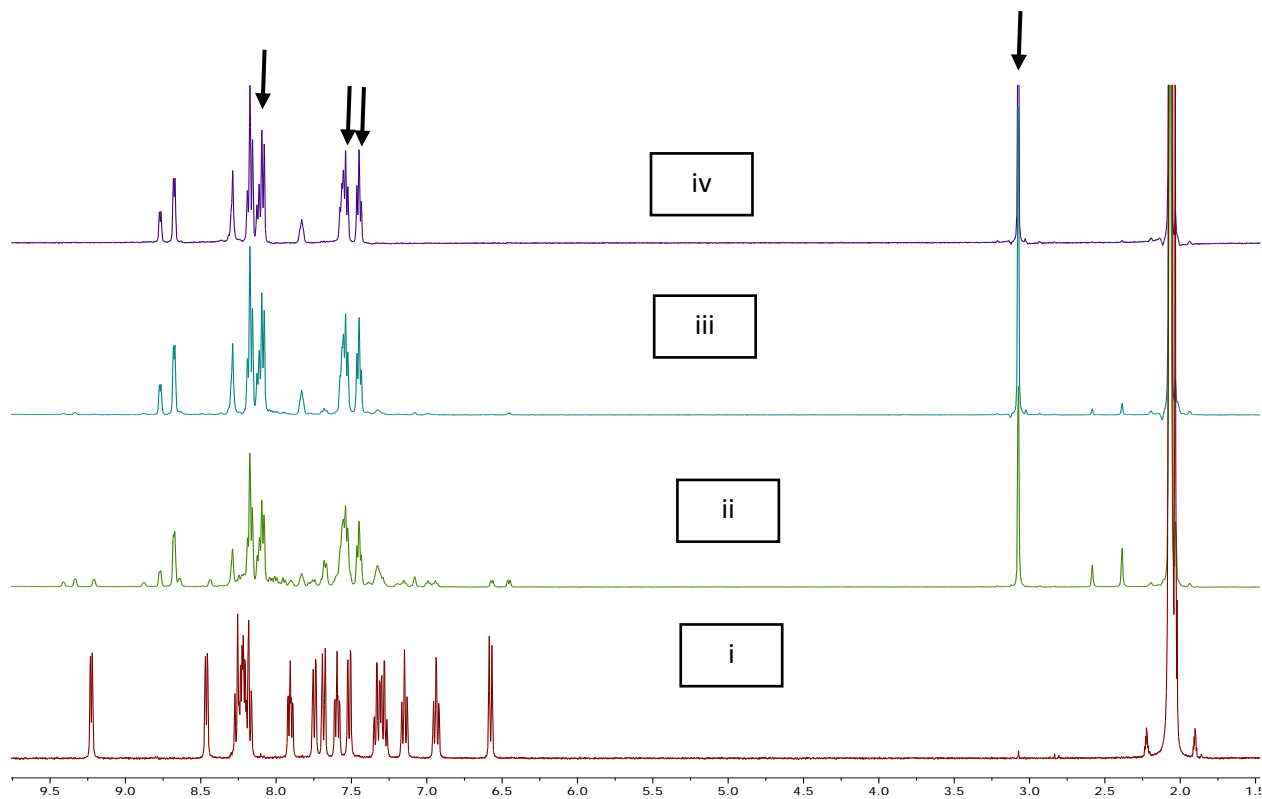
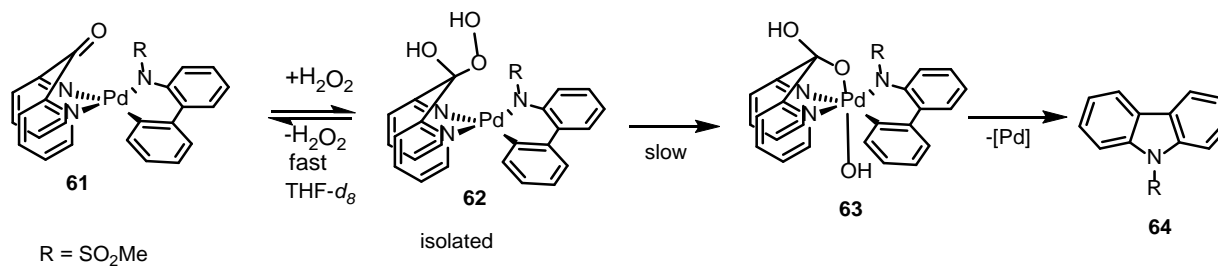


Figure 3.17 ^1H NMR monitoring of the reaction of **61** with 3 equiv H_2O_2 in AcOD at $22\text{ }^\circ\text{C}$. Arrows show the carbazole **64** (i) **61** in solution before addition of H_2O_2 , (ii) 5 minutes after addition (iii) 20 minutes after addition (iv) 30 minutes

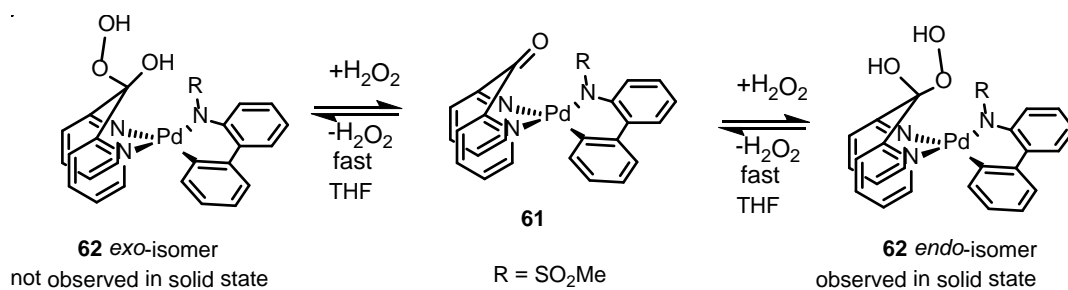
3.4.2.3 THF (Scheme 3.13)

A combination of a yellow solution of **61**(MeOH) in $\text{THF-}d_8$ with 3 equivalents of H_2O_2 led to a rapid color change to a very light yellow. ^1H NMR analysis of the resulting solution showed the formation of one major and one minor new species in about 4:1 ratio which could be assigned to the isomers of **62** with the OOH group positioned *endo*- or *exo*- with respect to the metal chelate ring (Scheme 3.14). For both species the resonances of the *ortho*-pyridine hydrogen atoms were shifted upfield, as compared to the starting material (Fig. 3.18). The isomer *endo*-**62** was observed to slowly precipitate out of solution. Using crystallization at a lower temperature, $0\text{ }^\circ\text{C}$, this

compound could be isolated in 76% yield. The so-produced crystals were suitable for single-crystal X-ray diffraction analysis.



Scheme 3.13 Reactivity of **61** toward H_2O_2 in $\text{THF-}d_8$ to form the intermediates **62**, **63** and the carbazole **64**.



Scheme 3.14 The interconversion between the *endo* and *exo* isomers of **62**.

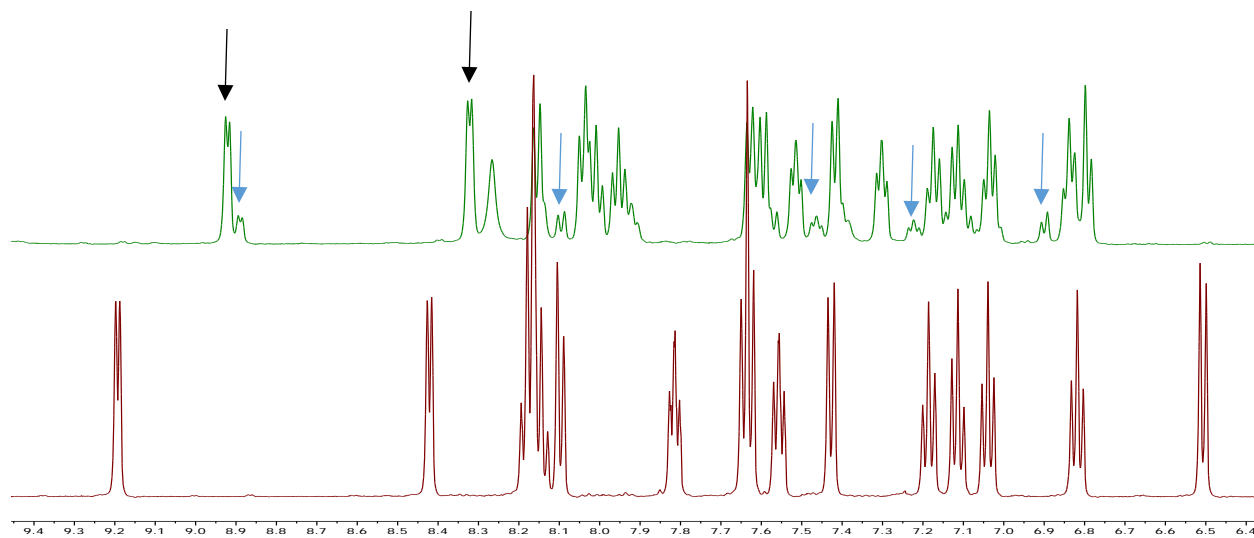


Figure 3.18 ^1H NMR spectra of **61** (below) and **62** (above) in $\text{THF-}d_8$. The major set of signals (black arrows) in **62** was assigned to the endo-isomer while the minor set of signals (blue arrows) were assigned to the endo-isomer.

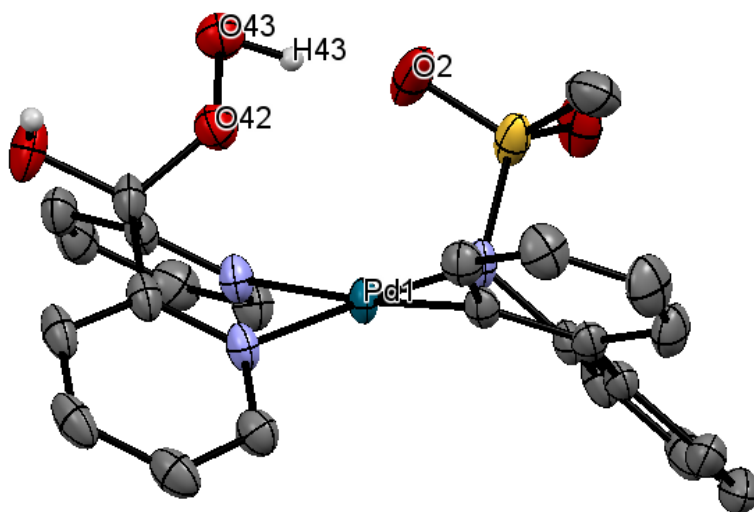


Figure 3.19 ORTEP plot of complex **62** with the *endo*-orientation of the OOH group. Selected bond lengths (\AA): Pd1-O42 2.888, O42-O43 1.465 (3), H43-O2 1.764

The X-ray diffraction analysis of **62** shows the expected square planar geometry around the palladium(II) center. The dpk fragment is coordinated to Pd in the κ^2 -*N,N*-fashion, and H₂O₂ added across the ketone group to form the peroxyketal. Notably, the hydroperoxo group in **62** is in the *endo*-configuration with respect to the metal chelate ring. The O43-O42 bond length (1.465(2) Å) of the peroxy fragment of the peroxyketal is comparable to the O-O bond length (1.49 Å) of H₂O₂.⁶⁹ The hydroperoxo group hydrogen atom H43 was found to be hydrogen-bonded to the sulfonyl group oxygen atom O2 with a bond length of 1.764 Å which is slightly longer than a typical H-bond in H₂O (1.74 Å).⁷⁰ This intramolecular interaction may be responsible for some additional stability of the *endo*-isomer of **62** crystallized from the reaction mixture. The Pd1-N31 bond *trans*- to the aryl ligand is elongated (2.148(2) Å) relative to the Pd1-N51 bond (2.058(2) Å) *trans*- to the amido group nitrogen atom due to the stronger *trans*-influence of the aryl group. Also, the metal-aryl carbon bond, Pd1-C21, is shorter (1.986(2) Å) as compared to the metal – amide nitrogen bond, Pd1-N1(2.020(2) Å), which may reflect a greater ionic character of the latter. Importantly, the hydroperoxo group found in **62** in the *endo*-position is perfectly suitable for a nucleophilic attack by the Pd(II) atom utilizing its d₂₂ electrons to cause a Pd(II)-to-Pd(IV) transformation. The corresponding distance Pd1-O42 is 2.888 Å which is equal to the sum of the Pd and O atoms' van der Waals radii. Based on the previous work from our group,⁵⁹ the *endo*-isomer of **62** may be a few kcal/mol more stable than the *exo*-adduct, in perfect agreement with the results of this study (Fig. 3.14).

When **62** dissolved in THF-*d*₈ was left for several hours at 22 °C, it slowly reacted to produce a mixture of the corresponding carbazole **62** and the Pd(IV) hydroxo complex **63**, along with the starting material, **61**, (Fig. 3.20) with apparent evolution of O₂ gas. The reaction was complete after 24 hours to form the corresponding carbazole **64** in 67% yield and the starting Pd(II)

amido aryl complex **61** in 21% yield. This observation suggests that the addition of H₂O₂ across the C=O bond of the dpk ligand in **61** is reversible and that **62** could lose H₂O₂ to produce **61** or be transformed to the isomeric Pd(IV) amido aryl complex **63** which, in turn, can reductively eliminate the carbazole **64** at 22 °C. The simultaneous observation in THF solutions of the Pd(II) peroxoketal complex **62**, its Pd(IV) hydroxo derivative **64** and the product of the C-N elimination from the latter of the carbazole **64** allow us to conclude that in THF the rates of both redox reactions can be comparable.

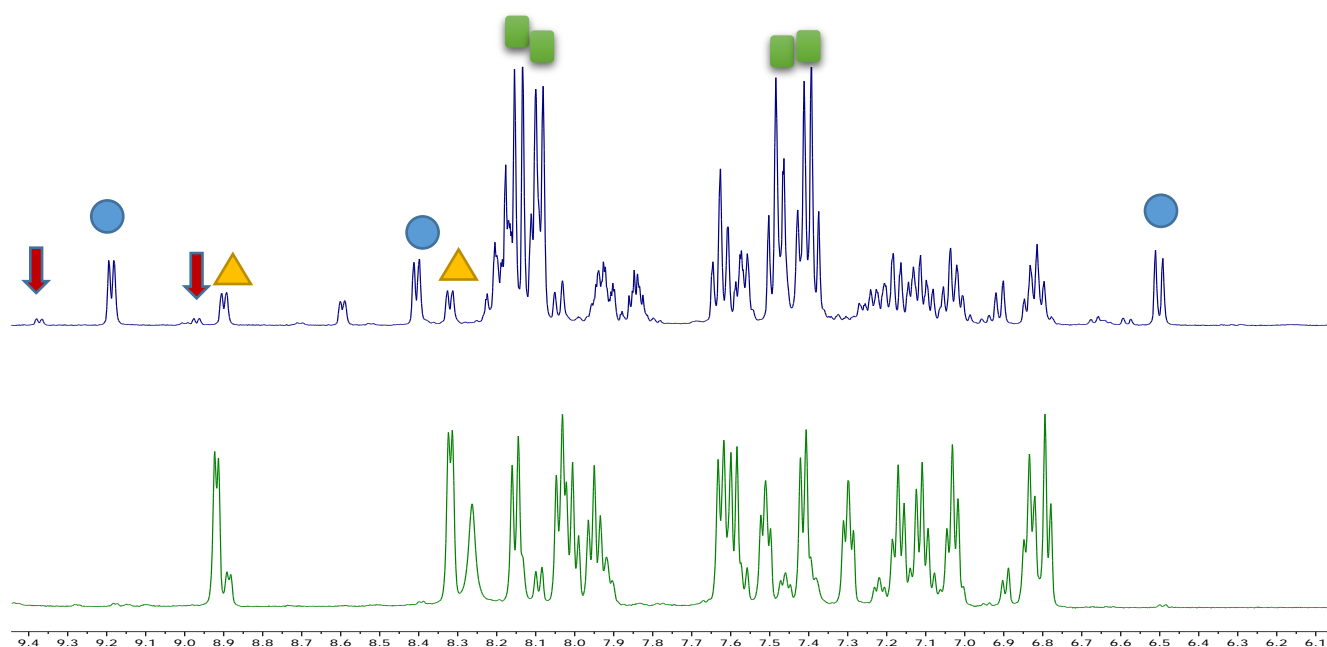
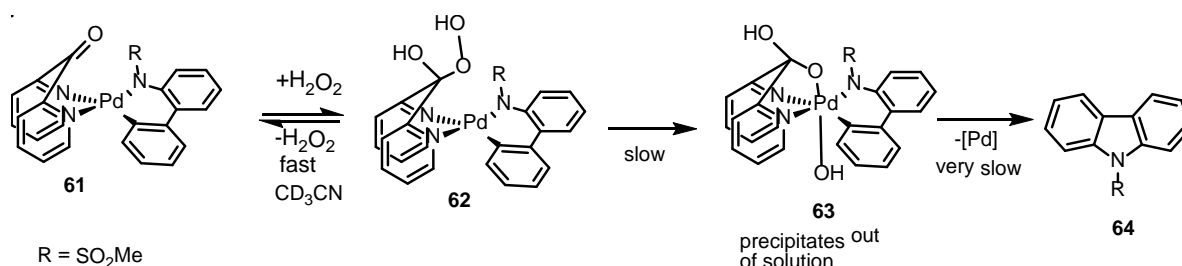


Figure 3.20 ¹H NMR spectrum of the Pd(II) hydroperoxo ketal complex **62** (bottom) and its mixture with the Pd(IV) hydroxo derivative **63** and the carbazole **64** (top) after 24 hours in THF-*d*₈ at 22 °C. Blue circles: **61**, yellow triangles: **62**, green squares: **64**. The signals assigned to **63** are marked with red arrows.

3.4.2.4 CH₃CN (Scheme 3.15)

A combination of a yellow solution of **61**(MeOH) in CD₃CN with 3 equivalents of H₂O₂ led to a rapid color change to produce a deep orange solution. ¹H NMR spectral analysis of the solution showed the formation of a new species which was assigned to **62** because of the presence of the characteristic signal of the peroxyketal fragment OOH at 11.79 ppm. When produced in high concentration, complex **62** could be crystallized out of solution. In turn, when the heterogeneous mixture was left for 24 hours at 22 °C, a new solid formed which was assigned as the Pd(IV) hydroxo complex **63** (*vide infra*), along with 7% of the corresponding carbazole **64** in solution. The fact that **63** could be crystallized out of solution without being much engaged in the subsequent elimination of the carbazole **64** suggests that the C-N coupling of **64** can only occur in solution and that the overall rate of the latter reaction was very slow because of the poor solubility of **63** in MeCN.



Scheme 3.15 Reactivity of **61** toward H₂O₂ in CD₃CN to form **63** at 22 °C.

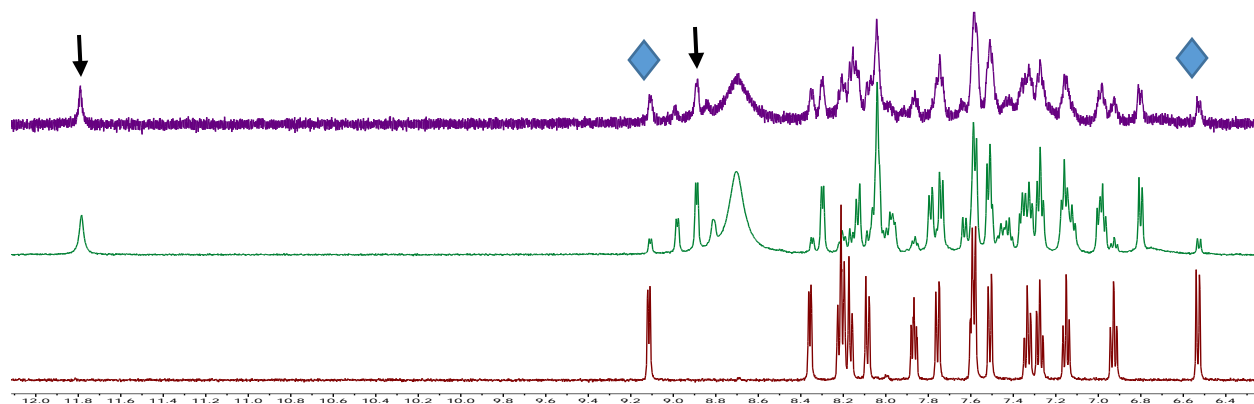


Figure 3.21 ^1H NMR spectrum of **61**(MeOH) in CD_3CN (bottom), 30 minutes after adding H_2O_2 (middle) and 60 minutes after addition of H_2O_2 (top). The intensity of the peak at 11.78 ppm was observed to decrease with time. Blue diamonds show **61** and arrows show **62**.

3.5 Isolation and characterization of the methanesulfonyl Pd(IV) amido aryl complex **63**

The Pd(IV) amido aryl complex **63** could be prepared in the most pure form from the dpk hydroperoxoketal – derived Pd(II) complex **62** isolated from a cold solution in THF and dried at room temperature. The solid **62** so-produced was stirred in MeCN and after 5 minutes was observed to dissolve completely. In 15 minutes after dissolution, a new precipitate formed and was isolated. ^1H NMR spectral analysis of this precipitate in $\text{DMSO}-d_6$ suggests that the solid is **63** containing less than 5% of **62** as the impurity (Fig. 3.22). The ^1H NMR spectrum of **63** exhibits two signals of the hydrogen atoms in the 6th positions of its two pyridine rings, each integrating as 1H and appearing as a doublet, one at 9.19 ($J = 5.9$ Hz) ppm and another at 9.00 ($J = 5.7$ Hz) ppm. The signal of the OH fragment of the hydrated dpk ligand integrating as 1H is observed as a sharp singlet at 8.22 ppm. The Pd(IV)-OH group proton produces an upfield shifted broadened singlet at 3.74 ppm. The signal of the SO_2Me group methyl is observed at 2.29 ppm. Due to the remarkable

availability of the amido aryl Pd(IV) complex **63**, its C-N reductive elimination reactivity could be studied in detail (see Chapter 4). To reveal existing reactivity trends in this high-valent Pd(IV) chemistry, we explored synthetic approaches to its more electron poorer analog bearing trifluoromethanesulfonyl group at the amido nitrogen atom.

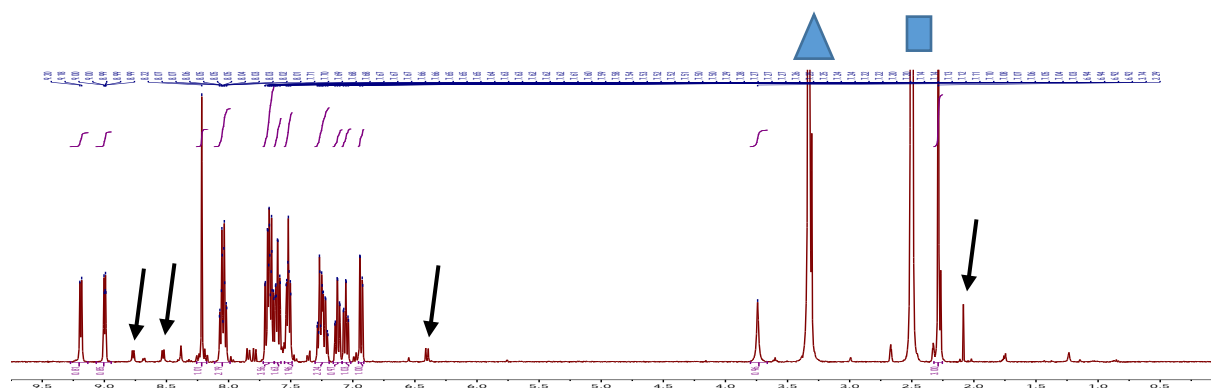


Figure 3.22 ^1H NMR spectrum in $\text{DMSO-}d_6$ of the Pd(IV) amido aryl complex **63** containing <5% of the dpk hydroperoxoketal – derived Pd(II) complex **62** as a major impurity. Black arrows show **62**, blue triangle shows (HOD + H_2O) and blue rectangle shows solvent residual signal $\text{DMSO-}d_6$

3.6 Characterization and reactivity of the N-trifluoromethanesulfonyl Pd(II) complex **66**·MeCN

3.6.1 Characterization of the N-trifluoromethanesulfonyl Pd(II) complex **66**·MeCN

Complex **66**·MeCN was prepared and isolated from MeCN solutions without using MeOH and shown by ^{13}C NMR spectroscopy to exist in CD_3CN in the keto-form **66**. There was no peak at about 95 ppm in its ^{13}C NMR spectra characteristic of the dpk ketal carbon whereas the signal

of the dpk carbonyl group at about 188 ppm was observed. ^{19}F NMR spectrum of **66** confirmed the presence of only one fluorine-containing species in solution. No signals were observed in the ESI(+)/MS spectrum of a methanol solution of **66** confirming the target compound as being neutral. In turn, ^1H NMR spectroscopy showed the presence of one mole of MeCN of crystallization per one formula unit of **66**. The composition **66**·MeCN was also confirmed by elemental analysis. Finally, the X-ray diffraction analysis of crystals of **66** grown from CH_3CN confirmed that **66** crystallized with one molecule of CH_3CN .

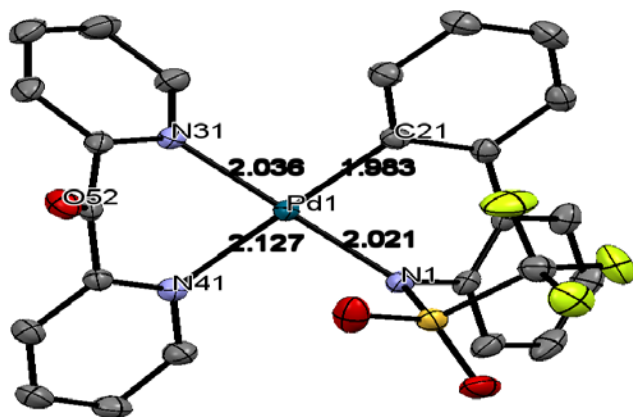


Figure 3.23 X-ray crystal structure of **66**·MeCN (the solvent of crystallization is not shown).

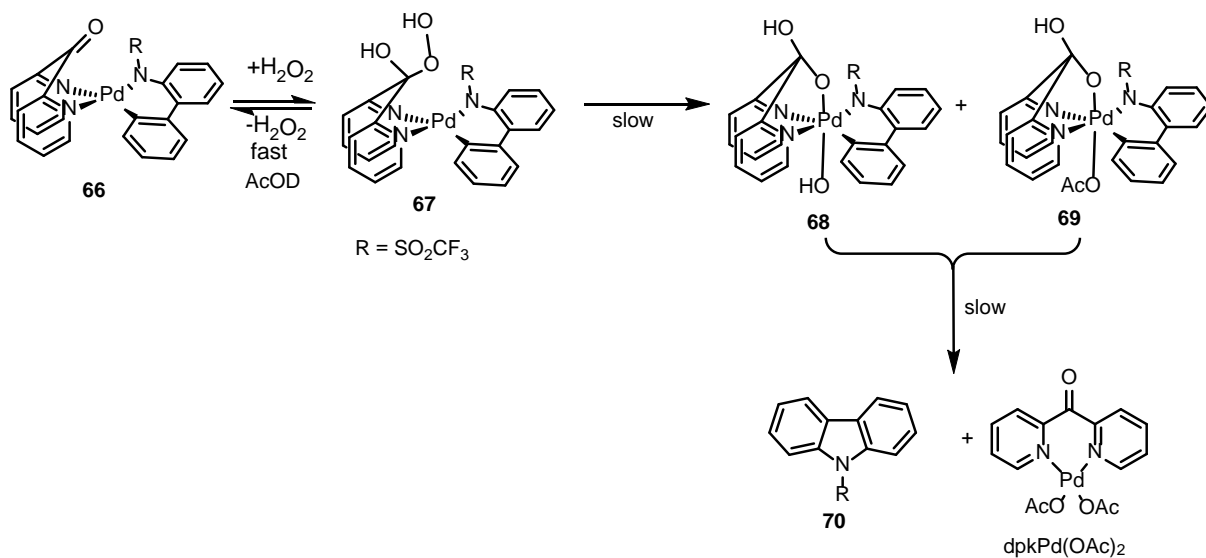
The X-ray diffraction of **66**·MeCN (Fig. 3.25) shows the square planar geometry around the palladium center, typical for Pd(II) complexes. The dpk fragment is coordinated to Pd in the $\kappa^2\text{-}N,N$ mode and the C=O group is out of the planes of either of the pyridine fragments forming a boat-like metal chelate ring. The C=O bond length of 1.212(2) Å is in strong agreement with a double bond character between C and O. The Pd1-N31 bond *trans*- to the aryl is longer (2.135(1) Å) relative to the Pd1-N21 (2.039(1) Å) bond *trans*- to the amido nitrogen atom which shows the stronger *trans*-influence of the aryl group in comparison to the amido fragment of the Pd bound

2'-aminobiphenyl-2-yl fragment. Also, the bond Pd1-C19 is shorter (1.986(1) Å) compared to Pd1-N11 (2.051(1) Å).

3.6.2 Reactivity of **66**·MeCN towards H₂O₂ in different solvents

3.6.2.1 AcOD (Scheme 3.16)

The compound **66**·MeCN is poorly soluble in AcOD; it forms a pale yellow solution. ¹H NMR spectroscopy showed the presence of a single metal complex in the solution.



Scheme 3.16 Reactivity of **66** toward H₂O₂ to form **70** in AcOD.

Upon addition of 3 equivalents of H₂O₂ to a suspension of **66** and stirring for about 12 h, all the solid had dissolved and a reddish brown solution was produced. ¹H NMR spectral analysis of the solution showed the presence of 13% of unreacted **66**, 38% of each the carbazole **70** and Pd(dpk)(OAc)₂ which confirms that reductive elimination had taken place, and two intermediates,

68 and **69**, in 49 % combined yield (Fig. 3.24). No peaks of interest were observed in the ESI(+)/MS spectrum of the resulting solution. When the reddish brown solution formed after 12 h was warmed up at 60 °C for 30 min, the carbazole **70** was produced as the only organic product in 98% yield together with Pd(dpk)(OAc)₂. Our attempts to isolate intermediates **69** and **68** were not successful. The slow rate of dissolution, coupled with Pd(II)-to-Pd(IV) oxidation and carbazole elimination made us propose a mechanism, where the rates of the Pd(II)-to-Pd(IV) oxidation and the C-N reductive elimination are comparable.

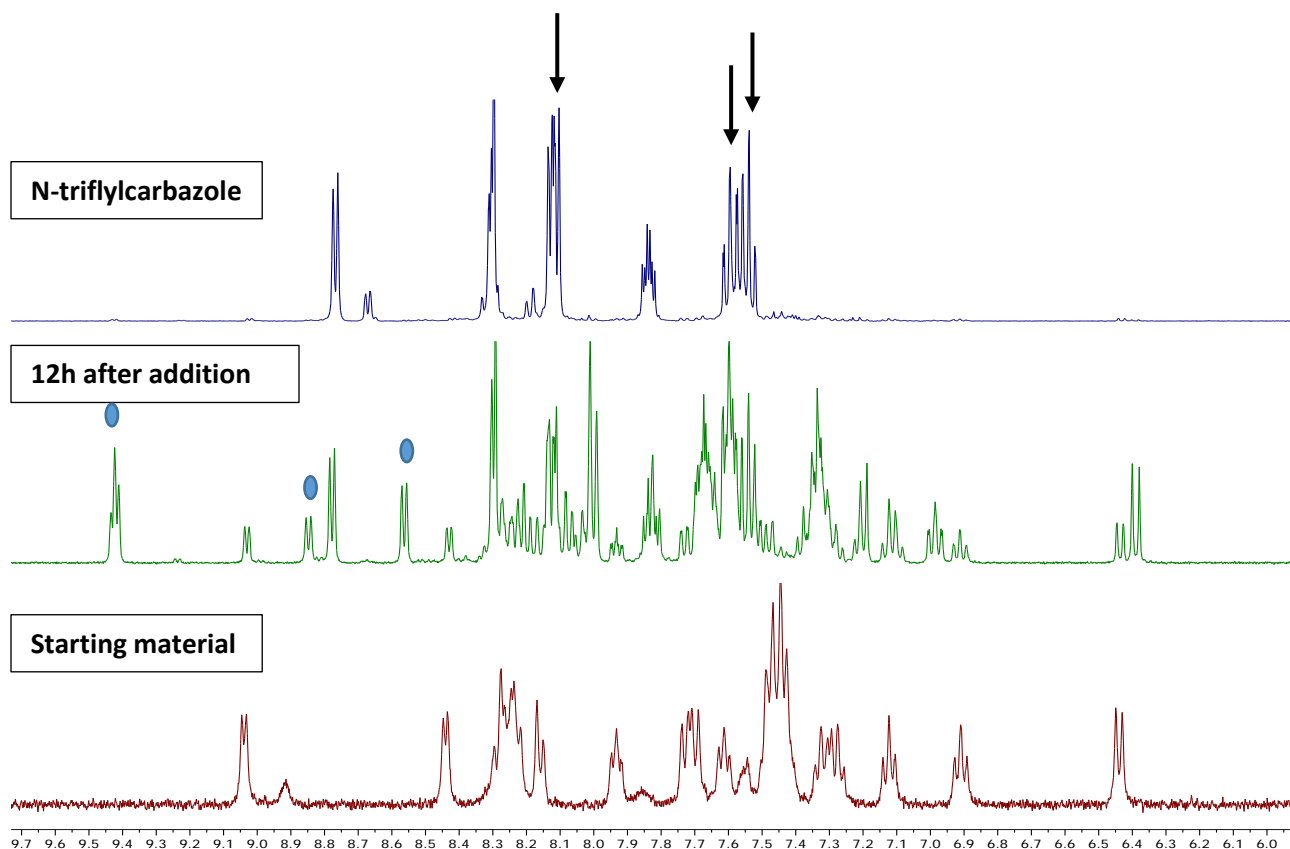


Figure 3.24 Oxidation of **65** with 3 eq of H₂O₂ in AcOD at 22 °C. Arrows show product peaks. Blue circles show two intermediates **68** and **69**.

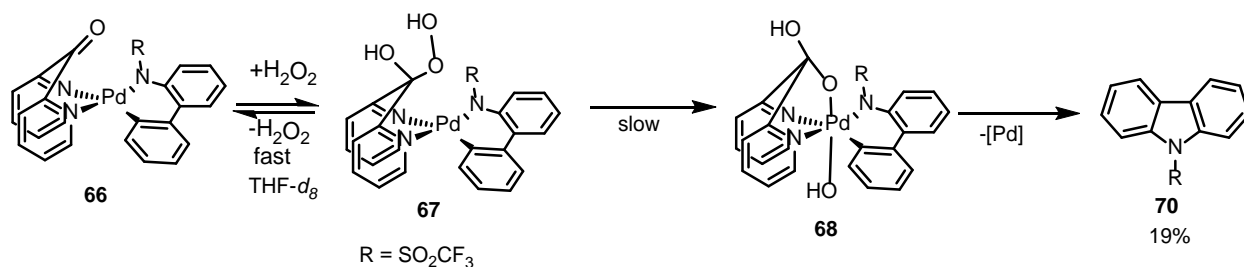
3.6.2.2 MeOD

The compound **66**·MeCN is virtually insoluble in MeOD; no signals were observed in the ^1H NMR spectrum of the mixture after stirring it for 12 h. Addition of 3 equiv of H_2O_2 led to a gradual dissolution of **66** to form a reddish brown solution. ^1H NMR spectrum after 12 hours showed the formation of 4 different species in solution in a ratio of 1:0.9:0.4:0.5, based on the intensity of their signals associated with the hydrogen atoms in the 6th position of the pyridine rings. The identity of the four species in solution could not be determined. When the mixture was left for 7 days, only one of the species was observed in solution; no **70** formed, according to ^{19}F NMR spectroscopy. These results suggest that the Pd(II)-to-Pd(IV) oxidation did not occur at any appreciable rate whereas the C-N reductive elimination was expected to be observable in MeOD under these conditions (*vide infra*).

3.6.2.3 THF (Scheme 3.17)

A combination of a yellow solution of **66**·MeCN in THF- d_8 with 3 equivalents of H_2O_2 led to a rapid change of color to a very light yellow. ^1H NMR spectral analysis of the resulting mixture after about 30 minutes showed the formation of two new species in 80% combined yield which were assigned to the isomeric dpk hydroperoxoketal – derived complexes **67** with *endo*- and *exo*-orientation of the OOH group with respect to the metal chelate ring. Unreacted **66** was observed in 20% yield. The signals of the hydrogen atoms in the 6th position of the pyridyl groups of the resulting species were upfield shifted as compared to the starting material **66** (Fig. 3.25). In turn, two signals assigned to the OOH group protons of *endo*- and *exo*-isomeric **67** appeared at

11.03 ppm and 10.59 in a ratio of 5:1, respectively, which is similar to other systems studied in this work previously.



Scheme 3.17 Reactivity of **66** toward H₂O₂ in THF-*d*₈ to form **70**.

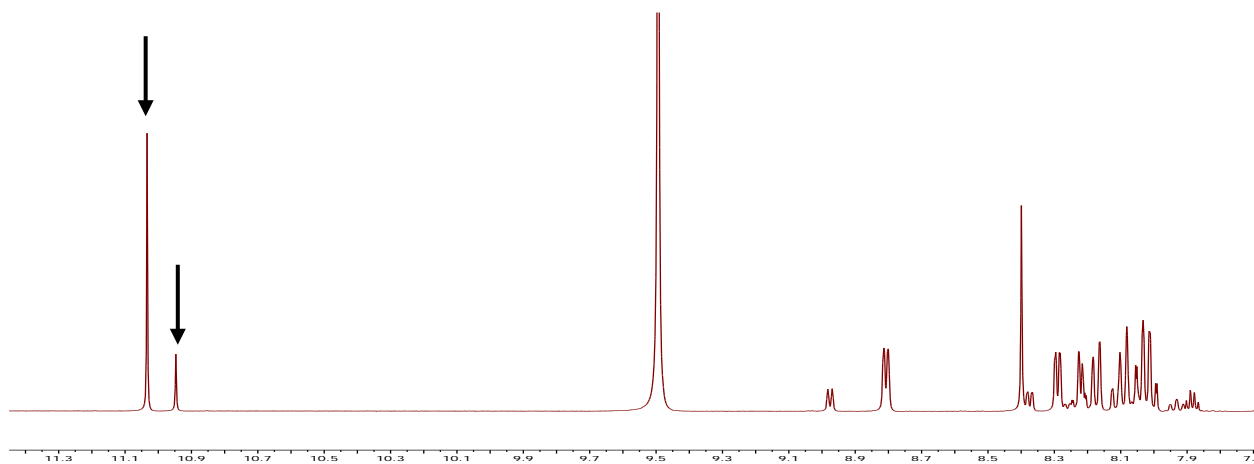


Figure 3.25 ¹H NMR spectrum of a 5:1 mixture of *endo*- and *exo*-isomers of **67** in THF-*d*₈ with arrows showing the peroxyketal signals at 11.03 ppm and 10.59 ppm.

When the solution containing **66** was left for 24 h at 22 °C, ¹H NMR spectroscopy showed the reformation of **66** so that its total fraction in the mixture was 55% whereas the fraction of **67** had decreased to 17%. Formation of a new species in 16% yield having more downfield shifted

signals of the *ortho*-pyridyl protons (9.21 ppm and 9.14 ppm), as compared to the starting material (8.97 ppm) was also observed in solution. This new species was assigned to the Pd(IV) amido aryl complex **68** by using an authentic sample of independently synthesized **68** (*vide infra*). Finally, about 12% of the carbazole product **70** was also present in the solution (^{19}F NMR).

The formation of the carbazole **70** and reformation **66** after 24 h suggest that the Pd(II)-to-Pd(IV) transformation (**67**-to-**68**) is slow and comparable with H_2O_2 decomposition. The slow oxidation may be attributed to the presence of a very strong electron withdrawing triflyl group placed on the amido nitrogen atom.

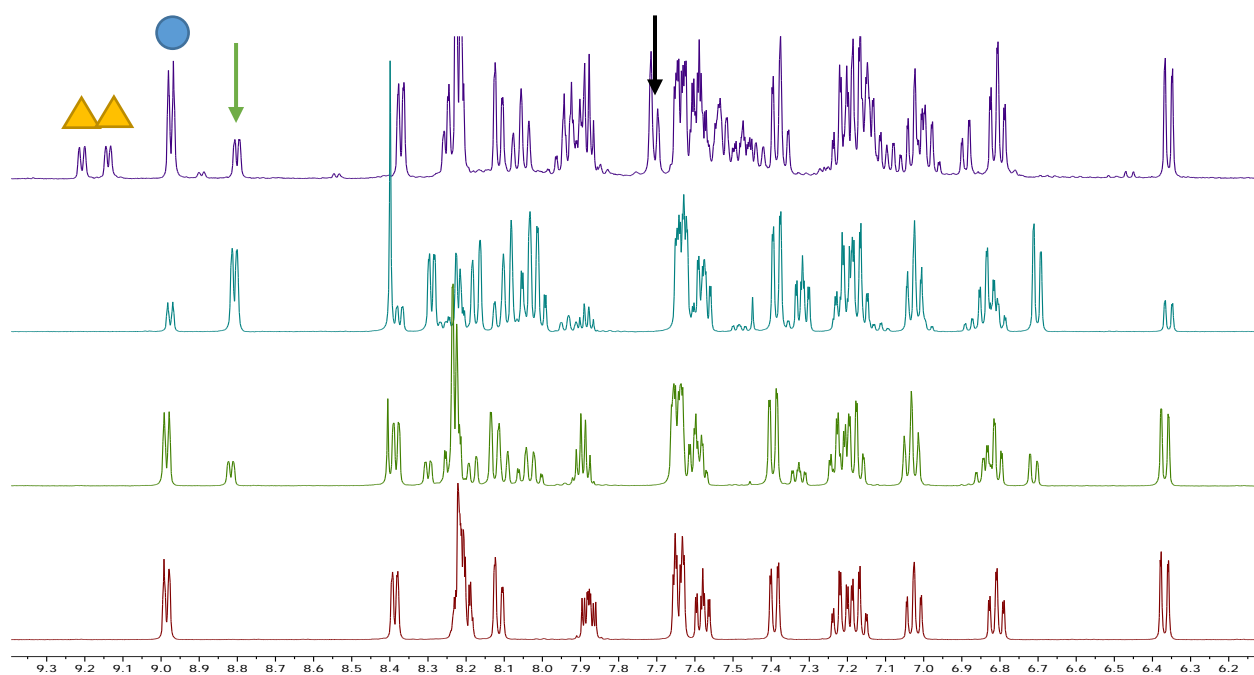
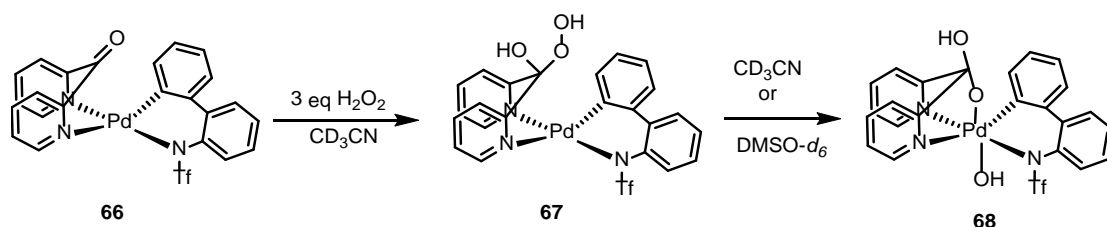


Figure 3.26 ^1H NMR monitoring of the reaction of **66** with H_2O_2 in $\text{THF-}d_8$ at $22\text{ }^\circ\text{C}$. Green arrow shows the major dpk hydroperoxoketal – supported complex **67**, yellow triangles show the derived Pd(IV) amido aryl complex **68**, blue circle labels **66** and black arrow shows **70** in solution: (i) **66** in solution before addition of H_2O_2 , (ii) 20 minutes after addition (iii) 60 minutes after addition (iv) 22 hours after addition.

3.6.2.4 CD₃CN (Scheme 3.18)

The compound **66**·MeCN dissolves readily in CD₃CN to give a yellow solution. When the resulting solution was combined with 3 eq of H₂O₂, there was no change in the ¹H NMR spectrum for about 30 minutes but after 1 h an off-white precipitate **67** formed which was isolated. ¹H NMR spectrum of this compound DMSO-*d*₆ showed the presence of a single species. Interestingly, solutions of **67** in DMSO-*d*₆ were observed to gradually change their color from an almost colorless to orange. ¹H NMR monitoring of these solutions showed the gradual conversion of **67** to the Pd(IV) amido aryl complex **68** (Fig. 3.27-3.28) following clean 1st order kinetics (Fig. 3.29) with the half-life of 50±3 min at 22 °C.



Scheme 3.18 Reactivity of **66** toward H₂O₂ to form **68** in CD₃CN.

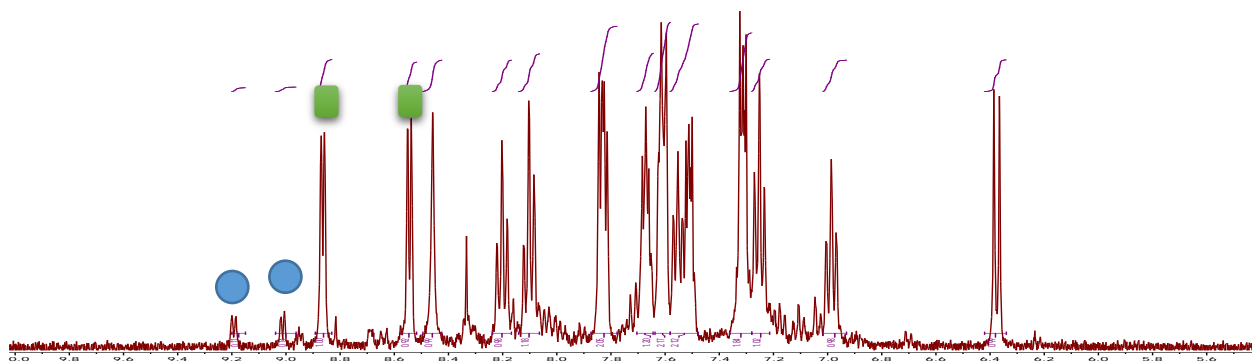


Figure 3.27 ¹H NMR spectrum showing the conversion of **67** into **68** DMSO-*d*₆. Green squares are ortho-pyridyl signals of **67**, blue circles are ortho-pyridyl signals for **68**.

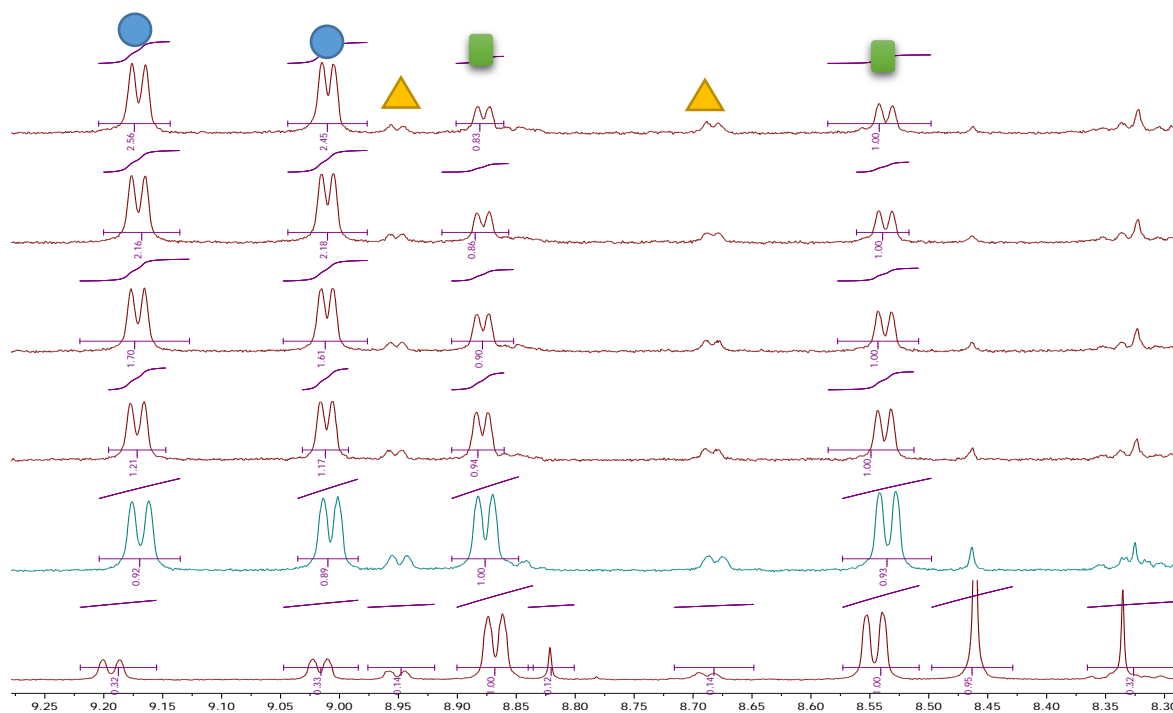


Figure 3.28. A detailed picture of the downfield region of ^1H NMR spectrum showing the conversion of **67** to **68** in $\text{DMSO-}d_6$. Green squares correspond to the *ortho*-pyridyl signals of **67**, blue circles correspond to **68** and yellow triangles are **66**.

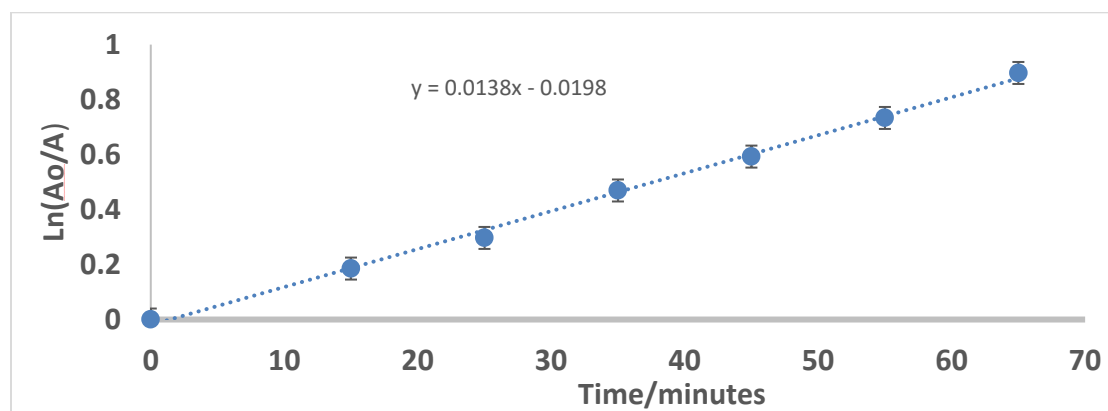


Figure 3.29. Plot of $\ln([\mathbf{67}]_0/[\mathbf{67}])$ vs time in $\text{DMSO-}d_6$. The reaction first order rate constant is $(1.38 \pm 0.03) \times 10^{-3} \text{ min}^{-1}$ giving the reaction half-life of $50 \pm 3 \text{ min}$.

3.7 Synthesis of the N-trifluoromethanesulfonyl Pd(IV) amido aryl complex **68**

The Pd(IV) amido aryl complex **68** could be synthesized in a reasonably pure (96%+) form by adding 10 equivalents of H₂O₂ to **66** dissolved in CH₃CN and stirring the solution for 24 hours. The off-white precipitate of **67** which forms initially gradually turns orange. The orange solid is filtered off and washed with cold CH₃CN to afford orange crystals of **68** in 83% yield. The product usually contains < 4% of **66** and **67** altogether even when more H₂O₂ is used and the reaction time increased to 7 days. Our attempts to recrystallize **68** to get rid of **67** and **66** were not successful.

The C-N reductive elimination reactivity of **68** could be studied in detail (see Chapter 4).

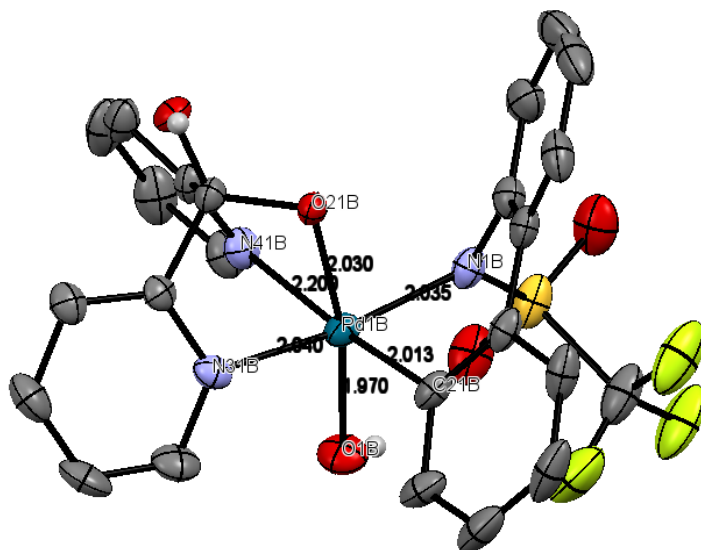


Figure 3.30 X-ray crystal structure of **68**. Selected bond lengths (Å): Pd1B-N1B 2.035 (3), Pd1B-O1B 1.970 (2), Pd1B-O21B 2.030 (2), Pd1B-N31B 2.040 (3), Pd1B-N41B 2.200 (2), Pd1B-C21B 2.013 (2)

3.8 Conclusions

In summary, we synthesized a number of N-substituted amido aryl Pd(II) complexes bearing various electron withdrawing groups R at the amido nitrogen atom (R = COCH₃, COCF₃, SO₂CH₃ and SO₂CF₃) supported by dpk ligand, **50**, **51**, **61**, **66**. For the first time, we have demonstrated clean oxidation of the latter complexes with H₂O₂ to form moderately stable or even very stable amido aryl Pd(IV) derivatives through the use of *fac*-chelating hydrated dpk ligand. The latter ligand provides both thermodynamic and kinetic stabilization to the Pd(IV) center. The rates of oxidation of the pallada(II)cycles **50**, **51**, **61**, **66** with H₂O₂ and subsequent C-N reductive elimination of the resulting Pd(IV) species are a function of solvent used and the nature of the R-group at the amido fragment. The N-acetyl substituted Pd(II) complex **50** (R=COCH₃) reacts at the fastest rate with H₂O₂ in all solvents (MeOH, THF, AcOH and CH₃CN). In MeCN solution we were able to observe the derived amido aryl Pd(IV) complex **53** as a major species and monitor its C-N coupling to produce a carbazole.

The N-methanesulfonyl substituted Pd(II) complex **61** (R=SO₂CH₃) reacts with H₂O₂ at slower rates, as compared to **50**. Notably, by exploiting the difference in solubility in THF of **61** and the derived hydroperoxyketal Pd(II) intermediate **62**, the latter Pd(II) compound could be isolated and characterized by single crystal X-ray diffraction. In turn, in CH₃CN solution, the hydroperoxyketal intermediate **62** could be cleanly converted to a poorly soluble isolable amido aryl Pd(IV) complex **63**, which appears to be less reactive in C-N coupling as compared to its N-acetyl analog **57**.

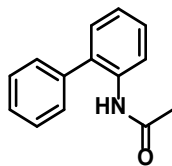
The use of an even more electron-withdrawing group $R = \text{SO}_2\text{CF}_3$, leads to an even more difficult oxidation of the derived Pd(II) amido aryl complex **66** to give the Pd(IV) species **68**. This reaction is only efficient in acetylperoxide-forming solvents, MeCN and AcOH. Once again, by using difference in solubility in MeCN of **66** and the derived Pd(II) hydroperoxoketal **67** and the Pd(IV) amido aryl complex **68** these two intermediates could also be isolated. The latter compound was also structurally characterized by XRD and was found to be poorly reactive in C-N coupling.

Finally, when R was changed to a more electron-withdrawing COCF_3 , the Pd(II)-to-Pd(IV) oxidation could be accomplished at 22 °C only in AcOD. In other solvents, MeOD, THF and CH_3CN , higher temperatures were needed to promote formation of the corresponding carbazole. Some of the amido aryl Pd(IV) intermediates could also be isolated from H_2O_2 -AcOH mixtures. These Pd(IV) compounds are very robust when it comes to C-N coupling.

Overall, the use of Pd(II) aryl complexes bearing electron-poor amido ligands was very fruitful in terms of our ability to get an access to the key intermediates involved in Pd-mediated oxidative $\text{C}(\text{sp}^2)$ -N coupling. Most of the anticipated intermediates could be isolated which allowed us to study their reactivity in more detail and establish some important structure-reactivity relationships.

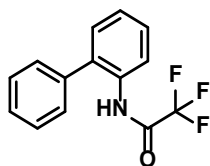
3.9 Experimental

N-acyl-2-aminobiphenyl, (46)



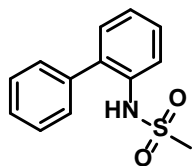
2.0 g of **25** was stirred in 5.0 mL of acetic anhydride vigorously for 10 min. A white precipitate forms which is poured onto ice, allowed to stand for about 1 hour and filtered. Recrystallization from water gives 2.2 g (87% yield) of target product. ^1H NMR (400 MHz, Chloroform-*d*) δ 8.27 (d, $J = 8.3$ Hz, 1H), 7.49 (dd, $J = 8.1, 6.5$ Hz, 2H), 7.45 – 7.41 (m, 1H), 7.37 (ddd, $J = 8.3, 5.2, 1.8$ Hz, 3H), 7.25 (d, $J = 8.9$ Hz, 1H), 7.16 (dd, $J = 18.0, 10.6$ Hz, 2H), 2.02 (s, 3H).

N-trifluoroacetyl-2-aminobiphenyl, (47)



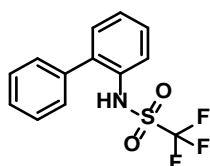
Trifluoroacetic anhydride (0.85 mL, 6.0 mmol, 1.25 equiv) was added dropwise to 1.0 g (6.0 mmol) of **25** in 15mL of dichloromethane in a round bottom flask cooled by an ice bath. This was allowed to warm to room temperature and stirred for 6 hours at room temperature. The solution was washed with 1N aqueous HCl (20mL) and dried with anhydrous Na_2SO_4 . Removal of the solvent on a rotavap yielded 1.2g (of crystals. ^1H NMR (400 MHz, Chloroform-*d*) δ 8.33 (dd, $J = 8.2, 1.1$ Hz, 1H), 8.01 (s, 1H), 7.60 – 7.44 (m, 4H), 7.42 – 7.30 (m, 4H).

Synthesis of N-methanesulfonyl-2-aminobiphenyl, (48)



1.0g (6.0 mmol) of **25** was dissolved in dry pyridine (15 mL flask equipped with a reflux condenser). Methanesulfonyl chloride (0.35 mL, 6.1 mmol, 1.05 equiv) was added dropwise at room temperature. The reaction mixture was stirred at room temperature for 12 h, then evaporated under reduced pressure. The crude product was dissolved in dichloromethane, washed with water and brine, dried over MgSO₄ and concentrated under reduced pressure and 1.1g(75% crude yield) of target compound was isolated. ¹H NMR shows the presence of pyridine signals. ¹H NMR (400 MHz, Chloroform-*d*) δ 8.70 – 8.55 (m, 3H), 7.76 – 7.62 (m, 2H), 7.57 – 7.19 (m, 11H), 6.58 (s, 1H), 2.89 (s, 3H).

N-trifluoromethanesulfonyl-2-aminobiphenyl, (48):

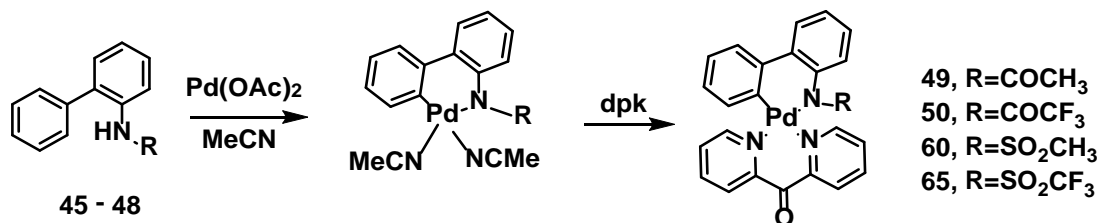


Triflic anhydride (0.45 mL, 6.0 mmol, 1.0 equiv) was added dropwise to a solution of 2-aminobiphenyl (1.0 g, 6.0 mmol, 1.0 equiv) and triethylamine(0.8 mL, 6.0 mmol, 1.0 equiv) in CH₂Cl₂ (20.0 mL) at -78°C(dry ice in acetone). The solution was allowed to warm to room temperature and stirred for 16 h. Then the mixture was washed with water (2 x 20 mL) and brine (20 mL), dried over MgSO₄ and evaporated under reduced pressure to give a brown liquid which solidifies after standing for over a week at room temperature. ¹H NMR (400 MHz, Chloroform-*d*)

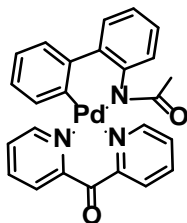
δ 7.70 – 7.65 (m, 1H), 7.58 – 7.46 (m, 3H), 7.43 (ddd, $J = 8.3, 5.9, 3.3$ Hz, 1H), 7.38 – 7.30 (m, 4H), 6.70 (s, 1H).

General procedure for the synthesis of 2-aminobiphenylPd dpk substrates (49, 50, 60 and 65)

0.50g (2.2 mmol) of Pd(OAc)₂ was weighed and combined in 20.0 mL of CH₃CN to form a suspension. Then 1.1 equivalents of substrates **45-48** was added to the suspension and heated at (60-80)°C for between 3-14 hours. Palladium black was observed and the resulting solution was filtered through Celite and used in further synthesis without isolation. 0.9 equivalents of dpk is dissolved in CH₃CN and the dpk solution was added dropwise to the palladacycle solution. After stirring the mixture for 4h, solvent is removed on a rotavap. 15mL of MeOH (**50** and **60**) or Et₂O(only for **49**) was added to the residue and stirred for 2h and the target compound crystallizes out of solution. The precipitate is washed with cold MeOH or Et₂O to afford target compound. **65** crystallized directly from CH₃CN solution.

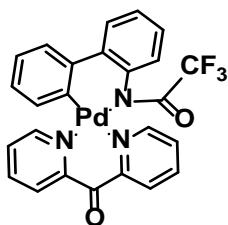


N-acyl-2-aminobiphenylPddpk (49) :



Yellowish orange solid, (63% yield) : ^1H NMR (400 MHz, Methanol- d_4) δ 8.69 (d, $J = 5.2$ Hz, 1H), 8.22 (dd, $J = 5.7, 1.6$ Hz, 1H), 8.15 – 8.10 (m, 1H), 8.08 – 8.02 (m, 2H), 7.98 (td, $J = 7.8, 1.7$ Hz, 1H), 7.66 (dd, $J = 7.7, 1.5$ Hz, 1H), 7.56 (td, $J = 5.4, 3.4$ Hz, 1H), 7.45 (ddd, $J = 10.3, 7.7, 1.4$ Hz, 2H), 7.31 – 7.20 (m, 2H), 7.14 (td, $J = 7.5, 1.3$ Hz, 1H), 7.10 – 7.04 (m, 1H), 6.96 – 6.87 (m, 2H), 2.21 (s, 3H) ^{13}C NMR (126 MHz, Acetic) δ 186.34, 173.64, 154.35, 152.35, 152.19, 150.84, 150.31, 149.28, 141.51, 141.25, 140.95, 140.49, 140.29, 139.83, 138.50, 138.25, 136.21, 135.51, 129.28, 128.83, 128.49, 128.24, 127.57, 127.22, 127.16, 126.62, 126.39, 125.98, 125.63, 125.53, 125.32, 125.10, 124.05, 123.94, 123.71, 48.61, 24.92, 16.66.

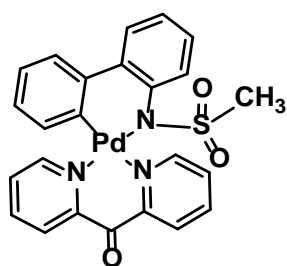
N-trifluoroacetyl-2-aminobiphenylPddpk, (50) :



Off white solid (65% yield) : ^1H NMR (400 MHz, Acetic Acid- d_4) δ 8.83 (d, $J = 5.2$ Hz, 1H), 8.31 – 8.18 (m, 4H), 8.15 (dd, $J = 8.0, 1.5$ Hz, 1H), 7.95 (td, $J = 5.5, 3.1$ Hz, 1H), 7.78 (dd, $J = 7.7, 1.5$ Hz, 1H), 7.69 – 7.62 (m, 1H), 7.58 (ddd, $J = 7.4, 5.5, 1.6$ Hz, 1H), 7.50 (dd, $J = 7.7, 1.4$ Hz, 1H), 7.38 (td, $J = 7.6, 1.5$ Hz, 1H), 7.35 – 7.28 (m, 1H), 7.12 (t, $J = 7.4$ Hz, 1H), 6.93 (d, $J = 6.9$ Hz,

1H), 6.46 (d, $J = 7.6$ Hz, 1H). ^{13}C NMR (126 MHz, Acetic) δ 186.59, 160.04, 159.77, 154.30, 152.51, 151.00, 150.52, 148.44, 140.61, 140.59, 140.39, 140.24, 140.19, 138.34, 135.04, 129.11, 128.28, 127.25, 127.17, 127.13, 126.25, 125.71, 125.53, 125.44, 125.24, 124.98, 124.51, 118.58, 116.30, 48.61. Anal. Found / Calculated ($\text{C}_{25}\text{H}_{16}\text{F}_3\text{N}_3\text{O}_2\text{Pd}$).MeOH: C:53.00/53.30, H : 3.67/3.44, N : 7.20 /7.17

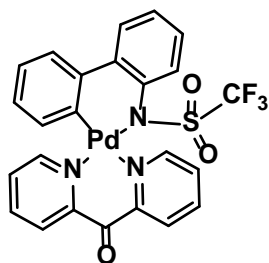
N-methanesulfonyl-2-aminobiphenylPddpk, (61):



Yellow solid, 1.38g (58% yield). ^1H NMR (500 MHz, $\text{THF-}d_8$) δ 9.29 (s, 1H), 8.52 (d, $J = 5.5$ Hz, 1H), 8.35 – 8.21 (m, 3H), 8.20 (d, $J = 7.9$ Hz, 1H), 7.96 – 7.88 (m, 1H), 7.77 – 7.70 (m, 2H), 7.66 (ddt, $J = 7.4, 5.5, 1.5$ Hz, 1H), 7.53 (dd, $J = 7.7, 1.6$ Hz, 1H), 7.32 – 7.25 (m, 1H), 7.25 – 7.19 (m, 1H), 7.17 – 7.11 (m, 1H), 6.97 – 6.85 (m, 1H), 6.65 – 6.54 (m, 1H), 1.88 (s, 3H). ^{13}C NMR (126 MHz, Acetic) δ 186.83, 154.71, 152.63, 151.25, 150.36, 148.39, 143.16, 139.94, 139.80, 139.62, 139.06, 136.29, 128.67, 128.54, 128.16, 127.30, 126.97, 126.36, 125.56, 125.44, 124.95, 124.66, 37.49.

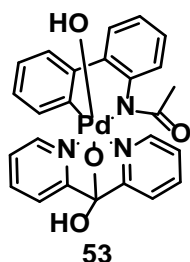
Anal. Found / calc for $\text{C}_{24}\text{H}_{19}\text{N}_3\text{O}_3\text{PdS}$: C: 53.53/53.79, H: 3.38/3.57, N: 7.96 /7.84

N-trifluoromethanesulfonyl-2-aminobiphenylPddpk, (66):



Yellow solid, (65% yield): ^1H NMR (400 MHz, Acetic Acid- d_4) δ 8.84 – 8.77 (m, 1H), 8.31 – 8.15 (m, 4H), 8.12 (d, $J = 8.0$ Hz, 1H), 7.97 – 7.89 (m, 1H), 7.77 (dd, $J = 7.7, 1.7$ Hz, 1H), 7.64 (dd, $J = 7.7, 1.6$ Hz, 1H), 7.54 (ddd, $J = 7.5, 5.6, 1.6$ Hz, 1H), 7.48 (dd, $J = 7.7, 1.5$ Hz, 1H), 7.38 (dd, $J = 8.4, 6.7$ Hz, 1H), 7.30 (dd, $J = 8.3, 6.7$ Hz, 1H), 7.10 (s, 1H), 6.91 (t, $J = 7.5$ Hz, 1H), 6.45 (d, $J = 7.6$ Hz, 1H). ^{13}C NMR (101 MHz, CD_3CN) δ 187.66, 154.88, 153.06, 151.27, 151.23, 147.96, 142.81, 141.07, 140.68, 139.31, 138.98, 136.51, 129.08, 129.06, 127.98, 127.47, 127.44, 127.31, 126.89, 125.98, 125.74, 125.63, 125.08, 122.75, 119.50. ^{19}F NMR (376 MHz, CD_3CN) δ -76.27 Anal. Found / Calculated for $\text{C}_{24}\text{H}_{16}\text{F}_3\text{N}_3\text{O}_3\text{PdS}\cdot\text{CH}_3\text{CN}$: C : 49.37/49.50, H : 3.04/3.44, N : 8.40 /8.88

Synthesis and reductive elimination from 53



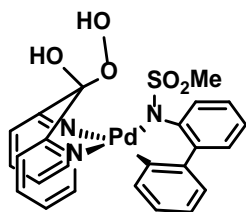
An NMR tube was charged with 10 mg of **49**. 0.6 mL of CD_3CN is added together with 3 equivalents of H_2O_2 and monitored by ^1H NMR at 22 $^\circ\text{C}$. **53** was observed to form in 88% yield

in solution 15 minutes after addition of H₂O₂ but could not be isolated. **53** was slowly observed to reductively eliminate **54**.

¹H NMR (500 MHz, Acetonitrile-*d*₃) δ 9.12 (d, *J* = 5.1 Hz, 1H), 8.73 (d, *J* = 5.4 Hz, 1H), 8.00 – 7.89 (m, 2H), 7.79 (d, *J* = 7.4 Hz, 1H), 7.73 (d, *J* = 8.1 Hz, 1H), 7.59 (d, *J* = 7.8 Hz, 1H), 7.41 – 7.31 (m, 1H), 7.24 (t, *J* = 7.4 Hz, 1H), 7.15 – 7.10 (m, 1H), 6.84 (d, *J* = 7.8 Hz, 1H), 1.96 (s, 3H).

Synthesis of 62

A combination of 15 mg of **61** in 0.6 mL THF with 3 equivalents of H₂O₂ led to a slow formation of **62** which, due to its poor solubility, could be isolated as a crystalline solid at 0 °C. The crystals were suitable for single crystal X-ray diffraction analysis.

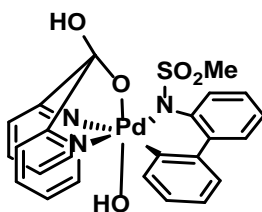


¹H NMR (500 MHz, THF-*d*₈) δ Major: 11.91 (s, 1H), 8.96 (d, *J* = 5.1 Hz, 1H), 8.36 (d, *J* = 5.3 Hz, 1H), 8.31 (s, 1H), 8.20 (d, *J* = 8.1 Hz, 1H), 8.07 (dd, *J* = 13.1, 7.8 Hz, 2H), 8.00 (t, *J* = 7.8 Hz, 1H), 7.65 (dd, *J* = 16.6, 7.7 Hz, 2H), 7.56 (t, *J* = 6.4 Hz, 1H), 7.46 (d, *J* = 7.4 Hz, 1H), 7.34 (t, *J* = 6.5 Hz, 1H), 7.22 (t, *J* = 7.5 Hz, 1H), 7.15 (t, *J* = 7.6 Hz, 1H), 7.08 (t, *J* = 7.2 Hz, 1H), 6.88 (t, *J* = 7.1 Hz, 1H), 6.83 (d, *J* = 7.5 Hz, 1H), 2.07 (s, 3H).

Minor δ 8.93 (d, *J* = 5.2 Hz, 1H), 8.14 (d, *J* = 8.0 Hz, 1H), 7.51 (t, *J* = 6.4 Hz, 1H), 7.26 (t, *J* = 6.6 Hz, 1H), 6.94 (d, *J* = 7.4 Hz, 1H)(Other minor peaks are buried under the major ones)

Synthesis of 63

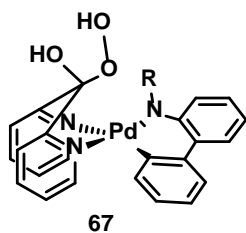
A combination of 15 mg of **61** in 1.0 mL with 3 equivalents of H₂O₂ in CH₃CN led to a slow formation of **63** as an orange solid in 4 h. The orange solid was filtered off and washed with cold CH₃CN; yield 68%. All attempts to grow crystals suitable for X-ray diffraction for **63** were not successful.



¹H NMR (400 MHz, DMSO-*d*₆) δ 9.19 (d, *J* = 5.9 Hz, 1H), 9.07 – 8.94 (m, 1H), 8.22 (s, 1H), 8.04 (tdd, *J* = 7.7, 6.5, 1.5 Hz, 2H), 7.72 – 7.63 (m, 3H), 7.63 – 7.58 (m, 2H), 7.52 (ddd, *J* = 7.6, 5.6, 1.7 Hz, 2H), 7.30 – 7.19 (m, 2H), 7.12 (td, *J* = 7.4, 1.5 Hz, 1H), 7.06 (td, *J* = 7.6, 1.6 Hz, 1H), 6.93 (dd, *J* = 7.9, 1.4 Hz, 1H), 3.74 (s, 1H), 2.29 (s, 3H). ¹³C NMR (101 MHz, DMSO-*d*₆) δ 164.94, 162.01, 148.65, 146.68, 145.73, 140.68, 139.51, 138.55, 137.26, 130.57, 128.80, 128.13, 127.47, 127.30, 126.27, 126.18, 125.99, 124.78, 121.99, 102.60.

Synthesis of 67

Addition of 3 equivalents of H₂O₂ to 10mg of **66** in THF-*d*₈ led to formation of **67** containing presumably its minor isomer with an *exo*-orientation of the -OOH group.

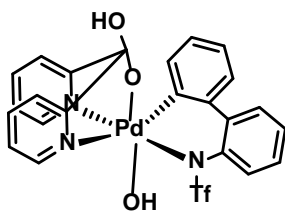


¹H NMR (400 MHz, THF-*d*₈) Major: δ 11.03 (s, 1H), 8.81 (dt, *J* = 5.3, 1.1 Hz, 1H), 8.40 (s, 1H), 8.29 (dd, *J* = 5.6, 1.6 Hz, 1H), 8.23 – 8.20 (m, 1H), 8.17 (dd, *J* = 8.0, 1.4 Hz, 1H), 8.09 (dt, *J* = 8.0, 1.1 Hz, 1H), 8.07 – 7.98 (m, 2H), 7.64 (ddd, *J* = 7.7, 4.0, 1.7 Hz, 1H), 7.61 – 7.56 (m, 1H), 7.39 (dd, *J* = 7.7, 1.5 Hz, 1H), 7.32 (ddd, *J* = 7.3, 5.5, 1.5 Hz, 1H), 7.19 (dtd, *J* = 17.6, 7.4, 1.7 Hz, 2H), 7.03 (td, *J* = 7.3, 1.3 Hz, 1H), 6.87 – 6.80 (m, 1H), 6.70 (dd, *J* = 7.6, 1.3 Hz, 1H).

Minor: δ 10.95 (s, 1H), 8.98 (d, *J* = 5.2 Hz, 1H), 8.37 (dd, *J* = 6.0, 1.2 Hz, 2H), 7.98 – 7.92 (m, 1H), 7.89 (dt, *J* = 9.5, 4.4 Hz, 2H), 7.48 (ddd, *J* = 7.6, 5.2, 1.3 Hz, 1H), 7.45 (s, 1H), 7.11 (td, *J* = 7.4, 1.5 Hz, 1H), 6.88 (dd, *J* = 7.6, 1.4 Hz, 1H), 6.36 (dd, *J* = 7.6, 1.2 Hz, 2H).

Synthesis of 68

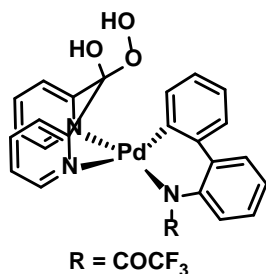
68 was synthesized by adding 10 equivalents of H₂O₂ to 50 mg of **66** dissolved in CH₃CN (5.0 mL) and stirring the solution for 24 hours. The off-white precipitate which forms initially gradually turns orange. The orange solid was filtered off and washed with cold CH₃CN; yield 83%. The product usually contains < 4% of **66** and **67** even when more H₂O₂ is used and the reaction time increased to 7 days. Attempts at getting an elemental analysis of **68** was not successful since it slowly decomposes at room temperature.



^1H NMR (400 MHz, $\text{DMSO-}d_6$) δ 9.19 (dd, $J = 5.9, 1.3$ Hz, 1H), 9.01 (dd, $J = 5.3, 1.2$ Hz, 1H), 8.33 (s, 1H), 8.07 (tdd, $J = 7.7, 3.5, 1.4$ Hz, 2H), 7.71 (dt, $J = 8.0, 1.2$ Hz, 1H), 7.69 – 7.64 (m, 3H), 7.60 (dd, $J = 7.8, 1.6$ Hz, 1H), 7.50 (td, $J = 7.6, 1.9$ Hz, 2H), 7.25 (pd, $J = 7.1, 1.6$ Hz, 2H), 7.17 (td, $J = 7.5, 1.5$ Hz, 1H), 7.10 (td, $J = 7.6, 1.6$ Hz, 1H), 7.03 (dd, $J = 8.0, 1.4$ Hz, 1H), 3.71 (s, 1H). ^{13}C NMR (126 MHz, DMSO) δ 164.78, 161.60, 148.23, 146.09, 144.97, 142.22, 140.67, 138.94, 138.01, 136.58, 131.11, 128.46, 127.67, 127.59, 127.49, 127.31, 127.13, 126.16, 126.09, 124.97, 121.84, 120.86, 102.13. ^{19}F NMR (376 MHz, DMSO) δ -74.23.

Synthesis of **56**

Addition of 3.0 equiv of H_2O_2 to 15 mg of **50** in THF rapidly produced **56** in solution.



56

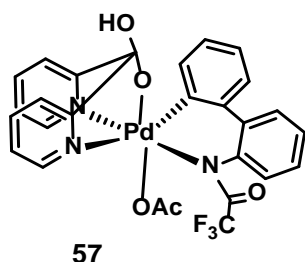
^1H NMR (500 MHz, $\text{THF-}d_8$) δ (Major) 14.12 (s, 1H), 9.04 (dd, $J = 5.2, 1.5$ Hz, 1H), 8.76 (dd, $J = 5.6, 1.5$ Hz, 1H), 8.69 (s, 1H), 8.60 (dd, $J = 8.1, 1.4$ Hz, 1H), 8.54 (d, $J = 8.0$ Hz, 1H), 8.44 (dtd, $J = 17.3, 7.8, 1.7$ Hz, 2H), 8.39 – 8.30 (m, 1H), 8.07 (dd, $J = 7.3, 1.9$ Hz, 1H), 7.96 – 7.86 (m, 2H),

7.78 – 7.69 (m, 2H), 7.66 – 7.55 (m, 2H), , 7.44 (td, $J = 7.4, 1.3$ Hz, 1H), 7.08 (dd, $J = 7.5, 1.2$ Hz, 1H)

Minor δ 11.37 (s, 1H), 9.20 (d, $J = 5.3$ Hz, 1H), 9.12 (d, $J = 5.3$ Hz, 1H), 8.66 – 8.62 (m, 1H), 8.50 (d, $J = 5.7$ Hz, 1H), 8.38 – 8.30 (m, 2H), 8.05 – 7.97 (m, 2H), 7.82 (dt, $J = 7.5, 2.0$ Hz, 2H), 7.48 (d, $J = 7.8$ Hz, 1H), 7.38 (d, $J = 7.5$ Hz, 1H), 7.28 (d, $J = 1.4$ Hz, 1H), 6.84 (d, $J = 7.5$ Hz, 1H).

Synthesis of 57

30 mg of **50** was oxidized with 3 equivalents of H_2O_2 in AcOH at 22 $^\circ\text{C}$. The solvent was removed under vacuum after 50 minutes. The precipitate (69% yield) was washed with water and dried to give a brown precipitate.

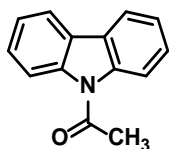


^1H NMR (400 MHz, Acetic Acid- d_4) Major δ 9.42 (ddd, $J = 5.3, 1.6, 0.8$ Hz, 1H), 8.96 – 8.91 (m, 1H), 8.61 (s, 1H), 8.06 (td, $J = 7.7, 1.2$ Hz, 1H), 7.98 (td, $J = 7.7, 1.6$ Hz, 1H), 7.69 (dd, $J = 8.0, 1.5$ Hz, 1H), 7.67 – 7.62 (m, 2H), 7.62 – 7.58 (m, 1H), 7.55 (dd, $J = 8.4, 1.0$ Hz, 1H), 7.50 (ddt, $J = 7.6, 3.4, 1.4$ Hz, 2H), 7.29 (td, $J = 7.2, 0.9$ Hz, 1H), 7.25 – 7.17 (m, 2H), 7.09 (td, $J = 7.6, 1.5$ Hz, 1H), 6.64 (dd, $J = 7.9, 1.5$ Hz, 1H), 2.01 (s, 3H). ^{19}F NMR (376 MHz, Acetic Acid- d_4) δ -64.66.

General procedure for oxidation of dpk ligated 2-aminobiphenyl substrates (54, 58, 63, 69)

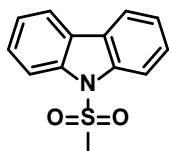
15 mg of the dpk ligated palladacycle was dissolved in 0.60 mL of solvent. 3 or 5 equivalents of H₂O₂ was added to the solution. The solution is then monitored by ¹H NMR until no further change was observed or peaks corresponding to the product were observed. All solutions were monitored at 22 °C unless otherwise stated. Isolation was by removing solvent on a rotavap, stirring the residue in CH₂Cl₂ and passing the solution through silica gel to adsorb any Pd containing species. All reductively eliminated products were compared to literature data except **70** and **58** which were confirmed by independent synthesis.

N-acylcarbazole(**54**):



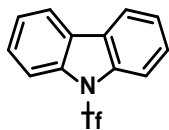
¹H NMR (400 MHz, Chloroform-*d*) δ 8.25 (d, *J* = 8.4 Hz, 2H), 8.03 (ddd, *J* = 7.6, 1.4, 0.7 Hz, 2H), 7.56 – 7.47 (m, 2H), 7.42 (td, *J* = 7.5, 1.0 Hz, 2H), 2.92 (s, 3H).

N-methanesulfonylcarbazole(**64**):



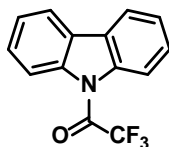
¹H NMR (400 MHz, Chloroform-*d*) δ 8.19 (d, *J* = 8.3 Hz, 2H), 8.03 (ddd, *J* = 7.6, 1.4, 0.7 Hz, 2H), 7.53 (ddd, *J* = 8.4, 7.3, 1.4 Hz, 2H), 7.45 (td, *J* = 7.5, 1.1 Hz, 2H), 2.91 (s, 3H).

N-trifluoromethanesulfonylcarbazole(70):



^1H NMR (400 MHz, Acetic Acid- d_4) δ 8.15 – 8.07 (m, 4H), 7.58 (ddd, $J = 8.4, 7.3, 1.5$ Hz, 2H), 7.52 (td, $J = 7.5, 1.1$ Hz, 2H). ^{19}F NMR (376 MHz, Acetic) δ -75.82. ^{13}C NMR (101 MHz, Acetic) δ 138.10, 128.34, 126.92, 125.87, 120.81, 115.05.

N-trifluoromethanesulfonylcarbazole(58):

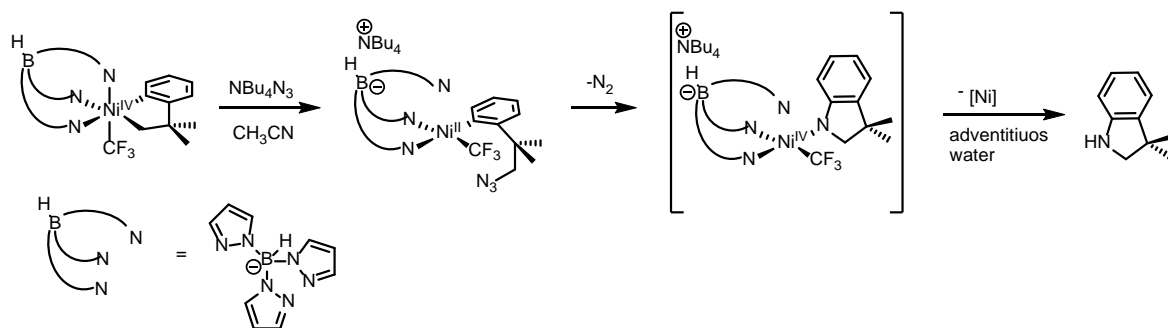


^1H NMR (400 MHz, Acetic Acid- d_4) δ 8.23 (dd, $J = 8.3, 0.9$ Hz, 2H), 8.06 (ddd, $J = 7.4, 1.5, 0.7$ Hz, 2H), 7.54 (ddd, $J = 8.5, 7.3, 1.6$ Hz, 2H), 7.49 (td, $J = 7.4, 1.1$ Hz, 2H). ^{19}F NMR (376 MHz, Acetic Acid- d_4) δ -70.92. ^{13}C NMR (101 MHz, Acetic Acid- d_4) δ 138.14, 128.12, 127.37, 125.75, 120.28, 119.12, 116.58 (q, $J = 3.7$ Hz, CF_3), 110.91.

Chapter 4: Reactivity of κ^2 -C,N-2'-(N-R-amido)biphenyl-2-yl Pd(IV) complexes

4.1 Introduction

Even though some detailed information is available on C-C, C-O, C-X (C= F, Cl, Br, S, Se) reductive elimination from isolated Pd(IV) complexes, surprisingly, the corresponding C(sp²)-N reductive elimination reactivity eluded such characterization.³⁷ Only recently has Sanford characterized a few examples of the C(sp³)-N reductive elimination reactivity of an isolated Pd(IV) alkyl aryl amido complex. Previously, the Goldberg group has also reported C(sp³)-N reductive elimination from a series of Pt(IV) complexes.⁶¹ In both cases, mechanistic studies made them propose a two-step pathway which involves initial dissociation of the amido ligand from the metal center, followed by a nucleophilic attack of the amido ligand on the metal-bound alkyl group carbon of the transient cationic 5-coordinate species. The transformations reported by the Sanford group are shown in Scheme 1.17.⁵⁴ It should be noted that, no C(sp²)-N reductive elimination has never been reported for group 10 monohydrocarbyl M(IV) complexes. To study the reactivity at the corresponding Ni(IV) compounds, the Sanford group synthesized the TpNi(IV) complex in scheme 4.1.⁷¹ The Ni(IV) complex reacts slowly with tetrabutylammonium azide to form 3,3'-dimethylindoline in quantitative yield. This reaction was proposed to go through an S_N2 attack by the azide at the Ni(IV)-CH₂ group and subsequent insertion of the azide group into the Ni(II)-C(sp²) bond concomitant with loss of N₂ to give the target product in quantitative yield. Holding this information in mind, we wanted to explore the C(sp²)-N reductive elimination reactivity of our isolated Pd(IV) complexes and characterize the mechanism of this reaction.

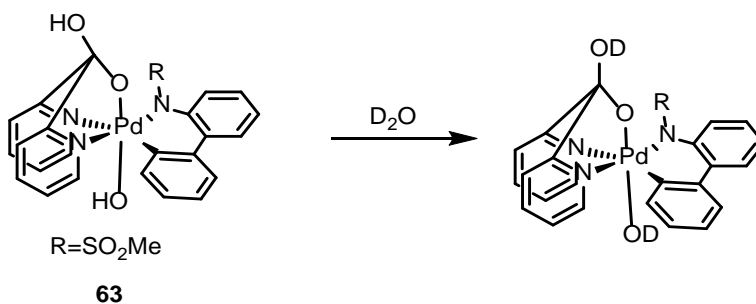


Scheme 4.1 Reactivity of a TpNi(IV) complex to form 3,3'-dimethylindoline as reported by Sanford.

4.2 Characterization and reactivity of N-methanesulfonylamido Pd(IV) complex, **63**

4.2.1 H/D exchange of **63** (Scheme 4.2)

To confirm the assignment of the OH group signals, addition of 2 drops of D_2O to a solution of **63** in $\text{DMSO}-d_6$ leads to the disappearance of two singlets at 8.22 ppm and 3.74 ppm (Scheme 4.2, Fig. 4.1) which are attributed to the OH of the hydrated dpk ligand and the Pd(IV)-OH group, respectively.



Scheme 4.2 The H/D exchange of **63** with D_2O .

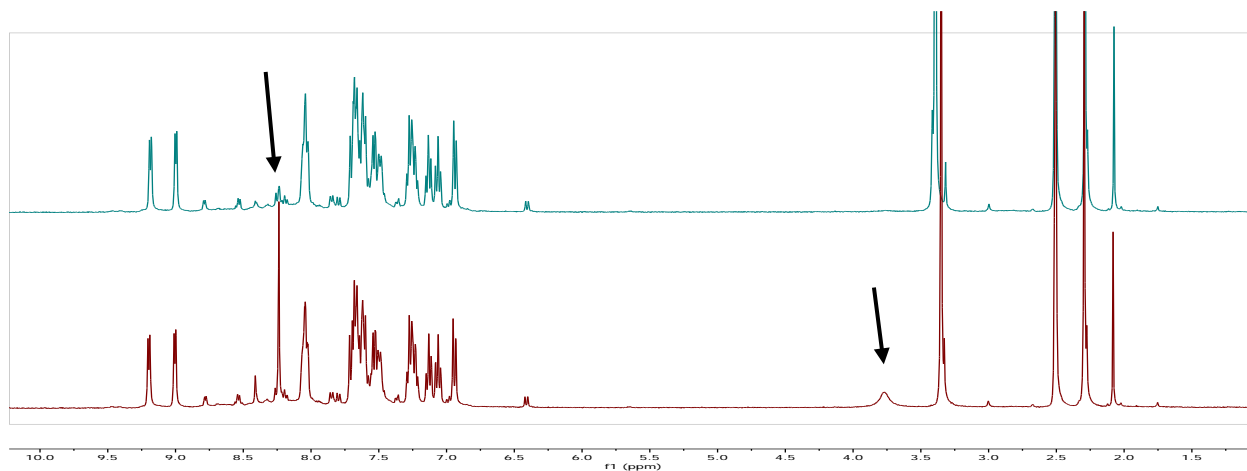
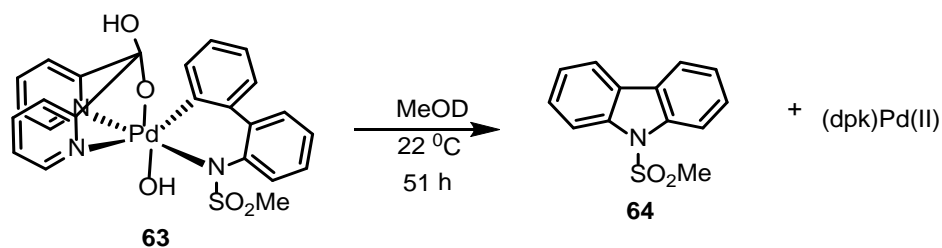


Figure 4.1 ^1H NMR spectra of **63** in $\text{DMSO-}d_6$ before (bottom) and after addition of D_2O (top). The arrows show the peaks affected.

4.2.2 $\text{C}(\text{sp}^2)\text{-N}$ Reductive elimination of **63** (Scheme 4.3)

When a freshly prepared solution of **63** in $\text{DMSO-}d_6$ was left to stand at $22\text{ }^\circ\text{C}$ and checked after 46 h, formation of the carbazole **64** in 76% yield was evident. An unknown species was observed in 18 % yield, and **61** was observed in 5 % yield, presumably, originating from the 5% impurity of the parent peroxy compound **62**.

The kinetics of the C-N coupling of the amido aryl $\text{Pd}(\text{IV})$ complex **63** to form the carbazole **64** and unidentified $\text{Pd}(\text{II})(\text{dpk})$ complex was monitored in CD_3OD (Scheme 4.3). An orange solution of **63** in the latter solvent was monitored by ^1H NMR spectroscopy at $22\text{ }^\circ\text{C}$. The reaction followed a clean 1^{st} order kinetics with a half-life of 37 ± 2 minutes (Fig. 4.2).



Scheme 4.3 Reductive elimination of **63** to form **64** in MeOD at 22 °C.

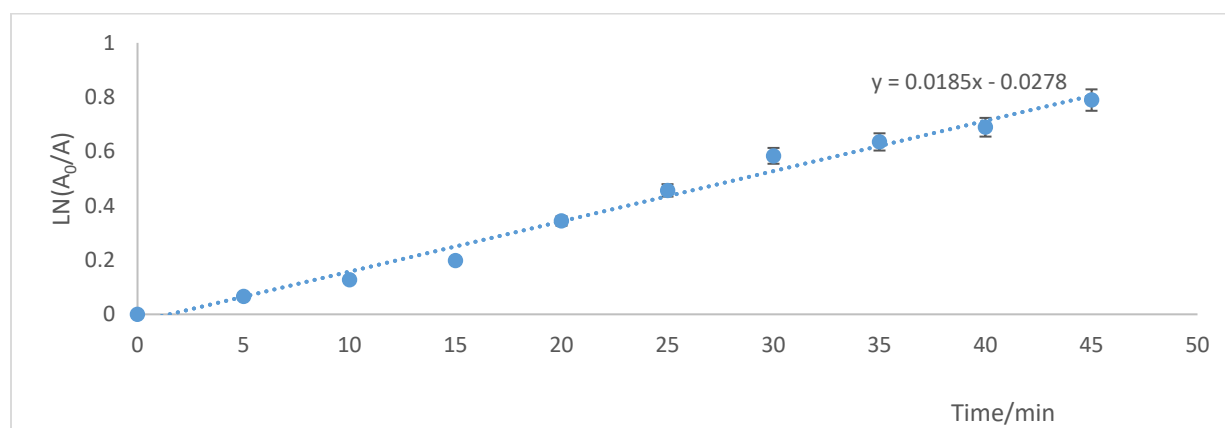


Figure 4.2. A plot of $\ln([\mathbf{63}]_0/[\mathbf{63}])$ vs time for **63** in MeOD at 22 °C. The first order rate constant is $(1.85 \pm 0.07) \times 10^{-2} \text{ min}^{-1}$ giving a half-life of $37 \pm 2 \text{ min}$.

This was our first observation of the C(sp²)-N reductive elimination from an isolated aryl amido Pd(IV) complex.

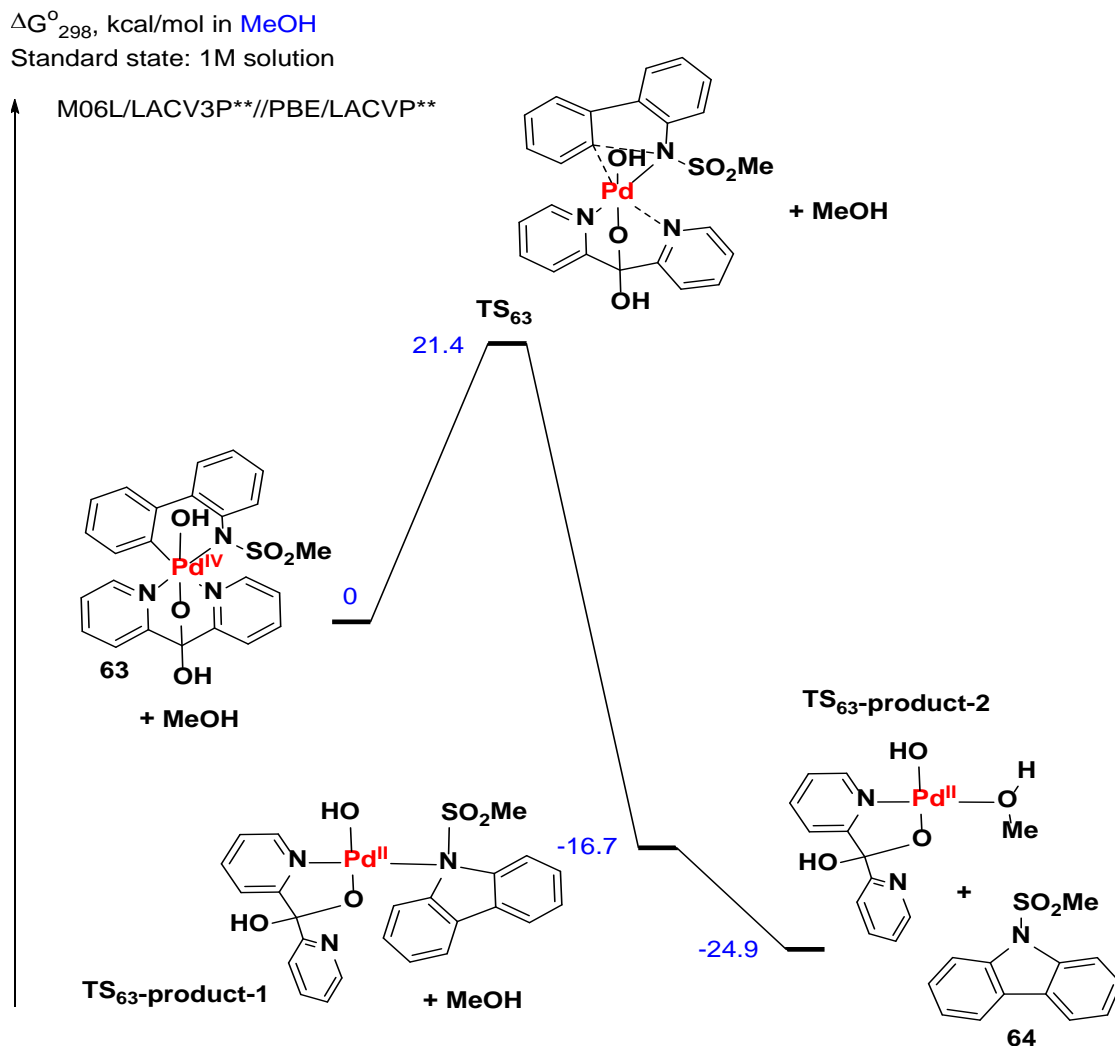


Figure 4.3. The DFT-calculated Gibbs energy profile for the C-N reductive elimination of **63** in MeOH.

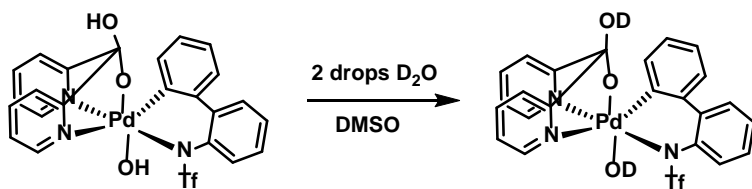
Our DFT study of this reaction⁷² in MeOH suggests that this concerted reductive elimination occurs directly from a six-coordinate Pd(IV) complex. This reaction goes through a transition state **TS₆₃** ($\Delta G = 21.4$ kcal/mol) which involves a partial dissociation of one of the pyridine fragments of the hydrated-dpk ligand situated *trans*-to the aryl ligand. Overall, the C-N

bond forming reaction of **63** leading to the liberation of the carbazole **64** and formation of a Pd(II) dpk complex **TS₆₃-product-2** (Fig. 4.3) is strongly exergonic ($\Delta G = -24.9$ kcal/mol).

4.3 Characterization and reactivity of N-trifluoromethanesulfonylamido Pd(IV) complex **68**

4.3.1 H/D exchange (Scheme 4.4)

The Pd(IV) amido aryl complex **68**·MeCN is insoluble in CH₃CN, CH₃COCH₃, toluene, H₂O, poorly soluble in MeOH, THF, acetone, CH₂Cl₂ and perfectly soluble in DMSO at room temperature. An ¹H NMR spectrum of **68**·MeCN in DMSO-*d*₆ showed the presence of the following most characteristic signals: two downfield shifted multiplets of the *ortho*-pyridyl protons at 9.19 ppm and 9.01 ppm, as compared to the starting material (8.97 ppm), one sharp singlet at 8.33 ppm of the hydrated dpk ligand OH group and one broad singlet at 3.71 ppm assigned to the Pd(IV)OH group, all integrating as 1H. To prove the assignment of the singlets at 8.33 ppm and 3.71 ppm, an H/D exchange experiment with D₂O was carried out. The addition of 2 drops of D₂O to a solution of **68** in DMSO-*d*₆ leads to the disappearance of both singlets (Fig. 4.3).



Scheme 4.4 H/D exchange reaction involving **68** and D₂O.

The spectra in Fig. 4.3 also show the presence of a small impurity of the starting amido aryl Pd(II) complex **66** and derived hydroperoxoketal **67**. When MeCN, MeOH or THF solvents were used to prepare solutions of **66**, these impurities produced stronger signals due to their greater solubility in these solvents, as compared to **68**.

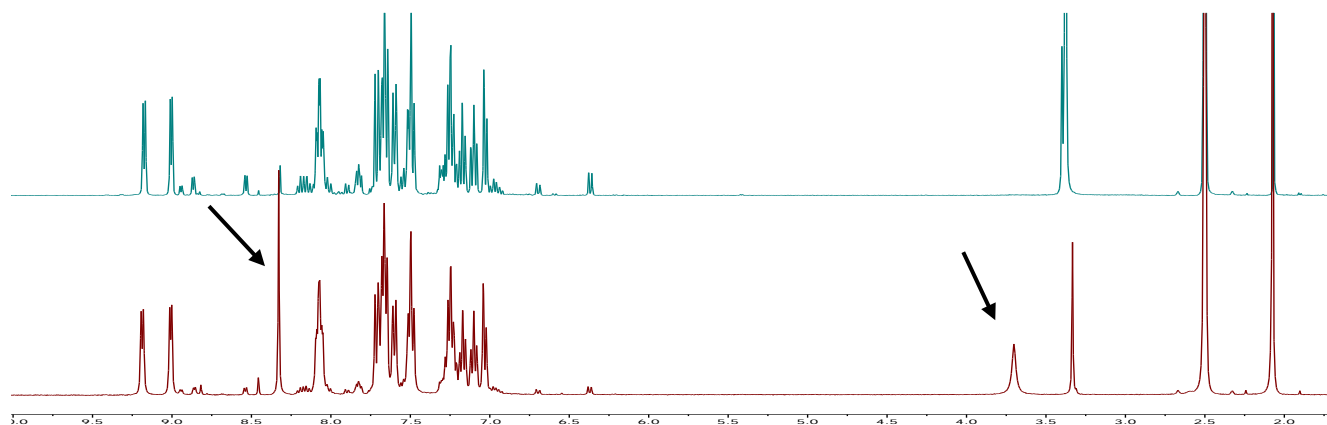


Figure 4.4. ^1H NMR spectra of **68**·MeCN in DMSO- d_6 before (bottom) and after addition of D_2O (top). The arrows show the peaks affected.

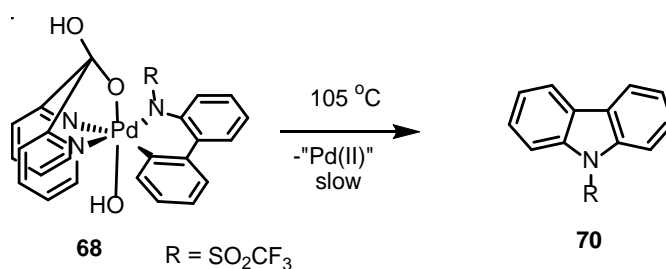
Interestingly, in the course of ^1H NMR our experiments with DMSO solutions of complex **67** it was found that the compound appears to be somewhat oxidizing: monitoring solutions of **68** in DMSO- d_6 showed a slow gradual transformation of **68** to **66**, so that after about 90 h all **68** has reacted to produce the Pd(II) complex **66** in 64% yield together with another product whose identity could not be determined in 33% yield.

4.3.2 C(sp²)-N Reductive elimination of **68**·MeCN in CD_3CN at 105 °C (Scheme 4.5)

Since **68**·MeCN is insoluble in CD_3CN at room temperature, the temperature in the following experiments was raised to 60 °C and 105 °C. Heating **68** in MeCN at 60 °C led to an increase in its solubility and formation of an orange solution in equilibrium with the solid sample of **68**. ^1H NMR spectral analysis of the resulting solution showed the presence of **68** along with an impurity of the starting Pd(II) complex **66** which has a much better solubility in this solvent.

Leaving this solution at room temperature for 5 h led to slow crystallization of **68**·MeCN and subsequent disappearance of any ^1H NMR signals in the solution.

Warming up of the suspension of **68**·MeCN in CD_3CN at $105\text{ }^\circ\text{C}$ for 14 h led to the formation of a brownish solution containing the carbazole **70** in a low 4% yield by ^{19}F NMR along with some unidentified products (Fig. 4.4). These experiments showed that the C-N reductive elimination from **68** containing a strong electron-withdrawing triflyl group at the amido nitrogen atom is not facile in CD_3CN even at $105\text{ }^\circ\text{C}$.



Scheme 4.5 Reactivity of **68** at $105\text{ }^\circ\text{C}$ in CD_3CN .

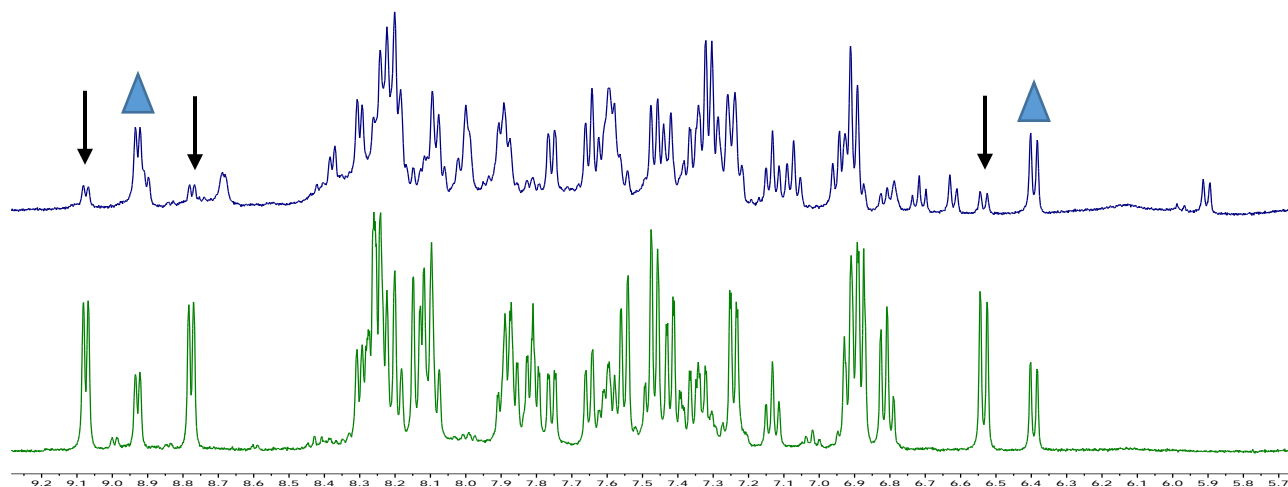
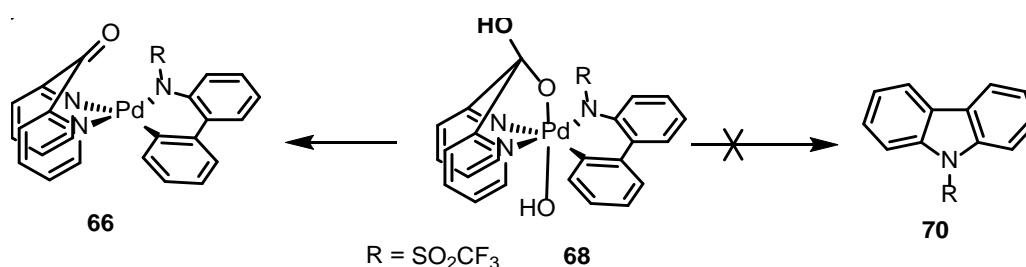


Figure 4.5 ^1H NMR spectra of complex **68** (bottom) after heating for 14 hours at $60\text{ }^\circ\text{C}$ and $105\text{ }^\circ\text{C}$ (top). Arrows show **68** while blue triangles show **66**.

4.3.3 Reactivity of **68**·MeCN in THF-*d*₈ (Scheme 4.6)

In spite of poor solubility of **68**·MeCN in THF-*d*₈, the resulting orange solutions of **68** in THF-*d*₈ could be monitored by ¹H NMR at 22 °C (Fig. 4.5). After 46 h, similar to the solutions of **68** in DMSO, a reduction of **68** to **66** was observed with the solution colour turning from orange to yellow. No product of C-N reductive elimination was detected. This experiment shows that reductive elimination of **68** to form **70** is not facile in THF-*d*₈.



Scheme 4.6 Reactivity of **68** in THF-*d*₈.

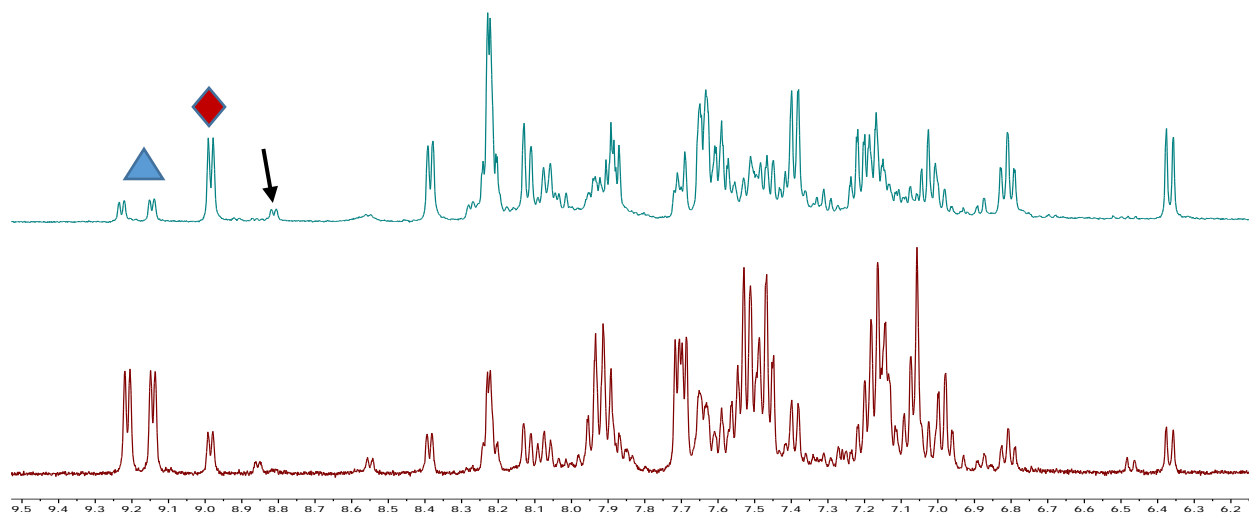
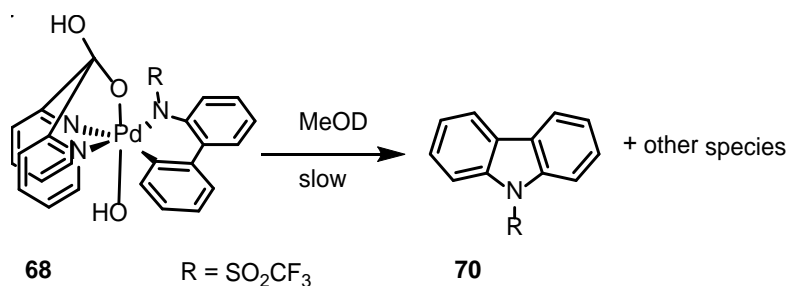


Figure 4.6 ¹H NMR spectra of complex **68** containing a more soluble impurity of **66** and some **67** in THF-*d*₈ after 5 minutes upon dissolution (bottom) and after 46 hours (top). Blue triangle shows **68**, red diamonds show **66** and arrow shows **67**.

4.3.4 Reactivity of **68**·MeCN in MeOD (Scheme 4.7)

Complex **68**·MeCN is slightly soluble in MeOD to form orange solutions. A solution of **68**·MeCN in MeOD was monitored by ^{19}F NMR at 22 $^{\circ}\text{C}$ for 95 h (Fig. 4.6). ^{19}F NMR analysis showed the presence of three species in a ratio of 0.15:1:3.7. The major component (76%) was assigned to **68**. The next major species (21%) was assigned to **67** which is more soluble in methanol than **68** and was extracted in a large extent from the sample of **68** contaminated with **67**. The smallest peak (2%) was assigned to the impurity of the starting Pd(II) dpk complex **66**.



Scheme 4.7 Reactivity of **68** in MeOD at 22 $^{\circ}\text{C}$.

After 24 h, ^{19}F NMR spectrum of the solution showed a decrease in the fraction of **68** from 76% to 44% and a slight decrease of the fraction of **67** from 21% to 15%. Two new major species present in 1:1 ratio were observed in solution in 35% combined yield which could be attributed to products of some modification of **68** where the OH group on the hydrated dpk ligand has been replaced with OMe from the solvent. The fraction of these two new species increased to a 55% and the reductively eliminated product **70** was observed in 1.3% yield after 72 hours. After 95 h the corresponding numbers were 94% and 3.6%, respectively (Fig. 4.6). This result shows that

C-N reductive elimination from **68** in MeOD is not facile at room temperature but is faster than in THF or MeCN.

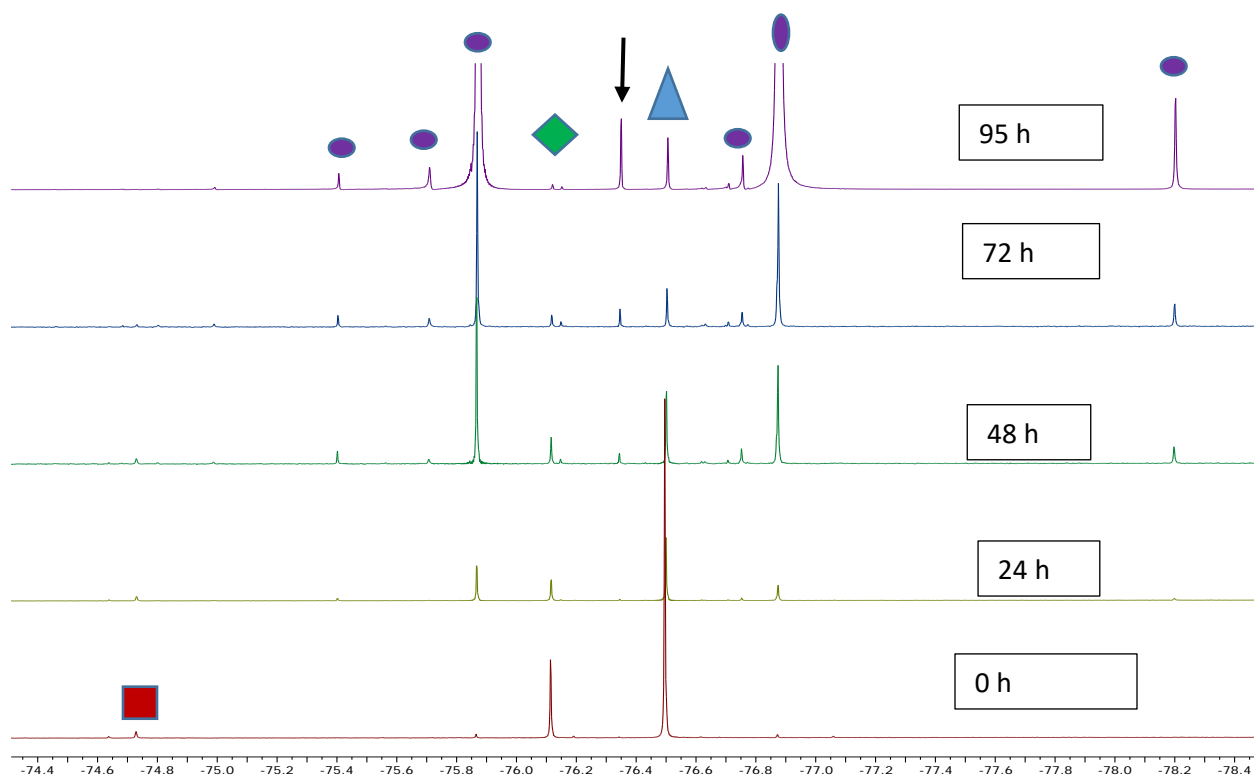
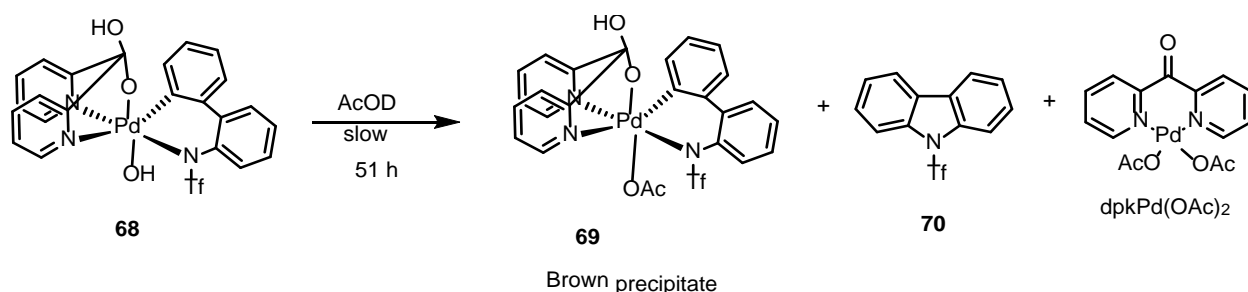


Figure 4.7. ^{19}F NMR spectrum in MeOD of **68** containing impurities of **67** and **66**. The arrow points to the peak for **70** which was formed only in 3.6% yield after 95 h. Red square shows **66**, green diamond shows **67** and blue triangle shows **68**. Purple circles show unknown intermediates observed in solution.

4.3.5 Reactivity of **68**·MeCN in AcOD (Scheme 4.8)

The compound **67**·MeCN dissolves slowly in AcOD (about 20 minutes). Analysis of the ^1H NMR spectrum of the resulting solution showed the presence of **67** and two other species in solution (Fig. 4.7, top). The peak at 9.28 ppm was assigned to the hydrogen atoms in the *ortho*-position of the pyridyl group of **69**, and the multiplet at 9.42 ppm was assigned to the carbazole **70**. Notably, **68** and **69** were also observed when the Pd(II) amido aryl precursor **66** was reacted with H_2O_2 in AcOD (Fig. 4.7, bottom). This result suggests that the reaction of **66** with 3 equivalents of H_2O_2 leads to the formation of Pd(IV) intermediates.



Scheme 4.8 Reactivity of **68** to form **69** and **70** in AcOD at 22 $^\circ\text{C}$.

After 24 h, the originally orange solution of **68** in AcOD had turned brown with some brown solid precipitating out of the solution. The peak corresponding to **68** had disappeared, but **69** was still present (Fig. 4.8). The yield of the carbazole **70** formed along with $\text{Pd}(\text{dpk})(\text{OAc})_2$ has increased to 26%. After 51 h, **70** was observed in 42% yield together with $(\text{dpk})\text{Pd}(\text{OAc})_2$. The brown solid precipitate was isolated in 53% yield and its identity was confirmed by ^1H and ^{19}F NMR spectroscopy and an independent synthesis (see below) to be **69**. The most probable pathway

for the formation of **69** is the protonation of the Pd(OH) group of **68** to form an aqua complex with subsequent displacement of the aqua ligand with the acetate ligand derived from the solvent.

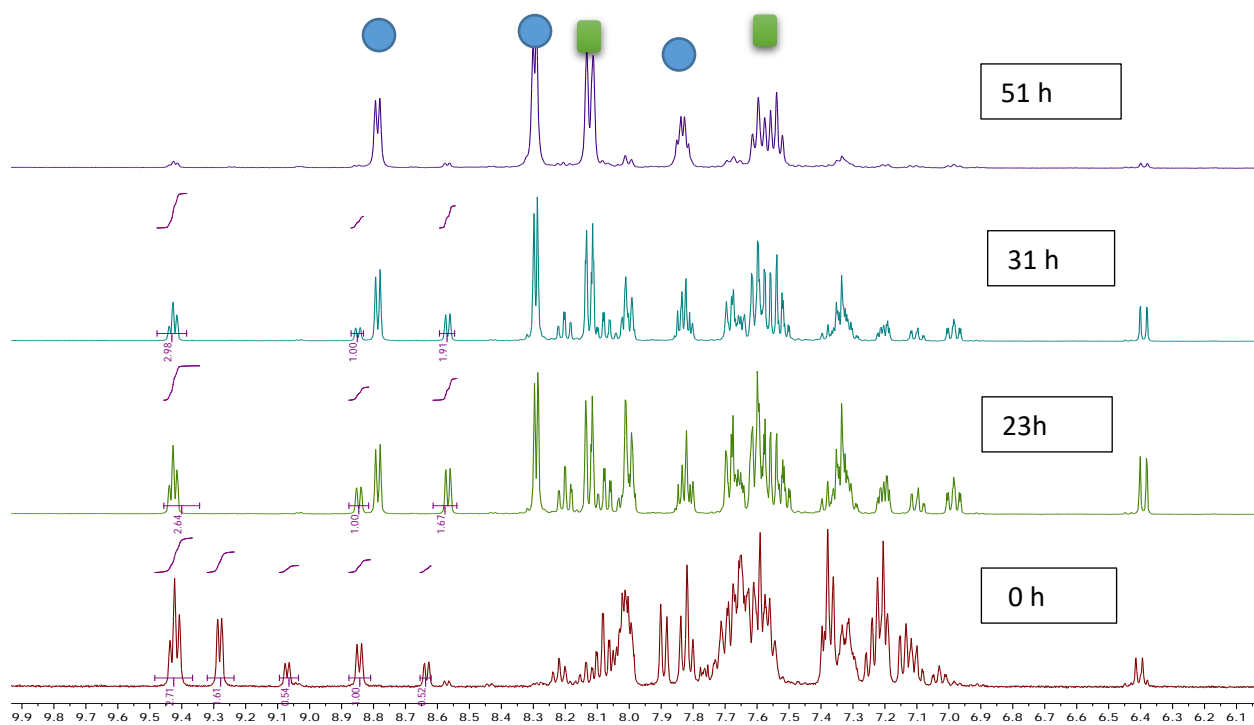


Figure 4.8. ¹H NMR spectral monitoring of **68** in AcOD for 51 hours. Green squares show **70** and blue circles show (dpk)Pd(OAc)₂.

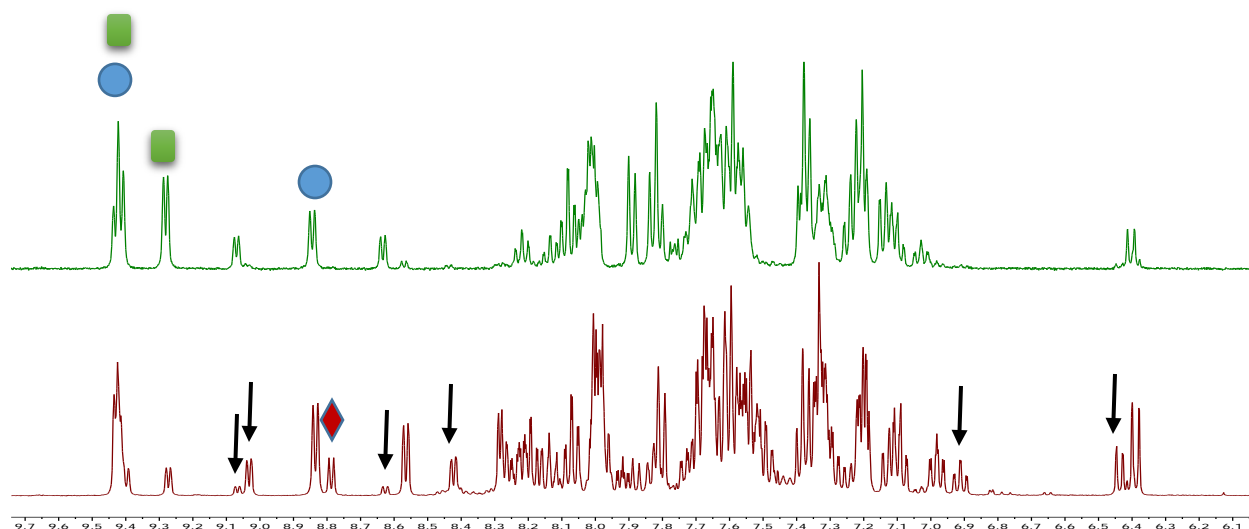


Figure 4.9 Comparison of ^1H NMR spectra of **68** observed in the direct oxidation of **66** with H_2O_2 in AcOD (bottom) and isolated **68** dissolved in AcOD (top). Green squares show **69**, blue circle shows **68**, Arrows show **67** and red diamond shows **66**.

In the experiments above the OAc ligand in **69** was not observed in the ^1H NMR spectra because it was derived from a deuterated solvent. To confirm the identity of the precipitate formed, **68**·MeCN was dissolved in neat CH_3COOH , the resulting solid collected and its ^1H NMR spectrum in $\text{DMSO}-d_6$ was analyzed. According to ^1H NMR analysis, the so-formed product **69** showed the presence of a single Pd complex in solution. Since **68** and **69** are similar except in the apical ligand, their ^1H NMR spectra in $\text{DMSO}-d_6$ were also expected to be very similar which was, in fact, observed (Fig. 4.9). Notably, complex **69** crystallized with one molecule of AcOH, so that two OAc signals were present in the ^1H NMR spectra of **69**·AcOH, one attributable to the OAc ligand at 1.71 ppm and another assignable to AcOH of crystallization at 2.07 ppm (Fig. 4.9, top). The signals of two hydrogen atoms in the *ortho*-positions of the pyridine fragments were observed as doublets at 9.16 (d, $J = 5.3$ Hz) ppm and 8.91 (d, $J = 5.8$ Hz) ppm. The OH fragment of the

hydrated dpk ligand produced a singlet at 8.71 ppm. ^{19}F NMR spectra also showed a single fluorine-containing species in solution.

Upon standing for 48 h at 22 °C a solution of **69**·AcOH in DMSO- d_6 produced a new species **71** in 45% yield (Scheme 4.9, Fig. 4.10). An ^1H NMR spectrum of the new species showed two signals of *ortho*-pyridyl hydrogen atoms observed as doublets at 9.39 (d, $J = 5.4$ Hz) ppm and 8.46 (d, $J = 5.7$ Hz) ppm. The OH fragment of the hydrated dpk ligand produced a singlet at 9.01 ppm, and the CH_3 ligand was observed as a singlet at 1.25 ppm integrating as 3H. The product **71** was proposed to be an isomer of **69**.

After the continued monitoring of the mixture for nine days, the carbazole **70** was observed in 5% yield together with the Pd(II) species **66** in 15% yield and a minor unidentified species in less than 5% yield. A new Pd(IV) species was observed in solution in 68% yield whose identity we could not determine but was proposed to form from a DMSO solvent modification of **69**.

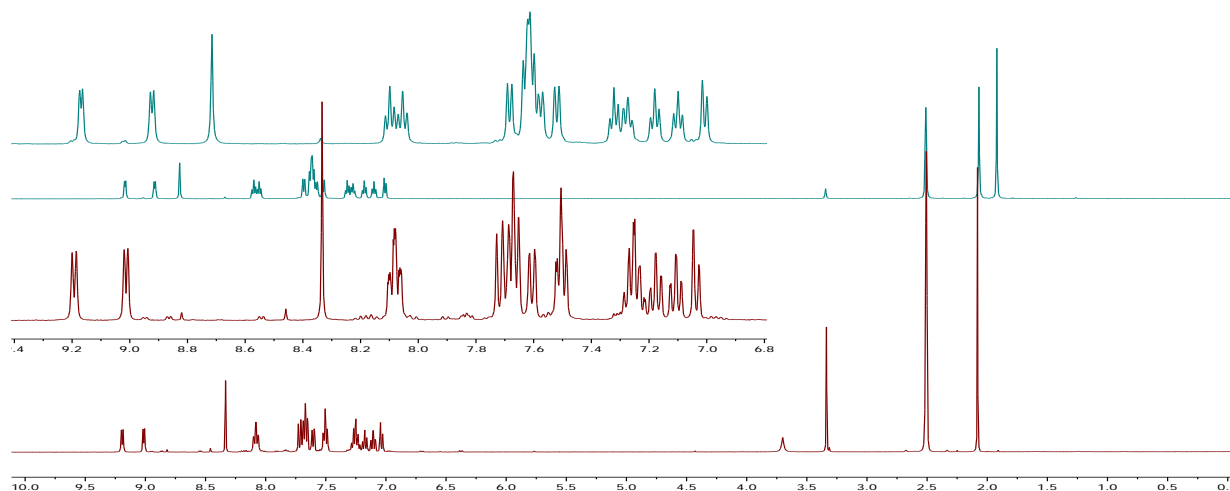
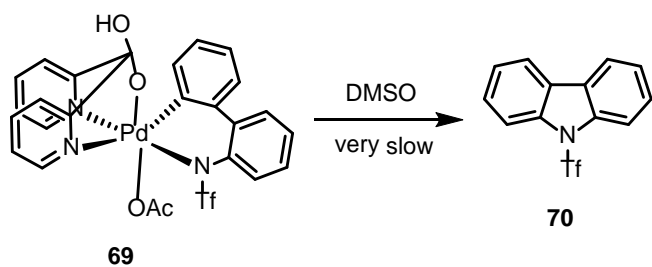


Figure 4.10. ^1H NMR spectrum of **68**·MeCN (bottom) and **69**·AcOH (top) in DMSO- d_6 . The aromatic region is expanded for clarity. The apical ligand OAc could be observed at 1.71 ppm for **69**·AcOH.



Scheme 4.9 Reactivity of **69** in DMSO to form **70** at room temperature.

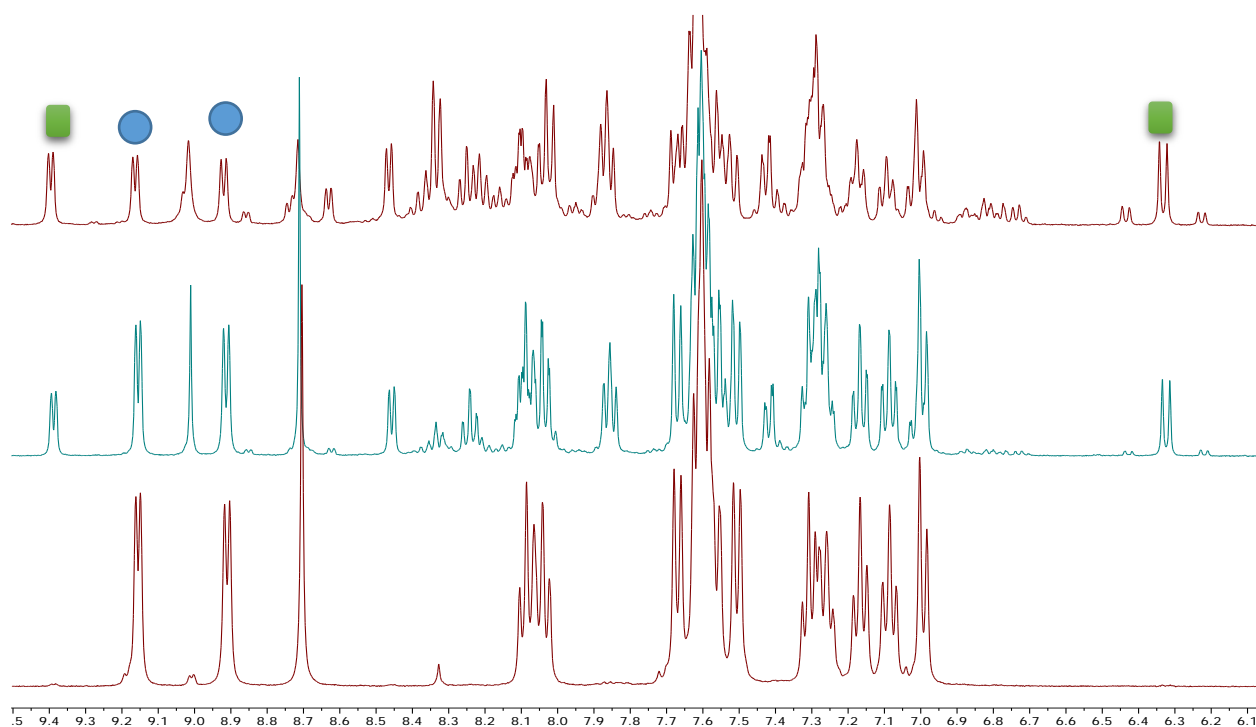


Figure 4.11 ^1H NMR spectrum of **69**·AcOH in DMSO- d_6 after 5 minutes (bottom), 48 hours (middle) and nine days (top). Blue circles show **69** and green squares show **71**.

4.3.6 Reactivity of **69**·AcOH in CD₃CN

The compound **69**·AcOH is soluble in CD₃CN and a solution of **69** in CD₃CN was monitored for nine days. No carbazole **70** was observed after that time.

4.3.7 Reactivity of **68** in the presence of different acids

Since there was no reductive elimination from **68** in CD₃CN at room temperature, we decided to ‘force’ the reaction using additives which could make reductive elimination more facile. We envisioned that the addition of an acid would protonate the OH ligand of **68** thereby producing a more electrophilic cationic species which can reductively eliminate **70** more readily.

4.3.7.1 HClO₄

The addition of 3 equivalents of 70% HClO₄(aq) to a suspension of **68** in CD₃CN at room temperature led to the formation of a purple solution. ¹H NMR spectral analysis of the solution showed the formation of the carbazole **70** in 98% yield in 5 minutes; no intermediates were observed in the reaction. The purple solution turned light yellow by the moment the NMR tube was removed from the probe. A single Pd(dpk) complex was observed in solution which was tentatively assigned to [Pd(dpk)(MeCN)₂](ClO₄)₂. No Pd-black was observed.

4.3.7.2 CF₃SO₃H

We next use trifluoromethanesulfonic acid. The addition of 3 equivalents of anhydrous CF₃SO₃H to a suspension of **68** in CD₃CN at room temperature led to the formation of a purple solution. ¹H NMR spectral analysis of the solution showed the formation of the carbazole **70** in 97% yield in 5 minutes, and no intermediates were observed in the reaction. The purple solution had turned light

yellow by the moment the NMR tube was removed from the probe. Two different Pd(dpk) complexes were observed which were assigned to $[\text{Pd}(\text{dpk})(\text{MeCN})_2](\text{CF}_3\text{SO}_3)_2$ and $\text{Pd}(\text{dpk})(\text{CF}_3\text{SO}_3)_2$.

4.3.7.3 H_2SO_4

The addition of 3 equivalents of H_2SO_4 to a suspension of **68** in CD_3CN at room temperature led to the formation of a purple solution. ^1H NMR spectral analysis of the solution showed the formation of the carbazole **70** in 98% yield in 5 minutes, and no intermediates were observed in the reaction. The purple solution had turned light yellow by the moment the NMR tube was removed from the probe after 5 minutes. Two different Pd(dpk) complexes were observed and were assigned to $[\text{Pd}(\text{dpk})(\text{MeCN})_2](\text{HSO}_4)_2$ and $\text{Pd}(\text{dpk})(\text{HSO}_4)_2$.

4.3.7.4 HBF_4

The addition of 3 equivalents of 50% $\text{HBF}_4(\text{aq})$ to a suspension of **68** in CD_3CN at room temperature led to the formation of a purple solution. ^1H NMR spectral analysis of the solution showed the formation of the carbazole **70** in 98% yield in 15 minutes. After about 5 minutes, two intermediates were observed in 8% and 19% yield respectively but have disappeared after 15 minutes. The purple solution had turned light yellow after 15 minutes. Two Pd(dpk) complexes were observed in solution and were tentatively assigned to $[\text{Pd}(\text{dpk})(\text{MeCN})_2](\text{BF}_4)_2$ and $[\text{Pd}(\text{dpk})(\text{H}_2\text{O})_2](\text{BF}_4)_2$ and were found to be in a ratio of 1.00:1.76.

Since acids with weakly coordinating anions reacted fast to reductively eliminate the target product **70**, we switched to acids with more strongly coordinating anions.

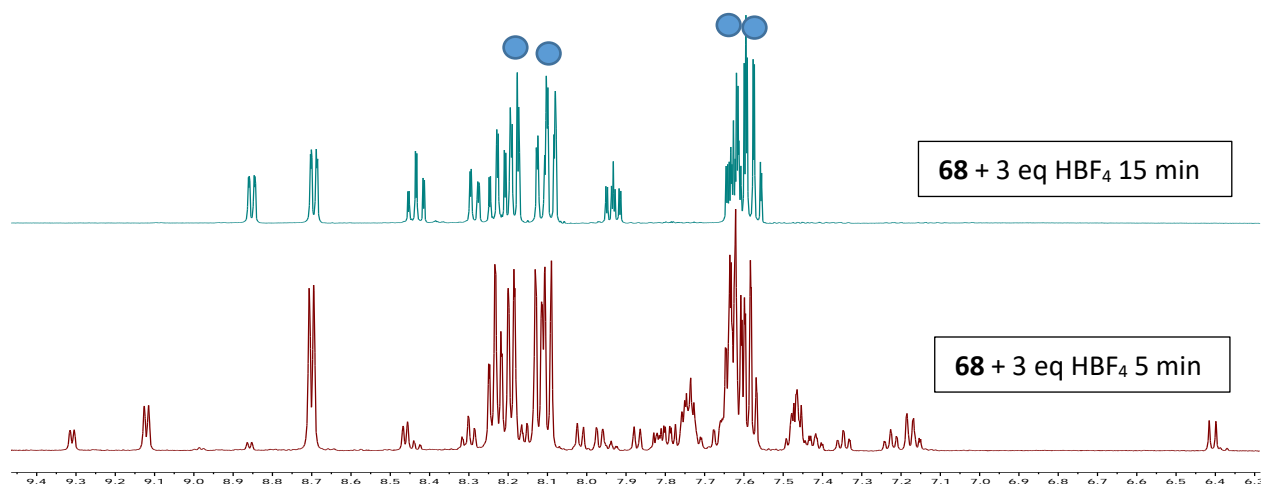
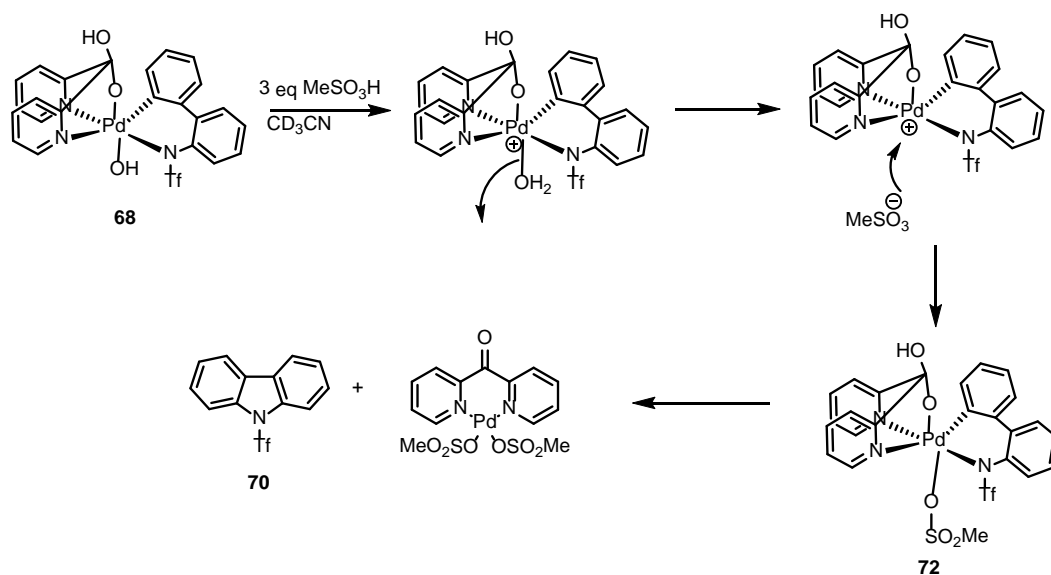


Figure 4.12. ^1H NMR spectrum of **68** 5 minutes after adding 3 equivalents of HBF_4 and 15 minutes after addition. Blue circles show **70**.

4.3.7.5 $\text{CH}_3\text{SO}_3\text{H}$

The addition of 3 equivalents of $\text{CH}_3\text{SO}_3\text{H}$ to a suspension of **68** in CD_3CN at room temperature led to the formation of a purple solution. ^1H NMR spectral analysis of the solution after about 5 minutes showed formation of a single intermediate. This intermediate, which we propose to be **72** (Scheme 4.10) was observed to form gradually the carbazole **70**. The rate of decomposition of **72** to form **70** followed a first order rate law with a half-life of 46 ± 2 minutes (Fig. 4.12). The slow rate of the C-N reductive elimination in the presence of $\text{CH}_3\text{SO}_3\text{H}$ additives, as compared to HClO_4 , $\text{CF}_3\text{SO}_3\text{H}$ and HBF_4 made us to propose that the presence of a more coordinating CH_3SO_3^- anion is responsible for this diminished reactivity involving the Pd(IV) species **72**.



Scheme 4.10 Proposed reactivity of **68** in CD_3CN with 3 equiv of MeSO_3H to form **72** and **70** at $22\text{ }^\circ\text{C}$

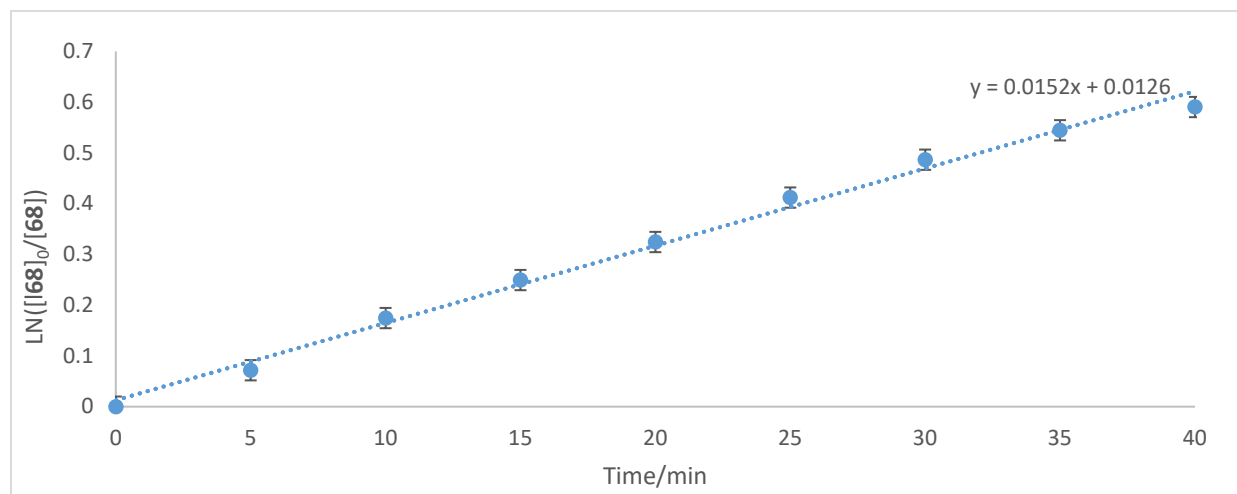
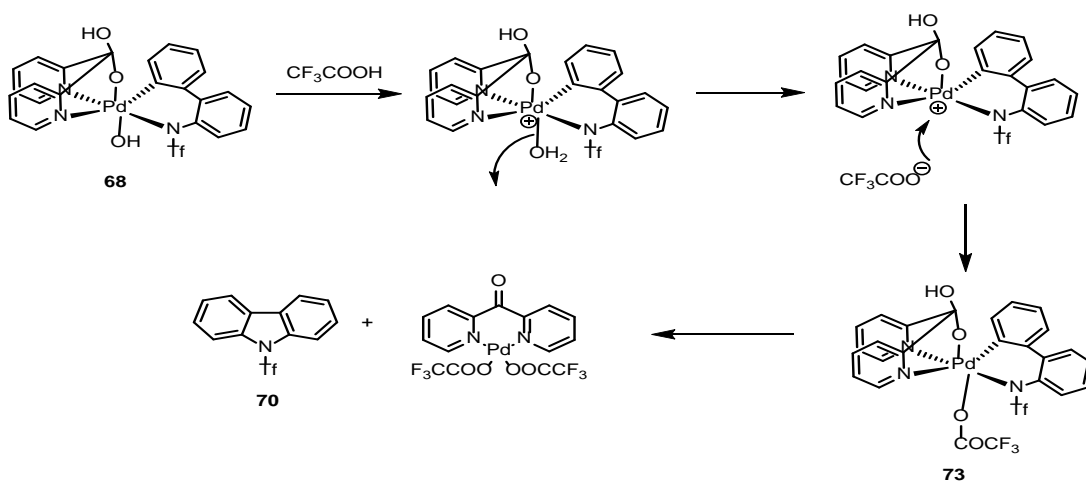


Figure 4.13 Plot of $\ln([68]_0/[68])$ vs time with 3 equivalent of MeSO_3H in CD_3CN . The slope of the straight line is $(1.53 \pm 0.05) \times 10^{-2} \text{ min}^{-1}$ giving a half-life of $46 \pm 2 \text{ min}$.

4.3.7.6 TFA

Since new Pd(IV) intermediates were observed when using MeSO₃H, we chose trifluoroacetic acid (CF₃COOH) with a similar pKa (-0.25 in H₂O) and reacted it with **68** in CD₃CN. Addition of 3 equivalents of CF₃COOH to a suspension of **68** in CD₃CN at room temperature led to the formation of a purple solution. According to ¹H NMR spectral analysis of the solution after about 5 minutes, a single intermediate was formed. This intermediate, which we tentatively assign to **73** (Scheme 3.28) was observed to gradually form **70**. The rate of decomposition of **73** to form **70** was observed to follow a first order rate law with a half-life of 66±1 minutes (Fig. 3.43). The slow rate of the C-N reductive elimination in the presence of CF₃CO₂H additives, as compared to HClO₄, CF₃SO₃H, HBF₄ and H₂SO₄, made us to propose that the presence of a more coordinating CF₃CO₂⁻ anion is responsible for this diminished reactivity involving the Pd(IV) species **73**.



Scheme 4.11 Proposed reactivity of **68** in CD₃CN with 3 equiv of CF₃COOH to form **73** and **70** at 22 °C.

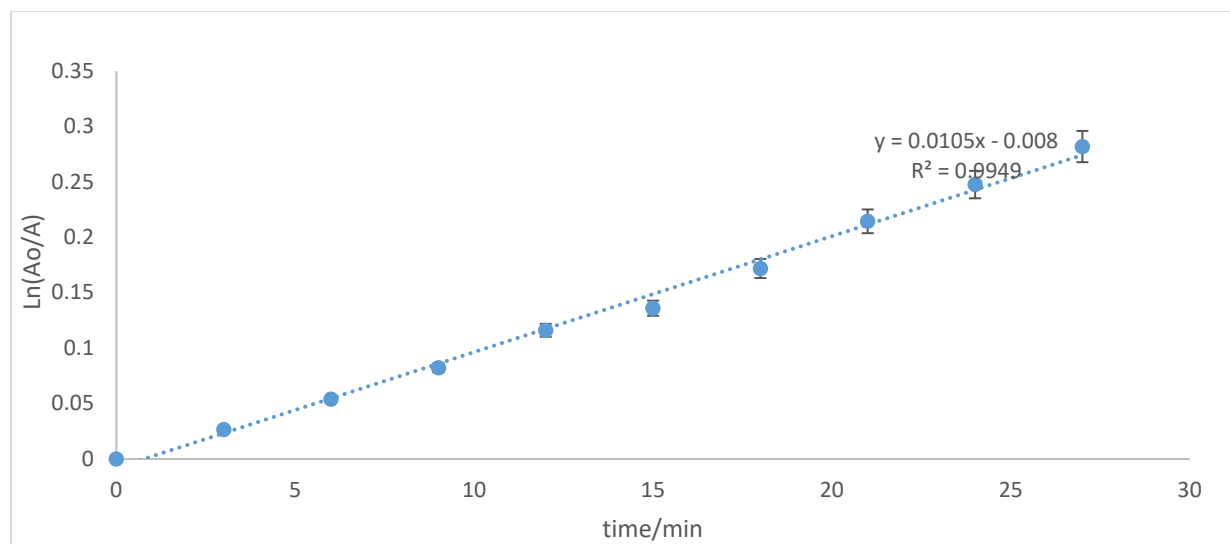
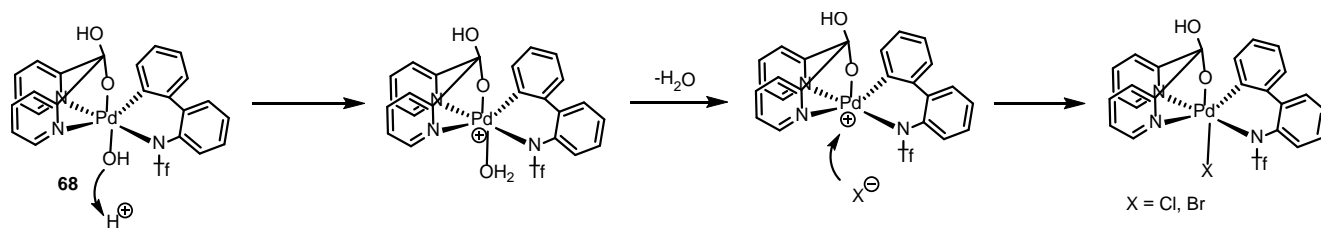


Figure 4.14 Plot of $\ln([\mathbf{68}]_0/[\mathbf{68}])$ vs time with 3 equivalent of TFA in CD_3CN . The slope of the straight line is $(1.05 \pm 0.03) \times 10^{-2} \text{ min}^{-1}$ giving a half-life of $66 \pm 1 \text{ min}$.

4.3.7.7 HBr and HCl

Based on the experiments above, we envisioned that, using strong hydrohalic acids with strongly coordinating anions might inhibit the C-N elimination reaction due to the formation of corresponding Pd(IV) halides (Scheme 4.12). Upon addition of 3 eq of HBr(aq) to a suspension of **68** in CD_3CN , the solution immediately turned dark red, and the resulting mixture was monitored by ^1H NMR spectroscopy. 5 different species were observed in solution whose identity was not determined except **68**. After 72 hours, a yellow solution was formed together with some brown precipitate. ^1H NMR spectrum of the solution showed that a partial reduction of the Pd(IV) amido aryl complex **68** has occurred to form the amido aryl Pd(II) complex **66** (34 % yield) (Fig. 4.14). The precipitate was isolated and dissolved in $\text{DMSO}-d_6$. ^1H NMR spectrum in of the isolated precipitate in $\text{DMSO}-d_6$ showed one major species whose identity we could not determine. It should be noted that the carbazole **70** was not produced.



Scheme 4.12 Proposed reactivity of **68** in CD₃CN with 3 equiv of HCl or HBr at 22 °C.

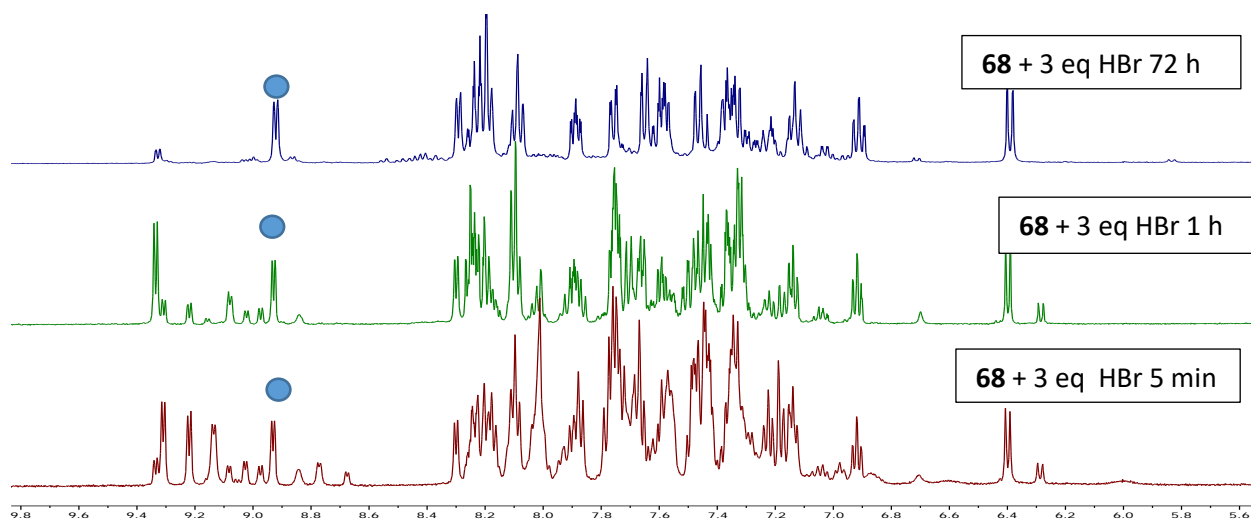


Figure 4.15. ¹H NMR spectrum of **68** 5 minutes after adding 3 equivalents of HBr, 60 minutes after addition and 72 h after addition. Blue circles show **66**.

The addition of 3 equivalents of HCl(aq) to a suspension of **68** in CD₃CN resulted in the formation of a reddish brown solution. ¹H NMR spectrum of the solution showed the presence of 5 different species whose identity was not determined. After 72 hours, a red solution was produced together with some precipitate. ¹H NMR spectrum of the solution showed a reduction of **68** to **66** in 14% yield (Fig. 4.15). No carbazole **70** was observed. The precipitate was isolated, dissolved in DMSO-

*d*₆. ¹H NMR spectrum in of the isolated precipitate in DMSO-*d*₆ showed one major species whose identity we could not determine. Notably, the reduction of **68** to **66** in CD₃CN in the presence of HBr was faster and the yield of **66** higher in comparison to HCl.

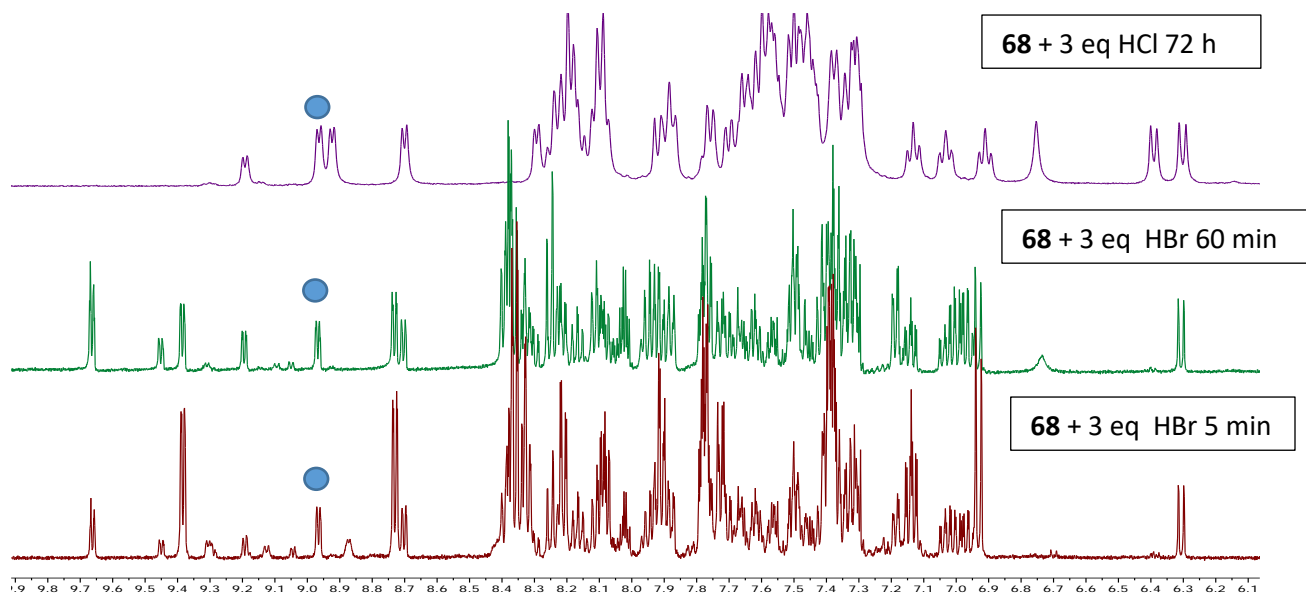


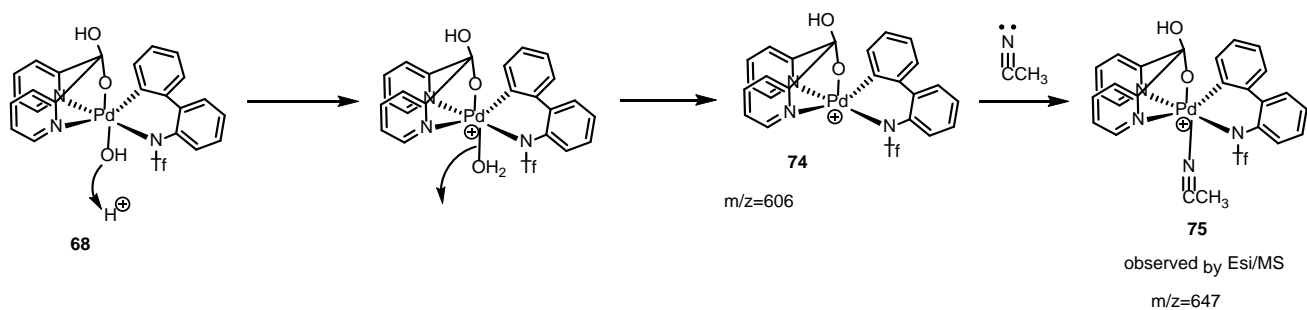
Figure 4.16 ¹H NMR spectrum of **68** 5 minutes after adding 3 equivalents of HCl, 60 minutes after addition and 72 h after addition. Blue circles show **66**.

4.3.8 Reaction of **68** in CD₃CN with different equivalents of HBF₄

4.3.8.1 With 1 equivalent of HBF₄ to form N-trifluoromethanesulfonamido Pd(IV)(MeCN), **75**(BF₄)

Since no appreciable amount of intermediates were observed in our previous systems where we used excess of strong acids with weakly coordinating anions, HClO₄, CF₃SO₃H and HBF₄, we decided to reduce the amount of acid to 1 equivalent. We used HBF₄ in these experiments.

The addition of 1 equivalent of HBF_4 to **68** in CD_3CN led to the formation of a purple solution which was monitored by ^1H NMR spectroscopy at 22°C . The NMR showed the presence of a single species (Fig. 4.16, bottom). The intermediate was observed to slowly produce **70** following a clean first-order reaction kinetics with the reaction half-life of 104 ± 2 min (Fig. 4.17). The identity of the reactive species formed by the addition of 1 equivalent of HBF_4 to **68** was revealed by running the reaction in neat CH_3CN and subjecting the resulting solution to ESI(+)/MS. Two mass envelopes were observed with m/z 605.9 and 646.9 and assigned to **74** and **75** (Scheme 4.13, Fig. 4.18), respectively. This shows that the species formed upon protonation of **68** may be the CH_3CN adduct **75** and not the aquo adduct.



Scheme 4.13 Reactivity of **68** with 1 equiv of HBF_4 in CD_3CN to form **75** at 22°C .

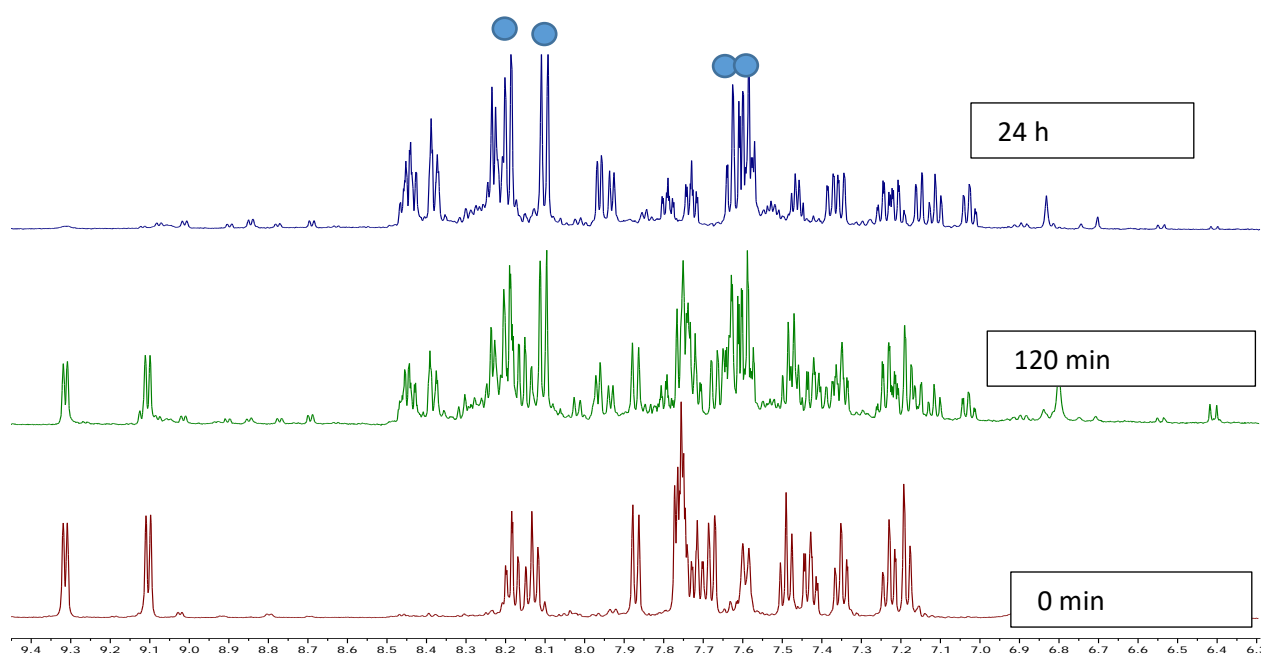


Figure 4.17. ^1H NMR spectrum of **68** + 1 equivalent HBF_4 upon mixing and after 24 hours. Blue circles show **70** (yield 83 %) peaks after 24 hours. **70** can be observed as a major component after 120 min.

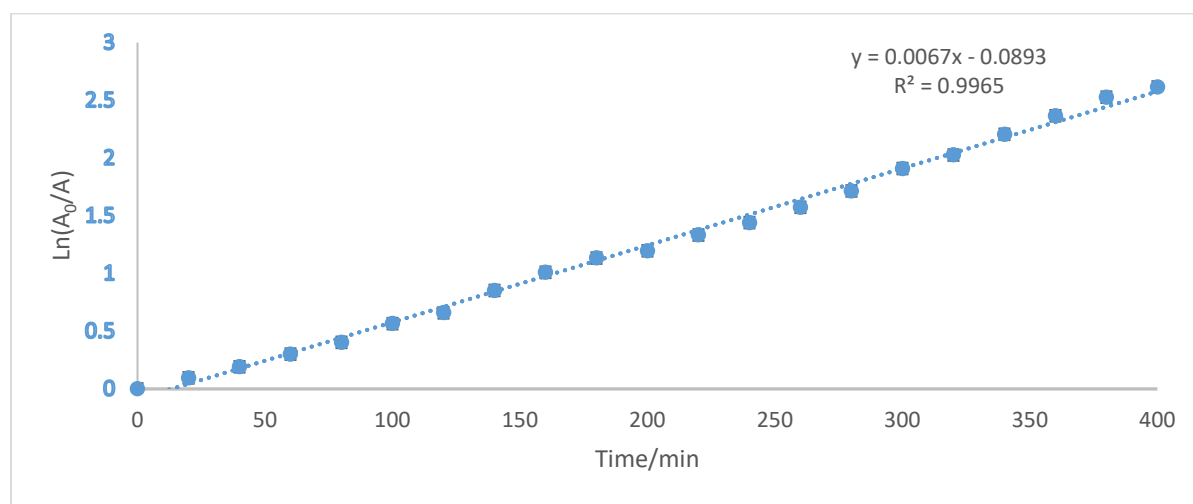


Figure 4.18. Plot of $\ln([\mathbf{75}]_0/[\mathbf{75}])$ vs time/min in CD_3CN at 22°C . The slope of the straight line is $(6.67 \pm 0.03) \times 10^{-3} \text{ min}^{-1}$ giving a half-life of $(104 \pm 2) \text{ min}$.

Acq. Data Name: 05_09_2016_N-trif2abpPd(IV).dpk_MeCN_HBF4
Creation Parameters: Average(MS[1] Time:0.65..0.69)
Comment: Bqpm5P1OH2 CH4 100C 1Product neg3

Experiment Date/Time: 5/9/2016 5:23:54 PM
Ionization Mode: ESI+

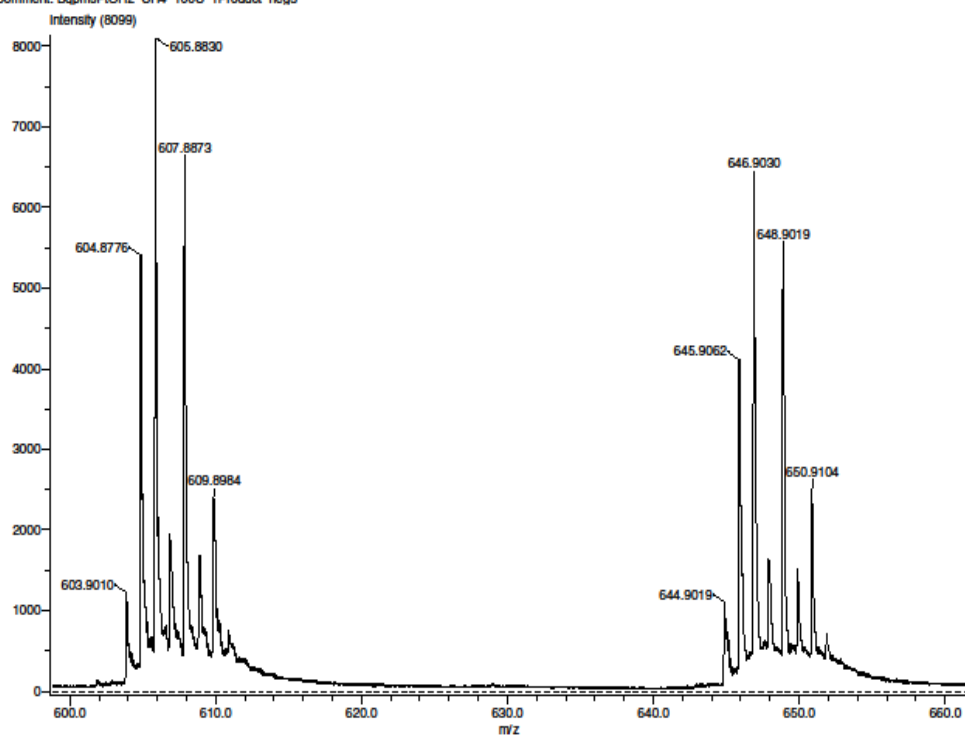


Figure 4.19. Mass spectrum of **68** in CH_3CN + 1 equivalent of HBF_4 . The peak at $m/z=605.90$ is assigned to a formally 5-coordinate Pd(IV) species **74** and the peak at $m/z= 646.99$ is attributed to **75**.

To additionally confirm the identity of **75**, **68** was combined with CH_3CN in which it is virtually insoluble at 0°C . 0.9 equivalent of HBF_4 was added to the mixture and stirred to cause the dissolution of most of the solid. Then the liquid was decanted, the solvent was quickly removed under vacuum at 0°C and the residue dissolved in CD_2Cl_2 . The ^1H NMR spectrum of the solution showed the presence of two types of CH_3CN molecule (Fig. 4.19). The CH_3CN bound to the Pd(IV) center in **75** was observed at 2.73 ppm, much more downfield shifted compared to free

CH₃CN in solution which was observed at 1.97 ppm. The peak at 2.73 integrates for 3H. The OH group of the dpk fragment was observed at 5.18 ppm.

Reductive elimination of **75** was then monitored by ¹H NMR spectroscopy to reveal first order kinetics behavior with the reaction half-life of 87 ± 2 min (Fig. 4.20).

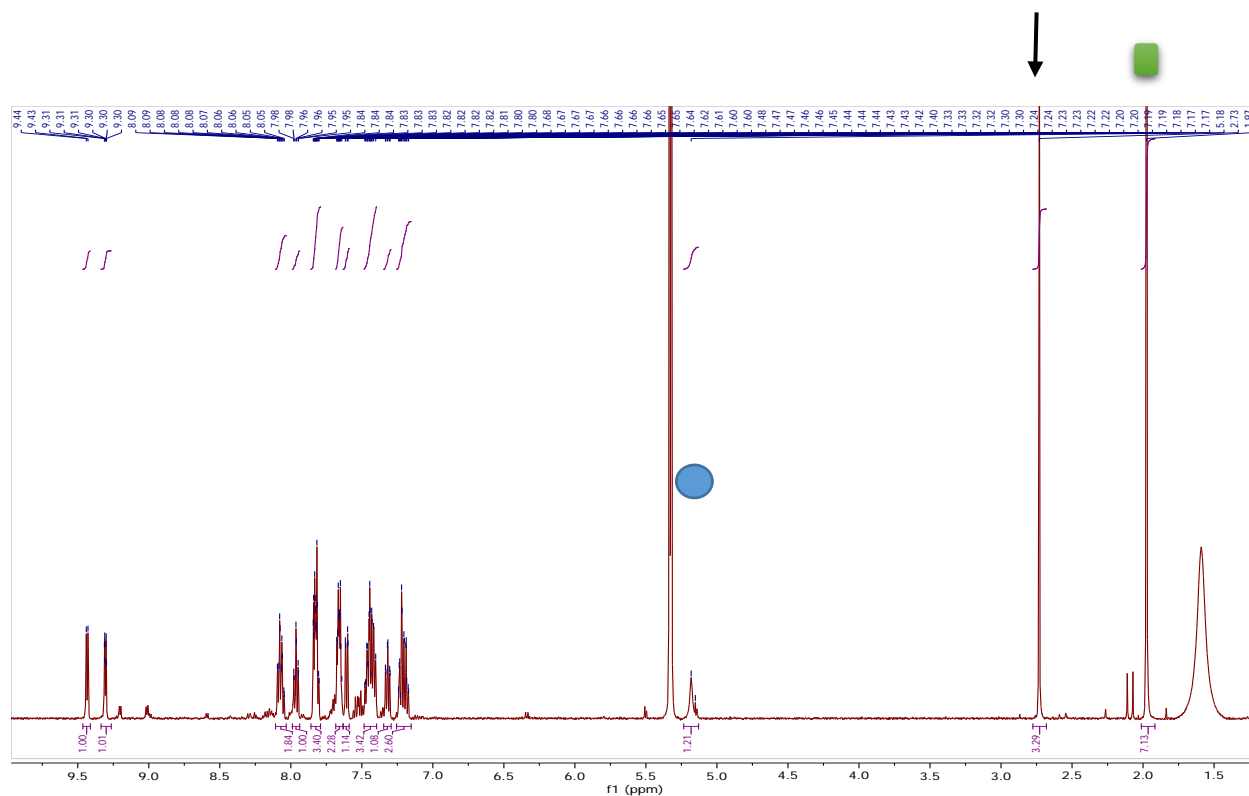


Figure 4.20 ¹H NMR spectrum of **75** in CD₂Cl₂. Blue circle shows dpk-OH. Arrow shows Pd(IV)-bound CH₃CN which integrates for 3H at 2.73 ppm and free CH₃CN at 1.97 ppm (green square).

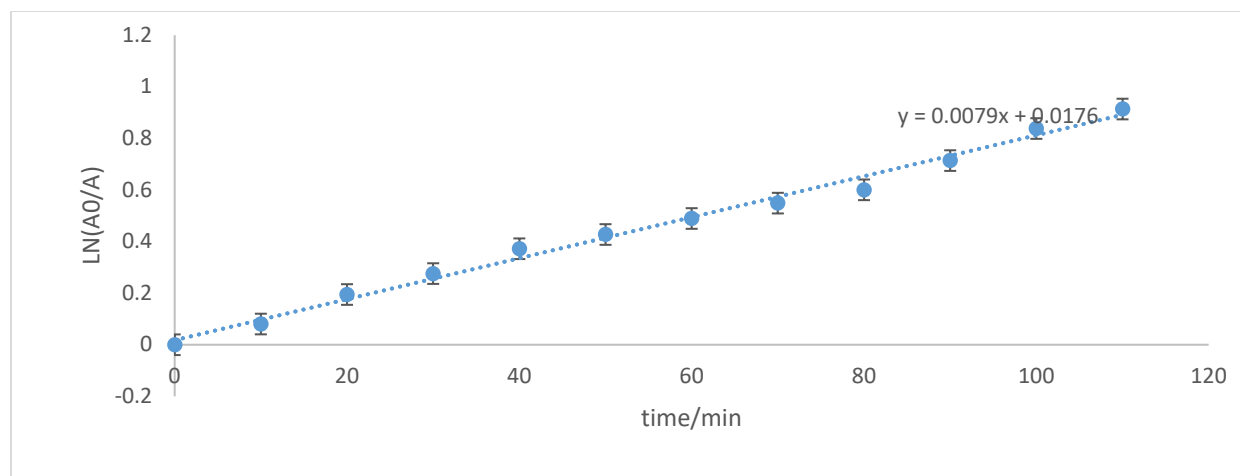


Figure 4.21 First order kinetic plot for the reductive elimination of **75** isolated as a BF_4 salts in CD_2Cl_2 . Slope is $(7.9 \pm 0.2) \times 10^{-3} \text{ min}^{-1}$ giving a half-life of 87 ± 2 minutes.

4.3.8.2 With 1.3 equivalents HBF_4

We repeated the same reaction as above but this time we combined **68·MeCN** with a small excess (1.3 equivalents) of HBF_4 . The rate of the C-N reductive elimination was monitored. The reaction plots in coordinates $\ln([\text{Pd(IV)}]_0/[\text{Pd(IV)}])$ vs. time (Fig. 4.21) and $1/[\text{Pd(IV)}]$ vs. time (Fig. 4.22) were not linear suggesting that, possibly, there are several reactions taking place. This confirms that the second equivalent of acid is critical to lower the activation energy for the C-N elimination reaction.

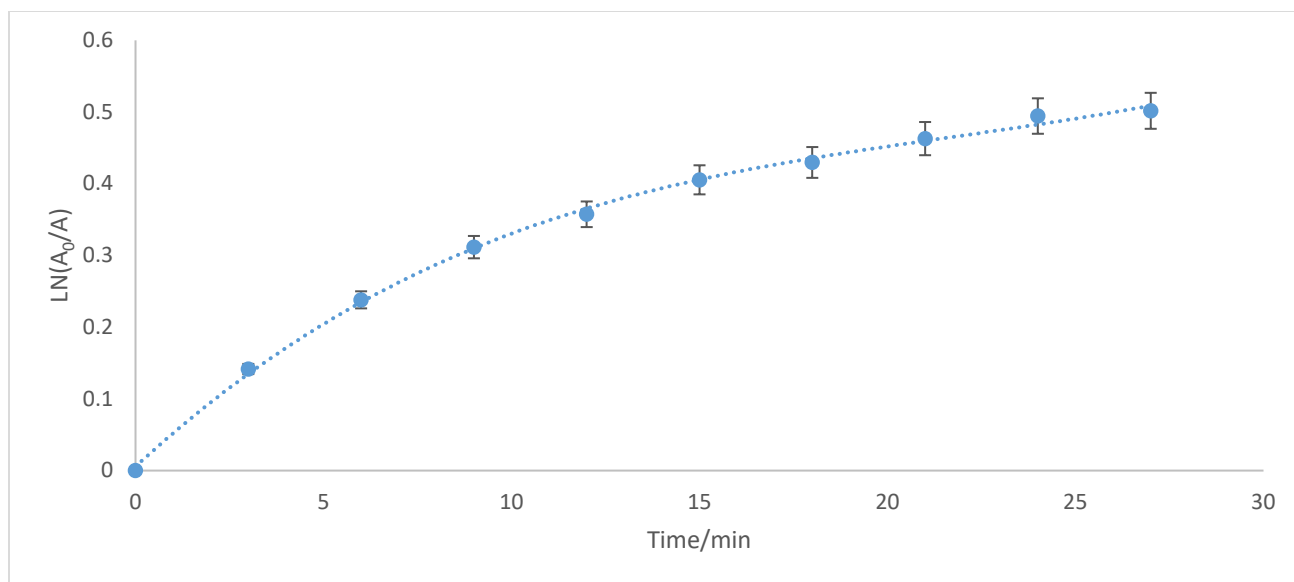


Figure 4.22. Plot of $\ln([\text{Pd(IV)}]_0/[\text{Pd(IV)}])$ vs. time/min for **68** with 1.3 equivalent of HBF_4 in CD_3CN at $22\text{ }^\circ\text{C}$

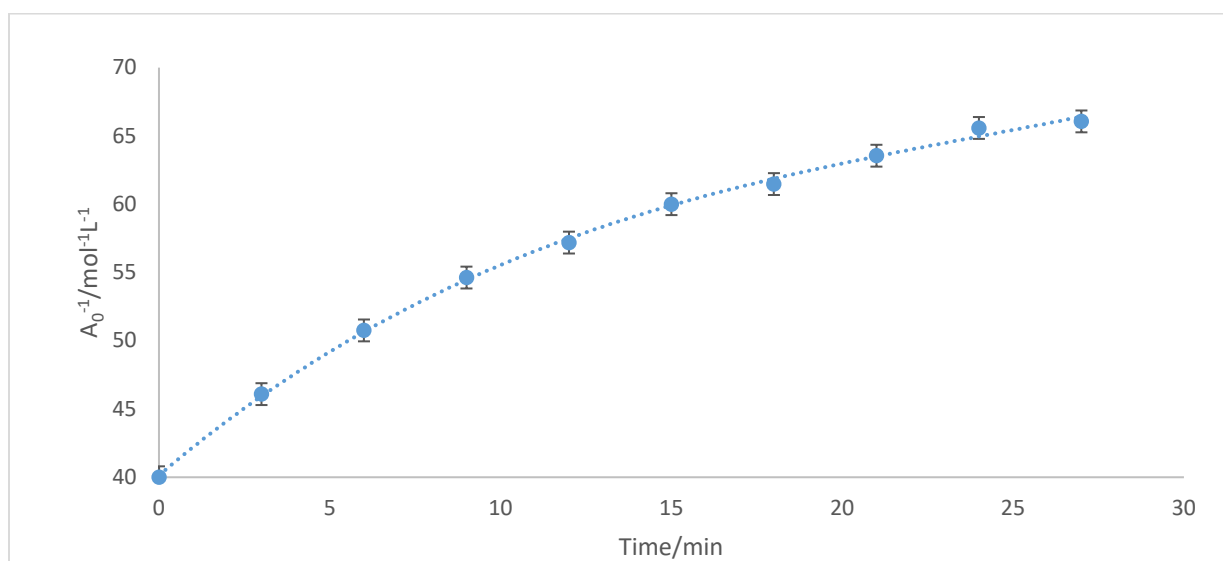
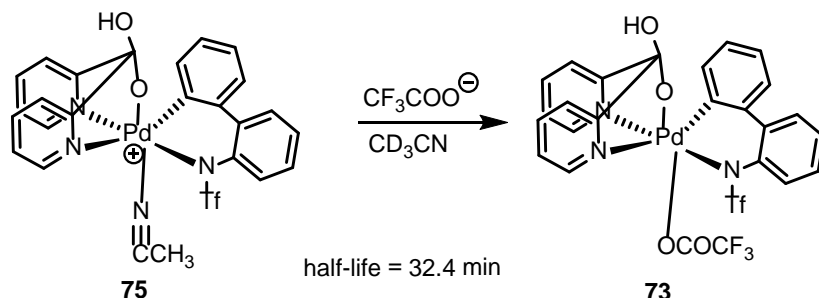


Figure 4.23. Plot of $[1/A]/\text{mol}^{-1}\text{L}^{-1}$ vs. time /min for **68** with 1.3 equivalents of HBF_4 in CD_3CN at $22\text{ }^\circ\text{C}$.

4.3.9 Lability of CD₃CN ligand in 75(BF₄)

4.3.9.1 Addition of CF₃COONa to a solution of 75(BF₄)



Scheme 4.14 Reactivity of **75** with CF₃COONa to form **78** at 22 °C.

To check how labile the CH₃CN ligand in **75** is we run an exchange reaction with CF₃COONa. 1.0 equivalent of CF₃COONa was added to a solution of **75** in CD₃CN. The mixture was stirred, allowed to settle for 5 minutes and the ¹H NMR spectrum was recorded. ¹H NMR spectrum of the resulting solution showed the formation of a new species in solution (Fig. 4.23). This new species observed in solution has an identical ¹H NMR spectral pattern to a trifluoroacetato Pd(IV) complex **73** (Fig. 4.24). We therefore assigned this new compound to **73**. The ligand exchange reaction was observed to follow a first order rate law with a half-life of 32±1 minutes (Fig. 4.25). It should be noted that, after 24 h, **73** was observed in solution in 73% yield together with other Pd-containing species whose identities we could not determine. Also, the carbazole **70** was observed in 17% yield. Our attempts to crystallize **73** were not successful.

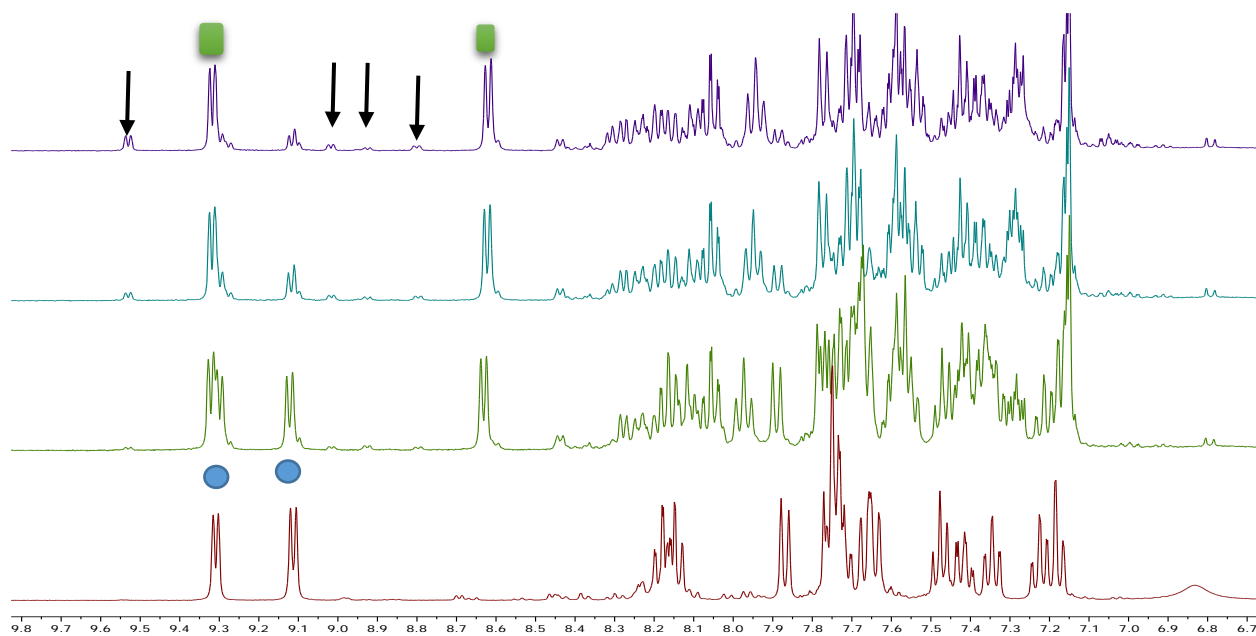


Figure 4.24. Exchange reaction of **75** with CF_3COONa . Blue circles show **75** and green squares show **70**. Arrows show intermediates or products which were observed in less than 5 % yield.

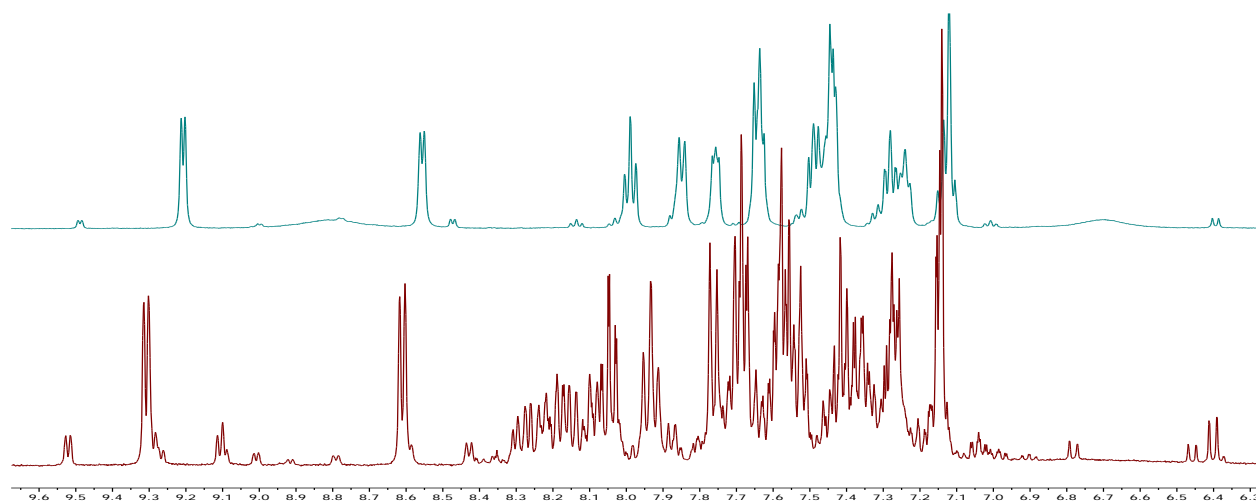


Figure 4.25 Comparison of the ^1H NMR spectrum of **73** (bottom) and **69** (top) in $\text{DMSO-}d_6$ at $22\text{ }^\circ\text{C}$

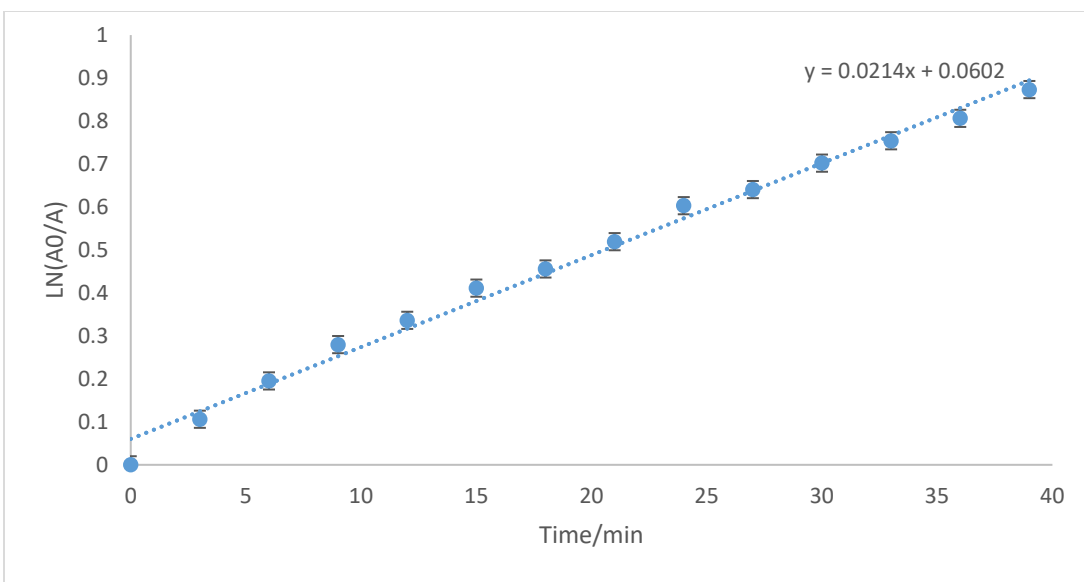


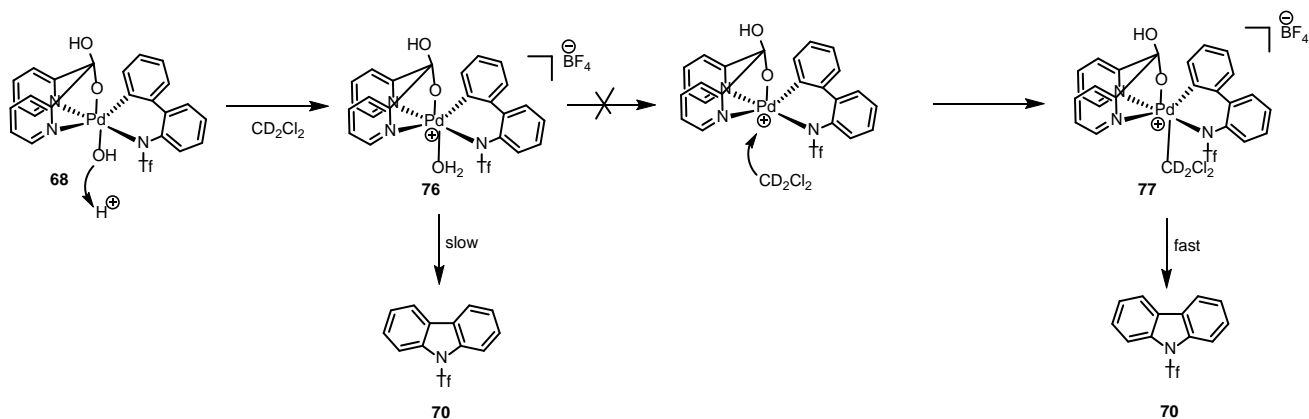
Figure 4.26 First order kinetic plot for the exchange reaction of the CH_3CN ligand in **75** with trifluoroacetate ion to form **73** in CD_3CN . The slope is $(2.14 \pm 0.06) \times 10^{-2} \text{ min}^{-1}$ giving a half-life of 32 ± 1 minutes

4.3.9.2 Addition of $\text{CF}_3\text{SO}_3\text{Na}$ to a solution of **75**(BF_4)

Since the more nucleophilic trifluoroacetate ligand was observed to undergo ligand exchange with CD_3CN as our apical ligand, we set out to see if a weakly nucleophilic trifluoromethyl sulfonate ligand can also undergo the same process. 1.0 equivalent of $\text{CF}_3\text{SO}_3\text{Na}$ was added to a solution of the cationic acetonitrile Pd(IV) complex **75** in CD_3CN and the mixture stirred and allowed to settle for 5 minutes, and the ^1H NMR spectrum was recorded. ^1H NMR spectrum of the resulting solution showed the formation of no new species in solution and no change in ^1H NMR pattern. This shows the trifluoromethyl sulfonate ligand is not nucleophilic enough to displace CD_3CN from **75**.

4.3.10 Reactivity of **68** in CD₂Cl₂ with 1 eq of HBF₄

We envisioned that the use of a very weakly coordinating solvent such as CD₂Cl₂ might help preserve the aqua ligand expected to form upon protonation of the Pd(IV)OH fragment with a strong acid. That, in turn, might help additionally speed up the reaction if the Pd(IV) aqua complex **76** is more reactive than the Pd(IV) MeCN complex **75** (Scheme 4.15). The displacement of the H₂O ligand in **76** with CH₂Cl₂ to form **77** might also be considered but is less likely. 1 equivalent of HBF₄(aq) was added to a suspension of **68** in CD₂Cl₂ and a purple solution was produced. The resulting solution was monitored by ¹H NMR spectroscopy and the rate of the C-N reductive elimination of **70** was monitored.



Scheme 4.15 Plausible reaction routes for **68** with 1 equiv of HBF₄ in CD₂Cl₂ at 22 °C.

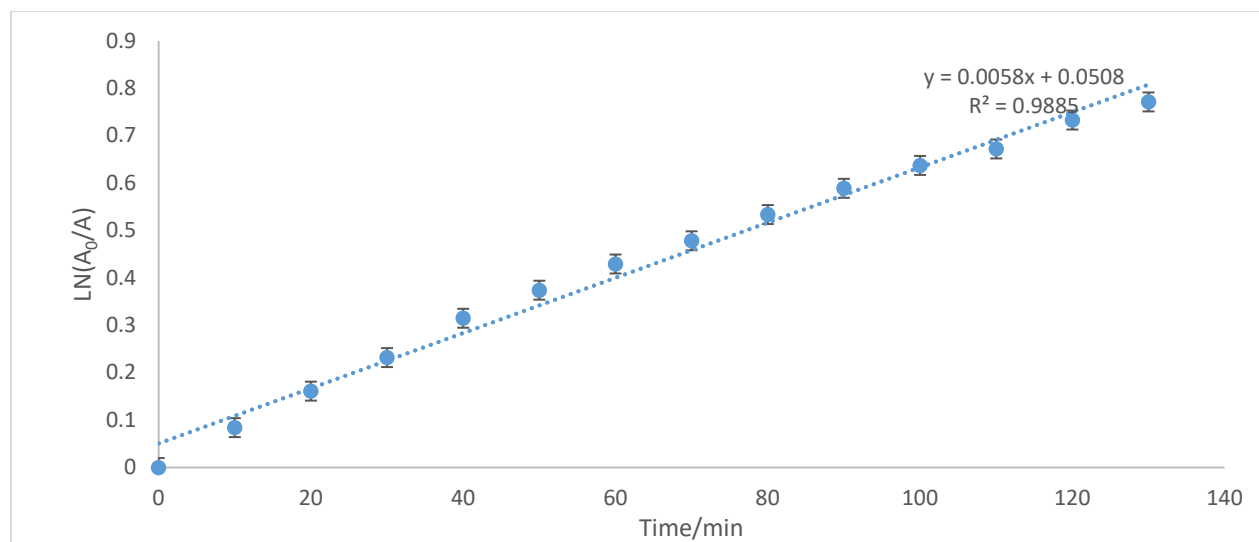
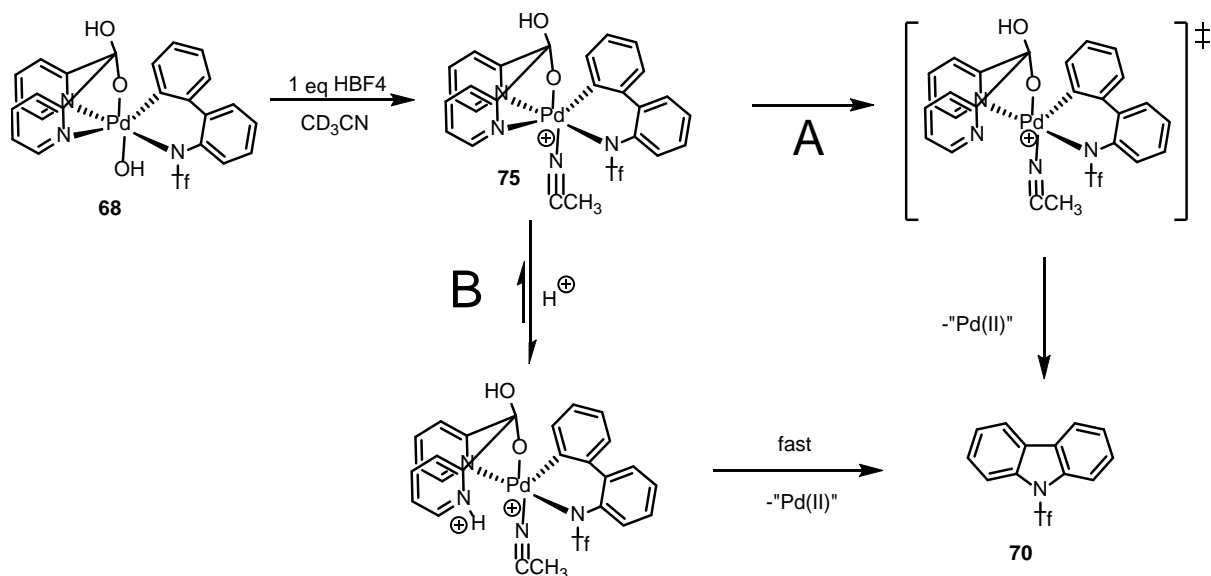


Figure 4.27. Plot of $\ln([\text{Pd(IV)}]_0/[\text{Pd(IV)}])$ vs time/min for **68** with 1 equivalent of HBF_4 in CD_2Cl_2 at 22°C . Slope is $(5.8 \pm 0.2) \times 10^{-2} \text{ min}^{-1}$ giving a half-life of (119 ± 4) minutes.

The reaction followed a clean first-order kinetics with the half-life of 119 ± 4 min at 22°C (Fig. 4.27). The rate of the C-N reductive elimination of this solution is comparable to that of **75** (half-life 87 ± 2 min at 22°C) which does not allow one to conclude if the C-N reductive elimination occurs from the aqua complex **76** or from the CH_2Cl_2 adduct **77**. To add to the complexity of the system, **75**, **76** and **77** are proposed to exist in CH_2Cl_2 solutions as ion-pairs with BF_4^- . Accordingly, our attempts to observe **75**, **76** or **77** in CH_2Cl_2 solutions by ESI(+)/MS were not successful.

4.3.11 Proposed mechanism for C-N bond elimination of **68** in MeCN containing HBF₄ additives



Scheme 4.16 Proposed reaction scheme for the C-N reductive elimination from **68** in the presence of 1 equivalent of HBF₄ in CD₃CN to form **70** at 22 °C.

Based on our observations presented in this Chapter, we can propose several mechanisms for the C-N coupling of **68** in the presence of HBF₄ in CD₃CN solutions (Scheme 4.16). In all the mechanisms the first step is just protonation of the most basic Pd(IV)OH fragment of **68** which produces the aqua complex **76**. In neat MeCN the weakly bound aquo ligand is easily displaced by CD₃CN to form the acetonitrile complex **75**. **75** can undergo a direct C-N reductive elimination to form **70** without prior loss of any ligand. The corresponding 6-coordinate transition state ($\Delta G = 25.4$ kcal/mol) has a partly dissociated pyridyl nitrogen *trans* to the aryl ligand (path A), as shown by our DFT calculations (Fig. 4.28). The cation **75** is involved in strong ion-pairing with BF₄⁻ counterion; the contact ion pairs **75**⁺,BF₄⁻, according to the DFT, are involved in the rate-limiting C-N reductive elimination step.⁷² Alternatively, **75** can be further protonated to form a

more electron-poor dicationic Pd(IV) species which might undergo reductive elimination more readily (**Path B**).

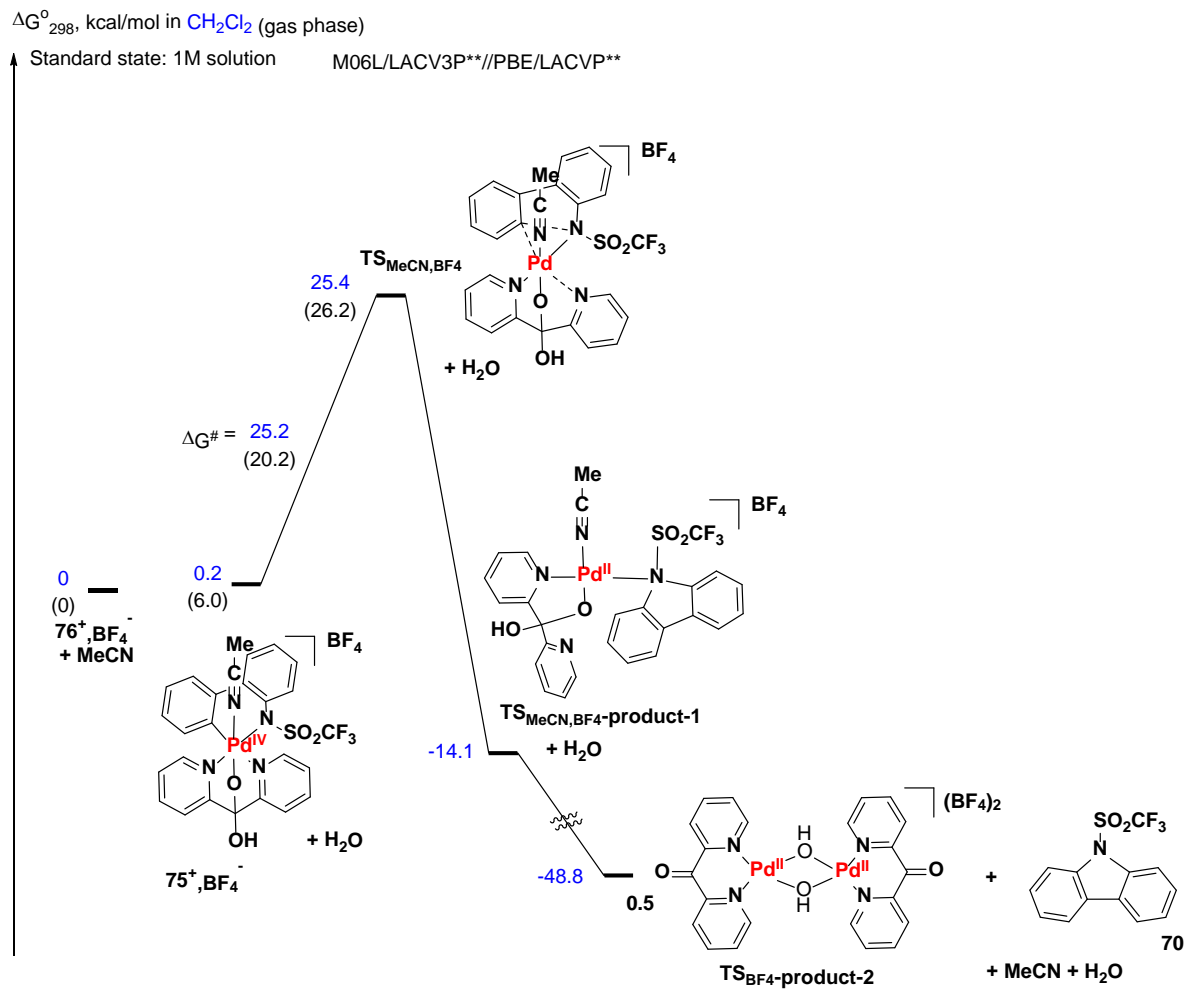


Figure 4.28. The Gibbs energy profile for the C-N reductive elimination of $75^+, \text{BF}_4^-$ in CH_2Cl_2 .

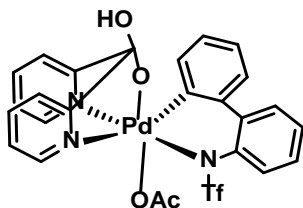
4.4 Conclusion

In conclusion, we explored reactivity of two similar N-sulfonylated amido aryl Pd(IV) complexes **62** and **68** and were able to characterize the C(sp²)-N elimination from Pd(IV) center for the first time. The electron richer N-methanesulfonyl complex **62** reductively eliminates the corresponding carbazole **65** under ambient conditions in MeOH and DMSO solutions. According to DFT calculations, the elimination occurs directly from a 6-coordinate Pd(IV) center. This mechanism is rare for d⁶ metal complexes and is enforced by the presence of a relatively rigid *fac*-coordinating hydrated dpk ligand. Conversely, the electron poorer N-trifluoromethanesulfonyl complex **68** was observed to undergo reductive elimination very slowly in MeOH at 22 °C and slightly faster in AcOH. In turn, an additive of a strong acid with a weakly coordinating anion such as HBF₄, HClO₄ or HOTf can speed up the reaction rate dramatically both in MeCN and in CH₂Cl₂ solutions. The reactions involve formation of reactive cationic MeCN or aqua complexes which, according to our DFT calculations, are expected to exist as ion-pairs in CH₂Cl₂ solutions. The rate of reductive elimination is also dependent on the amount of acids added which is proposed to alter the reaction mechanism to involve, presumably, dicationic 5-coordinate intermediates where one of the dpk nitrogen atoms is protonated and cannot participate in coordination with Pd(IV) center. Addition of 1 equivalent of acid showed a reductive elimination half-life of about a 100 minutes at 22 °C whereas 2 equivalents of strong acid lead to complete reductive elimination in about 15 minutes.

4.5 Experimental

Synthesis of 69

69 was synthesized by stirring 15 mg of **68** in AcOH (1.0 mL) for 24 h. A brown precipitate which formed was isolated and washed with cold Et₂O; yield of the target compound is 53%.

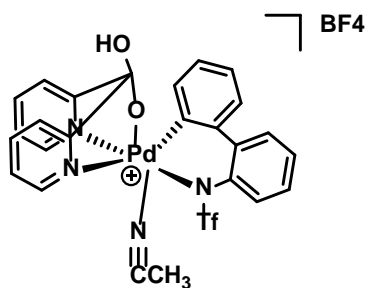


¹H NMR (500 MHz, DMSO-*d*₆) δ 9.17 (d, *J* = 5.3 Hz, 1H), 8.92 (d, *J* = 5.8 Hz, 1H), 8.72 (s, 1H), 8.10 (t, *J* = 7.7 Hz, 1H), 8.08 – 8.02 (m, 1H), 7.68 (d, *J* = 7.7 Hz, 1H), 7.65 – 7.55 (m, 5H), 7.52 (d, *J* = 7.7 Hz, 1H), 7.32 (t, *J* = 7.2 Hz, 1H), 7.27 (td, *J* = 7.7, 7.2, 1.9 Hz, 1H), 7.18 (t, *J* = 7.5 Hz, 1H), 7.10 (t, *J* = 7.6 Hz, 1H), 7.01 (d, *J* = 8.0 Hz, 1H), 2.07 (s, 3H). ¹³C NMR (126 MHz, DMSO) δ 174.06, 171.92, 163.35, 158.82, 150.93, 148.72, 147.41, 141.70, 139.70, 137.89, 137.79, 135.75, 129.88, 128.55, 127.80, 127.52, 127.31, 126.96, 125.82, 125.47, 123.58, 121.83, 119.63, 102.57, 23.66. ¹⁹F NMR (376 MHz, DMSO-*d*₆) δ -73.56

Synthesis of 75

In a small vial containing 12 mg of **68**, 0.40 mL of CH₃CN was added in which it is virtually insoluble at 0 °C. 0.9 equivalents of HBF₄ was added to the system and stirred for 5 minutes. The liquid turned purple; a small amount of precipitate remained on the bottom and the solution was

transferred into another vial. Solvent was quickly removed under vacuum at 0 °C and the residue dissolved in CD₂Cl₂



¹H NMR (500 MHz, CD₂Cl₂-d₂) δ 9.43 (d, *J* = 5.9 Hz, 1H), 9.31 (dt, *J* = 5.1, 1.2 Hz, 1H), 8.07 (tdd, *J* = 8.6, 6.2, 1.6 Hz, 1H), 7.96 (td, *J* = 7.7, 1.2 Hz, 1H), 7.86 – 7.79 (m, 3H), 7.68 – 7.63 (m, 2H), 7.61 (dd, *J* = 8.0, 1.4 Hz, 1H), 7.48 – 7.40 (m, 3H), 7.32 (td, *J* = 7.4, 1.6 Hz, 1H), 7.26 – 7.15 (m, 2H), 5.17 (s, 1H), 2.73 (s, 3H).

General procedure for the reactivity of **68** with acids

An NMR tube was charged with 10 mg of complex **68** and 0.60 mL of CD₃CN was added. To the resulting solution was added the appropriate equivalent of acid at 22 °C. The resulting solution was monitored by ¹H NMR spectroscopy for the C-N reductive eliminated product.

General procedure for the C-N reductive from **68** or **63**

An NMR tube was charged with 10 mg of complex **68** or **63** and 0.60 mL of appropriate solvent was added (MeOD, CD₃CN, AcOD, THF-*d*₈ or DMSO-*d*₆). The resulting solution at the stated temperature for the formation of the C-N reductively eliminated products.

Chapter 5. Synthesis and Reactivity of κ^2 -C,N-2'-(2',2'-dimethylethanediy)-N-R-anilido Pd(II) Complexes with Electron Withdrawing Group R=SO₂CF₃

5.1 Introduction and Background

The direct amination of C-H bonds is a unique synthetic approach towards the important class of alkylated nitrogen compounds.⁷³ In this context, the palladium-catalyzed intermolecular C(sp³)-H oxidative amination of alkyl groups is a notably unexplored process.⁷⁴ The Glorius group⁷⁵ reported the first direct intramolecular C(sp³)-H amination of 2-*tert*-butylanilines to form indolines with AgOAc as oxidant and Pd(OAc)₂ as a catalyst. Intermolecular competition experiments using differently 4-substituted anilines did not show any significant effect of the electronic properties of the aromatic ring on the reaction rate. A Pd(IV) complex was postulated as an intermediate which undergoes a direct reductive elimination to give the corresponding indolines.⁷⁵ The Muniz group, while working on the formation of alkyl–nitrogen bonds from σ -alkyl palladium intermediates in the context of developing intermolecular di-amination reactions of alkenes employing high-oxidation-state palladium catalysis, reported an oxidative C(sp³)-H amidation reactions.^{76, 77} DFT calculations and kinetic experiments showed the reaction of the amide group in an S_N2 like fashion with a highly electrophilic Pd(IV) intermediate.⁷⁸ The Yu group while working on synthesizing indolines from 2-phenethylamine substrates reported two novel approaches to achieve highly selective reductive elimination of an amino nucleophile from oxidized Pd(III) or Pd(IV) species to form indolines using either a one-electron Ce(IV) oxidant or a two-electron oxidant (F⁺).⁷⁹

Based on these findings, the Sanford group decided to study the direct C(sp³)-N reductive elimination from an isolated Pd(IV) complex. Both kinetic experiments and DFT calculations

showed an S_N2 like reductive elimination from the Pd(IV) center to give the target compound (Chapter 1).^{54, 55}



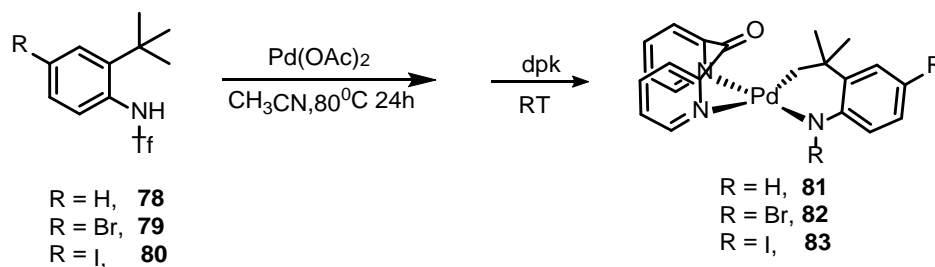
Scheme 5.1 Direct synthesis of substituted *N*-acylindolines from corresponding substituted *N*-acyl-2-*tert*butylanilides as reported by Glorius.

5.2 Preparation, characterization, and oxidation of dpk-supported amido alkyl Pd(II) complex, **81**

5.2.1 Preparation and characterization of *N*-(2-*tert*butylphenyl)trifluoromethanesulfonamidePd(II)(dpk), **81**

Based on the work done by Glorius,⁷⁵ we decided to study the intramolecular oxidative C(sp³)-H amination reaction involving cyclopalladated 2-*tert*-butylanilines to form the corresponding indolines (Scheme 5.1). Our attempts to produce the derived pallada(II)cycles by reacting Pd(OAc)₂ with various *N*-R-*tert*-butylanilines (R= H, acetyl, trifluoroacetyl and methanesulfonyl) were only successful with the *N*-triflyl-2-*tert*-butylaniline substrates **78-80** (Scheme 5.2). The dpk-supported palladacycles **81-83** were prepared by a one-pot synthesis from the corresponding *N*-R-2-*tert*-butylaniline precursors. The 2-*tert*-butylanilide precursors were combined with 0.9 equivalents of Pd(OAc)₂ in CH₃CN, and the resulting solution refluxed at 78 °C for between 4 to 8 hours until Pd black is observed. This solution is passed through Celite and 0.9 equivalents of

dpk was added. The mixture was stirred at room temperature for about 4 h to produce the target compounds **81-83** which could be isolated by crystallization.



Scheme 5.2 Synthesis of dpk ligated 2-*tert*butylaniline palladacycles **81-83**.

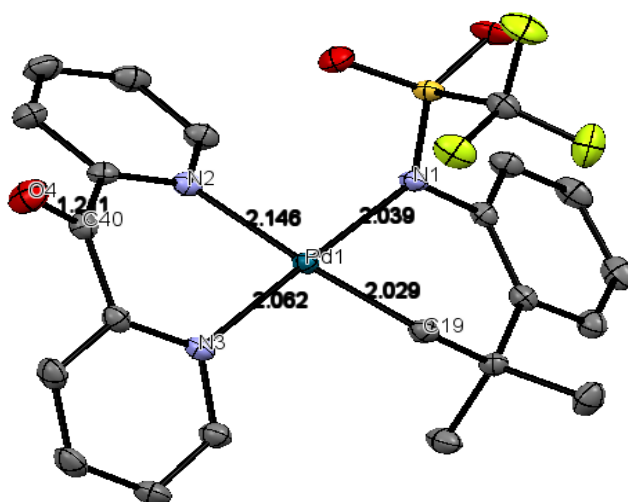


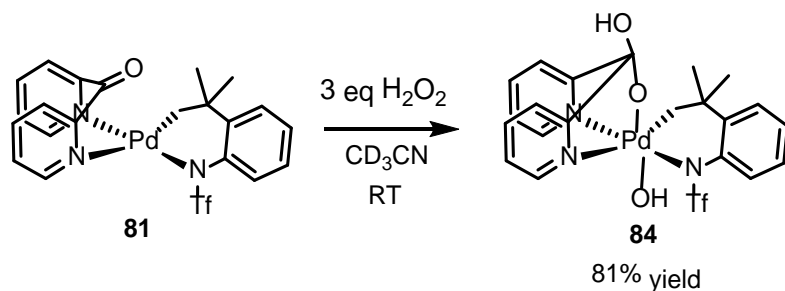
Figure 5.1 X-ray crystal structure of **81·MeCN** (the solvent of crystallization is not shown).

The so-prepared parent complex **81·MeCN** bearing no substituents on the anilide fragment was characterized by ^{13}C NMR spectroscopy in CD_3CN . In the absence of hydroxylic co-solvents the compound was found to exist in its keto-form **81**. There was no peak at about 95 ppm in its ^{13}C NMR spectra characteristic of the ketal carbon whereas the signal of the dpk carbonyl group at about 188 ppm was observed. ^{19}F NMR spectrum of **81** confirmed the presence of only one species

in solution. The composition **81**·MeCN was confirmed by elemental analysis. The presence of one molecule of CH₃CN of crystallization was confirmed by single crystal X-ray diffraction (Fig. 5.1).

The X-ray diffraction shows the square planar geometry around the palladium center in **81** which is expected for a d⁸ Pd(II) center. The dpk fragment is coordinated to Pd in the κ²-N,N mode and the C=O group is slightly bent out to form a boat-like structure. The C=O bond length of 1.216(2) Å is in strong agreement with a double bond character between C40 and O4. The Pd1-N2 bond is elongated (2.146 Å (3)) relative to the Pd1-N3(2.062(2) Å) bond which shows the stronger trans influence of the alkyl group in comparison to the amido fragment of the Pd bound 2-*tert*butylaniline fragment. Also, the bond between the Pd1-C19 is shorter (2.029(3) Å) compared to Pd1-N1(2.039(2) Å).

5.2.2 Oxidation of **81** with H₂O₂ to form **84** (Scheme 5.3)



Scheme 5.3 Synthesis of **84**

Upon addition of 3 equivalents of H₂O₂ to **81** dissolved in CD₃CN, the singlet at about 2.17 ppm assigned to the Pd(II)-bound CH₂ group was transformed to two doublets at 4.69 and 4.58 ppm, consistent with the formation of a more electron deficient Pd(IV) center and an increased rigidity of the resulting molecule **84** allowing for a convenient observation of signals of two

inequivalent diastereotopic protons of the CH_2Pd group. Also, the singlet at 1.46 ppm (6H), which was assigned to two methyl groups present in the metallacycle **81** was transformed to two singlets at 1.70 ppm and 1.58 ppm so additionally confirming the formation of an electron deficient and rigid Pd(IV) structure. After allowing the reaction to stand at room temperature, the intensity of the NMR signals diminished gradually with the formation of a precipitate. The identity of the precipitate as a solvate **84**·MeCN was confirmed by X-ray crystallography and its purity confirmed by elemental analysis.

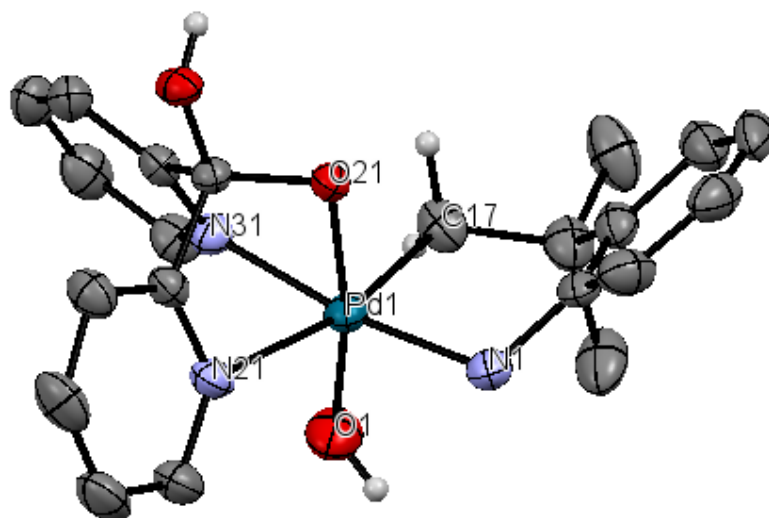


Figure 5.2 X-ray crystal structure of **84**·MeCN (the solvent of crystallization and trifluoromethylsulfonyl groups are not shown for clarity). Selected bond lengths (Å): Pd1-O21 2.032 (2), Pd1-O1 1.980 (3), Pd1-N1 2.052 (3), Pd1-C17 2.042 (4), Pd1-N21 2.283 (3), Pd1-N31 2.031 (3)

Table 5.1 Solubility of **84**·MeCN in different common solvents.

Solvent	Solubility
DMSO	good
MeOD	poor
Acetone	Negligible
Dichloromethane	poor
Toluene	Negligible
Acetic Acid	good
Acetonitrile	Negligible

¹H NMR spectrum of the isolated product in DMSO shows the presence of only one metal-containing species in solution. The two downfield shifted doublets at 9.0 ppm and 8.60 ppm were assigned to the *ortho*-pyridyl protons. The singlet at 8.21 ppm was assigned to the OH group of the hydrated dpk fragment. The multiplet at about 4.41 ppm was assigned to the Pd bound CH₂ fragment. The Pd bound OH group signal was observed at 2.67ppm.

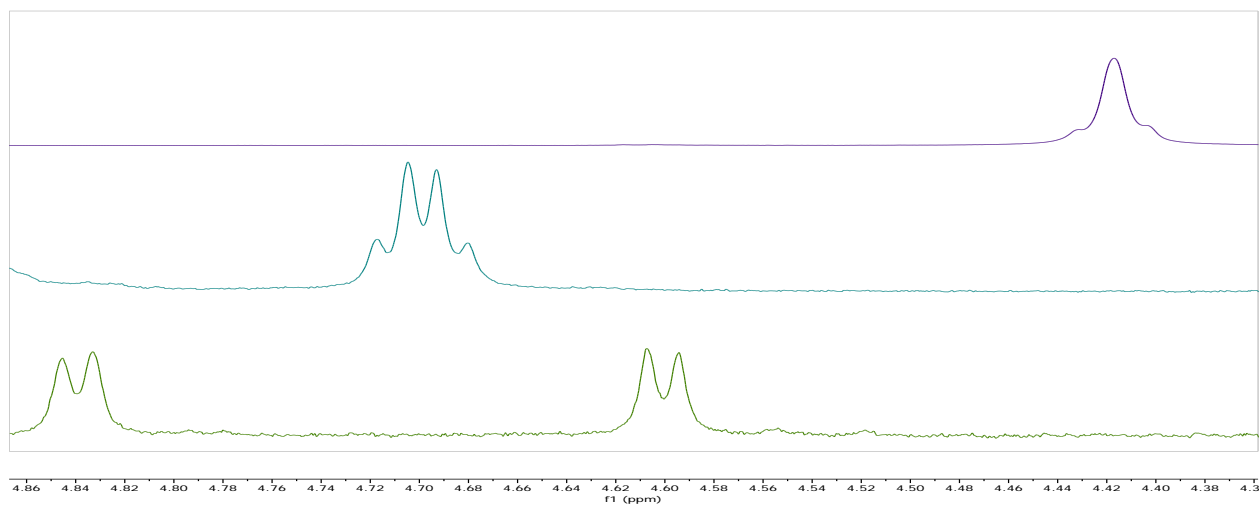
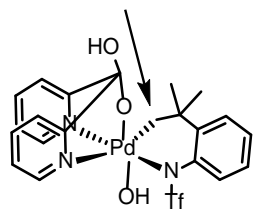
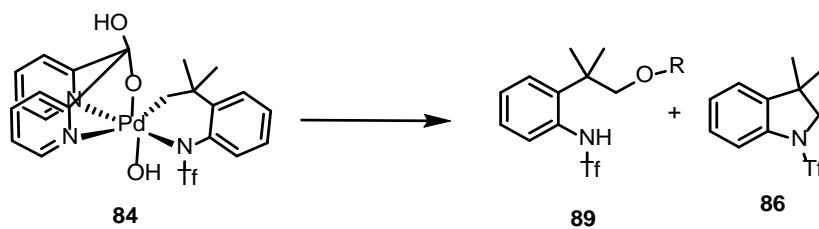


Figure 5.3 ^1H NMR spectrum of the $\text{CH}_2\text{Pd(IV)}$ fragment of **84** in different solvents: CD_2Cl_2 (bottom), MeOD (middle) and $\text{DMSO-}d_6$ (top). Arrow points to protons of interest.

5.3 Reactivity of **84** in different solvents



Scheme 5.4 Reductive elimination from **84** to form **86** and/or **89** ($\text{R} = \text{H}$).

5.3.1 Acetonitrile

Although **84** is not soluble in CD₃CN, the addition of 3 equivalents of TFA, led to its dissolution with a change in color from the yellowish orange crystals to a deep reddish brown solution. ¹H NMR spectrum analysis of this mixture showed the presence of a complex mixture. Analysis of chemical shift range between 3.5 ppm and 6 ppm shows the presence of three different species in solution in the ratio of 1: 0.3: 0.04. This is the chemical shift range where the characteristic signals of the methylene fragment bound to the Pd(IV) center show up (Fig. 5.4). The major component of the acidic solution of **84** produced two doublets at 5.04 ppm and 5.36 ppm. When this mixture was allowed to stand for 42 hours and then heated at 60 °C for 3h, the expected C-N coupled product, indoline **86**, formed only in 3% yield whereas the major organic product of the reaction was the C-O coupled compound, alcohol **89**, produced in about 40% yield. About four different species containing a rigid methylene fragment in the form of AB quartets were observed in solution.

5.3.2 Acetone

Similar to acetonitrile, **84** is not soluble in Acetone-*d*₆ but the addition of 3 equivalents of TFA leads to dissolution of **84** with a change in color from the yellowish orange crystals into deep orange solution. ¹H NMR analysis of the resulting solution in the chemical shift range between 3.5 and 6 ppm revealed the presence of 6 sets of signals originating from a CH₂Pd fragment. The major species produced two doublets at 5.06 ppm and 5.32 ppm each (*J* = 1.5 Hz). The C-O coupled product **89** was observed in about 5% yield with no C-N coupled product **86** present. After the solution had been allowed to stand at 22 °C for about 42 h and heated at 60 °C for 3 hours, the composition of the mixture showed no apparent change.

5.3.3 Methanol

84 is poorly soluble in MeOD and its Pd(IV)-CH₂ group signal is observed as a multiplet at 4.68 ppm. Addition of 3eq of TFA to **84** dissolved in MeOH led to the rapid formation of a deep yellow solution. ¹H NMR spectrum analysis of the solution showed the presence of four different sets of signals originating from a CH₂Pd fragment, together with the C-O coupled product **89**. After the solution was allowed to stand at 22 °C for about 42 h and heated at 60 °C for 3 hours, the C-O coupled product was the only organic product observed by ¹H NMR spectroscopy.

5.3.4 Toluene

84 is not soluble in Toluene-*d*₈ but addition of 3 equivalents of TFA leads to its dissolution with a change in color from the yellowish orange crystals to a deep reddish brown solution. ¹H NMR spectral analysis of the resulting solution showed the presence of six different sets of signals originating from a CH₂Pd fragment. The major species produces two doublets at 5.06 ppm and 5.32 ppm (*J* = 1.5 Hz). The C-O reductively eliminated product **89** was observed in about 5% yield; no C-N product was found. After the solution was allowed to stand at 22 °C for about 42 h and heated at 60 °C for 3 hours, the C-O coupled product **89** was observed in 27% yield.

5.3.5 Dichloromethane

84 is poorly soluble in CD₂Cl₂, and the CH₂Pd group signal is observed as a two doublets at 4.60 ppm and 4.84 ppm. The addition of 3eq of TFA to the solution of **84** led to the rapid formation of a deep yellow solution. ¹H NMR spectrum analysis of the solution showed the presence of four different species containing a PdCH₂ fragment together with the C-O coupled product **89**. After the solution was allowed to stand at 22 °C for about 42 h and heated at 60 °C for 3 hours, the C-O reductively eliminated product was the only organic product observed in the ¹H NMR.

5.3.6 Acetic acid

84 is soluble in AcOD and the PdCH₂ group signal is observed as a multiplet at 4.68 ppm. The addition of 3eq of TFA to the above solution of **84** led to the rapid formation of a deep yellow solution. ¹H NMR spectrum analysis of the solution showed the presence of four different species containing a PdCH₂ fragment together with a C-O coupled product. After the solution was allowed to stand at 22 °C for about 42 h and heated at 60 °C for 3 hours, the C-O reductively eliminated product **89** was the only organic product observed in the ¹H NMR spectrum.

5.3.7 DMSO

84 is soluble in DMSO, and the PdCH₂ group signal is observed as a multiplet at 4.41 ppm. The addition of 3eq of TFA to the solution of **84** led to the rapid formation of a deep reddish-yellow solution. ¹H NMR spectrum analysis of the solution showed the presence of one species containing a PdCH₂ fragment together with a peak at about 3.59. After the solution had been allowed to stand at 22 °C for about 42 h and heated at 60 °C for 3 hours, the peak at 3.59 ppm was persistent together with the C-N coupled product **86**. 3 different Pd(IV) containing species were also observed in addition to the C-N coupled product **86**.

5.4 Reactivity of **84** with different additives

5.4.1 Pyridine

In our previous work dealing with oxidative C-N coupling of 2-aminobiphenyl substrates (Chapter 4), we observed that various acid additives affect the rate of C-N reductive elimination of Pd(IV) amido aryl complexes. Based on these results, effect of additives of varied acidity was also

explored on the C-N reductive elimination of the Pd(IV) amido alkyl complex **84**. Free pyridine, its salt with trifluoroacetic acid (TFA) and TFA itself were used in these experiments.

No change in the ^1H NMR spectrum of **84** in $\text{DMSO-}d_6$ was observed after adding 5 equivalents of pyridine. The solution was then heated at $90\text{ }^\circ\text{C}$ for about 2 hours which led to the formation of Pd black. No C-N reductively eliminated product was observed.

5.4.2 Pyridine-TFA

We next used a more acidic compound, a pyridine-TFA adduct produced by mixing one equivalent of TFA to 1 equivalent to pyridine in ice. A white /colorless solid salt was isolated. When 3 equivalents of this salt was added to $\text{DMSO-}d_6$ solution of **84**, a change in the chemical shift was observed for the Pd- CH_2 group. Its original multiplet signal at 4.1 ppm was transformed to two doublets at 5.1 and 4.8 ppm whereas the color of the solution has changed from light orange to dark red. When the resulting solution was allowed to stand for 14 h, the C-N coupled product **86** was observed in 8% NMR yield. In addition to the indoline **86**, the C-O coupled product **89** was produced in 11% yield. 6 different sets of signals originating from minor Pd(IV) species were also observed between 4.5 ppm and 6.0 ppm. When the reaction was heated at $60\text{ }^\circ\text{C}$ for 3 hours, the yield of the indoline **86** has increased to about 23% whereas the amount of **89** did not change noticeably. Hence, the selectivity of the C-N coupling increased at higher temperatures.

5.4.3 Trifluoroacetic acid (TFA)

Based on the above observations, we expected a more dramatic consequences for the C-N coupling reaction in the presence free TFA. Therefore, the reaction was attempted in the presence of TFA. 3 equivalents of TFA was added to a solution of **84** in $\text{DMSO-}d_6$. Similar to the experiment with the py-TFA adduct, two doublets were produced at 5.1 ppm and 4.8 ppm. When the resulting

solution was allowed to stand for 18 h, the C-N coupled product was observed in 3% yield. In addition, 4 sets of signals originating from a Pd(IV)CH₂ fragment were observed between 4.5 ppm and 6.0 ppm. When the reaction was heated at 60 °C for 3 hours, the yield of the C-N coupled product has increased to about 5% yield. The C-O coupled product **89** producing a signal at 3.59 ppm was observed in about 2% yield.

To rationalize these results, we needed to find out if the reaction C-N vs. C-O coupling selectivity depends solely on a fine balance of the solution acidity or there may be other factors involved, such as the coordinating ability / nucleophilicity of the acid anion. As such, the effect of different acids on the **86:89** product ratio was explored.

5.4.4 Acetic acid

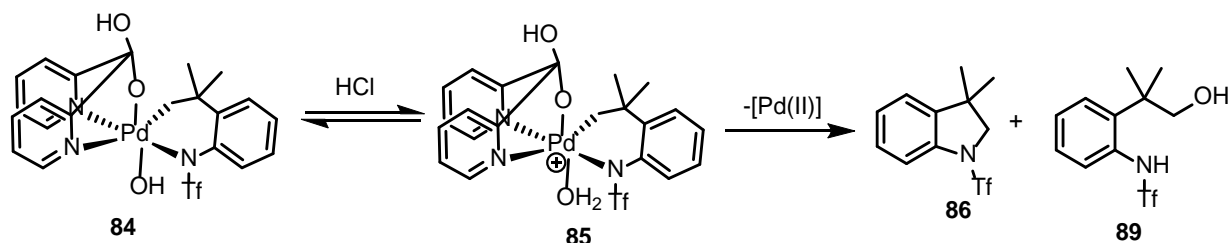
When 3 equivalents of acetic acid was added to a DMSO-*d*₆ solution of **84**, there was no change in color. ¹H NMR spectrum analysis of the resulting solution showed the presence of two doublets at about 4.47 and 4.43 ppm. No indoline was produced. Hence, the acetic acid is too weak to induce the C-N coupling.

5.4.5 Brookhart's acid

Brookhart's acid, [(Et₂O)₂H][BAr^F₄], was synthesized according to the literature.⁸⁰ In this case, the BAr^F₄⁻ counterion is virtually non-coordinating, and all the effects could be ascribed to the acidity change of the mixture. 2 equivalents of Brookhart's acid were added to a DMSO-*d*₆ solution of **84**. Immediately, the color of the solution changed from light orange to deep red. ¹H NMR spectrum analysis of the solution showed two doublets at 5.00 ppm and 4.82 ppm. When the resulting solution was allowed to stand for 60 hours, the C-N coupled product was observed in 6%

NMR yield and the C-O product was observed in about 86% yield. Hence, high acidity of the mixture alone favors formation of the C-O coupled product.

5.4.6 Hydrochloric acid



Scheme 5.5. Reactivity of **84** in the presence of HCl to form a rapidly equilibrating mixture of **84** and a derived aqua complex **85** which undergoes reductive elimination to produce **86** and **89**

Upon addition of 2 equivalents of HCl to DMSO solution of **84**, immediately, the color of the solution turned from light orange to deep red. ¹H NMR spectrum analysis of the solution showed two PdCH₂ group – containing intermediate species in solution; a major and minor one. The major signal at 5.33 ppm was broad and had an intensity-matching doublet at 4.76 ppm (*J* = 4.8 Hz). The minor species produced two doublets at 4.92 ppm and 4.50 ppm (*J* = 4.8 Hz). The major signals were observed to shift over time whereas those corresponding to the minor species were stationary (Figure 5.4). For instance, the original broad peak at 5.33 ppm shifted to 5.00 ppm, and the matching doublet shifted from 4.76 ppm to 4.70 ppm in about 1 hour. Both signals decreased in intensity with the simultaneous formation of the C-O and C-N coupled products. When the resulting solution was allowed to stand for 2 hours, and heated to at 60 °C for 1h, the C-N coupled product **86** was observed in 33% yield and the C-O coupled product **89** was observed in about 36% yield.

We assign the major signals observed in the 4-6 ppm range to a rapidly equilibrating mixture of **84** and a derived aqua complex **85**. The position of the equilibrium and the resulting averaged Pd(IV)CH₂ group signals are sensitive to changes of acid concentration in solution, so explaining their evolution in time as HCl was gradually consumed (Scheme 5.5).

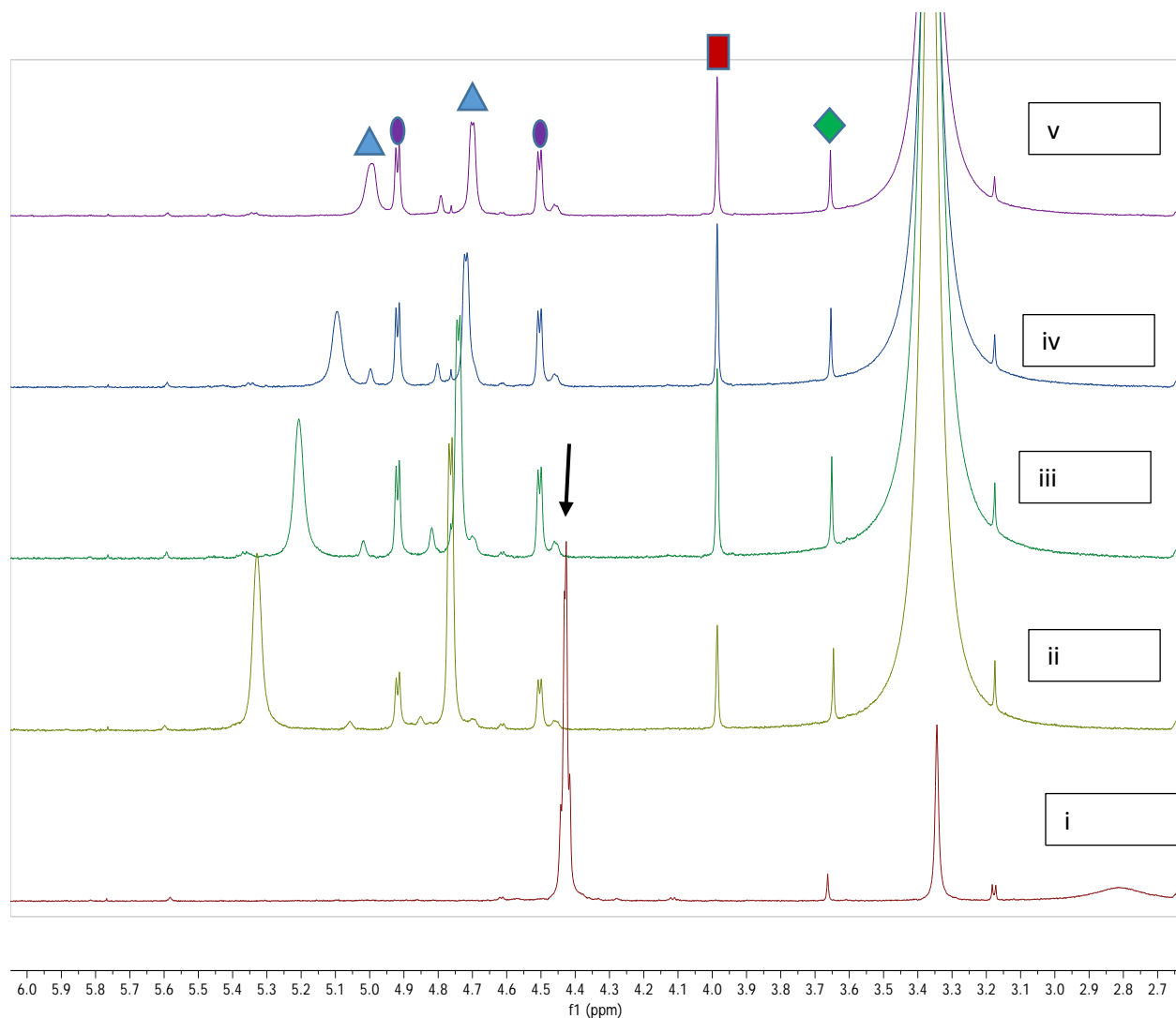


Figure 5.4 Reactivity of **84** with 2 equivalents of HCl. Blue triangle shows **85** in solution, purple circle shows an unknown intermediate observed, arrow shows **84**, red square shows **86** and green diamond shows **89**.(i) Before addition of HCl (ii) 15 minutes after addition of HCl (iii) 30 minutes after addition of HCl (iv) 45 minutes after addition of HCl (v) 60 minutes after addition of HCl.

5.4.7 Hydrobromic acid

Since the reaction of **84** with HCl was more selective with respect to the C-N coupled product than in the case of the Brookhart acid, we assumed that the nucleophilicity of the former acid counterion, Cl⁻, may be important for the reaction selectivity. Hence, we next tried aqueous HBr (48% v/v) that can produce an even more nucleophilic bromide anion. The addition of 3 equivalents of HBr to a DMSO-*d*₆ solution of **84**, led to the rapid formation of the C-N coupled product in about 58% yield after 15 min. At this time three sets of signals born by the PdCH₂ group were also apparent between 4.5 ppm and 6 ppm (Fig. 5.5). The major of these sets included two doublets in the ¹H NMR spectrum at 5.10 ppm and 4.81 ppm. The peak at 5.10 shifted to 5.01 in about 1 h, as the C-X coupling reaction progressed, whereas the corresponding peak at 4.81 ppm was only slightly affected. As previously, the major set of signals was assigned to a rapidly equilibrating mixture of **84** and **85**. The second major set of signals included two doublets at 5.26 ppm and 5.00 ppm. The third set of signals included a multiplet at 5.48 ppm. When the reaction was monitored by ¹H NMR for 7 hours, only trace amounts of intermediates were left unreacted. The C-O coupled product **89** formed in less than 5% yield whereas the major reaction product was the C-N coupled compound **86** produced in about 87% yield. These results suggest once more that the C-N reductive coupling of **84** is favored by strong acids having strongly nucleophilic counterions. Hence, we next tried HI additives that can produce the most nucleophilic halide anion in solution, I⁻.

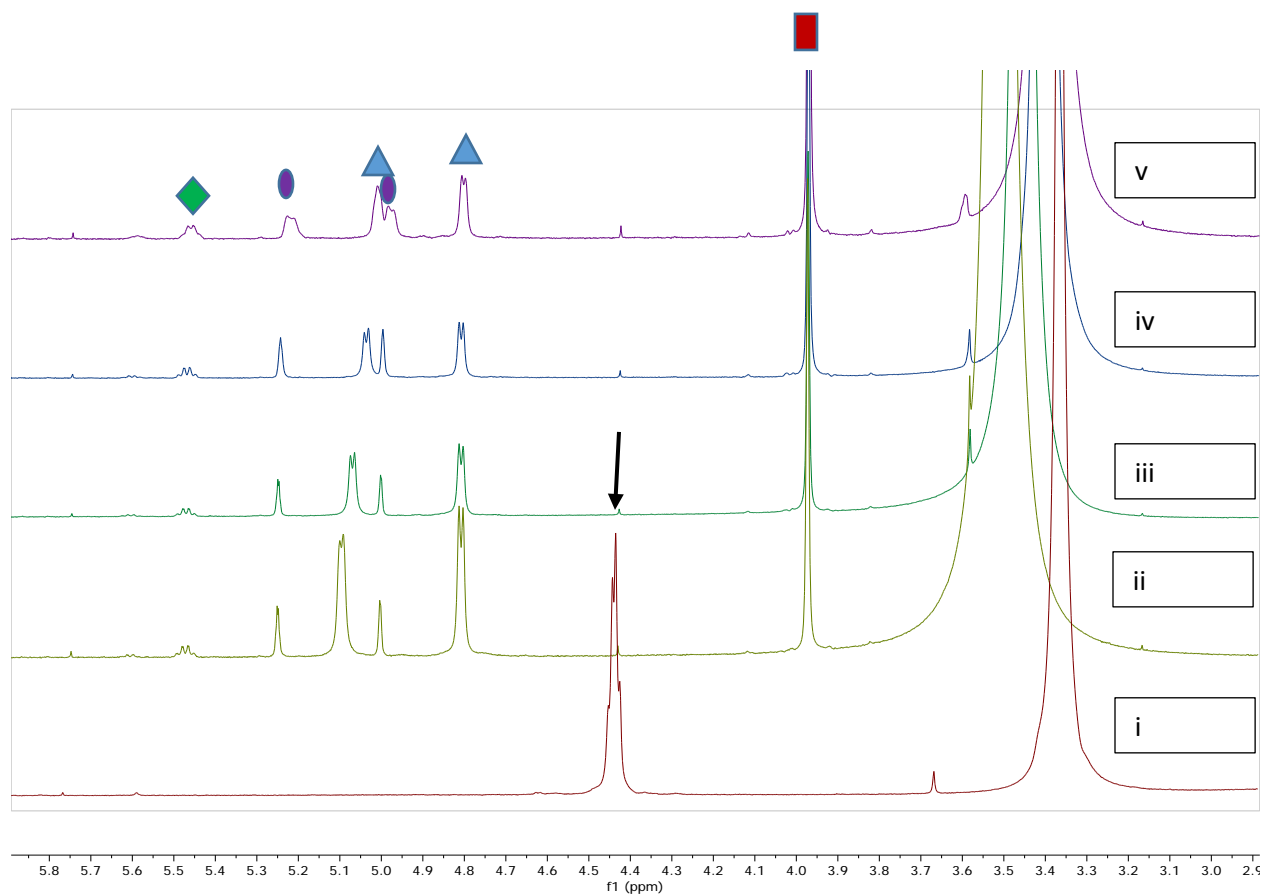


Figure 5.5 Reactivity of **84** with 2 equivalents of HBr. Blue triangle shows **85** in solution, purple circle shows an unknown intermediate observed, arrow shows **84**, red square shows **86** and green diamond shows a second unknown intermediate. (i) Before addition of HBr (ii) 15 minutes after addition of HBr, 58% yield of the indoline **86**, (iii) 30 minutes after addition of HBr (iv) 45 minutes after addition of HBr (v) 60 minutes after addition of HBr.

5.4.8 Hydroiodic acid

Addition of 3 equivalents of HI to a solution of **84** in DMSO- d_6 led to the appearance of only one set of signals born by the Pd(IV)CH₂ group in the ¹H NMR spectrum, two doublets, one at 4.97 ppm and another at 5.8 ppm. The C-N coupled product was observed in about 60% yield.

When the solution was monitored by ^1H NMR, no other presumed Pd(IV) species was observed. The disappearance of the peak at 4.97 ppm was accompanied by the increase of the amount of the C-N product. Notably, the starting Pd(II) complex **81** also formed in 30% yield. This observation shows that the iodide was also undergoing a competitive redox transformation by reducing Pd(IV) to Pd(II) species.

5.4.9 Addition of salts KBr and LiCl

The addition of 3 equivalents of KBr(aq) and LiCl(aq) to **84** in DMSO- d_6 showed no change in the ^1H NMR and no color change of the solution. When the solution was left for 5 hours, there was still no change in the ^1H NMR spectrum. These observations show that, in addition to a highly nucleophilic counterion, a proton source is needed for the C-N coupling reaction to proceed.

5.4.10 TFA/KBr

To confirm that the presence of both a proton source and a nucleophilic anion such as Br^- is needed for an efficient C-N coupling of **84**, we repeated the reaction of **84** with KBr as our source of Br^- and TFA as the source of acid in DMSO- d_6 . ^1H NMR spectral analysis of the solution after 14 h showed the formation of **86** in 78 % yield together with **89** in 13% yield

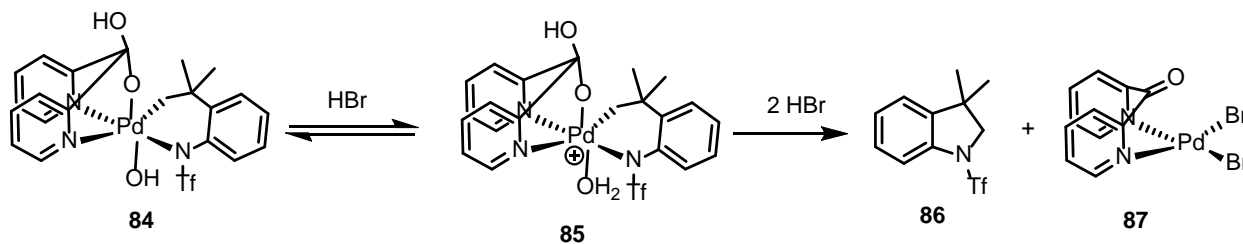
5.4.11 Tosyl Chloride

Instead of HCl, we tried out tosyl chloride. When 3 equivalents of tosyl chloride were added to DMSO- d_6 solution of **84**, two new sets of signals were observed. Two doublets at 5.26 ppm and 5.00 ppm were observed together with an AB multiplet at 5.47 ppm. The C-N coupled product **86** was observed in about 14% yield. When the solution was heated, the two doublets at 5.26 ppm and

5.5 Kinetics

5.5.1 Reaction with 2 equivalents of HBr(aq)

The highest 87% yield of the C-N coupled product **86** was observed with the addition of HBr to DMSO-*d*₆ solution of **84**. We, therefore, looked at the kinetic profile of the reaction highlighting the change in concentration of the starting material **84** plus its protonated form **85** that exist in equilibrium which is fast in NMR time scale (Scheme 4.4), the indoline **86**, and intermediates (Fig. 5.6). The cationic complex **85** formed upon addition of HBr undergoes a first order reaction with a half-life of (64 ± 2) minutes at 22 °C to form the indoline **86** and the Pd(dpk)Br₂ complex **87**. The latter could be isolated and characterized by single crystal X-ray diffraction (Fig. 5.8).



Scheme 5.7 Reaction of **84** with 2 equivalents of HBr at 22 °C.

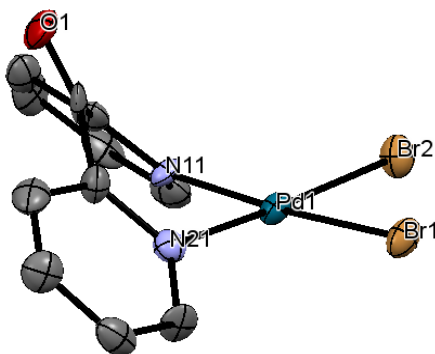


Figure 5.6 X-ray crystal structure of **87**

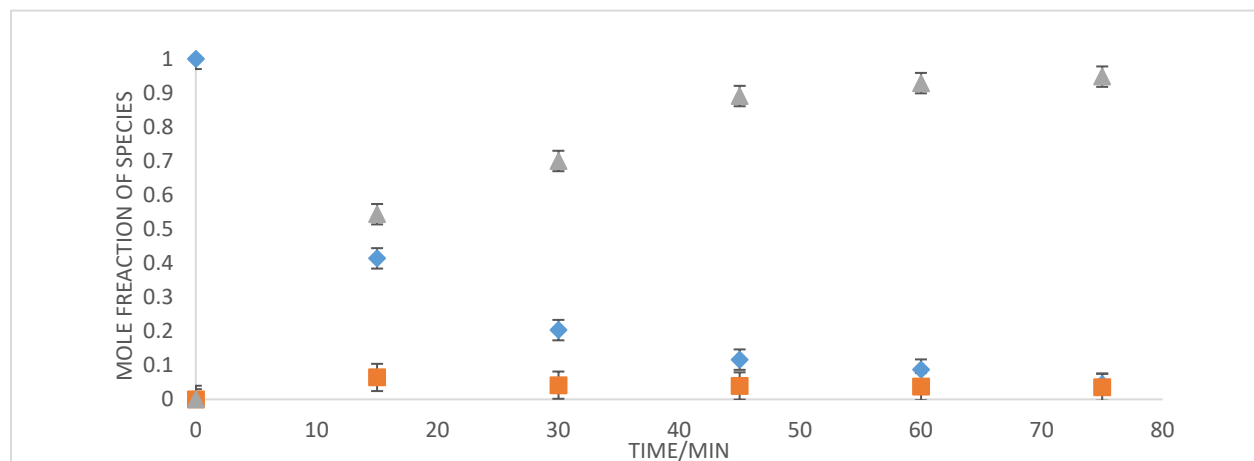
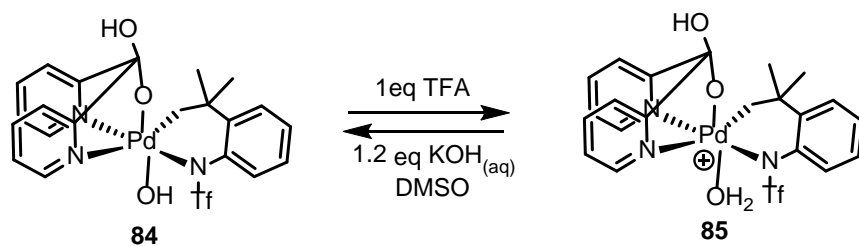


Figure 5.7 The kinetic profile of the reaction between **84** and 2 equivalents of HBr to form the indoline **86** (grey triangle) and Pd(dpk)Br₂, **87**. Blue diamonds correspond to a mixture of **84** and **85**. Orange circle square is an observed intermediate whose identity could not be accurately determined.

5.5.2 Reversibility of protonation



Scheme 5.8 Reversibility of protonation of **84** with in DMSO at 22 °C

To study the first part of our proposed mechanism, which involves protonation of **84**, we added 1 equivalent of TFA to a DMSO solution of **84**. Analysis of the ¹H NMR showed the transformation of the Pd-CH₂ group multiplet at 4.41 ppm into two doublets at 5.05 ppm and 4.82 ppm. After 5 minutes, 1.2 equivalents of aqueous KOH was then added to the mixture. ¹H NMR

analysis of the solution showed the reformation of the multiplet of the starting material **84** at 4.42 ppm. Two new signals were also observed. These new signals, one at 4.71 ppm and another at 4.48 ppm were most likely the effect of partial deprotonation of OH of dpk fragment present in **84**.

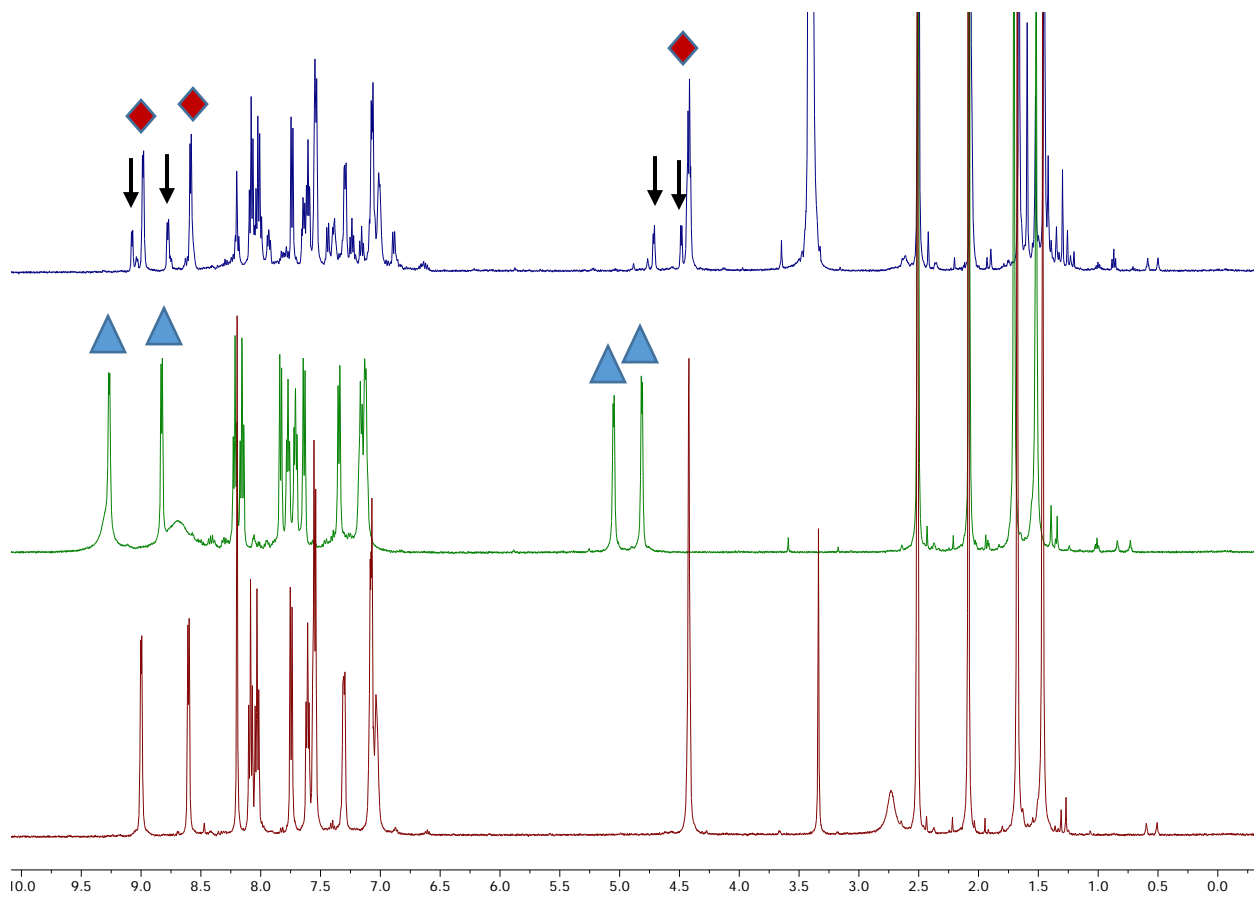


Figure 5.9 Reversibility of protonation of **84** in $\text{DMSO-}d_6$. Red diamonds show **84** in solution, blue triangles show **85** and arrows show deprotonated **84** in solution. **84** in solution before the addition of 1 equivalent of TFA (bottom). After addition of 1 equivalent of TFA (middle). Addition of 1.2 equivalent of KOH(aq) to the middle spectrum after 5 minutes.

5.5.3 Possible mechanisms of the C-N coupling of **84** in the presence of HBr

Since the C-X coupling does not occur in the absence of strong acids, we propose that the reaction begins with a reversible protonation of **84** to form **85**, as shown in Scheme 4.4. To study the effect of this protonation on the position of the signals produced by the Pd(IV)CH₂ group, different equivalents of Brookhart's acid were added to a DMSO solution of **84**. Analysis of the ¹H NMR chemical shifts of the resulting species shows a linear dependence between the amount of the acid added (0 – 1 equivalent) and the chemical shift of the most downfield shifted doublet of the Pd(IV)-CH₂ fragment which was monitored. This linear dependence discontinues after addition of 1.0 equivalent of acid. The addition of excess acid shows no change in the chemical shift of the monitored signal, consistent with a complete conversion of **84** to **85**. Since there was only one Pd(IV)CH₂ group – containing species present in solution, this observation suggests i) a relatively high basicity of **84** in DMSO, and ii) the existence of a fast proton transfer equilibrium involving **84** and **85**, so that the signals observed are weight-averaged, according to the fraction of each species present.

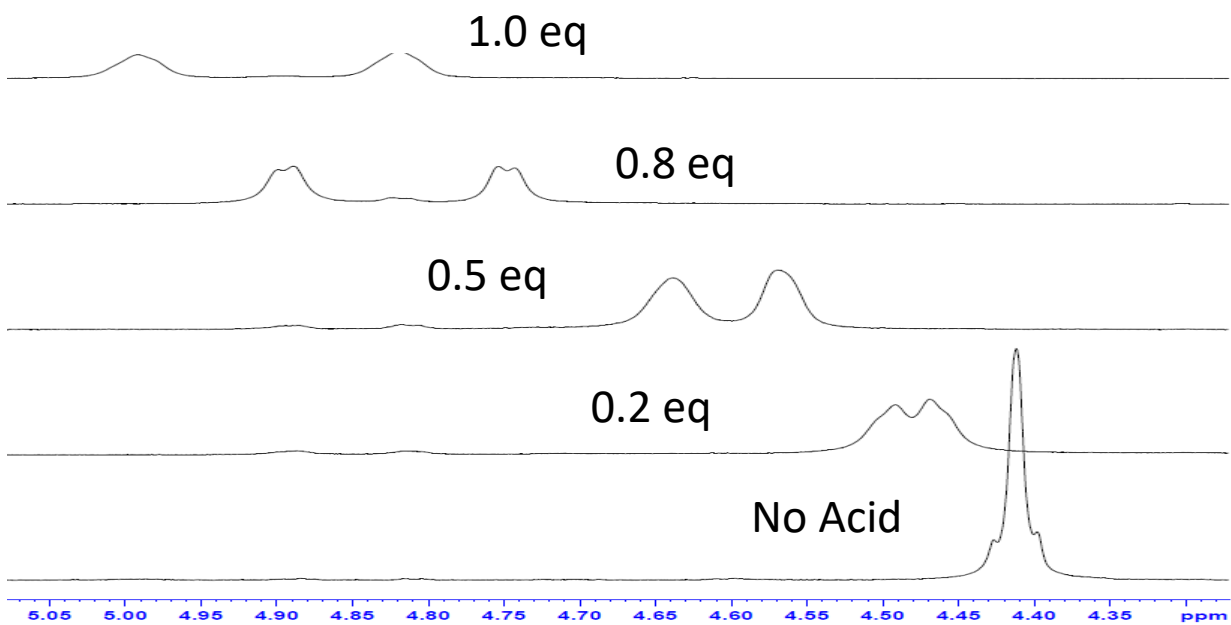


Figure 5.10 Addition of different equivalents of Brookhart's Acid to **84** in DMSO- d_6 at 22 °C.

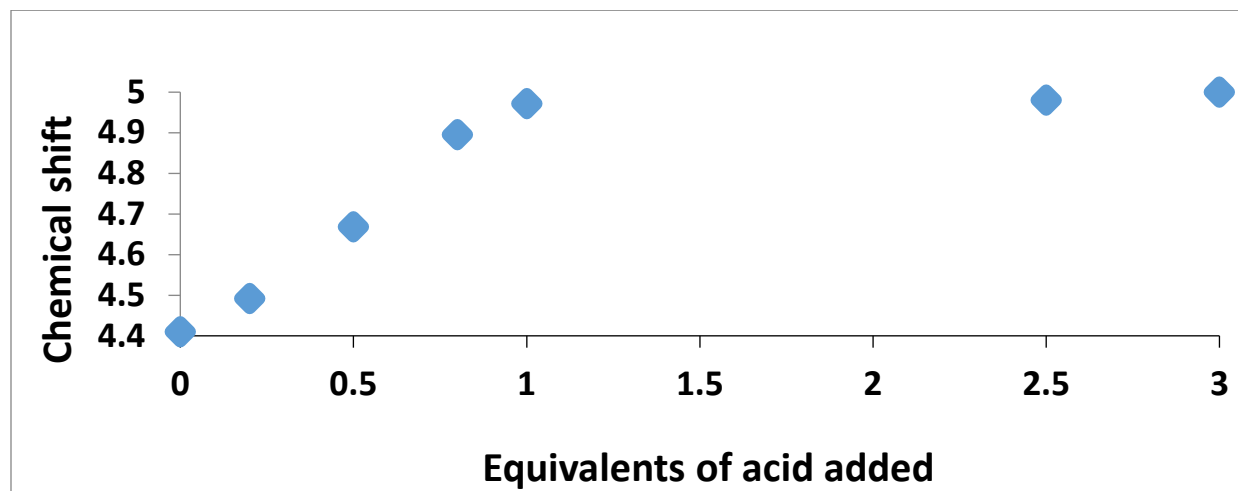


Figure 5.11 Plot of Chemical shift versus equivalents of acid added for figure 5.10 above.

5.5.4 Initial rates

To get more information about the reaction in Scheme 4.4, the initial rates of the reaction were studied by independently by varying concentrations of **84**, H^+ and Br^- (Table 2). The initial rates were determined by measuring the decrease of the combined concentrations $[84]+[85]$ during the reaction period corresponding to a less than 10% conversion of the Pd(IV) complex.

Table 5.2. Initial rates of reaction involving **84**, H^+ and Br^- .

Entry	[Pd(IV)], mM	$[H^+]$, mM	$[Br^-]$, mM	Initial Rate, $(d[Pd(IV)]/dt) \times 10^{-7} M \times s^{-1}$
1	13.0 ± 0.5	26.3 ± 0.5	25.6 ± 0.5	9.4 ± 0.8
2	25.8 ± 0.2	26.3 ± 0.5	25.6 ± 0.5	19.2 ± 0.4
3	25.8 ± 0.3	13.2 ± 0.7	25.6 ± 0.5	8.9 ± 0.3
4	25.8 ± 0.3	26.3 ± 0.7	52.2 ± 0.7	31.2 ± 0.2

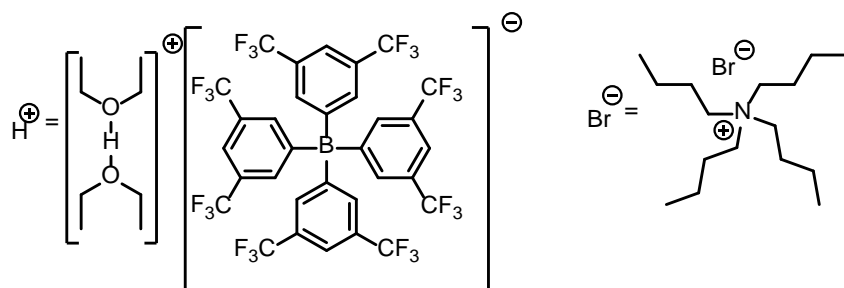


Figure 5.12 Structures of Brookhart's acid as our source of H^+ and tetra-*n*-butylammonium bromide as our source of Br^- .

We used tetra-*n*-butylammonium bromide as a source of Br⁻ ions and Brookhart's acid (Fig. 5.12) as an H⁺ source. The counterions, tetra-*n*-butylammonium and tetrakis[3,5-bis(trifluoromethyl)phenyl]borate are known as virtually non-coordinating, hence, they are not expected to interfere with the target reaction. Based on the results provided in Table 2, the C-X coupling reaction is first order in [**84**], first order in [H⁺] but has an order in [Br⁻] which is intermediate between 0 and 1.

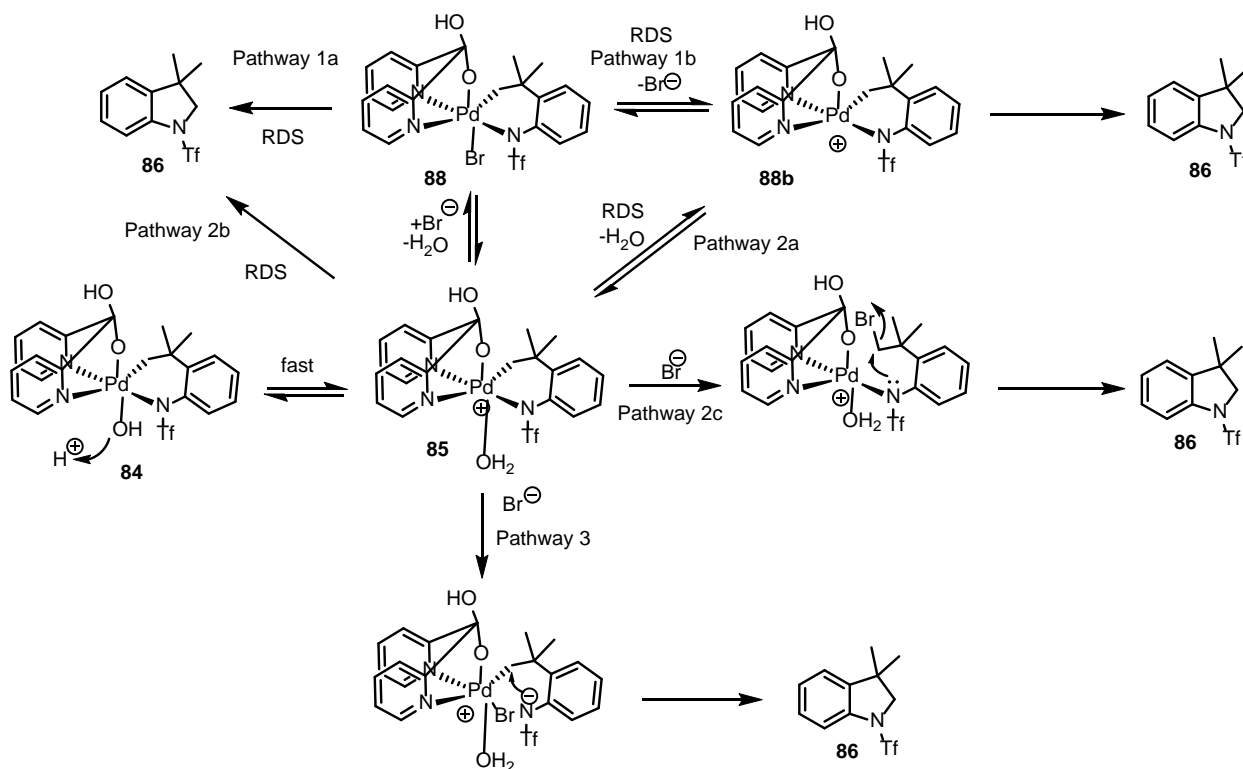
The transformations of **84** and the derived aqua complex **85** produced according to Scheme 4.4, may operate by several mechanisms shown in Scheme 4.6 and commented upon below.

As it is illustrated in Fig. 5.5-5.6, reaction mixtures containing 2 equivalents of HBr and **84** in DMSO solution show a relatively fast formation of the indoline **86** at 22 °C. The major species observed in the solutions for more than one reaction half-life is the cationic complex **85**. Two minor intermediates whose NMR chemical shifts are not affected by excess acid and are, therefore, not so basic as **84**. These intermediates may result from bromide or DMSO – for aqua ligand substitution in **85**. When the reaction in Scheme 4.4. was allowed to run for about 7 hours, complete conversion of **85** and both minor intermediates to C-X coupled products **86** and **89** was observed. Hence, the minor intermediates, presumably a bromo- and DMSO analogs of **84** and **85**, respectively, also react to form the C-X coupled products, perhaps, following an independent reaction pathway such as pathway 1 in Scheme 4.6.

5.5.5 Pathway 1 - direct C(sp³)-N reductive elimination from a Pd(IV) complex

This mechanism involves direct rate-limiting C-N reductive elimination from a six-coordinate Pd(IV) bromo complex **88** or a cationic DMSO complex analogous to **84**. The reaction rate for the pathway 1a involving **88** should be first order in [Br⁻].

Alternatively, Br⁻ can dissociate from **88** in a rate-determining step to form a five-coordinate complex **88b**, which then undergoes a direct C-N reductive elimination to give the target indoline **86**. In this case (pathway 1b) the effective reaction order in [Br⁻] may be between 0 and 1, as observed. The pathway 1b cannot be the only pathway operational since **88b** can be produced directly from **85** without participation of bromide anion (pathway 2a) resulting in 0 order in [Br⁻].



Scheme 5.9 Proposed mechanisms for the formation of **86** from **84**.

Hence, pathway 2a would be operational in the absence of bromide additive which does not correspond our observation that the C-N coupling does not happen in the absence of strong nucleophiles such as Br⁻. Altogether, this analysis suggests that the 5-coordinate Pd(IV) species **88b** is unlikely to be involved in the C-N coupling.

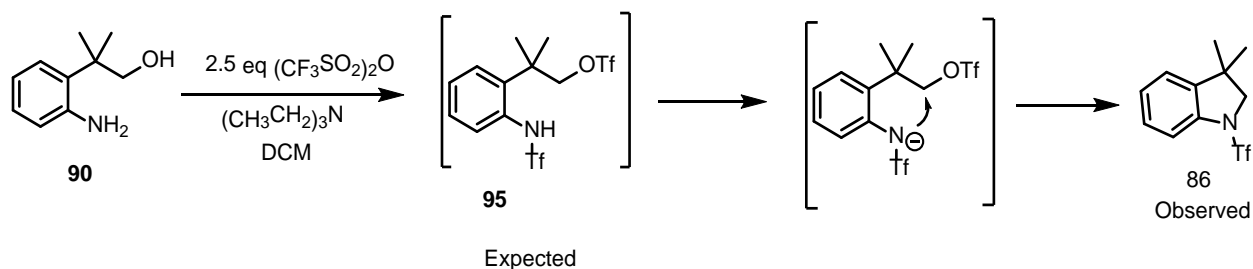
The pathway 1a is consistent with the available observations. Notably, it might compete with pathway 2b where the direct C-N coupling occurs from the aqua complex **85**, so that the overall reaction order in [Br⁻] for a combination of these two reactions may be between 0 and 1.

5.5.6 Pathway 2c –S_N2 attack at CH₂ fragment of Pd(IV)

Literature precedence (Sanford and Muniz)^{78, 81} shows that the Pd(IV)-CH₂ group may be very electrophilic and should be easily attacked by a nucleophile through an S_N2-like mechanism. This mechanism has the overall first reaction order in [Br⁻] and, therefore, to be consistent with our experimental observations should be accompanied with another process for which the order in [Br⁻] is less than 1.

5.5.7 Pathway 3 – dissociation of the amido donor atom

The third plausible pathway involves an intramolecular cyclization to form carbazole. This mechanism was proposed when we tried to independently synthesize the ester **95**. Instead of **95**, **86** was produced as the sole organic product observed by ¹H NMR spectroscopy.



Scheme 5.10 Independent synthesis of **86** from **90**.

The same result was observed when the reaction of **90** was run with only one equivalent of triflic anhydride. Even in that instance, **86** was isolated as the major product in 72% yield. The proposed mechanism for the formation of **86** from **90** and Tf_2O is shown in Scheme 5.7.

Based on these considerations, the C-N coupling of the Pd(IV) complex **85** may also follow pathway 3, where the amido ligand is displaced by bromide first, which is followed by intramolecular cyclization to give the target compound **86**.

In this mechanistically complex situation a DFT analysis the reaction pathways in Scheme 5.9 turned out to be very helpful. This analysis suggests that the cationic aqua complex **85** exists in DMSO as a tight H-bonded ($\text{OH}_2 \dots \text{Br}^-$) ion pair **85,Br⁻** (Figure 5.13). This ion pair reacts following the pathway 2c and involves the lowest energy transition state **TS_{SN2IP}** with the calculated Gibbs activation energy ΔG^\ddagger 19.5 kcal/mol vs. experimental value of 20.8 kcal/mol (see left part of the figure 5.13). The transition state **TS_{SN2IP}** corresponds to a nucleophilic attack of a Br^- on the Pd(IV)-bound CH_2 group of the ion pair.

Other competing reaction pathways have their transition states of prohibitively high energy. E.g., pathway 3 in Scheme 5.9 is represented in the right part of figure 5.13; its effective

Gibbs activation energy ($\text{TS}_{\text{c-CN}}$) is 9.6 kcal/mol higher than TS_{SN2IP} . A partial Gibbs energy diagram showing the preferred reaction mechanism is given in figure 5.13, left. Note, that the $\text{C}(\text{sp}^3)\text{-N}$ coupling step itself, according to our proposed mechanism, occurs outside of the Pd coordination sphere (see an insert on the bottom of figure 5.13). The C-N coupling step is very fast with the Gibbs activation energy of only 12.5 kcal/mol ($\text{TS}_{\text{a-CN}}$), consistent with our observations illustrated in Scheme 5.10.

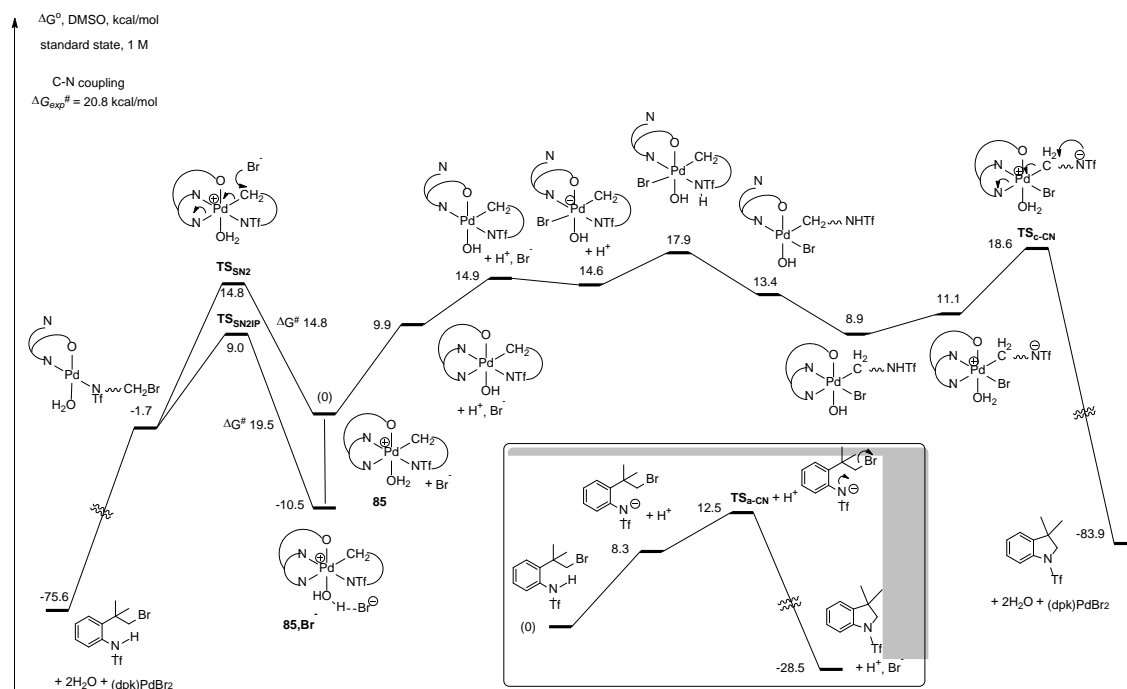
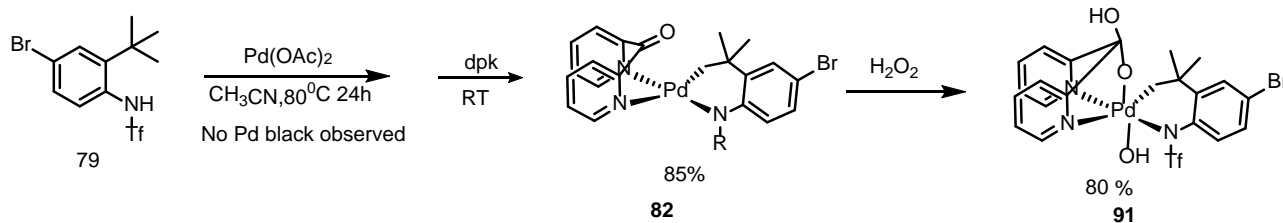


Figure 5.13 The reaction Gibbs energy profile corresponding to the most kinetically favorable $\text{C}(\text{sp}^3)\text{-N}$ coupling mechanism of the amido alkyl Pd(IV) complex **84** in the presence of HBr in DMSO solution.

5.6 Characterization and reactivity of a bromo-substituted analog of amido alkyl Pd(IV) complex **84**

To get additional insight into the reaction mechanism, we decided to look at the effect of substituents in the anilide ligand aromatic ring on the rate of reductive elimination. To study this behavior, we synthesized **82** which could be achieved from a one pot synthesis from **79** in MeCN solution.



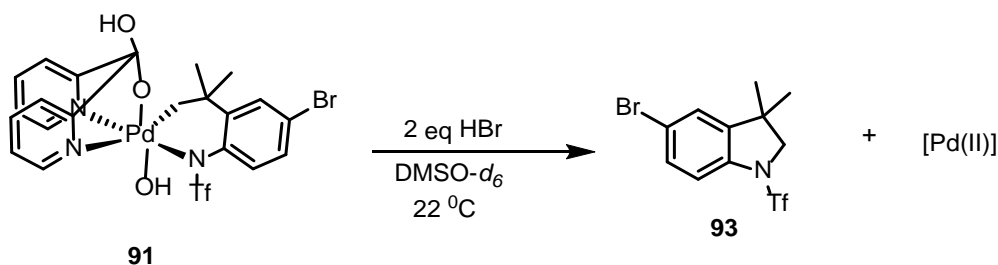
Scheme 5.11 Synthesis of complex **91**.

The Pd(II) alkyl amido complex **82** was shown by ^{13}C NMR spectroscopy in CD_3CN to exist in the keto form as expected. There was no peak at about 95 ppm in its ^{13}C NMR spectra characteristic of the ketal carbon whereas the signal of the dpk carbonyl group at about 188 ppm was observed. ^{19}F NMR spectrum of **82** confirmed the presence of only one species in solution.

82 was dissolved in CH_3CN to give a clear solution yellow solution. 5 equivalents of H_2O_2 was added to the solution which turned orange. ^1H NMR spectrum analysis of the resulting solution showed a single product which was assigned to structure **91**. The purity of **91** was confirmed by elemental analysis.

Upon the oxidation of **82** to **91** the PdCH₂ group signal has transformed from a singlet at 2.14 ppm to two doublets at 4.42 ppm and 4.34 ppm, which indicated a more electron deficient Pd(IV) center and the increased rigidity of the palladacyclic fragment. Also, the singlet at 1.43 ppm, which was assigned to two methyl groups in **82** has transformed to two singlets at 1.44 ppm and 1.65 ppm in **91**.

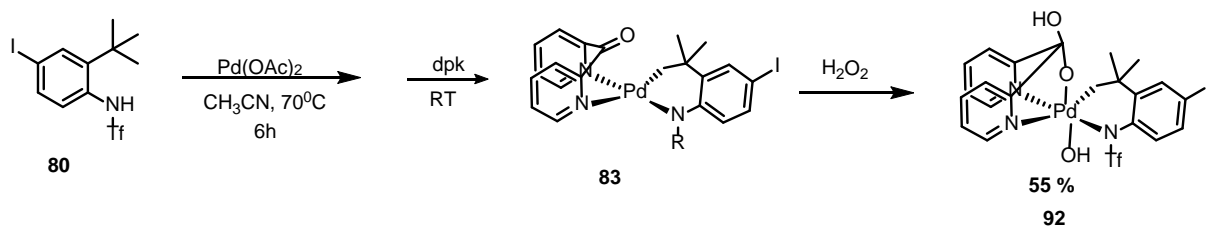
We next looked at the reductive elimination of **93** from **91** in the presence of 2 equivalents of HBr. The reaction followed a first-order kinetics with a half-life of (9.5 ± 0.4) minutes at 22 °C. This was observed to be much faster compared to reductive elimination from **84**, (17 ± 1) minutes. This shows that an electron withdrawing group at the para-position increases the rate of the C-N reductive elimination from the corresponding Pd(IV).



Scheme 5.12 Reactivity of **91** to form **93** with 2 equivalents of HBr in DMSO-*d*₆.

5.7 Characterization and reactivity of an iodo-substituted analog of amido alkyl Pd(IV) complex **84**

To further study the effect of substituents on the rate of reductive elimination, we synthesized the amido alkyl Pd(II) complex **83** bearing an iodo substituent in the aniline core. Complex **83** did not crystallize out of MeCN solution due to its high solubility and was used as is in the subsequent oxidation to the isolable Pd(IV) product **92**.



Scheme 5.13 Synthesis of **92** from **80**.

The PdCH₂ group signals in **92** were observed as two doublets at 4.40 ppm and 4.34 ppm, which indicated an electron deficient Pd(IV) center. The methyl groups of **92** were observed as two singlets at 1.43 ppm and 1.64 ppm confirming the presence of rigid palladacyclic fragment. The purity of **92** was confirmed by elemental analysis.

Reductive elimination of **92** to form **94** in the presence of 2 equivalents of HBr followed a first-order kinetics with a half-life of (9.5 ± 0.4) minutes at 22 °C. This was observed to be faster compared to reductive elimination from **84**, (17 ± 1) minutes and comparable to the reductive elimination of **91**, (6.9 ± 0.4) minutes. Similar to **91**, this results shows that an electron withdrawing group at the para-position increases the rate of reductive elimination from the corresponding Pd(IV) complex.



Scheme 5.14 Reactivity of **92** to form **94** with 2 equivalents of HBr in DMSO-*d*₆.

5.8 Conclusion

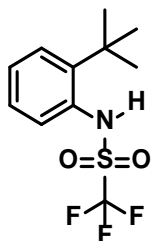
In conclusion, we have synthesized a series of κ^2 -C,N-2-(2',2'-dimethylethanediy)-N-(trifluoromethanesulfonyl)anilido Pd(II) complexes supported by dpk ligand. Two of the three complexes bear a halogen substituent (Br, I) in the anilide ligand core. We next performed their oxidation with H₂O₂ to produce the corresponding amido alkyl Pd(IV) derivatives. Hence, we have demonstrated again the power of our approach to enabling the employment of this environmentally benign oxidizing agent for production of Pd(IV) monoalkyl complexes, for the first time, through the use of *fac*-chelating hydrated dpk ligand. The reactivity of the resulting amido alkyl Pd(IV) complexes was probed in the intramolecular C-N coupling leading to N-triflylindolines. These compounds were observed to form the C-N coupled product as the major or the sole organic product only in the presence of HCl, HBr or HI.

Notably, intramolecular C(sp³)-N coupling at Pd(IV) center has never been observed and characterized before. Our combined experimental and computational mechanistic investigation of this new reaction showed that this intramolecular C(sp³)-N coupling at the Pd(IV) is assisted by an attack of external nucleophiles such as Cl⁻, Br⁻ or I⁻. The reaction mechanism that we proposed

includes first a nucleophilic attack of a halide anion at the Pd(IV)-bound alkyl group carbon atom in the derived cationic aqua complex – bromide ion pair. This reaction leads to a Pd(II) amido complex having a so-produced alkylhalide fragment in the amido ligand. The amido ligand nitrogen atom is next involved in an intramolecular nucleophilic attack at the haloalkane fragment. Electron withdrawing groups, Br and I, at the para position of the 4th position of the anilide ligand were shown to increase the rate of the C-N reductive coupling.

5.9 Experimental

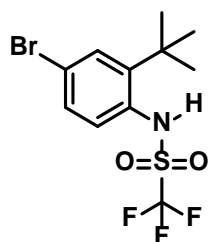
Synthesis of N-triflyl-2-*tert*butylanilide, 78



This was synthesized according to literature. 1.2 mL (7.6 mmol) of **N**- 2-*tert*butylaniline was added to 15mL of DCM at -78 °C using a dry-ice acetone bath together with 1.1 mL (7.7 mmol). After stirring for 10 min, 1.3 mL (7.7 mmol) of trifluoromethanesulfonic anhydride is added dropwise with stirring. When the addition was complete, the mixture was slowly allowed to warm to room temperature. After stirring at room temperature overnight, it is quenched with 15 mL of ice water. The mixture is extracted with 3 x 10mL of DCM, washed with sodium bicarbonate, then brine and dried with anhydrous Na₂SO₄. The solution was concentrated and eluted on a silica gel column with EtOAc/Hexane 20:80 to give the target compound in 73% yield.

¹H NMR (400 MHz, Acetonitrile-*d*₃) δ 7.62 (dd, *J* = 8.1, 1.6 Hz, 1H), 7.41 (dd, *J* = 7.9, 1.7 Hz, 1H), 7.35 – 7.29 (m, 1H), 7.26 (dd, *J* = 8.0, 1.6 Hz, 1H), 2.19 (s, 1H), 1.48 (s, 9H).

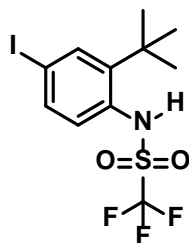
Synthesis of 79



This was synthesized according to literature.⁷⁵ *N*-(2-*tert*-butylphenyl)trifluoromethanesulfonamide (1.0 g, 2.7 mmol, 1.0 equiv) was dissolved in acetic acid (10 mL) and a solution of bromine (0.30 mL, 5.8 mmol, 2.0 equiv) in acetic acid (5 mL) was added over a period of 2 h. The reaction mixture was stirred at room temperature for 20 h. After addition of saturated aqueous NaHSO₃ (5 mL), the mixture was evaporated under reduced pressure. The residue was dissolved in CH₂Cl₂, washed with saturated aqueous Na₂CO₃ and brine, dried over MgSO₄ and concentrated under reduced pressure. After work-up as described above, the product was observed as white needles in 91% yield.

¹H NMR (400 MHz, Chloroform-*d*) δ 7.57 (d, *J* = 2.3 Hz, 1H), 7.38 (dd, *J* = 8.6, 2.3 Hz, 1H), 7.26 (d, *J* = 8.6 Hz, 1H), 6.67 (s, 1H), 1.47 (s, 9H).

Synthesis of 80

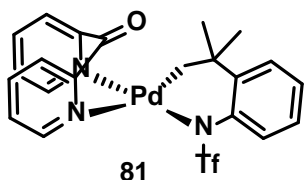


This was synthesized according to literature.⁸² H₂SO₄ acid (0.3 mmol) was dissolved in MeOH (3 mL); substrate (0.08 g, 0.2 mmol) and KI (0.2 mmol) were added into the solution. Finally, 30% H₂O₂ (0.4 mmol) was added and stirred at room temperature overnight. After the reaction was finished, the reaction mixture was poured into CH₂Cl₂ (30 mL), organic phase was washed with 0.1 M NaHSO₃ (5 mL), water (10 mL), dried (Na₂SO₄) and solvent was evaporated.

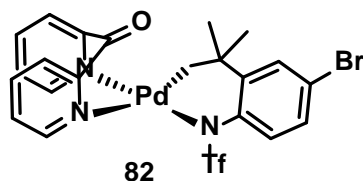
^1H NMR (400 MHz, Chloroform-*d*) δ 7.75 (d, $J = 2.1$ Hz, 1H), 7.58 (dd, $J = 8.5, 2.1$ Hz, 1H), 7.12 (d, $J = 8.5$ Hz, 1H), 6.64 (s, 1H), 1.46 (s, 9H).

General Procedure for the synthesis of N-triflyl-2-*tert*butylanilidePddpk

0.50 g (2.2 mmol) of $\text{Pd}(\text{OAc})_2$ was weighed and combined in 20.0 mL of CH_3CN to form a suspension. Then 1.1 equivalents of substrates **78 - 80** was added to the suspension and heated at (60-80) $^\circ\text{C}$ for between 3-14 hours. Palladium black was observed and the resulting solution was filtered through Celite and used in further synthesis without isolation. 1.0 equivalents of dpk is dissolved in CH_3CN and the dpk solution was added dropwise to the palladacycle solution. The target compounds except **83** are observed to crystallize out of solution after stirring for about 5 h.



^1H NMR (400 MHz, Acetonitrile- d_3) δ 8.95 (d, $J = 5.2$ Hz, 1H), 8.90 (d, $J = 5.5$ Hz, 1H), 8.20 (td, $J = 7.8, 1.6$ Hz, 1H), 8.15 (dd, $J = 7.7, 1.6$ Hz, 1H), 8.10 (d, $J = 7.7$ Hz, 1H), 8.00 (dd, $J = 7.9, 1.5$ Hz, 1H), 7.79 (ddd, $J = 7.7, 4.6, 2.0$ Hz, 2H), 7.53 – 7.44 (m, 2H), 7.15 – 7.00 (m, 2H), 2.17 (s, 2H), 1.47 (s, 6H). ^{13}C NMR (126 MHz, Methylene Chloride- d_2) δ 206.91, 187.15, 154.83, 152.84, 152.18, 151.48, 147.03, 140.13, 140.00, 139.65, 129.19, 128.84, 128.80, 127.03, 126.52, 125.81, 125.73, 124.16, 123.13, 120.51, 40.50, 36.30, 31.15. ^{19}F NMR (376 MHz, Acetonitrile- d_3) δ -73.57. Anal. Found/Calculated for $(\text{C}_{22}\text{H}_{20}\text{F}_3\text{N}_3\text{O}_3\text{PdS} \cdot \text{CH}_3\text{CN})$: C, 47.03/47.18; H, 3.78/3.79; N, 7.97/9.17;

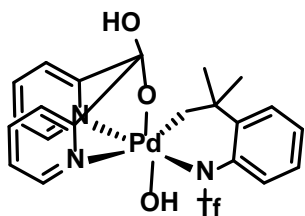


^1H NMR (400 MHz, Acetonitrile- d_3) δ 8.88 (d, $J = 5.3$ Hz, 1H), 8.84 (d, $J = 5.6$ Hz, 1H), 8.22 – 8.14 (m, 1H), 8.11 (dd, $J = 7.6, 1.5$ Hz, 1H), 8.07 (d, $J = 7.7$ Hz, 1H), 7.97 (dd, $J = 7.9, 1.5$ Hz, 1H), 7.75 (ddd, $J = 7.5, 5.4, 1.5$ Hz, 2H), 7.58 (d, $J = 2.4$ Hz, 1H), 7.37 (d, $J = 8.7$ Hz, 1H), 7.18 (dd, $J = 8.7, 2.4$ Hz, 1H), 2.14 (s, 2H), 1.43 (s, 6H).

Anal. Found / Calculated for ($\text{C}_{22}\text{H}_{19}\text{BrF}_3\text{N}_3\text{O}_3\text{PdS}$): C, 40.44/40.73; H, 2.66/2.95; N, 6.38/6.48;

General Procedure for oxidation of **81-83** with H_2O_2 in CH_3CN

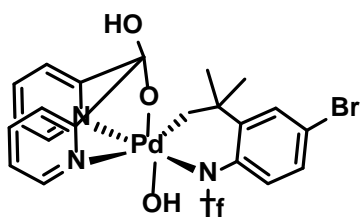
10.0 mg of **81-82** was dissolved in 0.60 mL of solvent to give a clear solution yellow solution. 5 eq of H_2O_2 was added to the solution which turned orange. After about 5 minutes, a precipitate was observed. The solution was then cooled to increase the rate of precipitation. The precipitate was isolated and washed with cold CH_3CN to afford the target compounds. X-ray quality crystals were grown by placing 30 mg of **81** in 1.0 mL of CH_3CN , and warming it slightly for full dissolution. The solution was placed in ice for about 10m and 3 drops of H_2O_2 was added and the resulting solution left in ice for a further 20 minutes. After that the solution was transferred into a freezer overnight.



84

^1H NMR (400 MHz, $\text{DMSO-}d_6$) δ 8.99 (d, $J = 5.1$ Hz, 1H), 8.59 (d, $J = 5.6$ Hz, 1H), 8.20 (s, 1H), 8.08 (td, $J = 7.6, 1.4$ Hz, 1H), 8.02 (td, $J = 7.7, 1.6$ Hz, 1H), 7.74 (d, $J = 7.8$ Hz, 1H), 7.60 (ddd, $J = 7.4, 5.6, 1.4$ Hz, 1H), 7.54 (ddd, $J = 7.5, 5.3, 1.2$ Hz, 2H), 7.29 (dd, $J = 6.2, 3.2$ Hz, 1H), 7.12 – 6.95 (m, 3H), 4.47 – 4.35 (m, 2H), 2.67 (s, 1H), 1.66 (s, 3H), 1.45 (s, 3H).

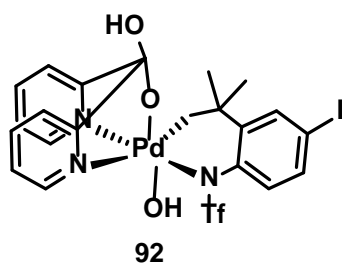
Anal. Found / Calculated for $(\text{C}_{22}\text{H}_{22}\text{F}_3\text{N}_3\text{O}_5\text{PdS}\cdot\text{CH}_3\text{CN})$: C, 44.34/44.69; H, 3.75/3.91; N, 8.37/8.69;



91

^1H NMR (500 MHz, $\text{DMSO-}d_6$) δ 8.99 (d, $J = 5.1$ Hz, 1H), 8.58 (d, $J = 5.7$ Hz, 1H), 8.21 (s, 1H), 8.09 (td, $J = 7.7, 1.4$ Hz, 1H), 8.03 (td, $J = 7.7, 1.6$ Hz, 1H), 7.74 (d, $J = 7.8$ Hz, 1H), 7.61 (ddd, $J = 7.4, 5.6, 1.5$ Hz, 1H), 7.55 (dd, $J = 7.8, 4.8$ Hz, 2H), 7.40 (d, $J = 2.4$ Hz, 1H), 7.28 (dd, $J = 8.6, 2.4$ Hz, 1H), 6.99 (d, $J = 8.6$ Hz, 1H), 4.42 (d, $J = 5.3$ Hz, 1H), 4.35 (d, $J = 5.3$ Hz, 1H), 2.67 (s, 1H), 1.65 (s, 3H), 1.45 (s, 3H).

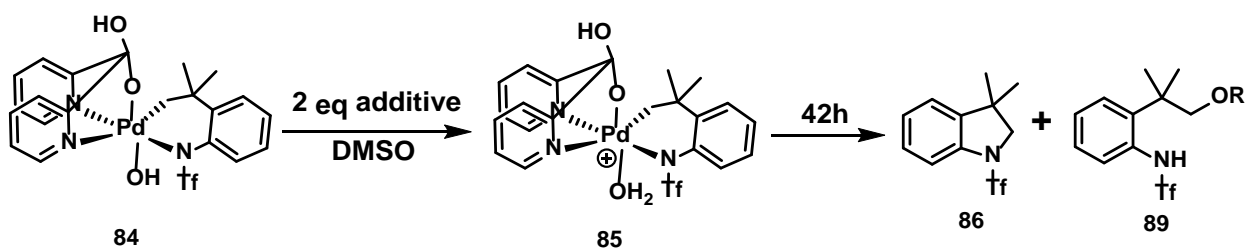
Anal. Found / Calculated for $(\text{C}_{22}\text{H}_{21}\text{BrF}_3\text{N}_3\text{O}_5\text{PdS})$: C, 38.43/38.70; H, 2.83/3.10; N, 6.15/6.15;



^1H NMR (500 MHz, $\text{DMSO-}d_6$) δ 8.99 (d, $J = 5.1$ Hz, 1H), 8.59 (d, $J = 5.7$ Hz, 1H), 8.22 (s, 1H), 8.10 (t, $J = 7.7$ Hz, 1H), 8.04 (t, $J = 7.6$ Hz, 1H), 7.75 (d, $J = 7.8$ Hz, 1H), 7.62 (t, $J = 6.7$ Hz, 1H), 7.56 (q, $J = 5.2$ Hz, 3H), 7.45 (dd, $J = 8.5, 2.0$ Hz, 1H), 6.85 (d, $J = 8.4$ Hz, 1H), 4.42 (d, $J = 5.3$ Hz, 1H), 4.36 (d, $J = 5.3$ Hz, 1H), 2.70 (s, 1H), 1.65 (s, 3H), 1.44 (s, 3H).

Anal. Found / Calculated for ($\text{C}_{22}\text{H}_{21}\text{IF}_3\text{N}_3\text{O}_5\text{PdS}$): C, 33.07/36.21; H, 2.64/2.90; N, 5.70/5.76;

General procedure for reaction of **84** with different additives

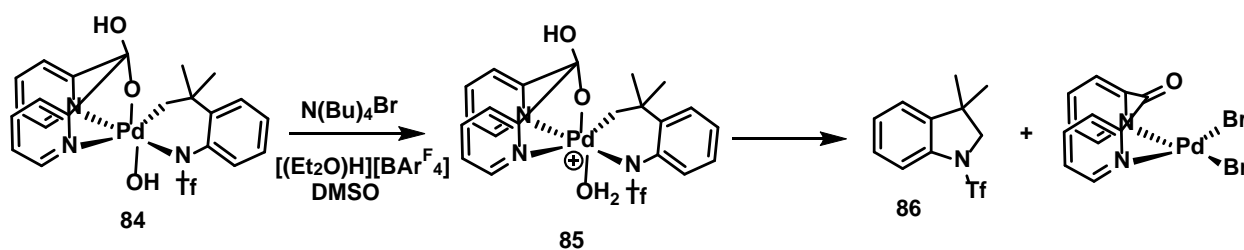


An NMR tube was charged with 10 mg of complex **84** and 0.60 mL of $\text{DMSO-}d_6$ was added. To the resulting solution was added 2 eq of the appropriate additive. The resulting solution was monitored and the yield of indoline which shows a peak at 3.97 ppm and the yield of the C-O product (peak at 3.60) were determined by ^1H NMR integration with the bound CH_3CN as internal standard. Yields were determined after 24 h.

ADDITIVE	PKA (H ₂ O / DMSO)	YIELD OF 86	YIELD OF 89
None		none	13
CH ₃ COOH	4.76 / 12.3	trace	48
CF ₃ COOH	-0.25 / 3.45	10	60
H ₂ SO ₄	-3 / 1.99	3	-
HCl	-8 / 1.8	32.5	30
HBr	-9 / 0.9	84	1
CF ₃ SO ₃ H	-14 / 0.3	3	-
KBr	none	none	21

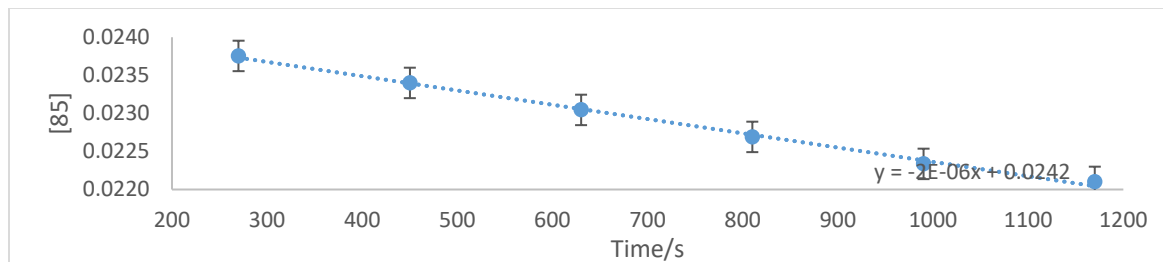
Kinetics

Determining order with respect to **84**

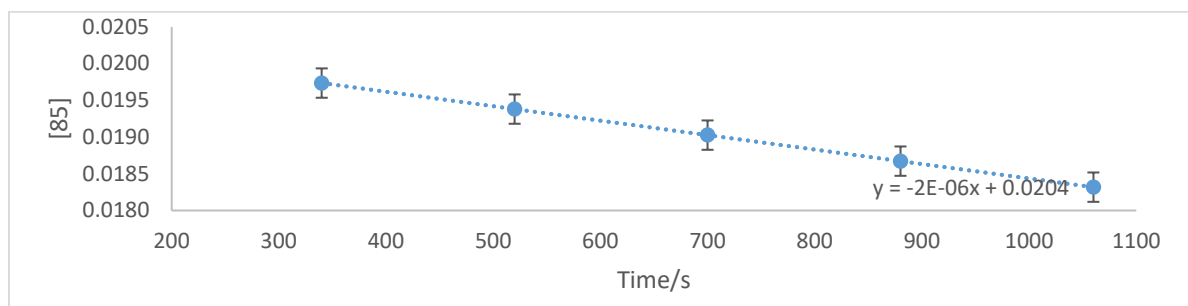


In a glove box, Young tubes were charged with different masses of **84** together with 5.00 mg of tetra-*n*-butylammonium bromide and 16.0 mg of Brookhart acid. 0.6 mL of DMSO is added and 2 μ L of benzyltrimethylsilane is added as internal standard. The rate of reductive elimination was

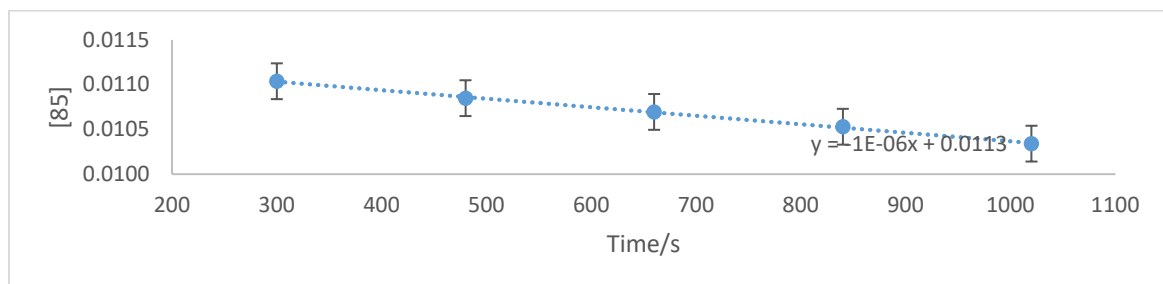
monitored by ^1H NMR spectroscopy with the integration of the Pd(IV) bound methylene group of **85**.

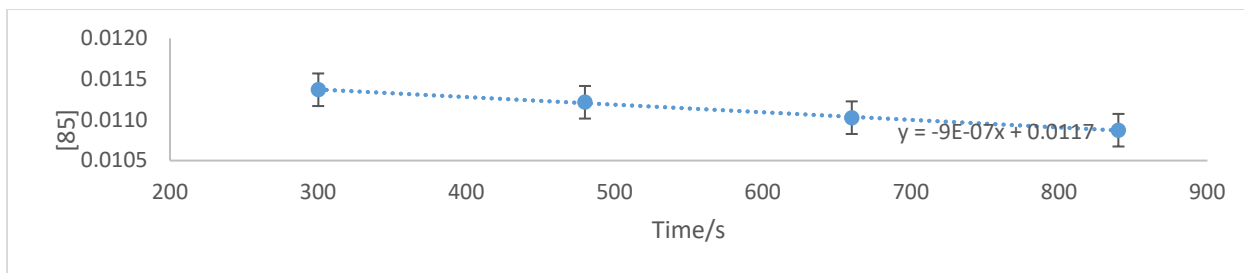


Initial rate plot for the reactivity of 10.1 mg (25.8 mM) of **84**. Slope is $1.97 \times 10^{-6} \text{ Mxs}^{-1}$

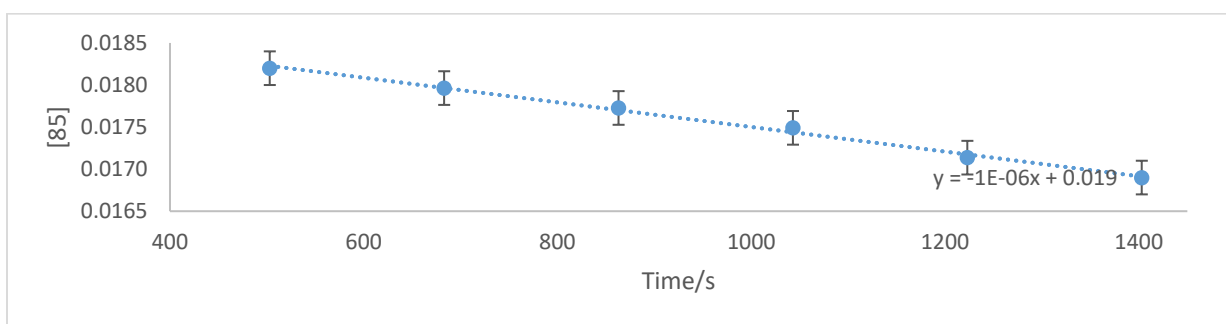


Initial rate plot for the reactivity of 5.5 mg (14 mM) of **84**. Slope is $9.5 \times 10^{-7} \text{ Mxs}^{-1}$

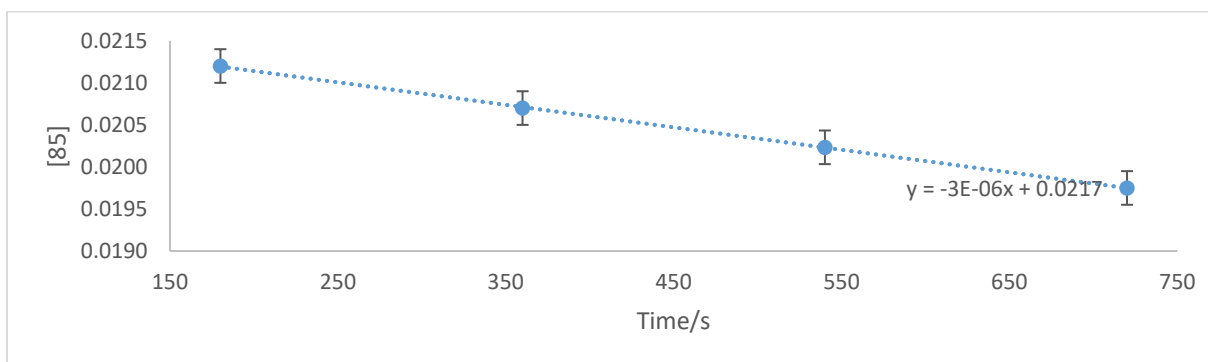




Initial rate plot for the reactivity of 5.5 mg (14 mM) of **84**. Slope is $9.3 \times 10^{-7} \text{ Mxs}^{-1}$



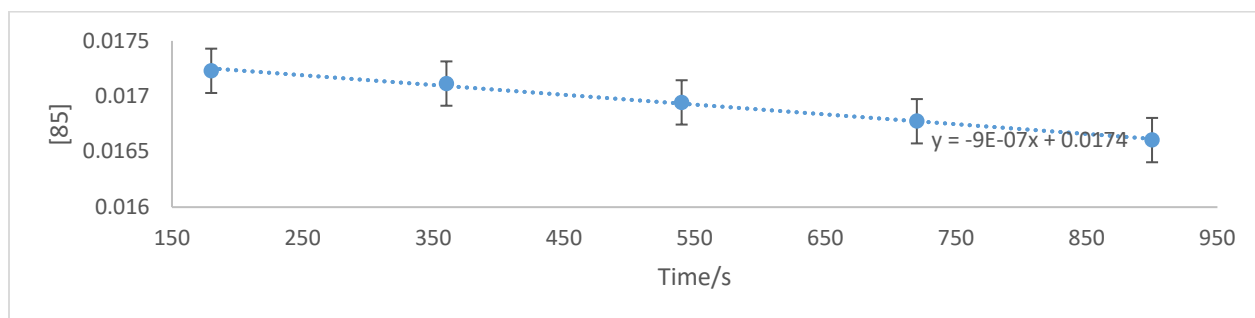
Initial rate plot for the reactivity of 8.1 mg (21 mM) of **84**. Slope is $1.46 \times 10^{-6} \text{ Mxs}^{-1}$



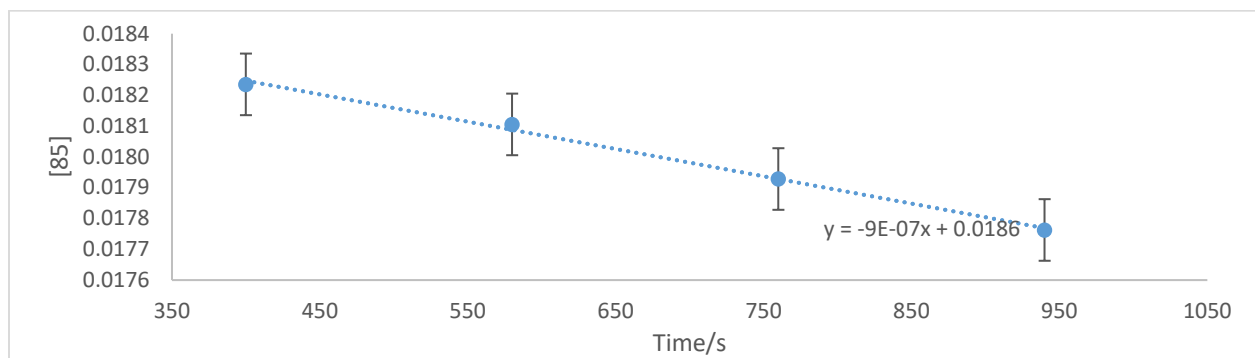
Initial rate plot for the reactivity of 8.5 mg (22 mM) of **84**. Slope is $1.42 \times 10^{-6} \text{ Mxs}^{-1}$

Determining order with respect to Acid

A Young tube was charged with 10.0 mg (26 mM) of **84** together with 5.00 mg of tetrabutylammonium bromide. 0.6 mL of DMSO is added and 2 μ L of benzyltrimethylsilane is added as internal standard. Different masses of Brookhart acid is dissolved in 0.2mL of DMSO.



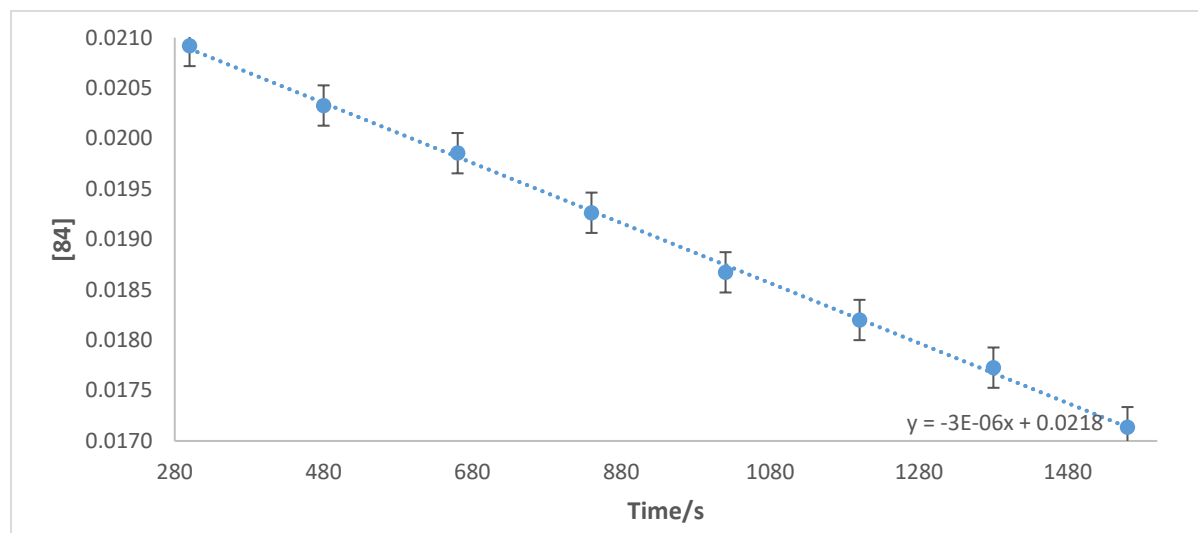
Initial rate plot for the reactivity of 8.3 mg (14 mM) of Brookhart's acid. Slope is $8.8 \times 10^{-7} \text{ Mxs}^{-1}$



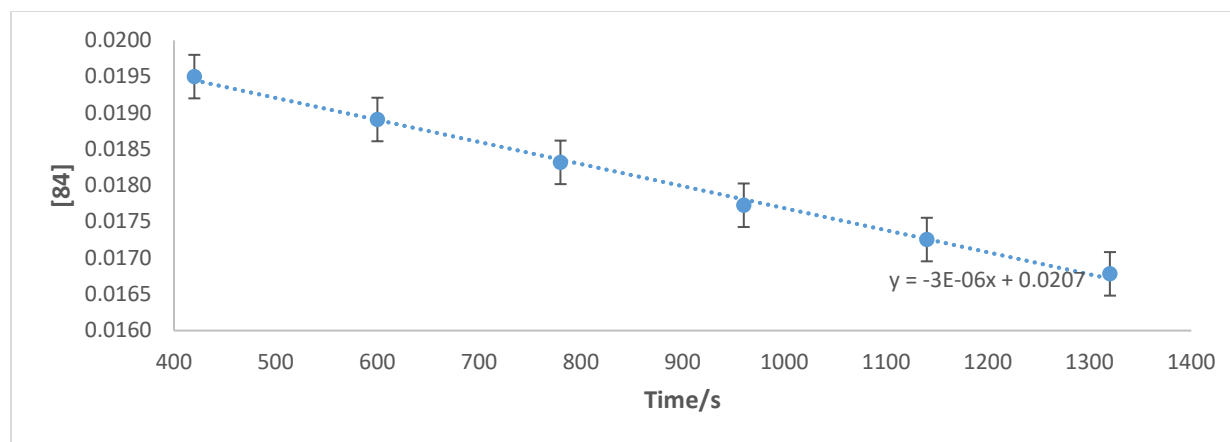
Initial rate plot for the reactivity of 8.5 mg (14 mM) of Brookhart's acid. Slope is $8.86 \times 10^{-7} \text{ Mxs}^{-1}$

Determining order with respect to bromide

A Young tube was charged with 10.0 mg of **84** together with a different mass of tetrabutylammonium bromide. 0.4mL of DMSO is added and 2uL of benzyltrimethylsilane is added as internal standard. 16 mg of Brookhart acid is dissolved in 0.2mL of DMSO. The Brookhart's acid solution is pulled into a syringe and capped. Both solutions are taken into the NMR room. The Young tube is partially opened, and the Brookhart's acid solution is added to make up the total volume to 0.6mL. The Young tube is quickly re-sealed and is placed in the 500MHz NMR probe at 295K. The rate of decomposition of the Pd(CH₂) signal is monitored by ¹H NMR.



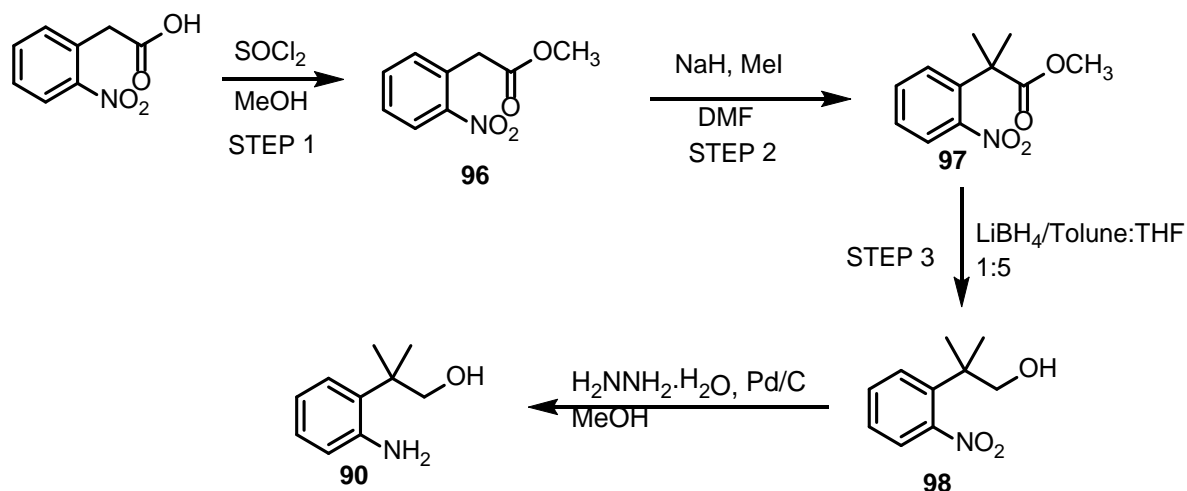
Initial rate plot for the reactivity of 10.1 mg (51.1 mM) of tetra-*n*-butylammonium bromide. Slope is $3.09 \times 10^{-6} \text{ Mxs}^{-1}$



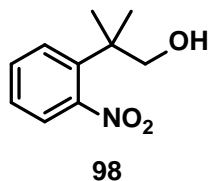
Initial rate plot for the reactivity of 10.3 mg (52.3 mM) of tetra-*n*-butylammonium bromide. Slope is $3.15 \times 10^{-6} \text{ Mxs}^{-1}$

Independent synthesis of 90

This was synthesized as reported by Glorius.⁷⁵

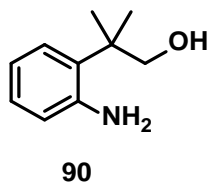


Total yield from starting material is 17%



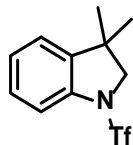
97 was dissolved in a mixture of toluene (20 mL) and THF (60 mL). LiBH₄ (600 mg, 27.5 mmol, 2.75 equiv) was added, and the mixture was heated at 100 °C for 12 h. After cooling to room temperature saturated aqueous NH₄Cl and H₂O were added and the mixture was extracted with EtOAc (2 X 100 mL). The combined organic phases were dried over MgSO₄ and the solvent was removed to give a **98**.

¹H NMR (400 MHz, Chloroform-*d*) δ 7.30 – 7.23 (m, 1H), 7.08 (ddd, *J* = 7.8, 7.2, 1.5 Hz, 1H), 6.82 (ddd, *J* = 7.8, 7.2, 1.4 Hz, 1H), 6.70 (dd, *J* = 7.8, 1.4 Hz, 1H), 3.80 (s, 2H), 3.52 (s, 3H), 1.45 (s, 6H).



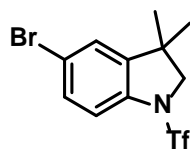
This was synthesized by reduction of **98** by a use of H₂NNH₂.H₂O on Pd/C system as reported by Li⁸³

¹H NMR (400 MHz, Chloroform-*d*) δ 8.22 (s, 1H), 7.29 – 7.25 (m, 1H), 7.08 (td, *J* = 7.5, 1.5 Hz, 1H), 6.81 (td, *J* = 7.7, 1.4 Hz, 1H), 6.69 (dd, *J* = 7.8, 1.4 Hz, 1H), 3.82 (s, 2H), 3.67 – 3.24 (s, 2H), 1.46 (s, 6H).

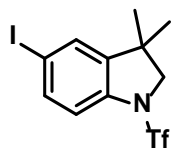


^1H NMR (500 MHz, $\text{DMSO-}d_6$) δ 7.39 (dt, $J = 7.4, 1.0$ Hz, 1H), 7.32 – 7.27 (m, 2H), 7.20 (ddd, $J = 7.4, 6.3, 2.2$ Hz, 1H), 3.97 (s, 2H), 1.33 (s, 6H).

^{13}C NMR (126 MHz, $\text{DMSO-}d_6$) δ 141.27, 138.10, 128.53, 125.99, 123.92, 121.56, 118.97, 113.77, 64.70, 27.52.



^1H NMR (400 MHz, $\text{DMSO-}d_6$) δ 7.65 (d, $J = 2.1$ Hz, 1H), 7.48 (dd, $J = 8.6, 2.1$ Hz, 1H), 7.23 (d, $J = 8.6$ Hz, 1H), 3.99 (d, $J = 1.1$ Hz, 2H), 1.33 (s, 6H).



^1H NMR (400 MHz, $\text{DMSO-}d_6$) δ 7.76 (s, 1H), 7.63 (d, $J = 9.1$ Hz, 1H), 7.10 (d, $J = 8.5$ Hz, 1H), 3.96 (s, 2H), 1.31 (s, 6H).

Chapter 6. Palladium-Catalyzed Oxidative C-H Amination with H₂O₂ as Oxidant

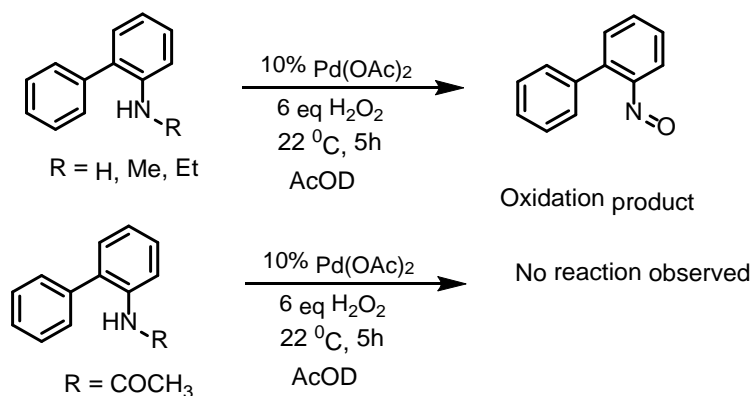
6.1 Introduction

The development of a mild and selective catalytic oxidative C-H amination reactions remains a challenge in modern organic synthesis. Traditionally, the Buchwald-Hartwig amination reactions have been used to construct C-N bonds. As an alternative to the Buchwald-Hartwig amination reactions, current research is focused on oxidative catalytic C-H amination without the use of pre-functionalized substrates. Palladium catalyzed C-H amination reactions have been reported in literature with different oxidants. Buchwald first reported the direct catalytic C-H amination of 2-aminobiphenyl substrates to form carbazoles with the use of the Cu(OAc)₂/O₂ as the terminal oxidant.⁶⁰ The Gaunt group used PhI(OAc)₂ as a terminal oxidant to achieve the same direct catalytic C-H amination of carbazoles.⁶² Youn and coworkers later reported the use of Oxone as the terminal oxidant for the direct catalytic C-H amination to form carbazoles. Mechanistic studies showed an electrophilic aromatic substitution (S_EAr) mechanism for the C-H activation step. A Pd(IV) intermediate was proposed, similar to Gaunt.⁸⁴ The Cho group later used a Pd catalyst together with O₂ in a Cp*Ir(III)-photoredox system to achieve a direct C-H amination to form carbazoles. The Antonchik group reported a metal-free oxidative C-H amination reaction to form carbazoles with AcOOH in a mixed hexafluoro-2-isopropanol/CH₂Cl₂ solvent system with 2,2'-diiodo-4,4',6,6'-tetramethylbiphenyl as an organocatalyst.⁸⁵ Interestingly, different research groups have also used different types of oxidants like K₂S₂O₈,⁸⁶ AgOAc,⁷⁵ Ce(SO₄)₂⁷⁹ or *N*-fluoro-2,4,6-trimethylpyridinium triflate⁷⁹ to achieve oxidative catalytic C-H amination of C(sp³)-H and

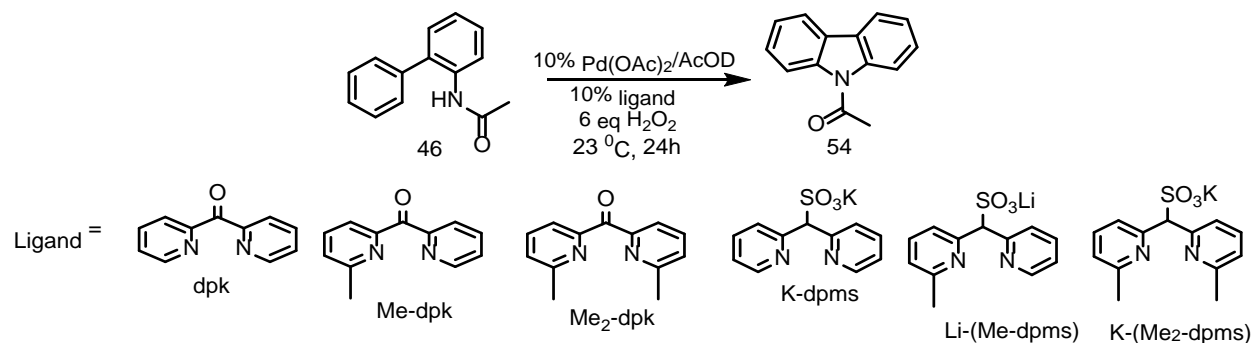
C(sp²)-H bonds. Based on these and the previous work by Oloo,⁴⁸ we attempted direct oxidative C-H amination of 2-aminobiphenyls and 2-tertbutylaniline substrates with H₂O₂.

6.2 Results and Discussion

We began our catalytic studies with the addition of 2 equivalents of H₂O₂ to a mixture of 5 mol% Pd(OAc)₂ and **25** in AcOD with no ligand present (Scheme 6.1). The solution was observed to turn greenish-blue which shows oxidation of the amino group by the H₂O₂ together with evolution of O₂ gas. ¹H NMR spectroscopy was not informative due to the formation of presumed free radicals during this process. We repeated the reaction with **26-28** which were all found to be oxidized by H₂O₂ to form most likely the corresponding nitrosobenzene. We then reacted **46** with only H₂O₂ in AcOD and no change in color was observed for 5 hours but **54** was not observed (Scheme 6.1). This confirmed that, the nitrogen atom in anilides were less reactive towards oxidation with H₂O₂ compared to anilines. We proceeded to optimize the catalytic C-H amination of **46** with Pd(OAc)₂ and H₂O₂. The optimal catalyst loading was found to be 10 mol % which led to only 4% yield of **54** upon addition of 6 equivalents of H₂O₂ after 24 h at 23 °C. We then screened different ligands which are common in our group (Scheme 6.2) at the initial conditions stated previously (Table 6.1).



Scheme 6.1 Screening of substrates towards reactivity with H_2O_2



Scheme 6.2 Screening of ligands for catalytic C-H amination with **46**

The ligands dpk and K(dpms) were observed not to support catalysis. This may be due to the formation of Pd(II)(dpk) or Pd(II)(dpms) complexes that are ineffective in the substrate C-H activation. We therefore switched our ligand systems to bulkier $\text{Me}_2\text{-dpk}$ and $\text{K(Me}_2\text{-dpms)}$ which have methyl groups at both 6-positions. We presumed that the ligands more loosely bound to the Pd center because of steric effects would allow the substrate to coordinate to the Pd center and undergo C-H activation. The use of $\text{Me}_2\text{-dpk}$ showed only a modest yield of 3% which was even lower than the ligandless system. Conversely, using $\text{K(Me}_2\text{-dpms)}$ showed over a 2 fold increase in the yield, as compared to the ligandless system, making $\text{K(Me}_2\text{-dpms)}$ a viable candidate for catalytic C-H amination. We then tried out the monomethylated ligands Me-dpk and Li(Me-dpms)

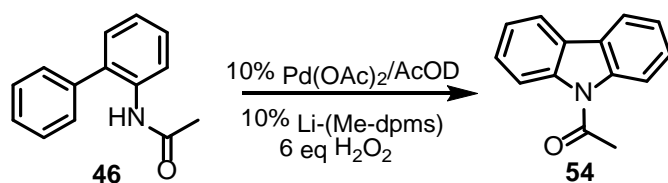
having a single methyl group at one of the 6-positions. Me-dpk showed a low yield of 2% which ruled out the use of dpk or any of its modified analogues (Me-dpk and Me₂-dpk) for catalytic C-H amination. The use of Li(Me-dpms) showed an increase in the yield of **54** to 14%.

Table 6.1. Effect of the ligand on the yield of N-acetylcarbazole (Scheme 6.2). Reaction conditions: **46** (30 mg, 0.14 mmol), Pd(OAc)₂ (10 mol%), Ligand (10 mol%), solvent(0.6 mL), 6 equivalents of 30 % H₂O₂ added at the beginning of reaction, 23 °C, 24 h. Yield (%) of **5f** determined by ¹H NMR spectroscopy with dioxane as internal standard.

Entry	Ligand	Yield
1	No Ligand	4
2	dpk	0
3	Me-dpk	2
4	Me ₂ -dpk	3
5	K-dpms	0
6	Li-(Me-dpms)	14
7	K-(Me ₂ -dpms)	10

This shows the dpk ligand might be perfect for studies involving stoichiometric reactions and isolation of intermediates but may not be viable for catalytic applications. After selecting the best ligand for our reaction, Li(Me-dpms), we tried to optimize the yield of **54** by varying temperature and rate of addition of H₂O₂ since H₂O₂ can decompose over time. C-H activation has been implicated in different catalytic reactions and previous work showed this process occurs

faster at higher temperatures.⁸⁷ We increased the temperature of our reaction to 50 °C and upon addition of 6 equivalents of H₂O₂ small bubbles were observed which is indicative of the formation of O₂ due to decomposition of H₂O₂. The yield of **54** after 6 hours was observed to be 20%. The modest yield was attributed to slow decomposition of H₂O₂. We therefore added the 6 equivalents of H₂O₂ in 0.5 equivalent portions over specific time intervals. When the time between additions was 15 minutes, the yield of **54** was observed to be 13% after 180 minutes.



Scheme 6.3 Catalytic C-H amination with **46** to form **54** with Li-(Me-dpms) as ligand.

Table 6.2. Effect of the reaction conditions on the yield of N-acetylcarbazole Reactants loading: **46** (30 mg, 0.14 mmol), Pd(OAc)₂ (10 mol%), Ligand (10 mol%), solvent(0.6 mL), 0.5 equivalent of H₂O₂ added each time. Yield (%) of **54** determined by ¹H NMR

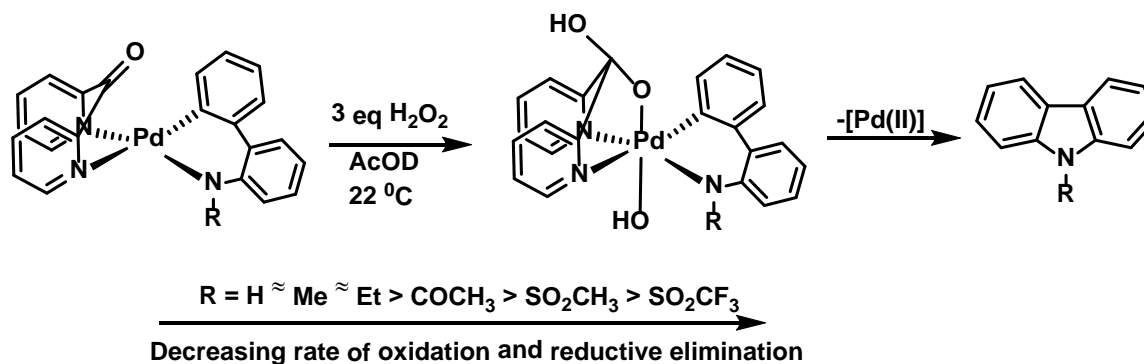
Entry	Time between additions / min	50°C		
		Yield (%)	Conversion (%)	Total Time / min
1	15	13	19	180
2	30	22	29	360
3	60	38	45	720
		70°C		
4	15	37	43	180

Increasing the time between additions to 30 minutes increased the yield of **54** to 22% after 360 minutes. The time between additions was further increased to 60 minutes and the yield of **54** was observed to increase to 38% after 720 minutes. This shows the yield of **54** was dependent on the amount of oxidant present in the system at constant temperature. The temperature of the catalytic reaction was then increased to 70 °C and adding 0.5 equivalents of H₂O₂ at a time with 15 minutes in between additions. The yield of carbazole formed was observed to be 37%. We propose an increase in temperature increases the rate of C-H activation and thereby increases overall, the rate of C-H amination since previous work had shown that C-H activation is usually the rate limiting step of this process.⁸⁸ Repeating the reaction in table entry in the absence of the Li(Me-dpms) ligand gave 6% yield of **54**.

6.3 Conclusions

In conclusion, we synthesized N-acyl carbazole through a direct C-H functionalization with H₂O₂ as terminal oxidant and Pd(OAc)₂ as catalyst. N-*R*-2-aminobiphenyl substrates with R = H, Me and Et were observed to undergo oxidation of the aniline fragment to form nitrosamine. N-acetyl-2-aminobiphenyl, **46**, was the only substrate observed to undergo catalytic C-H amination with Li(Me-dpms) as the desired ligand. The use of other electron withdrawing N-*R*-2-aminobiphenyl (R = COCF₃, SO₂CH₃, SO₂CF₃) substrates apart from **46** did not lead to the formation of the target carbazoles. The yield of the C-N coupled product, **54**, was observed to be dependent on the temperature of the reaction and the rate of addition of the terminal oxidant, H₂O₂.⁸⁹ The dependence of the yield on temperature implicates the C-H activation step as turnover limiting for this catalytic C-H oxidative amination reaction.

Chapter 7: Conclusion and Future Directions



Scheme 7.1 Trends for the reactivity of dppf ligated Pd(II) 2-aminobiphenyl substrates towards H₂O₂.

In conclusion, in this work we have synthesized the first amido aryl Pd(IV) complexes including a series of different cationic κ^2 -C,N-2'-(N-R-amino)biphenyl-2-yl Pd(II) and neutral κ^2 -C,N-2'-(N-R-amido)biphenyl-2-yl Pd(II) complexes (Scheme 7.1). As a result, the intermediacy of amido aryl Pd(IV) complexes in oxidative C-N coupling was unambiguously demonstrated for the first time. The reactions of the amido aryl Pd(II) precursors toward H₂O₂ and C(sp²)-N coupling of the resulting amido aryl Pd(IV) intermediates were explored in detail.

In general, the rates of oxidation and C(sp²)-N reductive elimination followed a common trend corresponding to the nature of the R group involved. The stronger the electron withdrawing ability of the R group, the slower the rates of both oxidation and reductive elimination. These reactivities can be related to the pK_a of the corresponding NH acids of the R group involved. The higher the pK_a of the corresponding acid, the faster the rates of oxidation and reductive elimination reactions. The outlier was R = COCF₃ which, based on the NH acidity trend, was expected to have a reactivity intermediate between that for R=COCH₃ and R=SO₂CH₃ but was observed to be the

least reactive towards H_2O_2 of all the Pd(II) complexes synthesized. Overall, according to our DFT calculations, the $\text{C}(\text{sp}^2)\text{-N}$ coupling in all our systems occurred as a concerted process from a 6-coordinate Pd(IV) center. The reactivity trend observed at the Pd(IV) center was found to be similar to that found earlier by other groups for C-N coupling at Pd(II); in both cases more electron-rich amido complexes react faster. These results may become useful for design of various systems relying on the utilization of high-valent metal mediated $\text{C}(\text{sp}^2)\text{-N}$ coupling step. Finally, based on our observations related to the isolation of high oxidation state amido aryl Pd(IV) complexes, we conclude that the use of a combination of a strong electron withdrawing ligands on the nitrogen and the use of weakly polar, weakly coordinating and non-reducing aprotic solvents for the oxidation process is the best strategy for success at isolating these otherwise very reactive and elusive species.

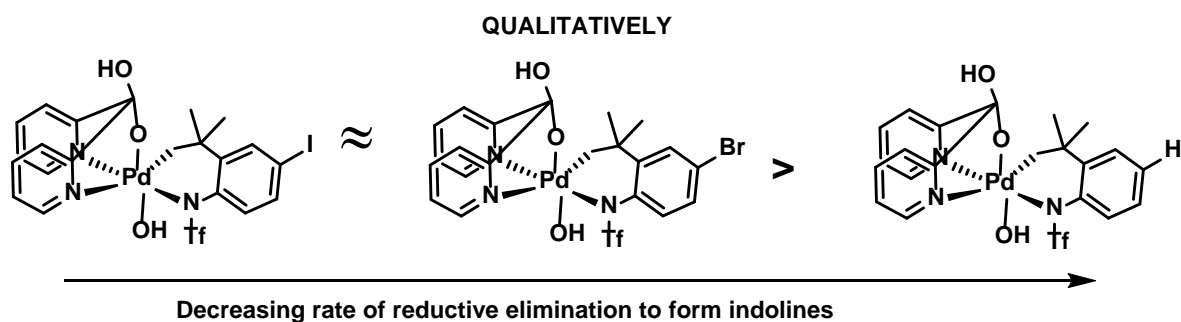


Figure 7.1 Trend for reductive elimination from substituted dpk-ligated Pd(IV) alkyl *N*-anilido complexes.

In this work we have also synthesized the first monohydrocarbyl amido alkyl Pd(IV) complexes (Figure 7.1) and explored the mechanism of their intramolecular $\text{C}(\text{sp}^3)\text{-N}$ reductive

eliminations leading to the formation of corresponding indolines. Notably, intramolecular C(sp³)-N coupling at Pd(IV) center has never been observed and characterized before. Our mechanistic investigation of this new reaction showed that the intramolecular C(sp³)-N coupling at the Pd(IV) is mediated by an attack of external nucleophiles such as Cl⁻, Br⁻ or I⁻. The reaction mechanism that we proposed includes first a nucleophilic attack of a halide anion at the Pd(IV)-bound alkyl group carbon atom. This reaction leads to a Pd(II) amido complex having an alkylhalide fragment. The amido ligand nitrogen atom is next involved in an intramolecular nucleophilic attack at the haloalkane fragment to form a corresponding indoline. Accordingly, in the C(sp³)-N coupling reaction, electron withdrawing halogen atoms in the aniline core were observed to slightly speed up the rate of reductive elimination from the Pd(IV) center. These results may become useful for design of various systems relying on the utilization of high-valent metal mediated C(sp³)-N coupling step.

Finally, in this work we were able to demonstrate a catalytic C(sp²)-H oxidative amination reactions utilizing H₂O₂ in acetic acid solutions. The reaction was enabled through the use of weakly binding *fac*-chelating ligands. Future work may be focused on optimization of reaction conditions for this catalytic process and its expansion to a broad range of substrates.

Appendices

(NMR Spectra)

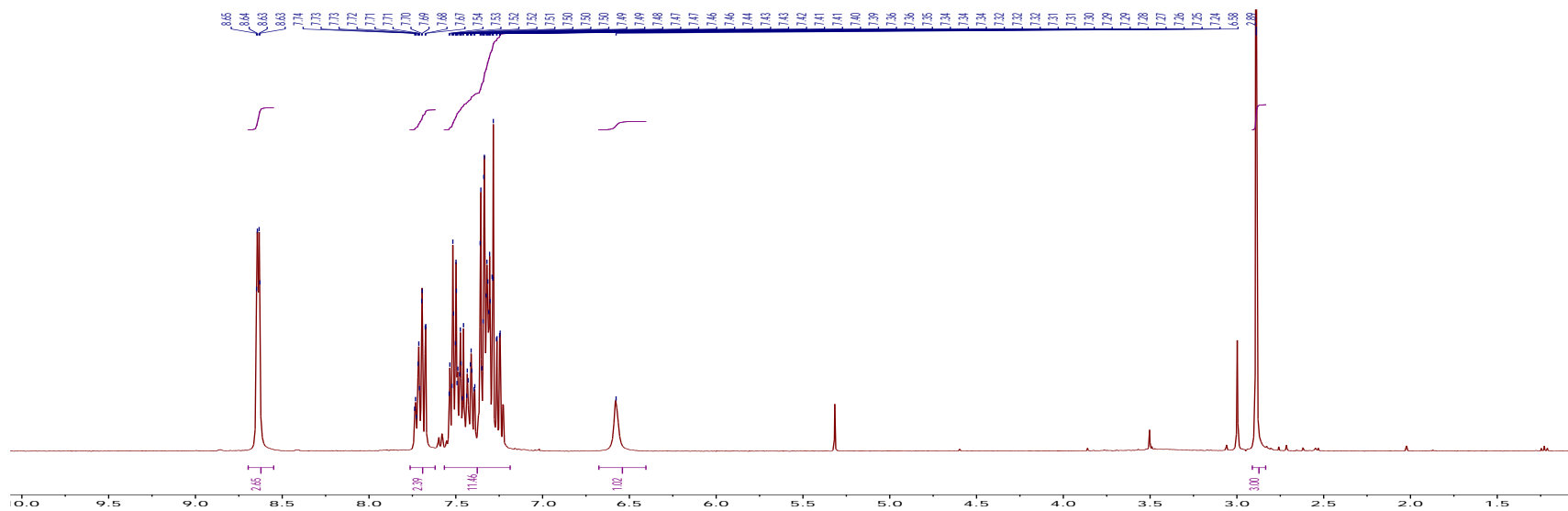
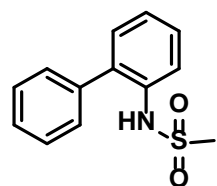


Figure A1. ^1H NMR of **48** in CDCl_3 at 22 °C.

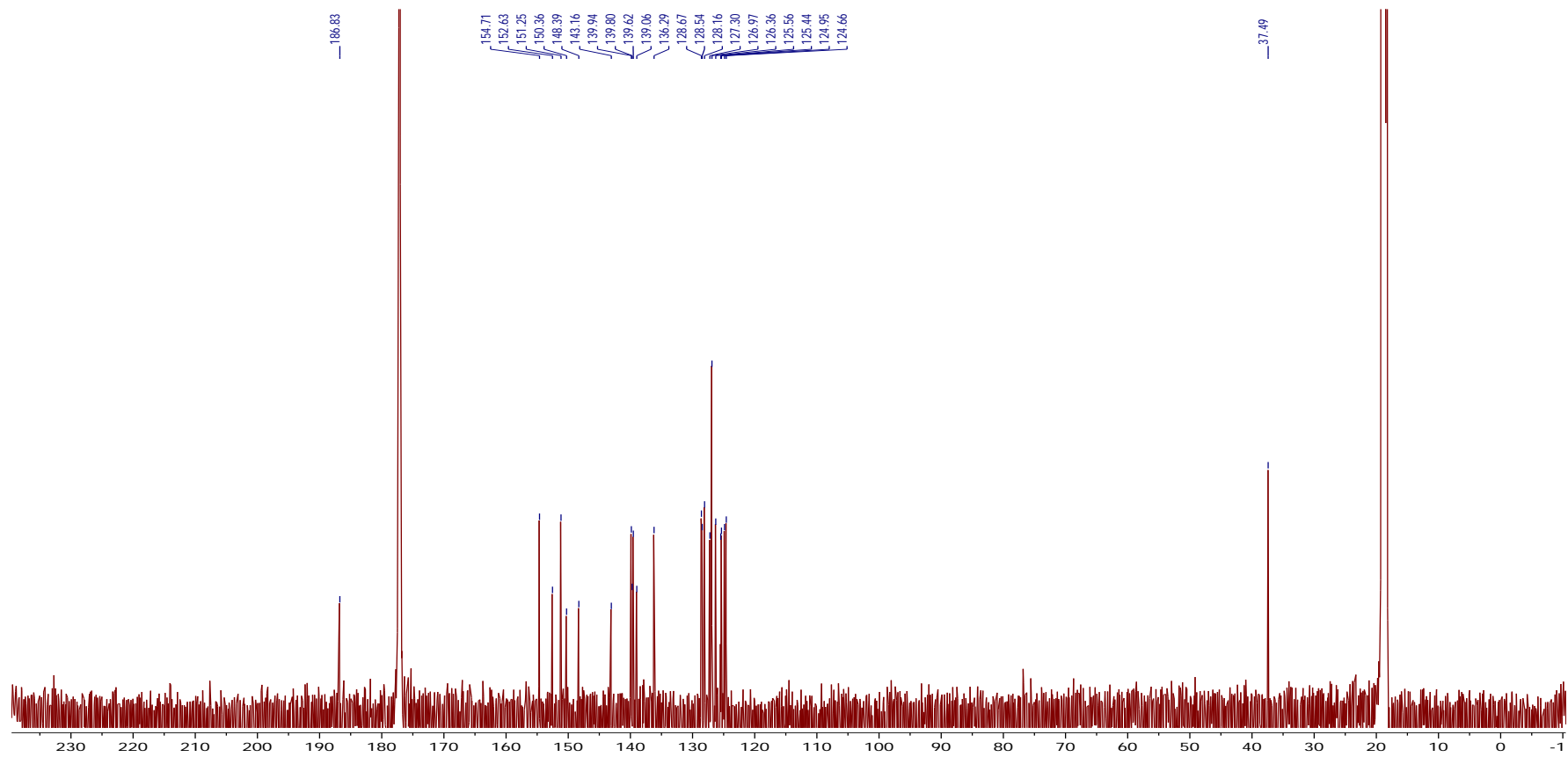
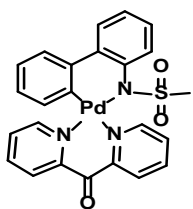


Figure A3. ^{13}C NMR of **61** in Acetic acid- d_4 at 22 °C

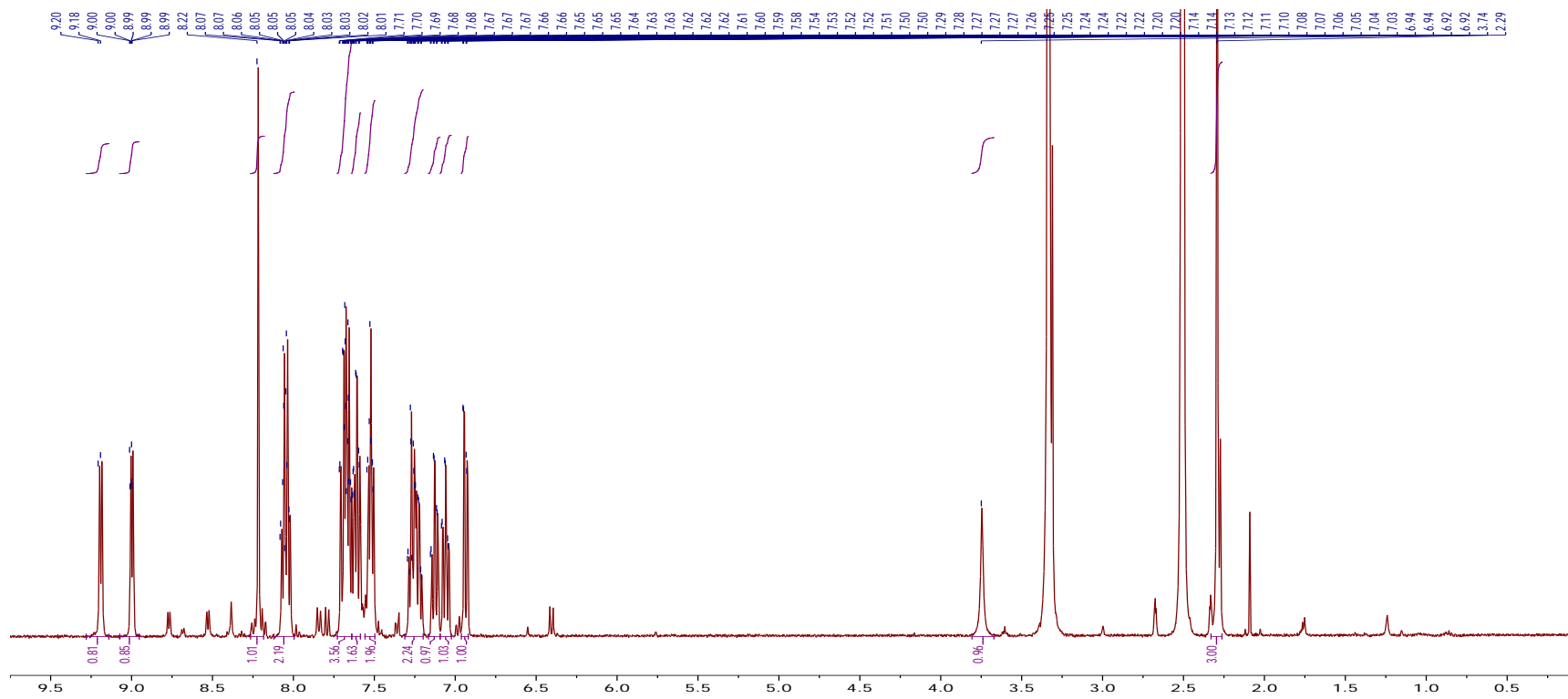
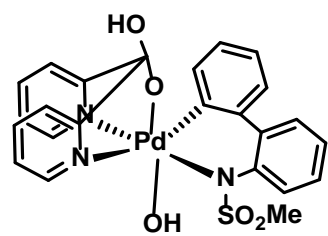


Figure A4. ^1H NMR of **63** in DMSO-d_6 at 23 °C. Minor signals in the aromatic region correspond to 6% impurity of **2a** and **3a**.

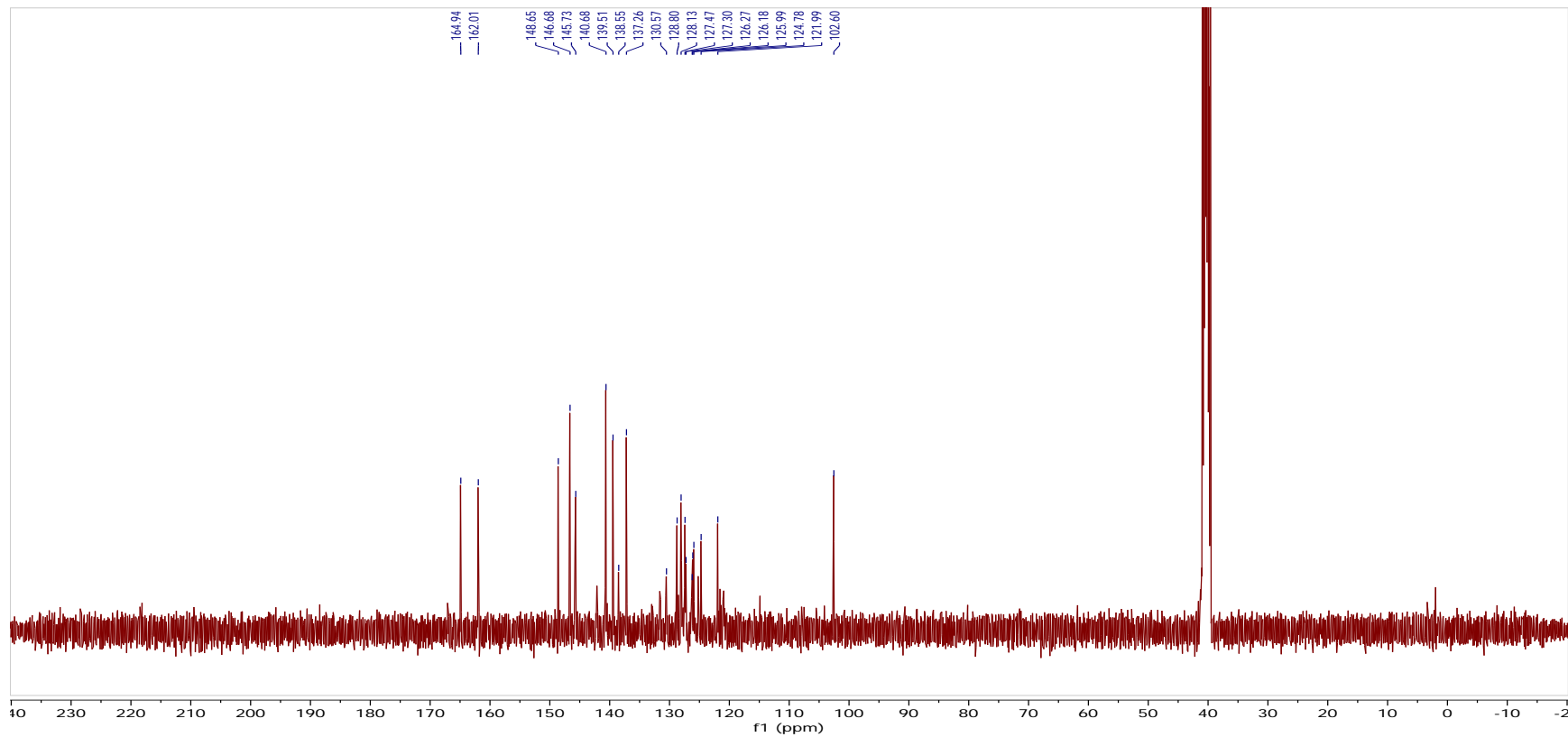
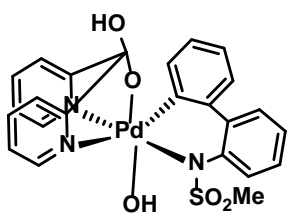


Figure A5. ¹³C NMR of **63** in DMSO-d₆ at 22 °C

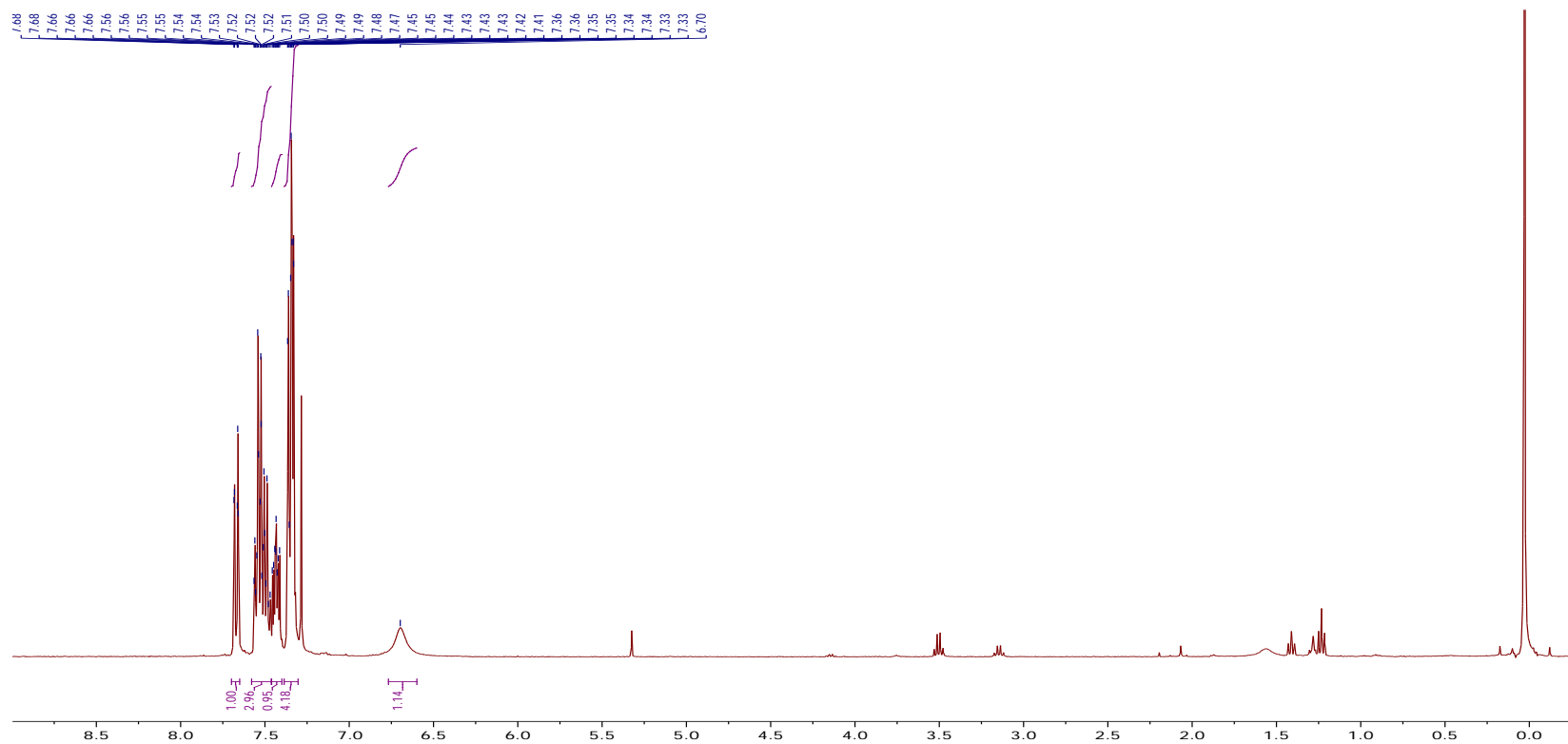
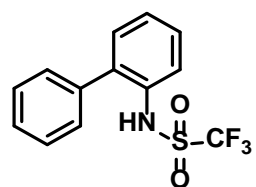


Figure A7. ¹H NMR of 49 in CDCl₃ at 22 °C.

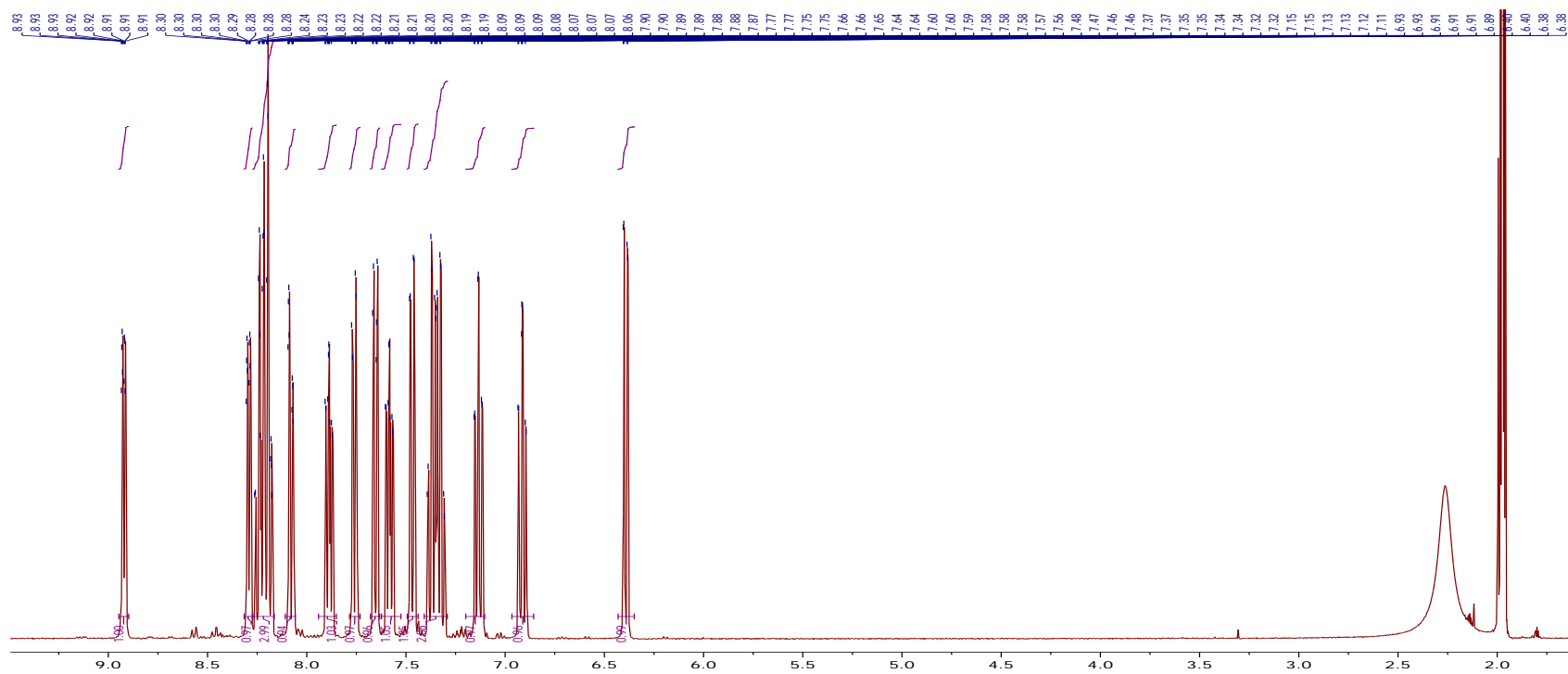
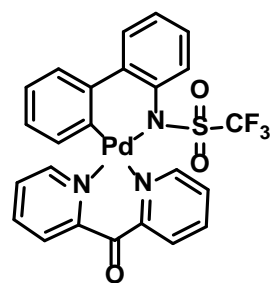


Figure A8. ^1H NMR of **66** in CD_3CN at 22 $^\circ\text{C}$.

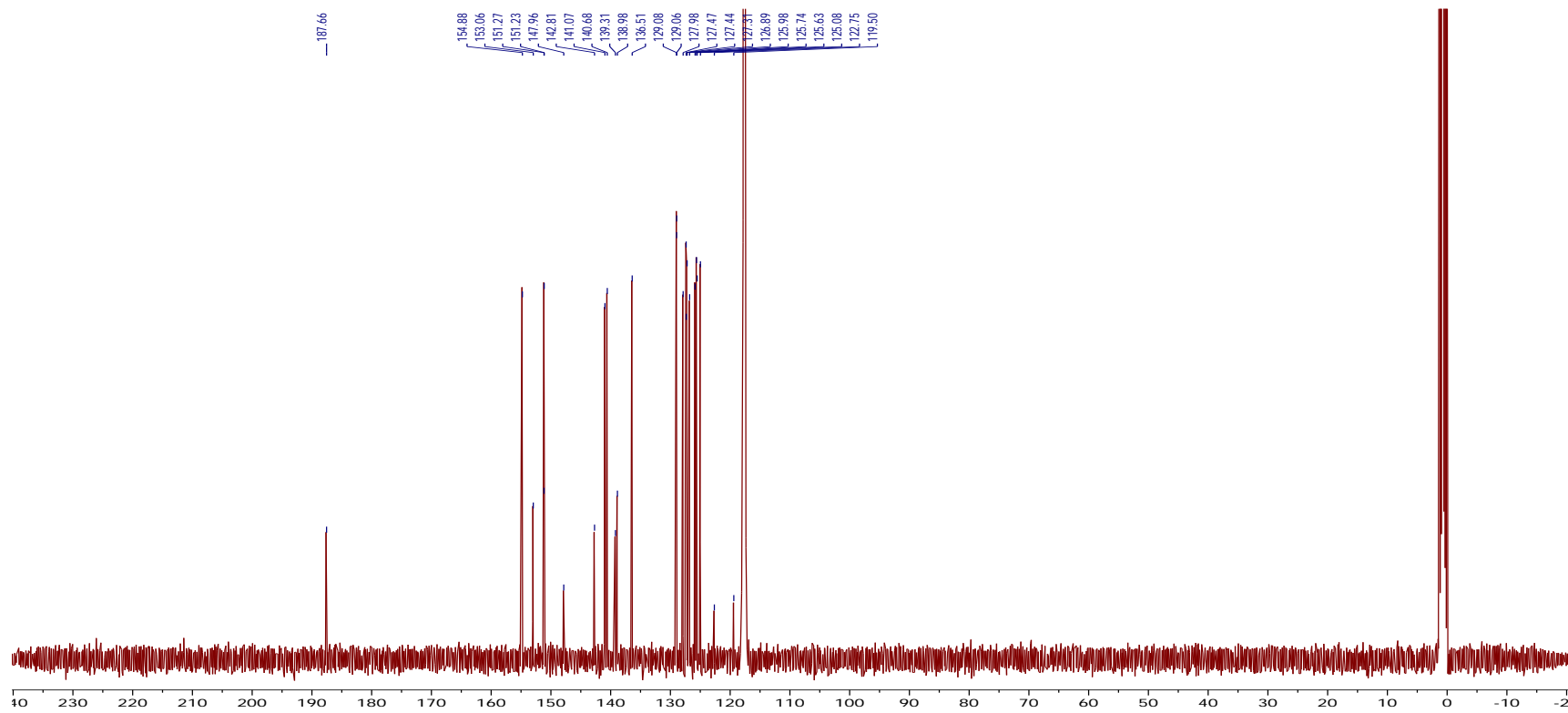
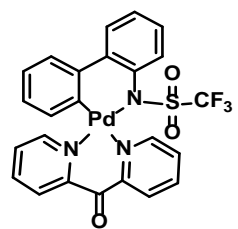


Figure A9. ¹³C NMR spectrum of **66** in CD₃CN at 22 °C.

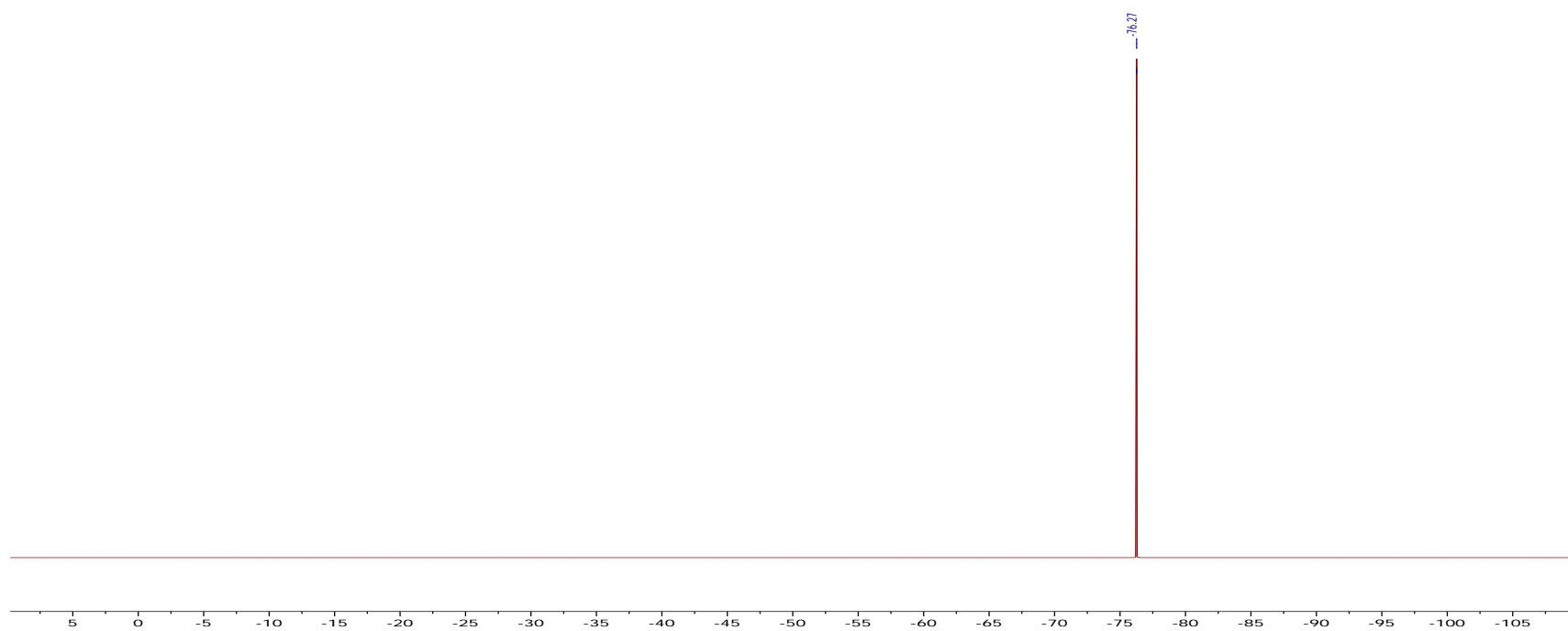
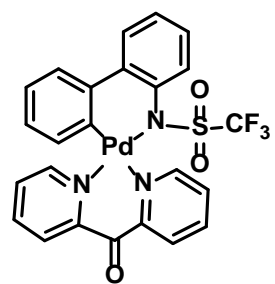


Figure A10. ^{19}F NMR spectrum of **66** in CD_3CN at $22\text{ }^\circ\text{C}$.

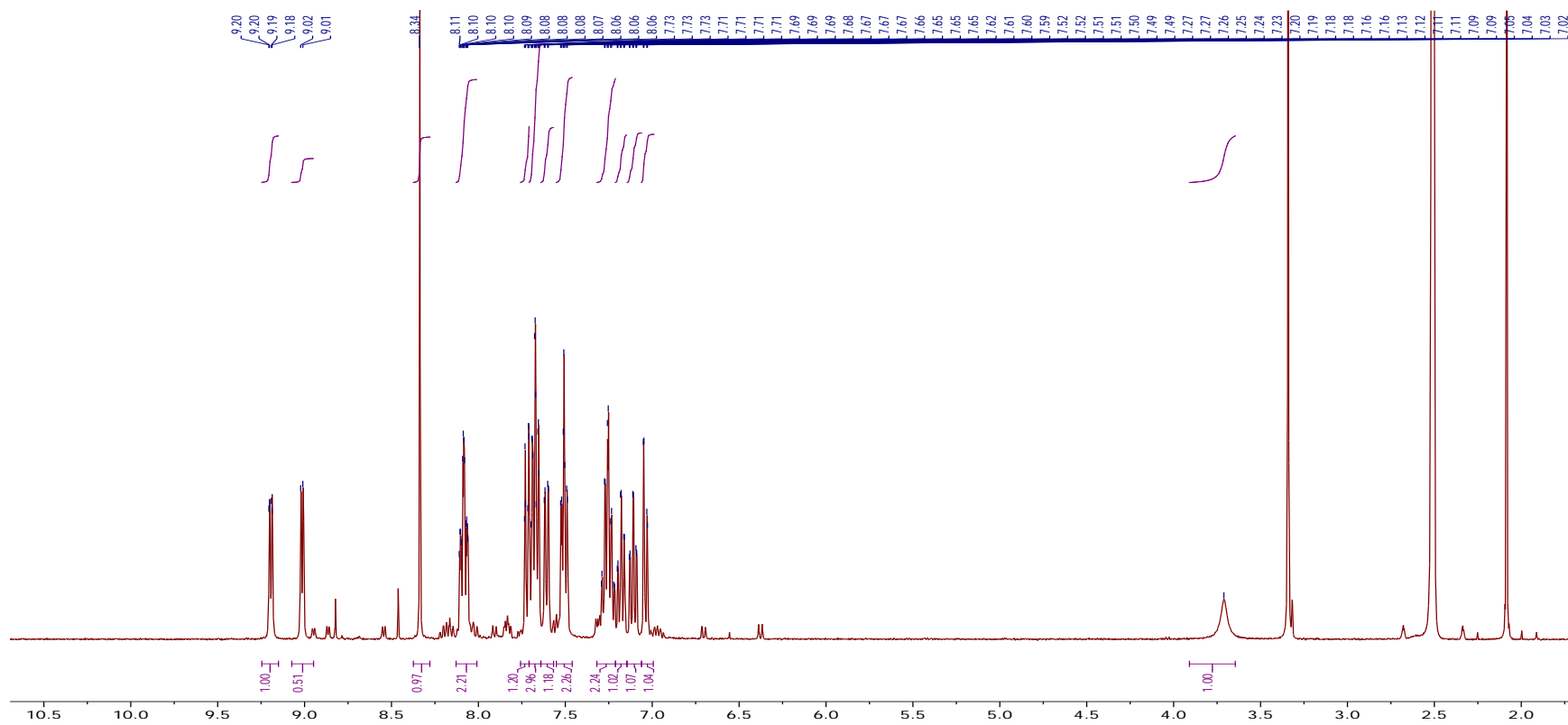
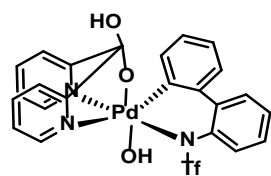


Figure A11. ¹H NMR of **68** in DMSO-*d*₆ at 22 °C. Minor signals in the aromatic region correspond to 4% impurity of **67** and **66**

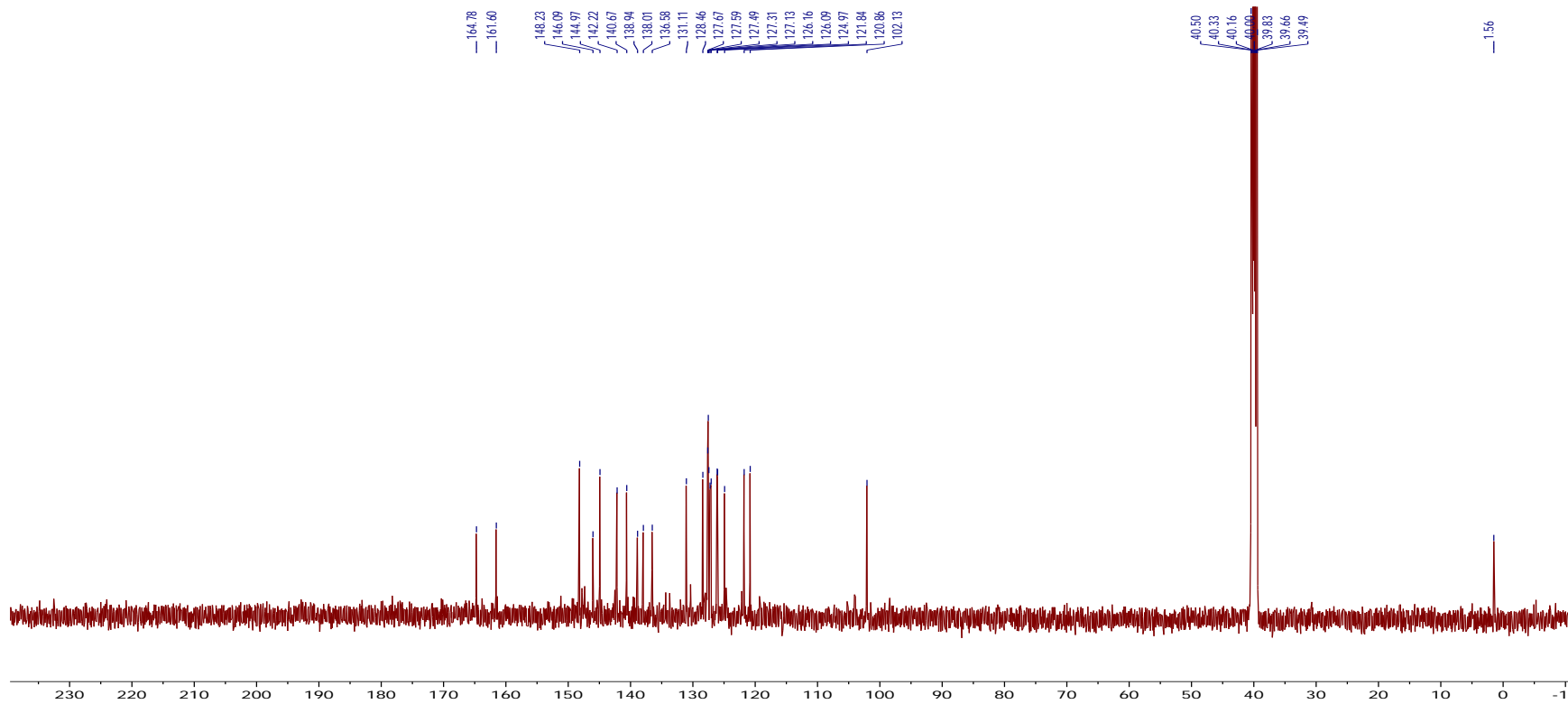
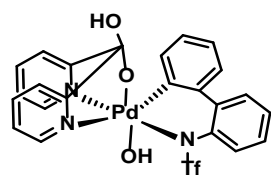


Figure A12. ^{13}C NMR of **68** in $\text{DMSO-}d_6$ at 22°C .

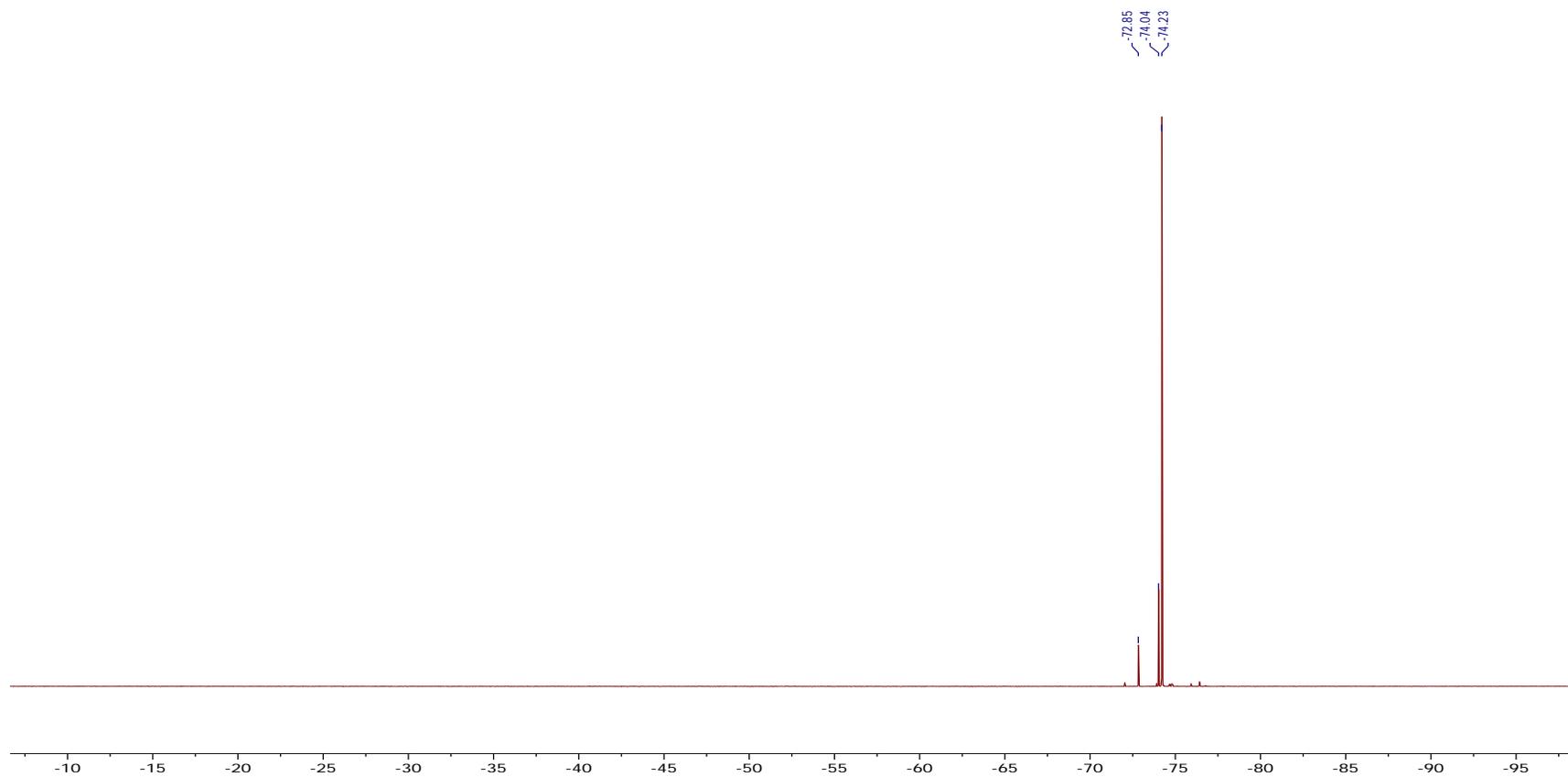
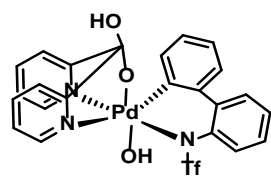


Figure A13. ^{19}F NMR of **68** in $\text{DMSO-}d_6$ at 22 °C. Minor signals to 5% impurity of **67** and **66**

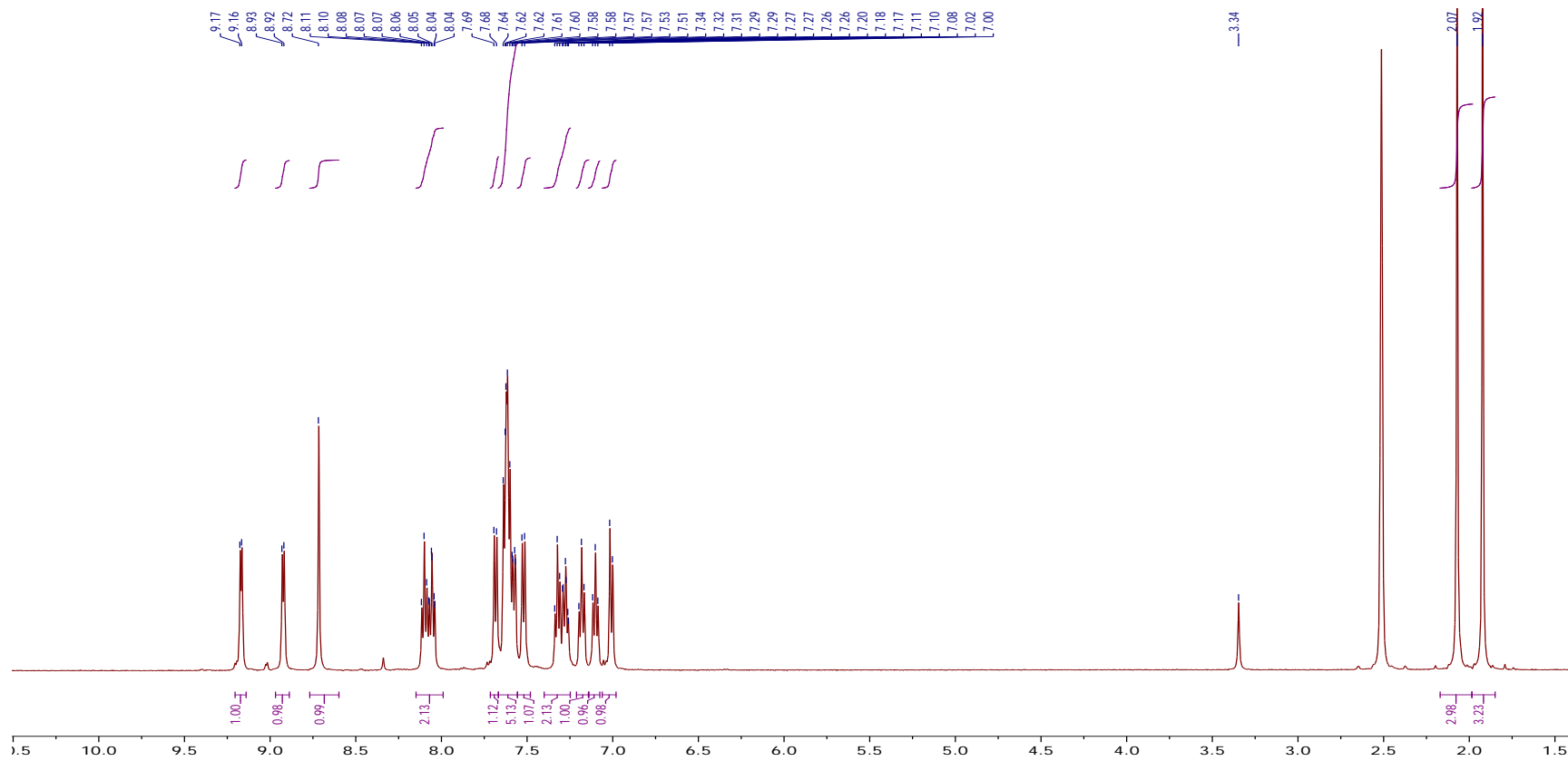
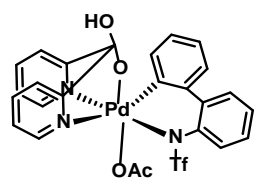


Figure A14. ^1H NMR of **69** in $\text{DMSO-}d_6$ at 22 °C.

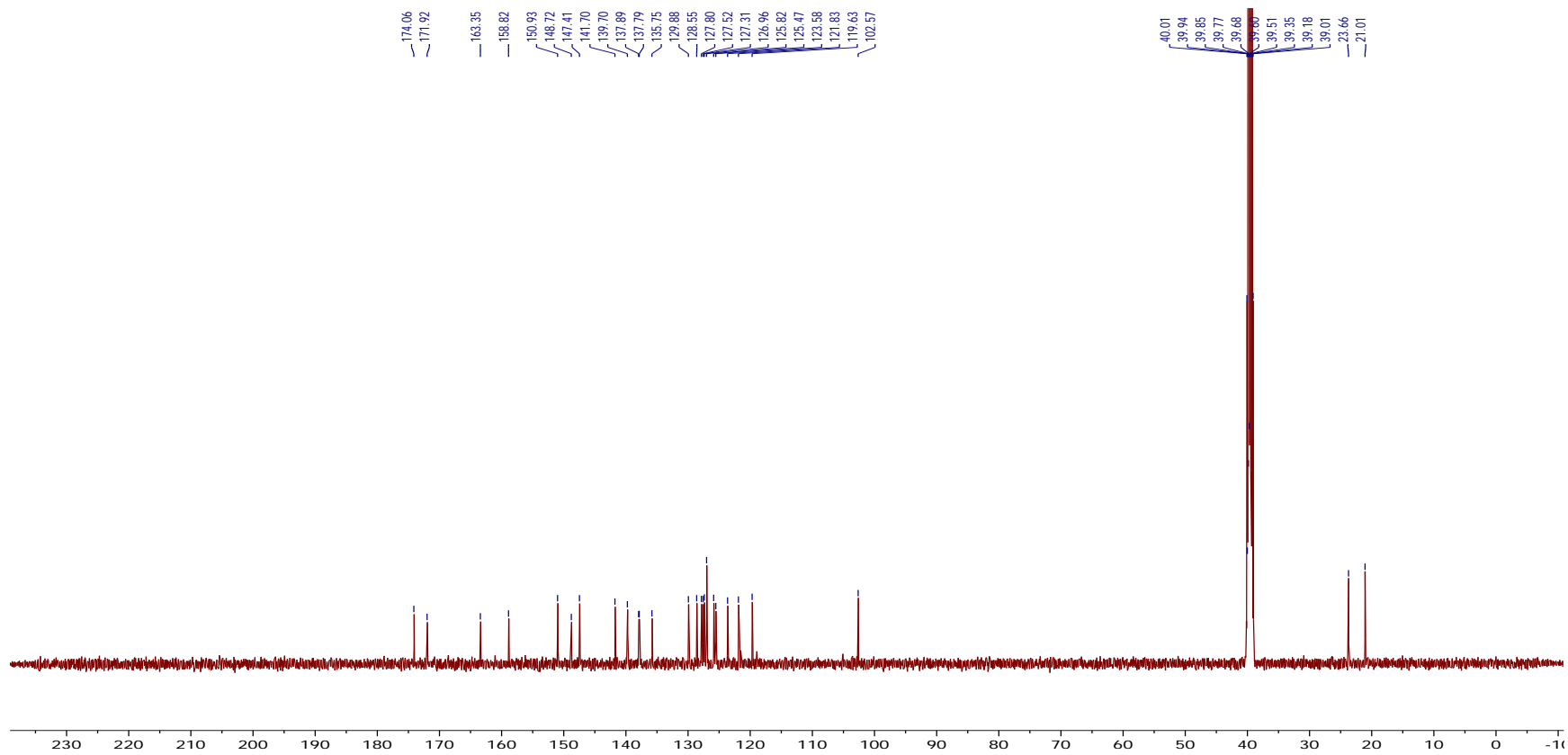
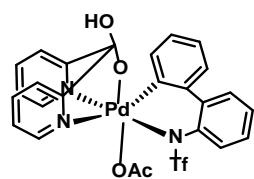


Figure A15. ^{13}C NMR of **69** in $\text{DMSO-}d_6$ at 22 °C.

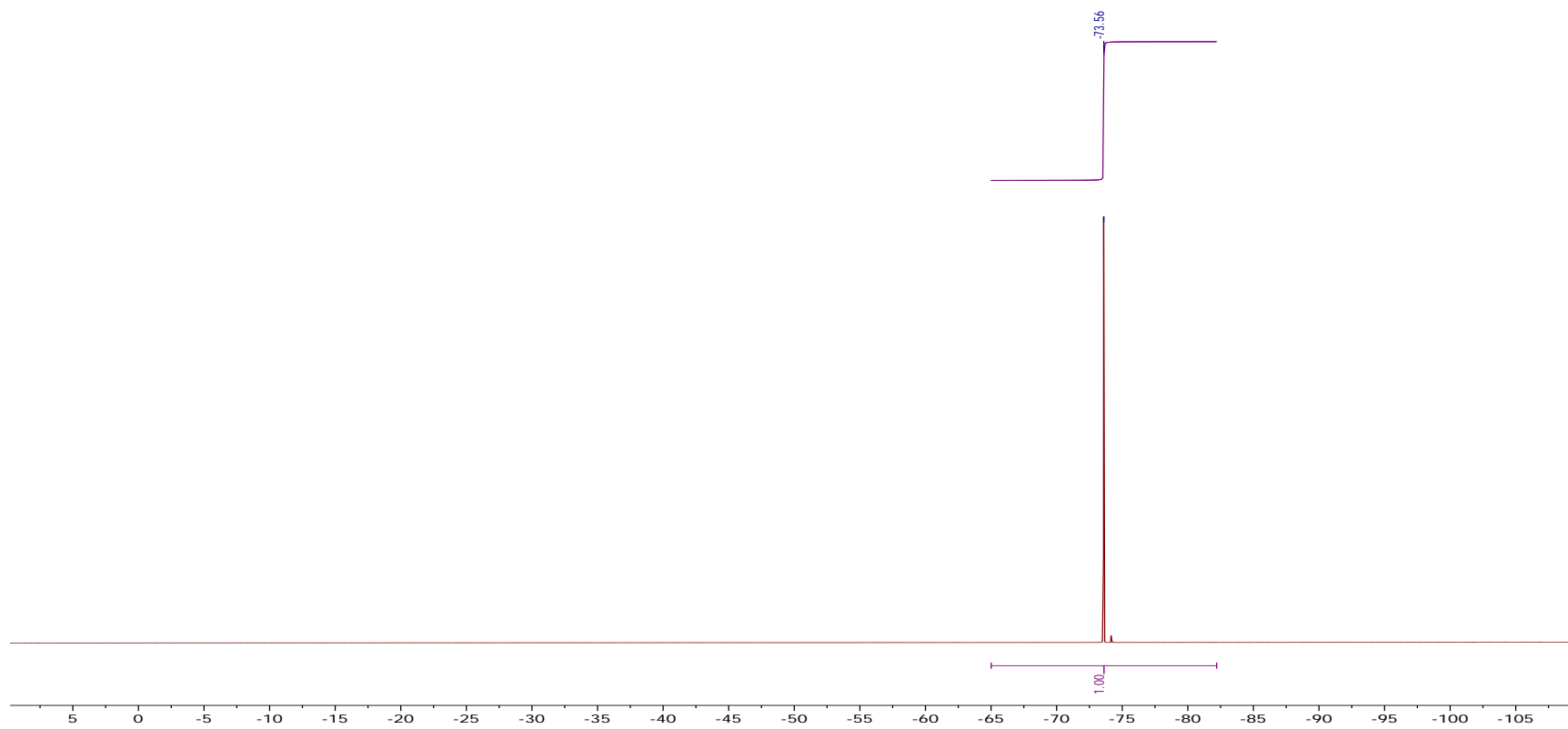
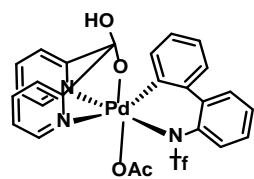


Figure A16. ^{19}F NMR of **69** in $\text{DMSO-}d_6$ at $22\text{ }^\circ\text{C}$.

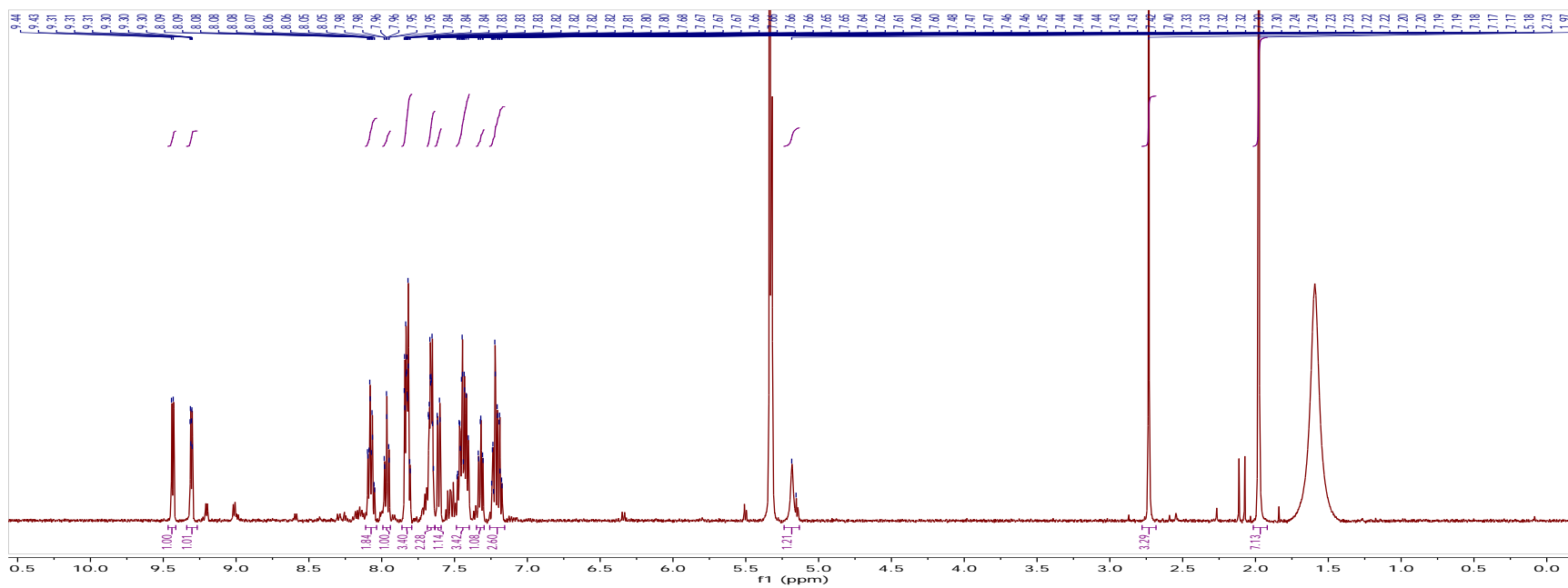
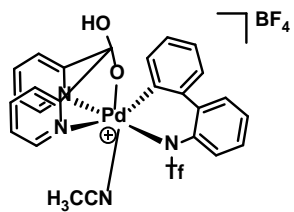


Figure A17. ^1H NMR of **75BF₄** in $\text{DMSO-}d_6$ at 22 °C. Minor signals in the aromatic region correspond to 4% impurity of **66** and **67**

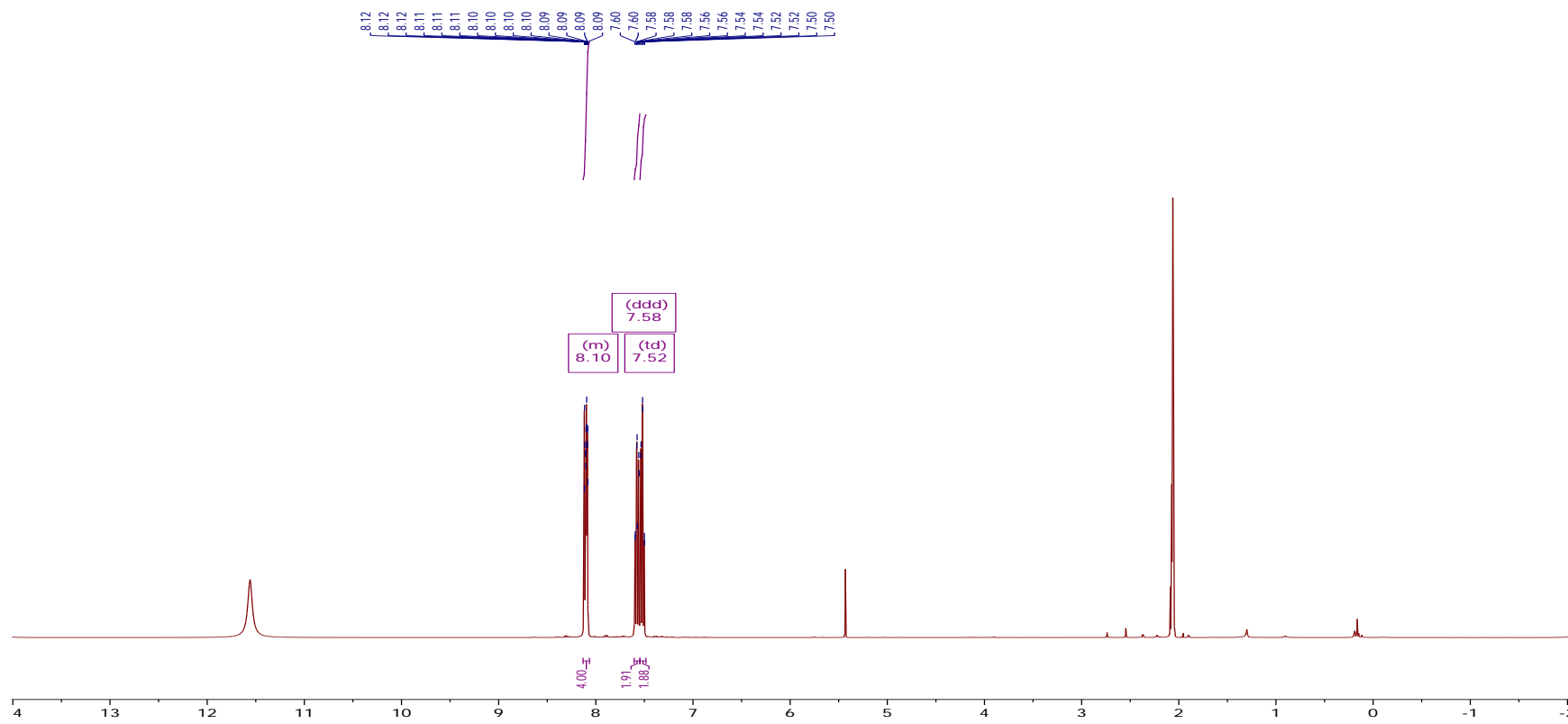
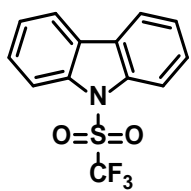


Figure A18. ^1H NMR of **70** in AcOD-d_4 at $22\text{ }^\circ\text{C}$.

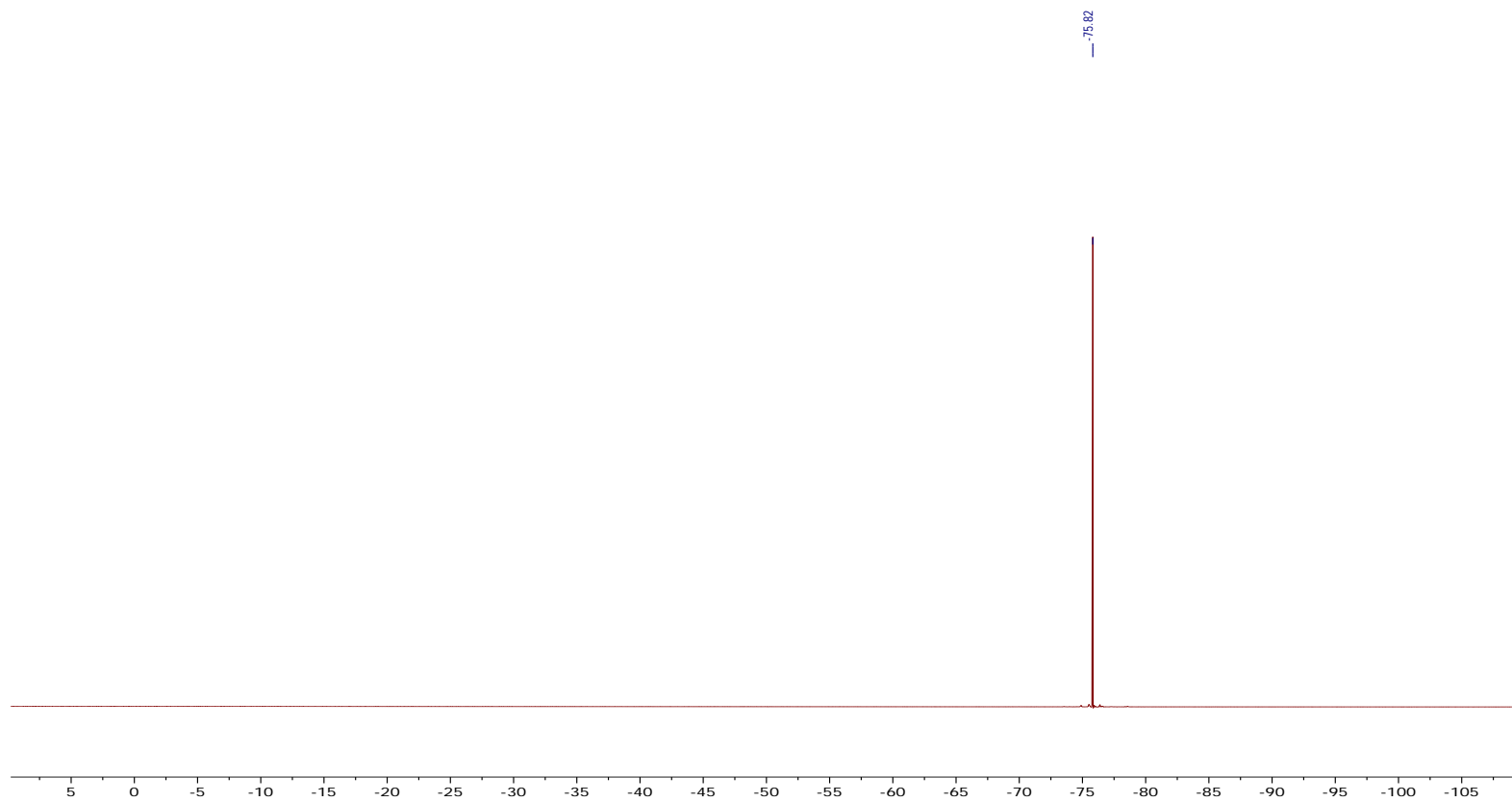
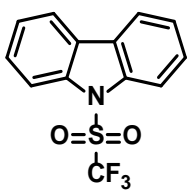


Figure A19. ¹⁹F NMR of **70** in AcOD-d₄ at 22 °C.

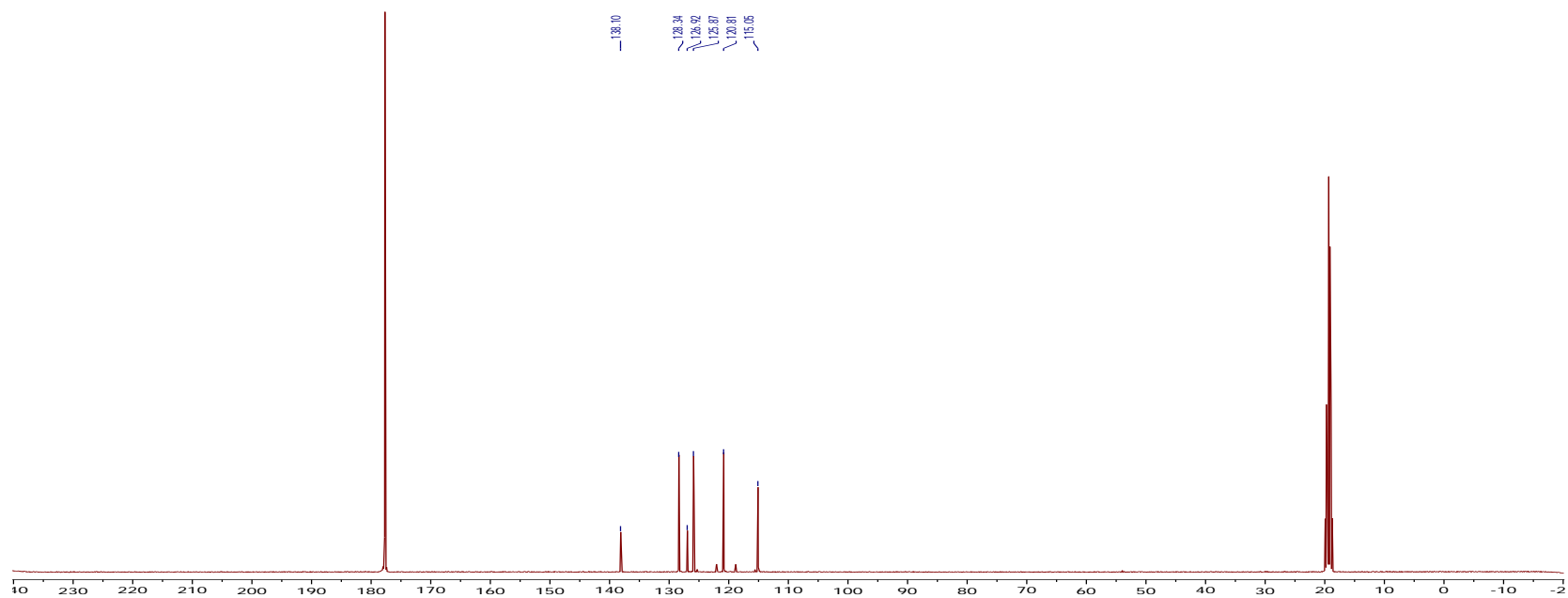
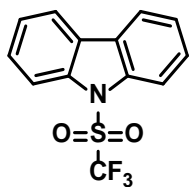


Figure A20. ^{13}C NMR of **70** in AcOD- d_4 at 22 °C.

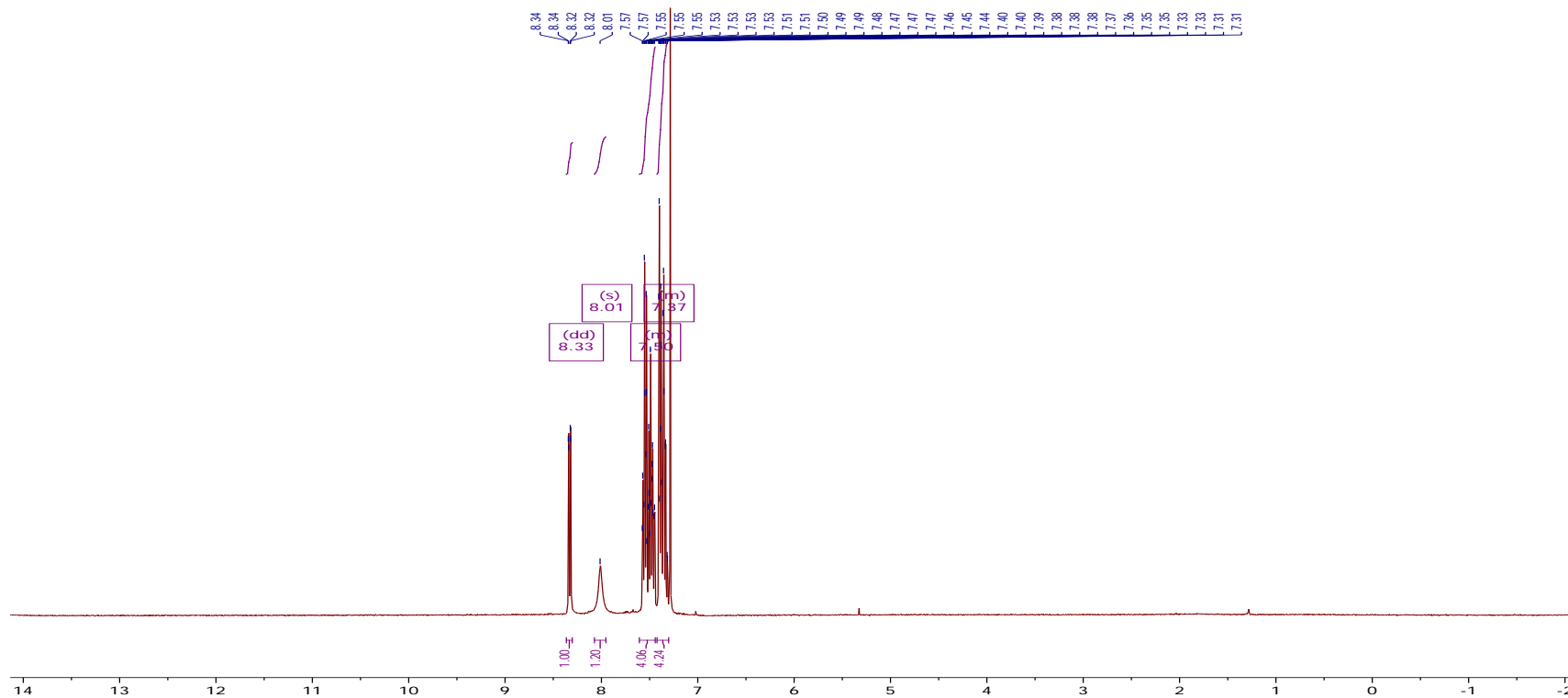
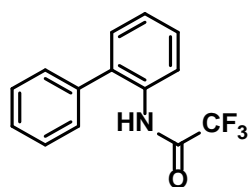


Figure A21. ¹H NMR of 47 in CDCl₃ at 22 °C

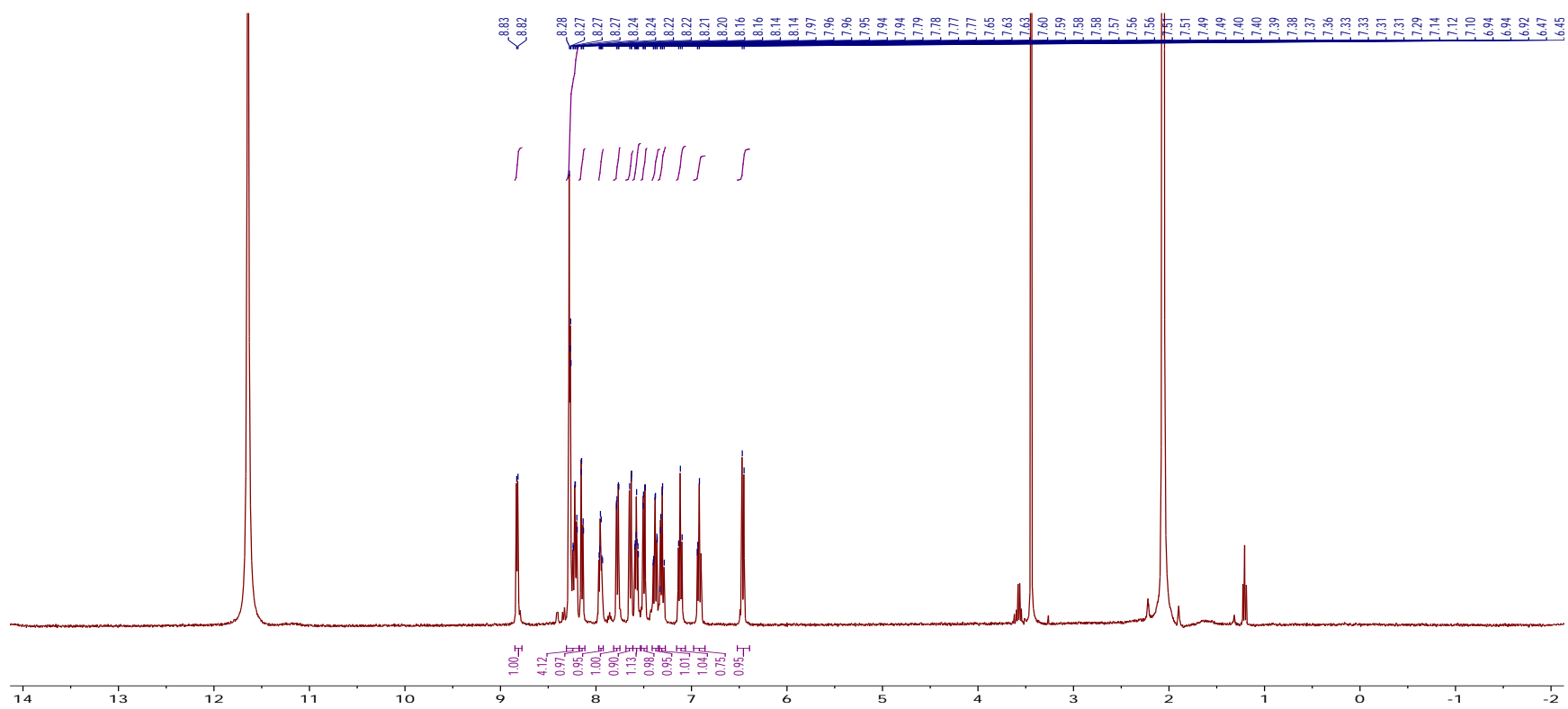
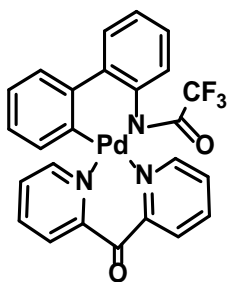


Figure A22. ^1H NMR of **51** in Acetic Acid- d_4 at 22 °C.

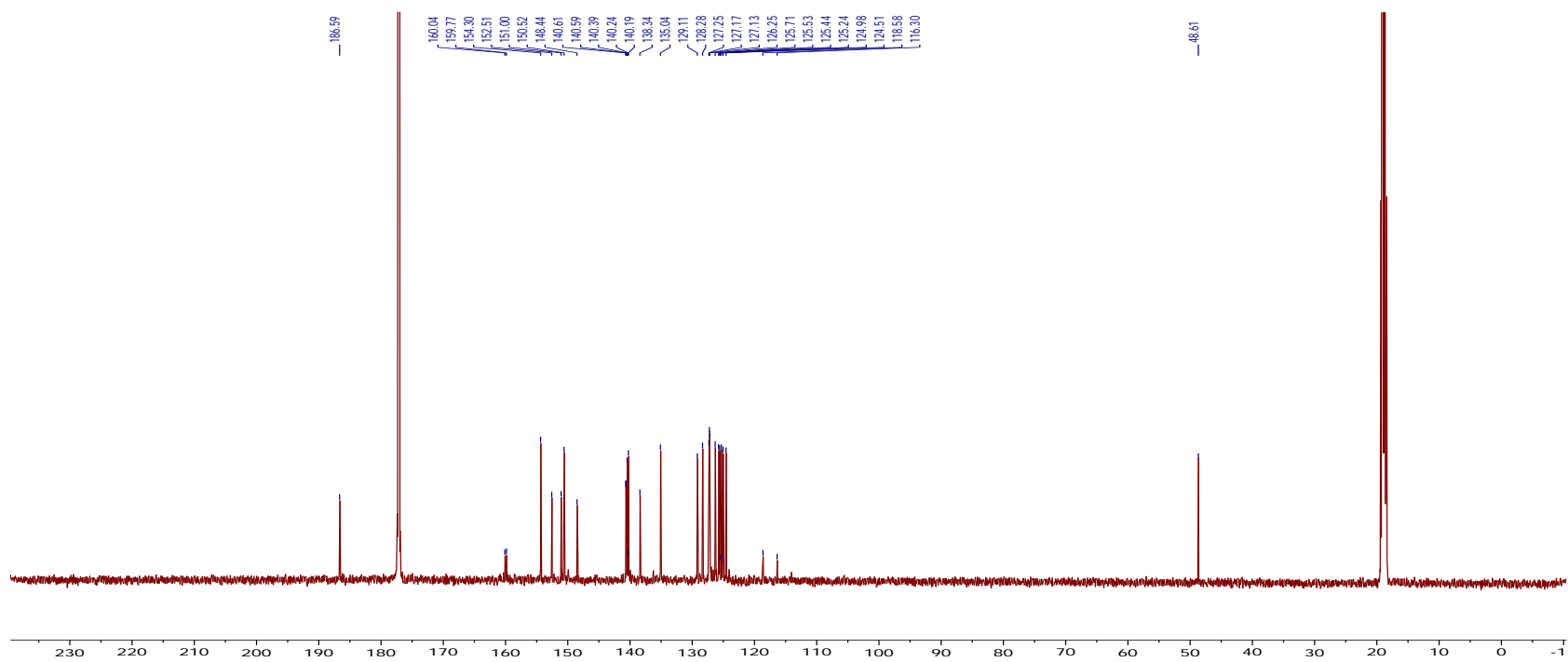
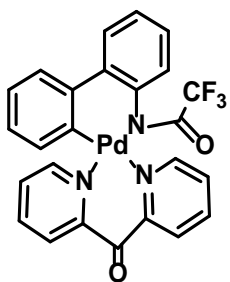


Figure A23. ¹³C NMR of 51 in Acetic Acid-*d*₄ at 22 °C.

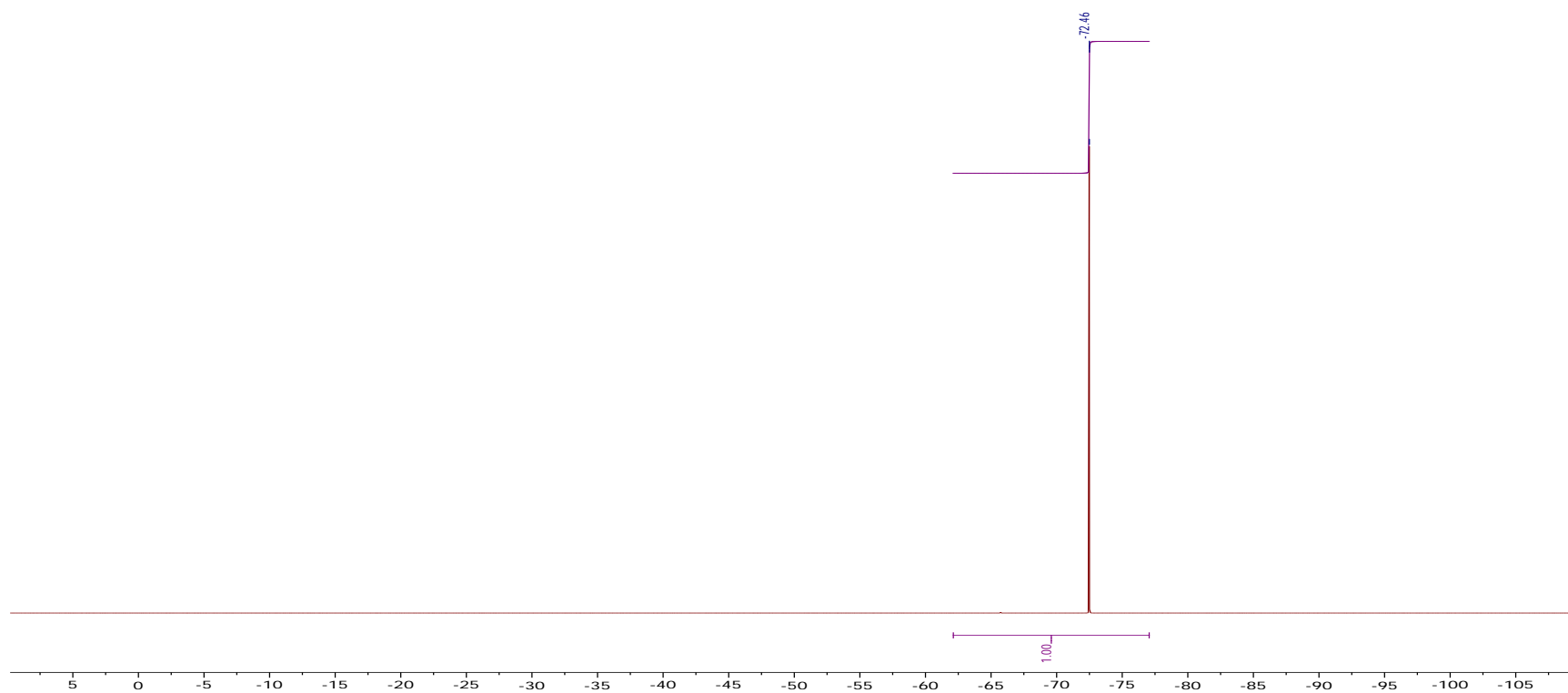
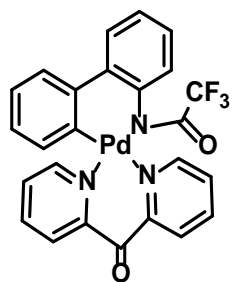


Figure A24. ¹⁹F NMR of **51** in Acetic Acid-*d*₄ at 22 °C.

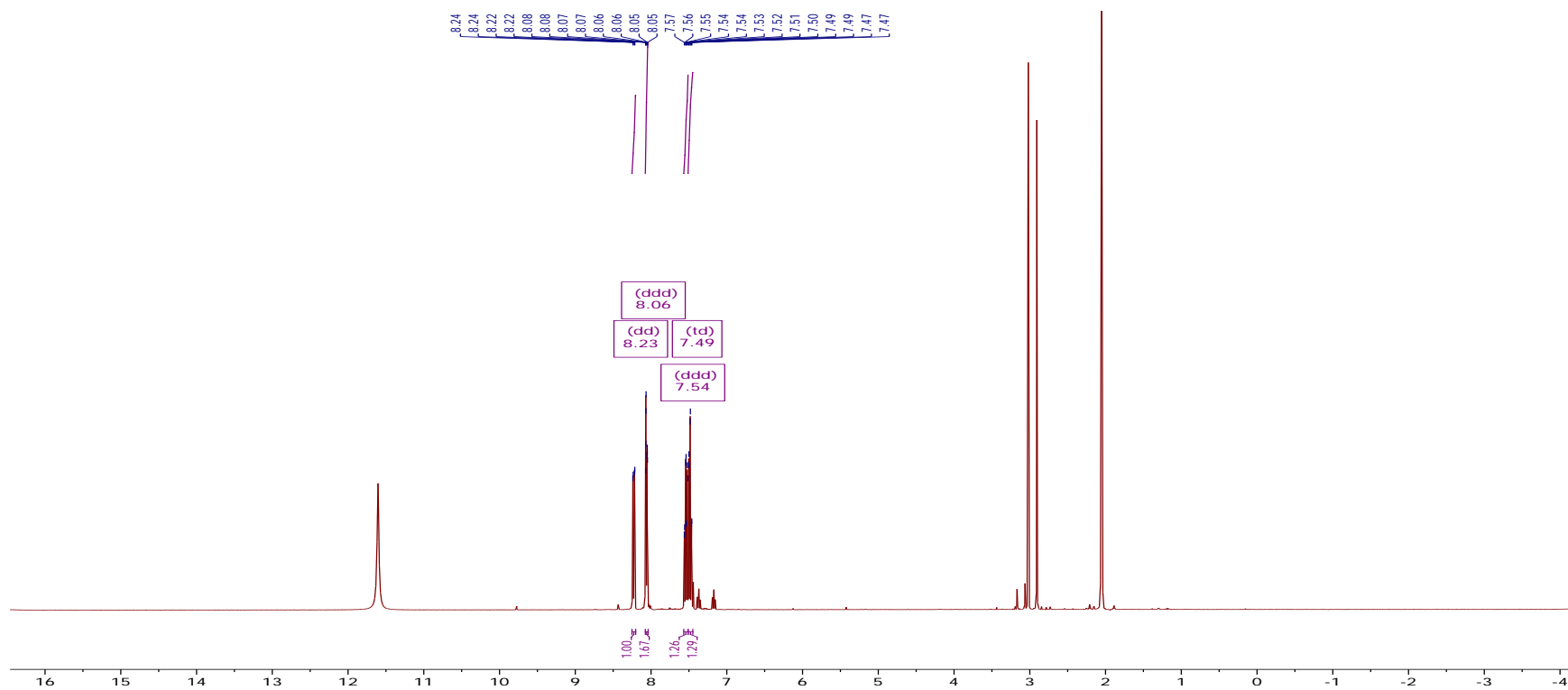


Figure A25. ¹H NMR of **58** in Acetic Acid-*d*₄ at 22 °C.

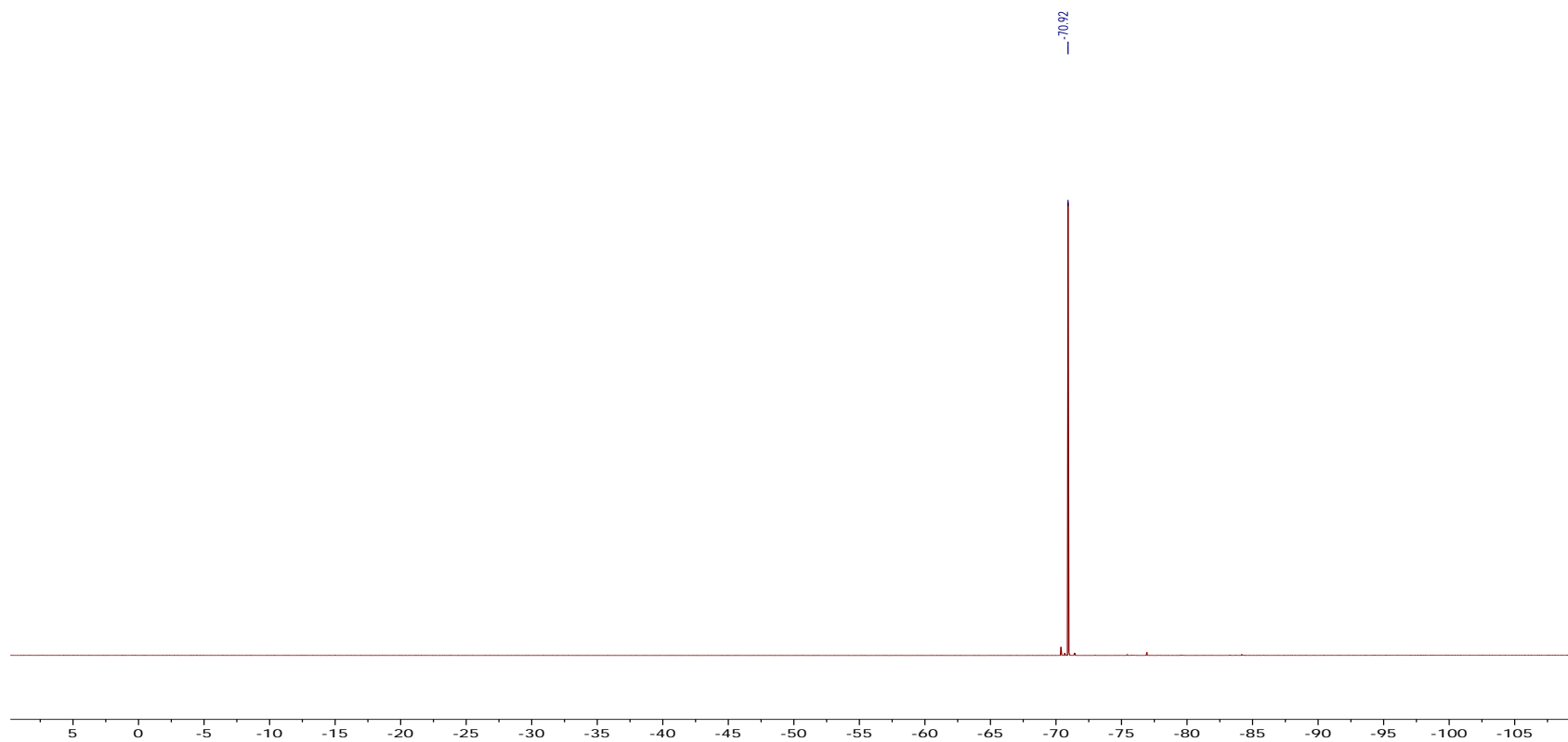


Figure A26. ¹⁹F NMR of **58** in Acetic Acid-*d*₄ at 22 °C.

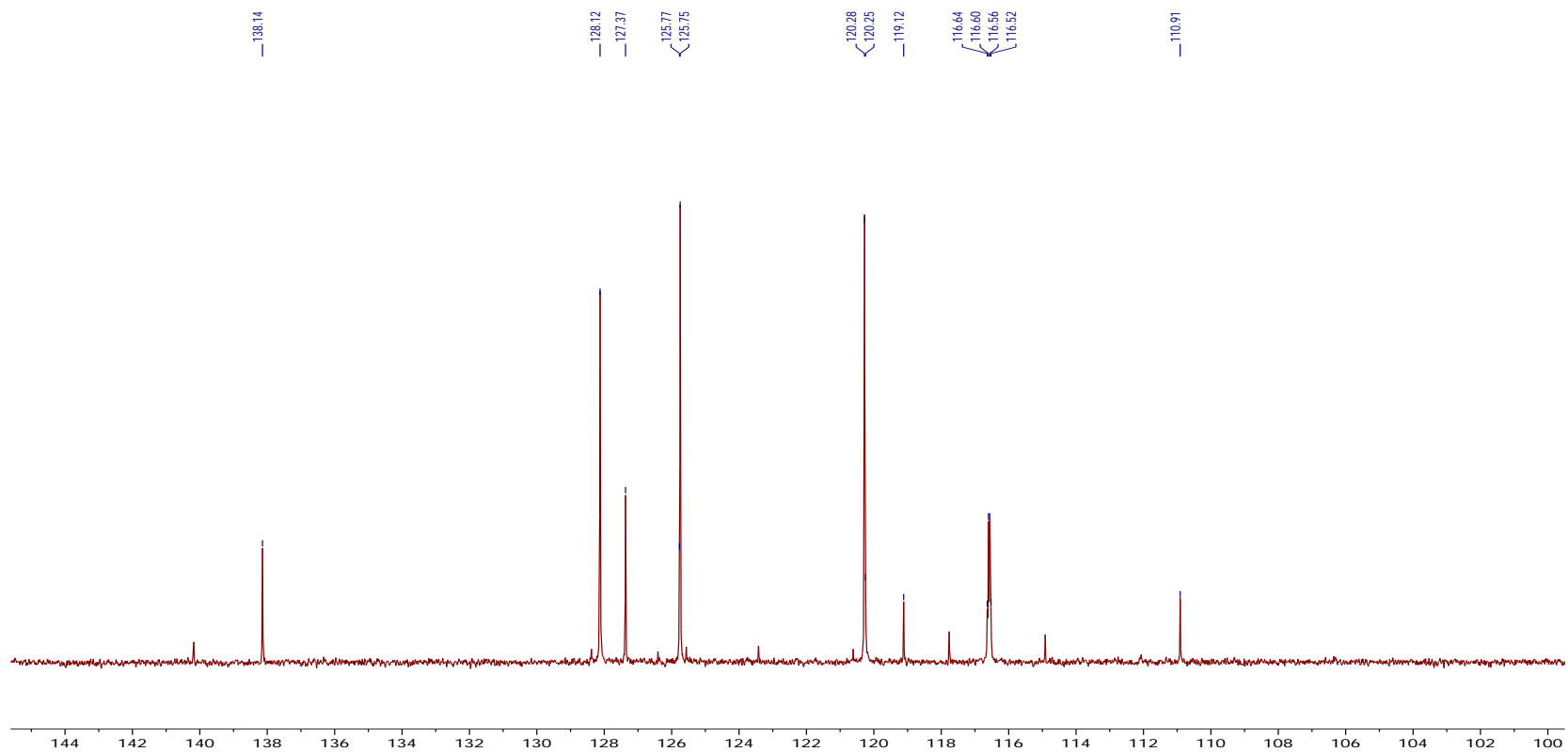


Figure A27. ^{13}C NMR of **58** in $\text{Acetic Acid-}d_4$ at $22\text{ }^\circ\text{C}$.

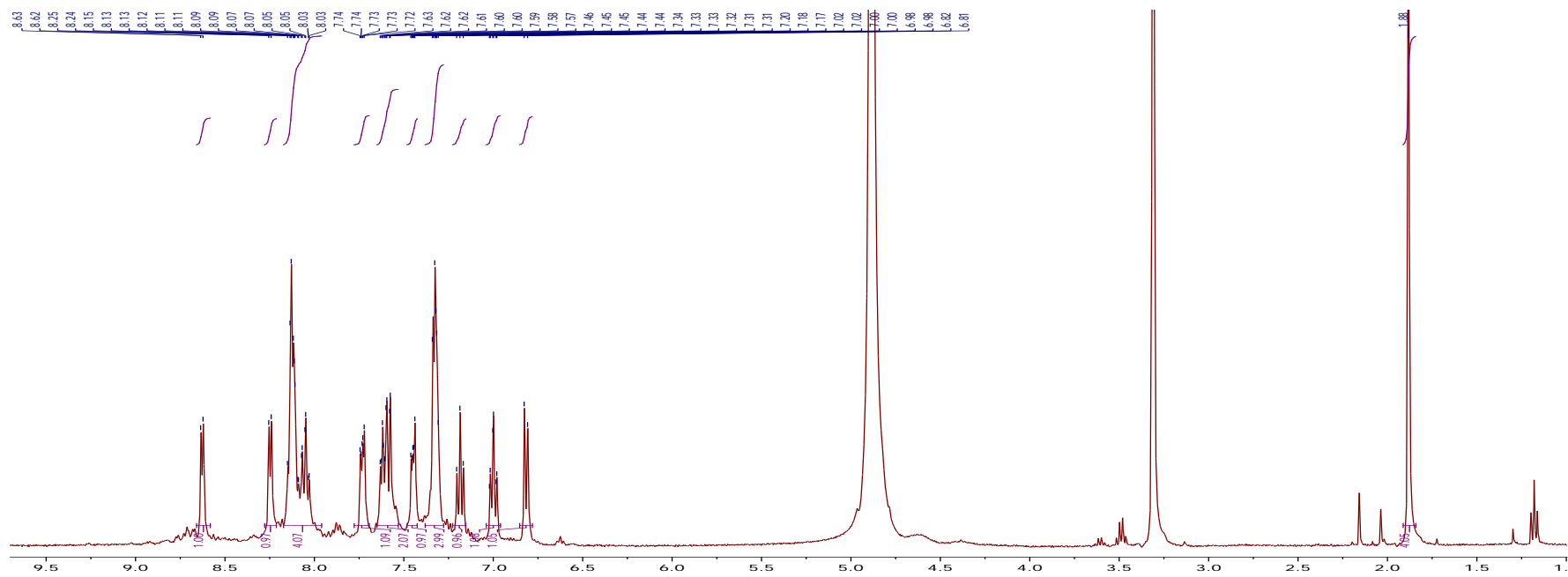
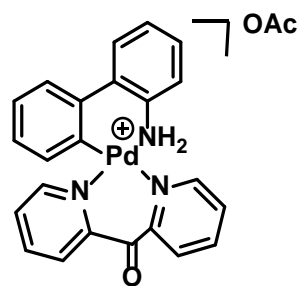


Figure A28. ¹H NMR of 30 in methanol-d₄ at 22 °C.

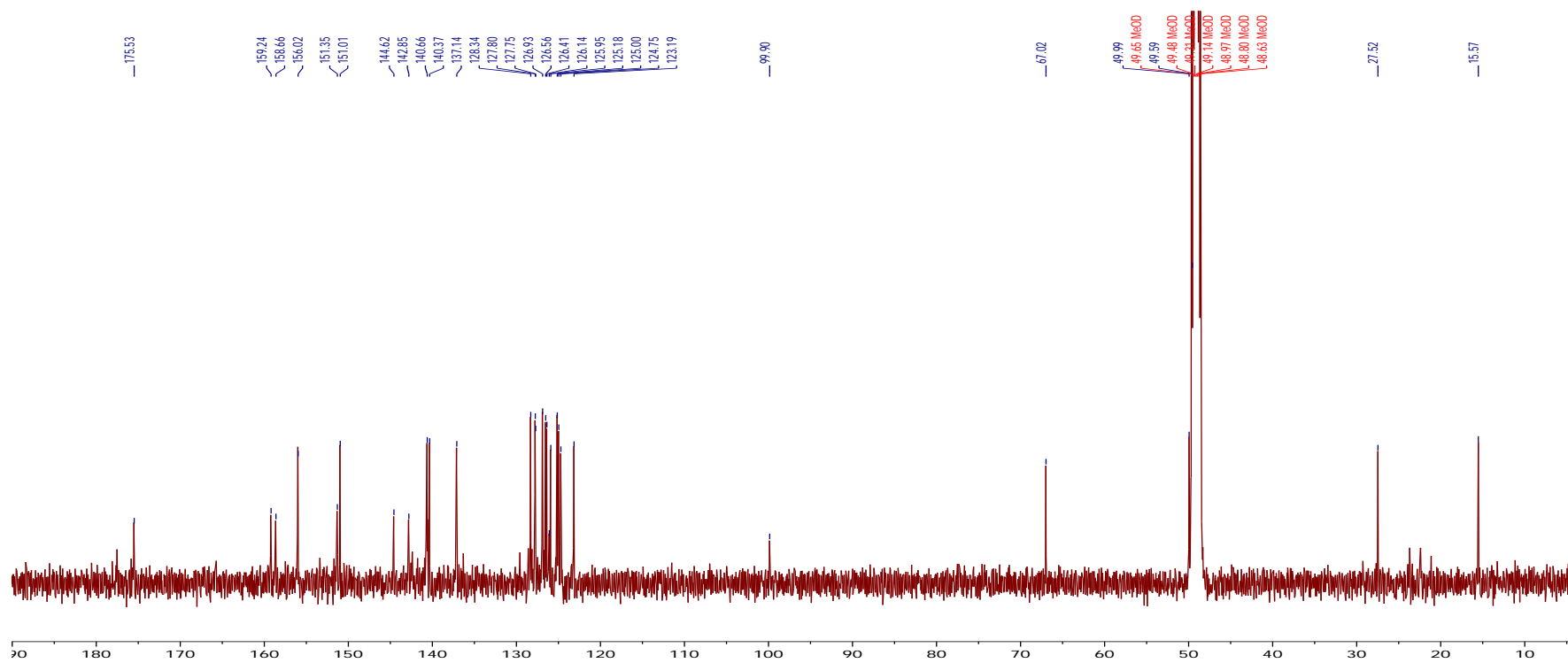
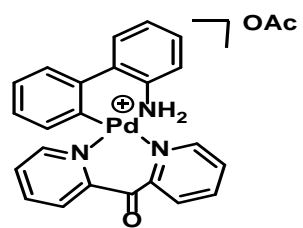


Figure A29. ¹³C NMR of **30** in methanol-d₄ at 22 °C.

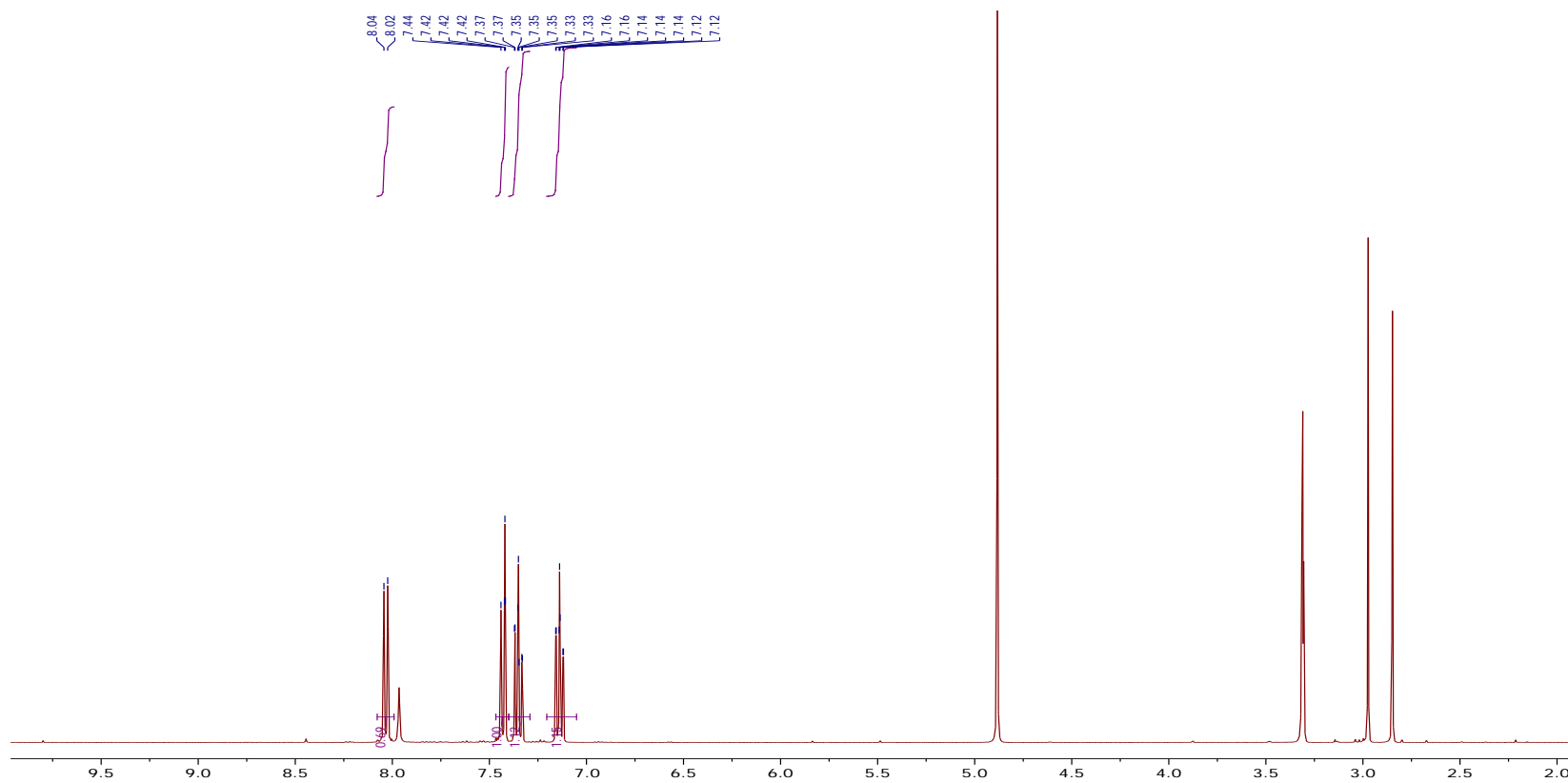
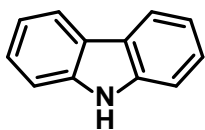


Figure A30. ¹H NMR of **45** in methanol-d₄ at 22 °C.

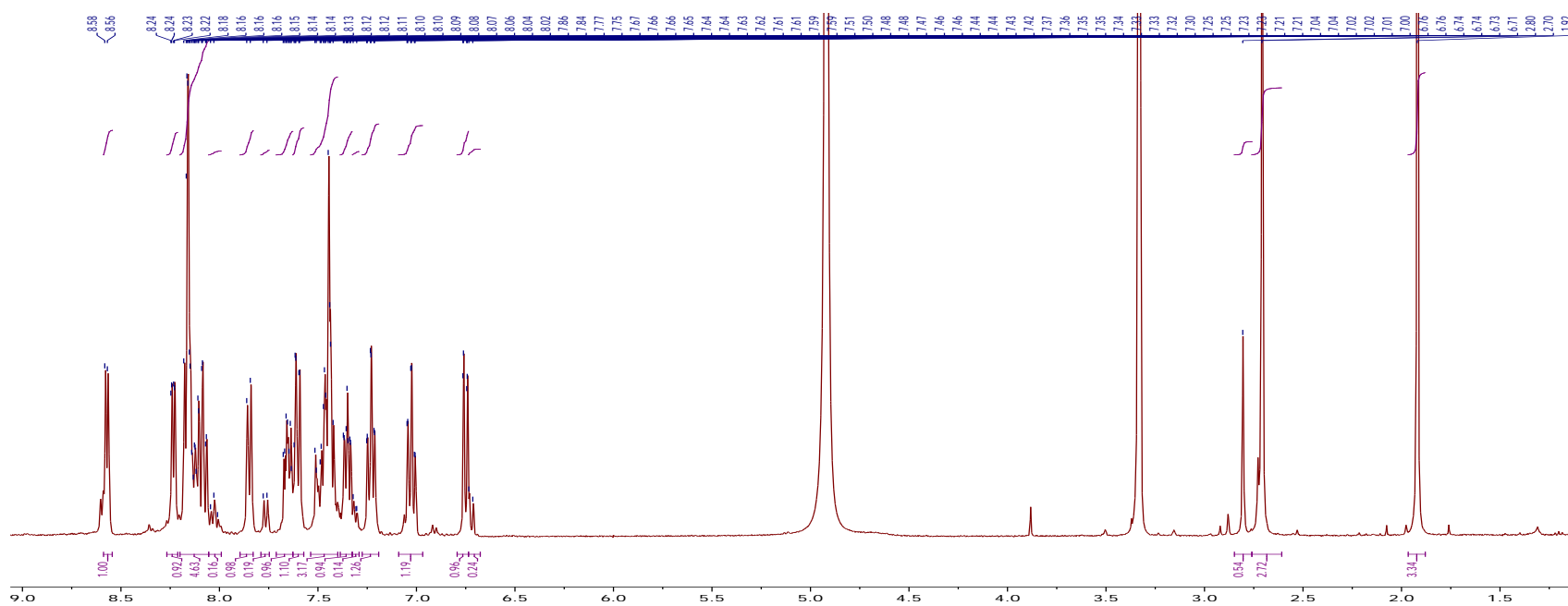
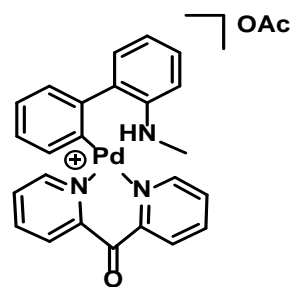


Figure A31. ^1H NMR of **32** in methanol- d_4 at 22 °C.

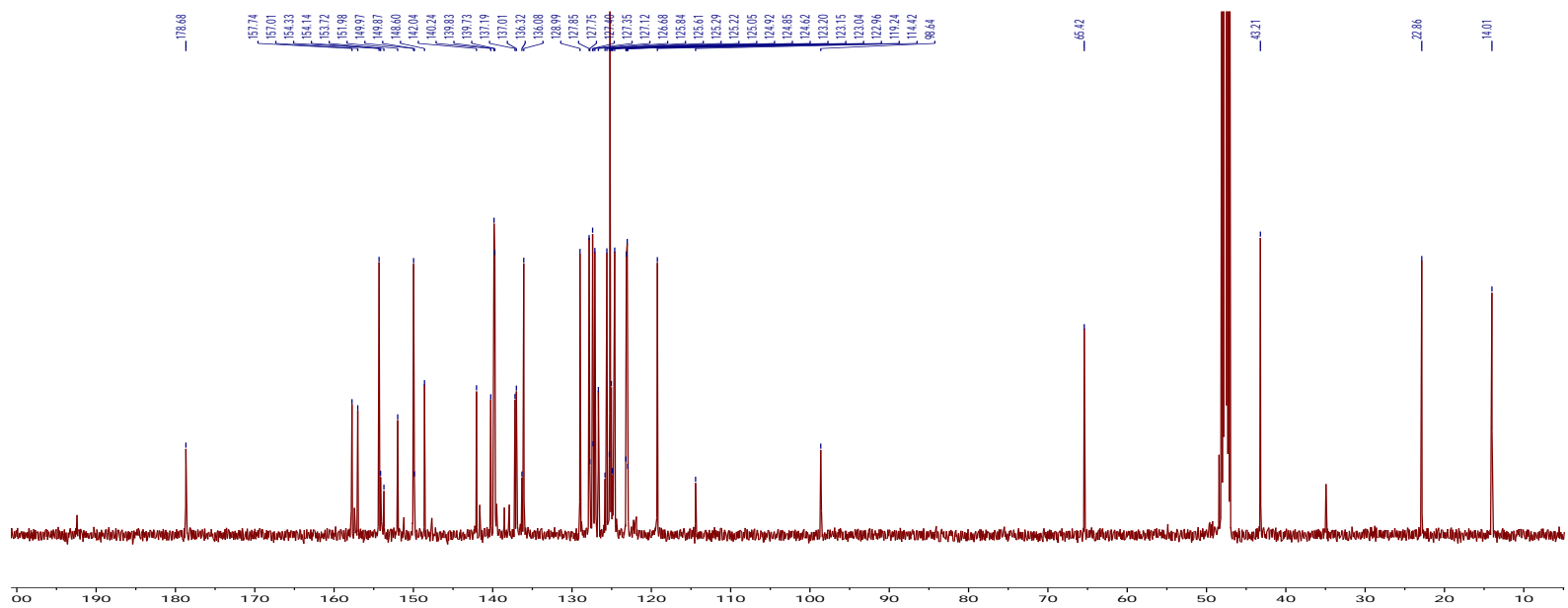
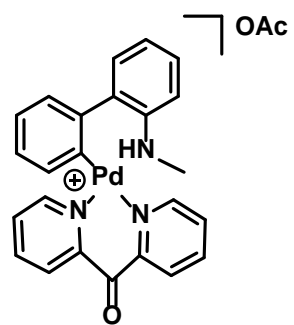


Figure A32. ^{13}C NMR of **32** in methanol- d_4 at 22 °C.

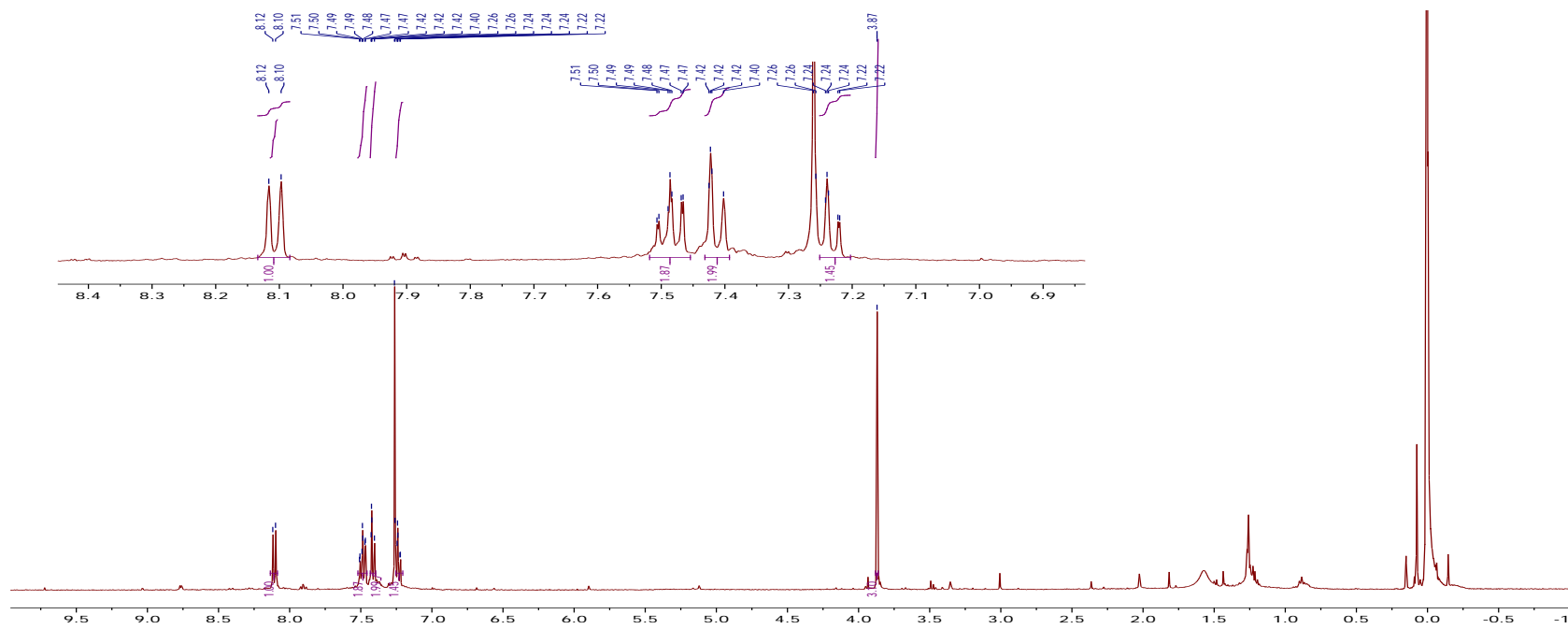
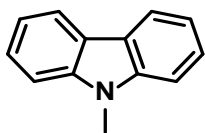


Figure A33. ^1H NMR of **34** in CDCl_3 at 22 °C.

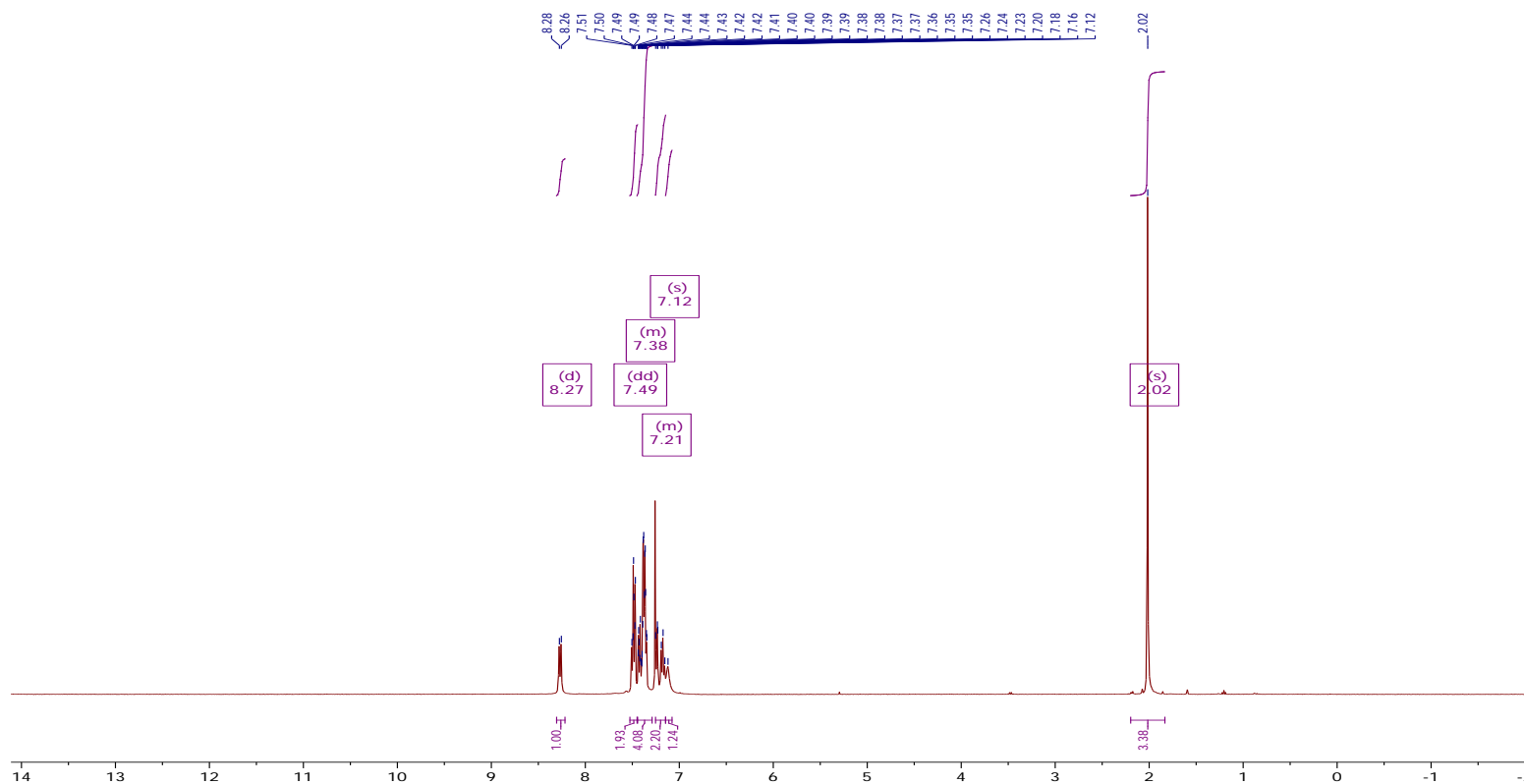
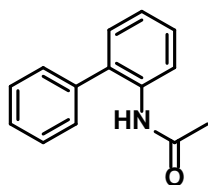


Figure A34. ^1H NMR of 46 in CDCl_3 at 22 °C.

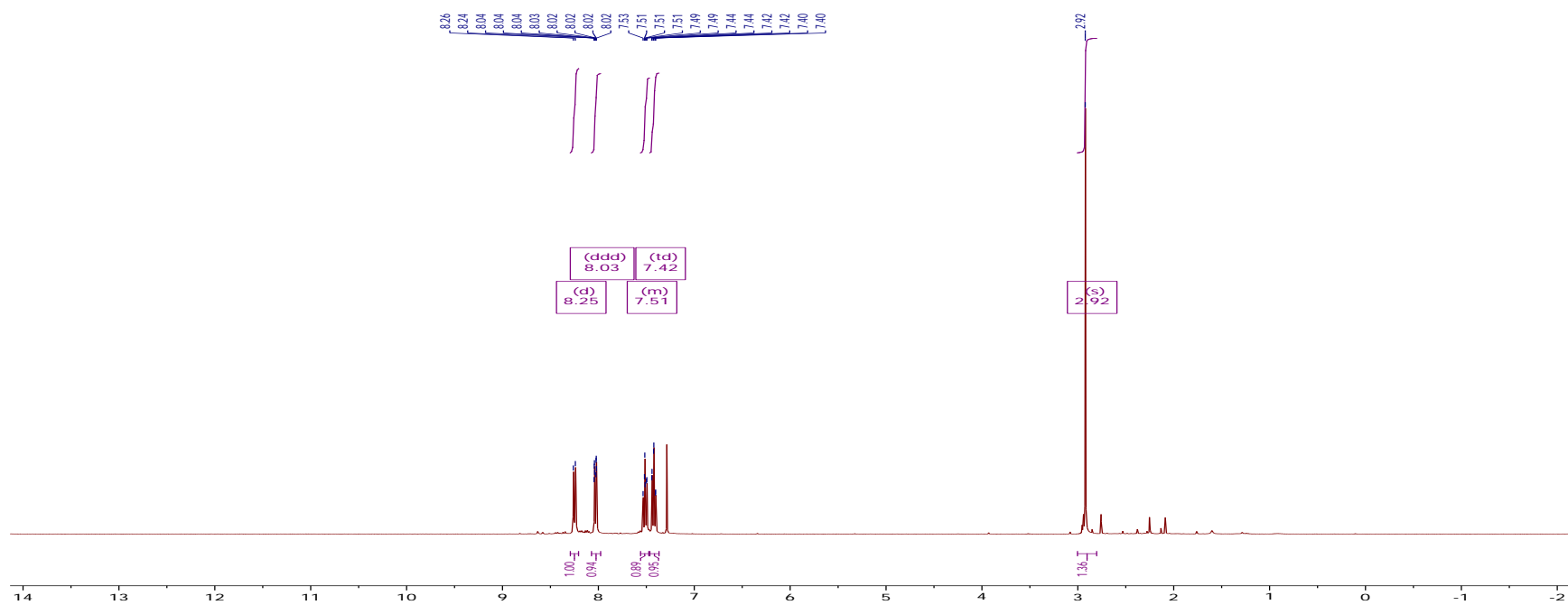
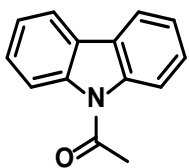


Figure A35. ¹H NMR of **54** in CDCl₃ at 22 °C.

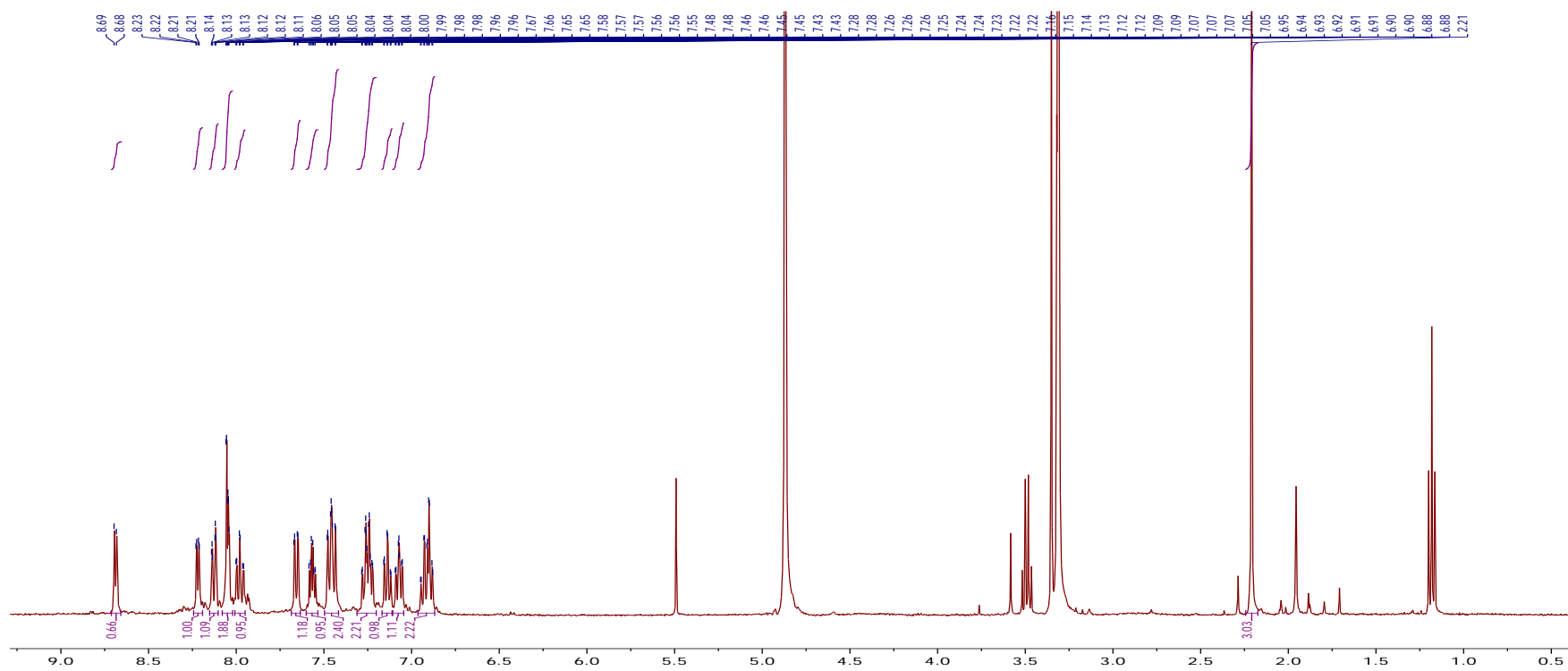
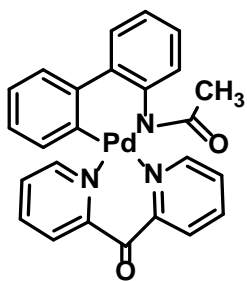


Figure A35 ^1H NMR of **50** in methanol- d_4 at 22 °C

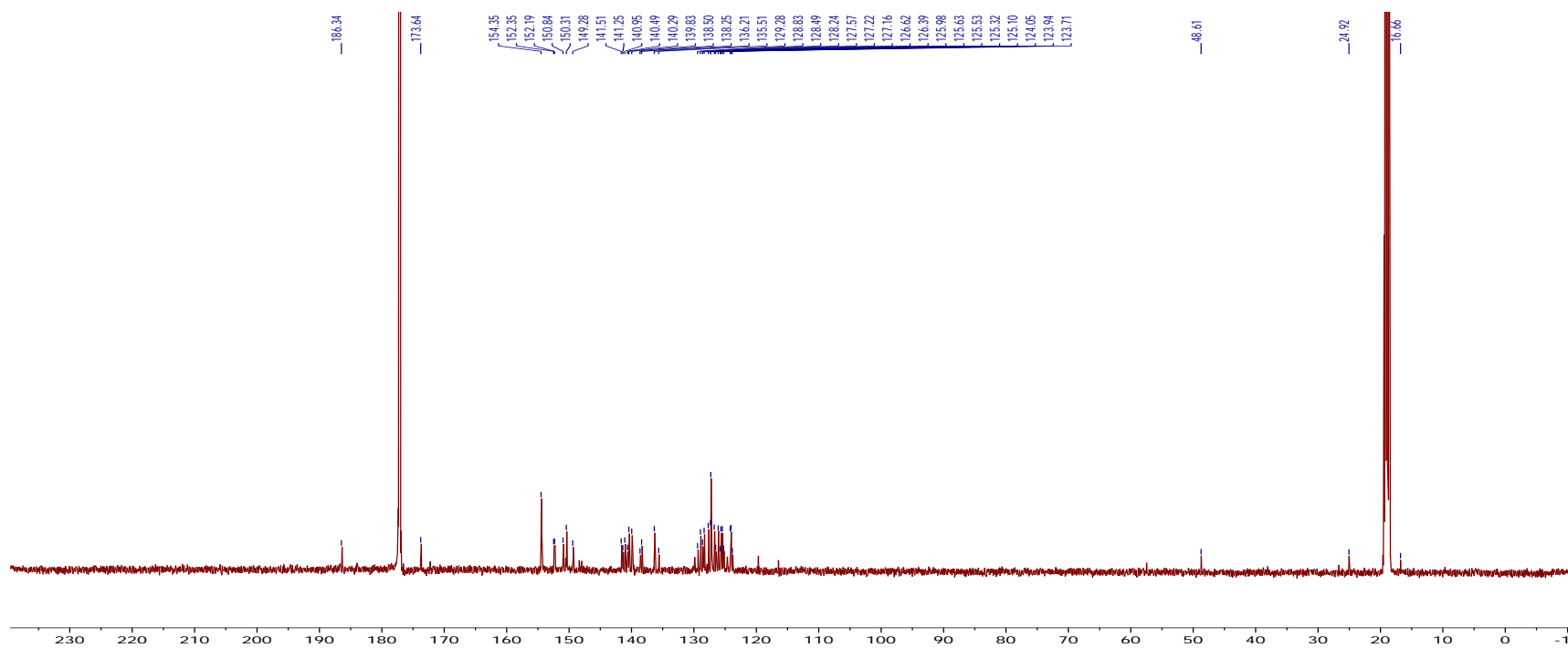
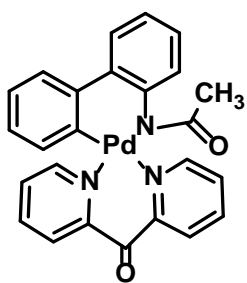


Figure A36 ¹³C NMR of 50 in methanol-d₄ at 22 °C

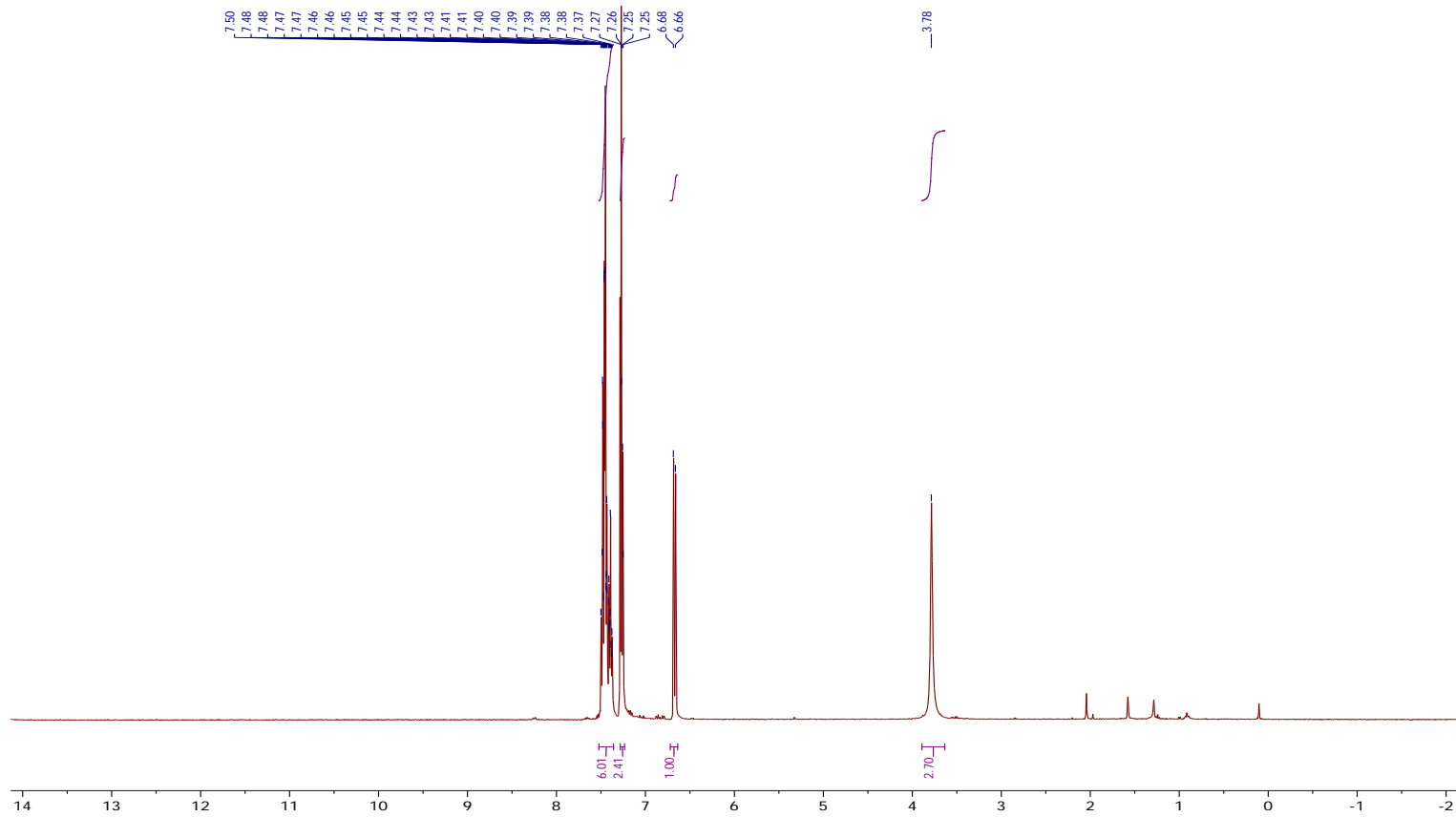
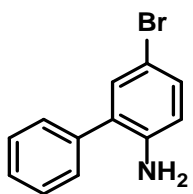


Figure A37 ¹H NMR of 27 in CDCl₃ at 22 °C

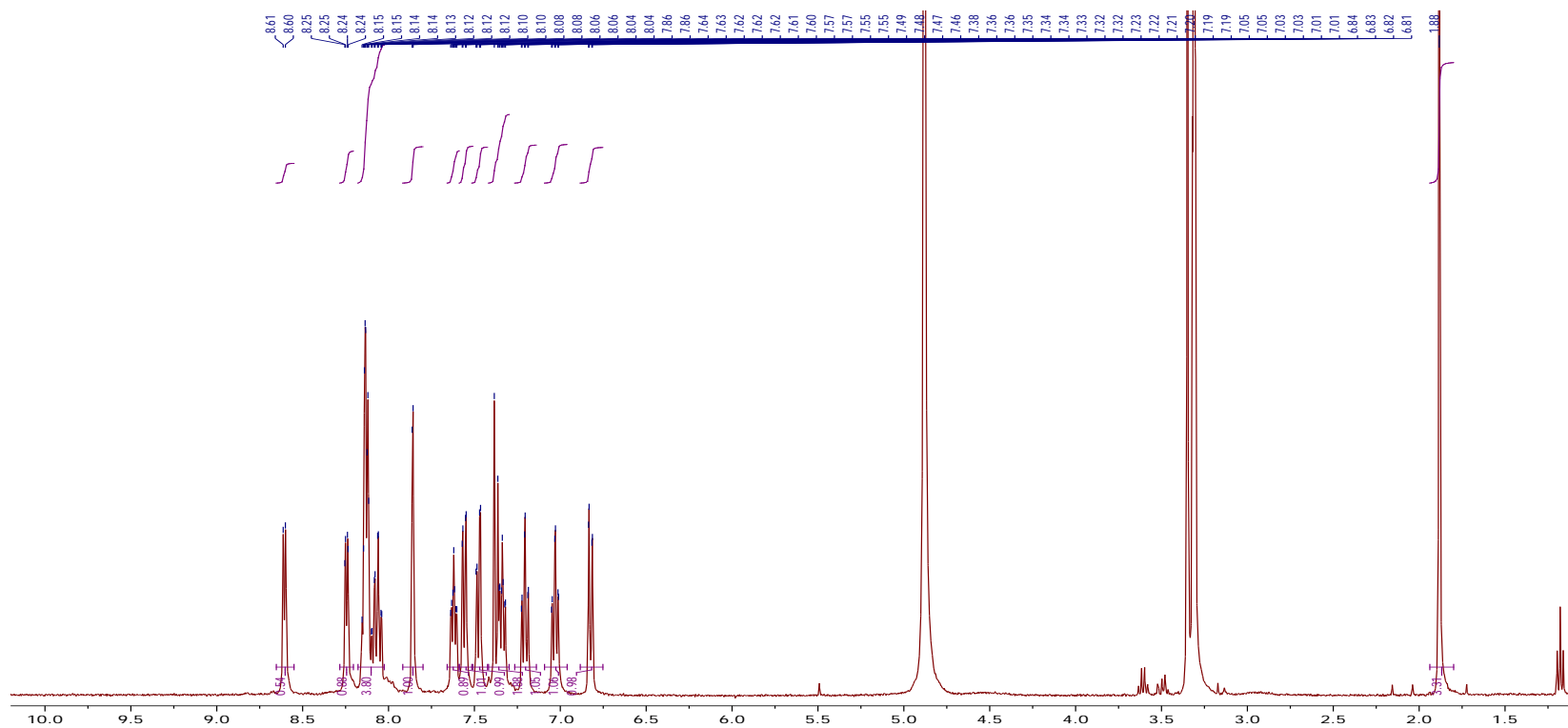
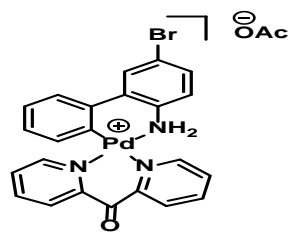


Figure A38 ¹H NMR of **31** in methanol-d₄ at 22 °C

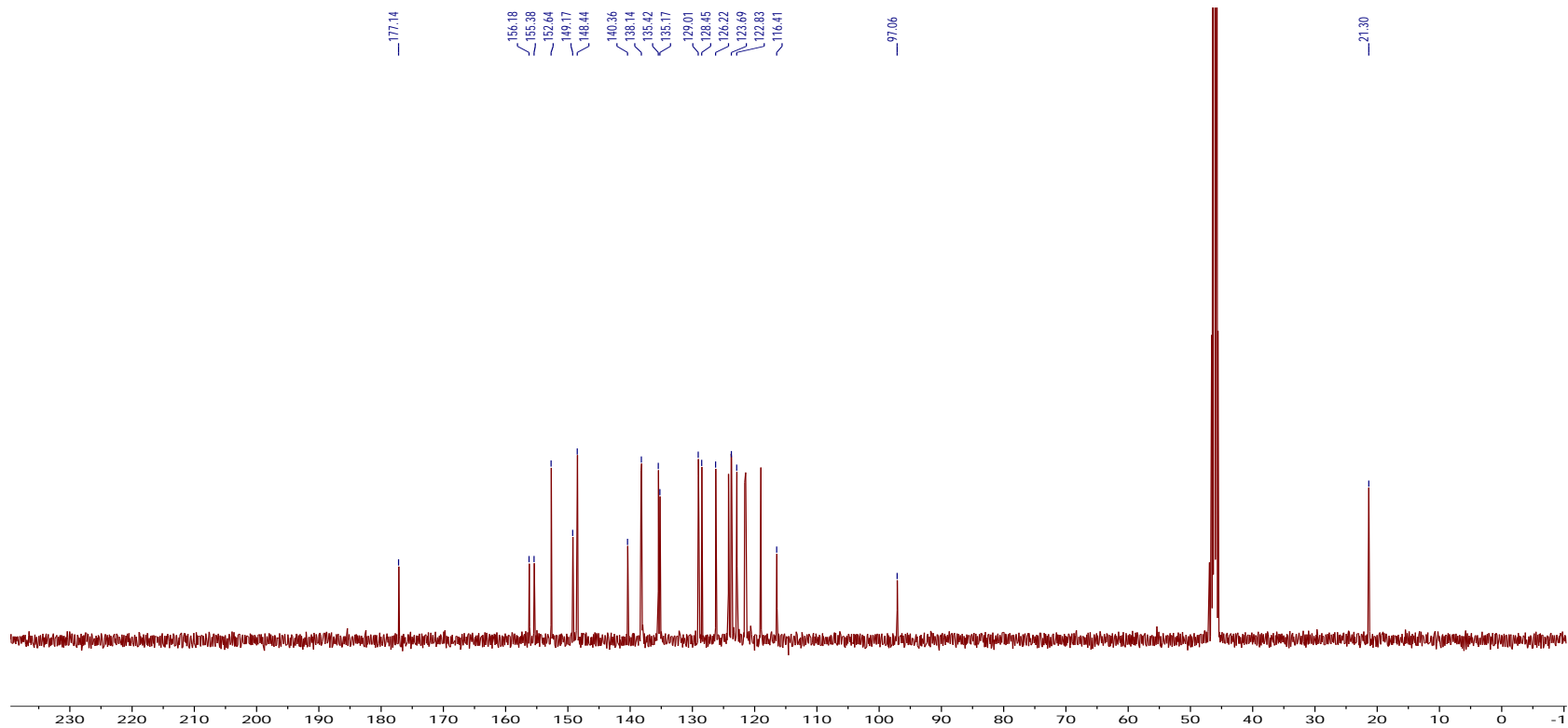
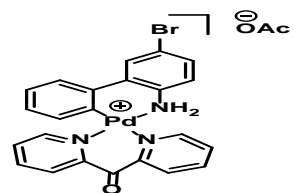


Figure A39 ¹³C NMR of **31** in Methanol-d₄ at 20 °C

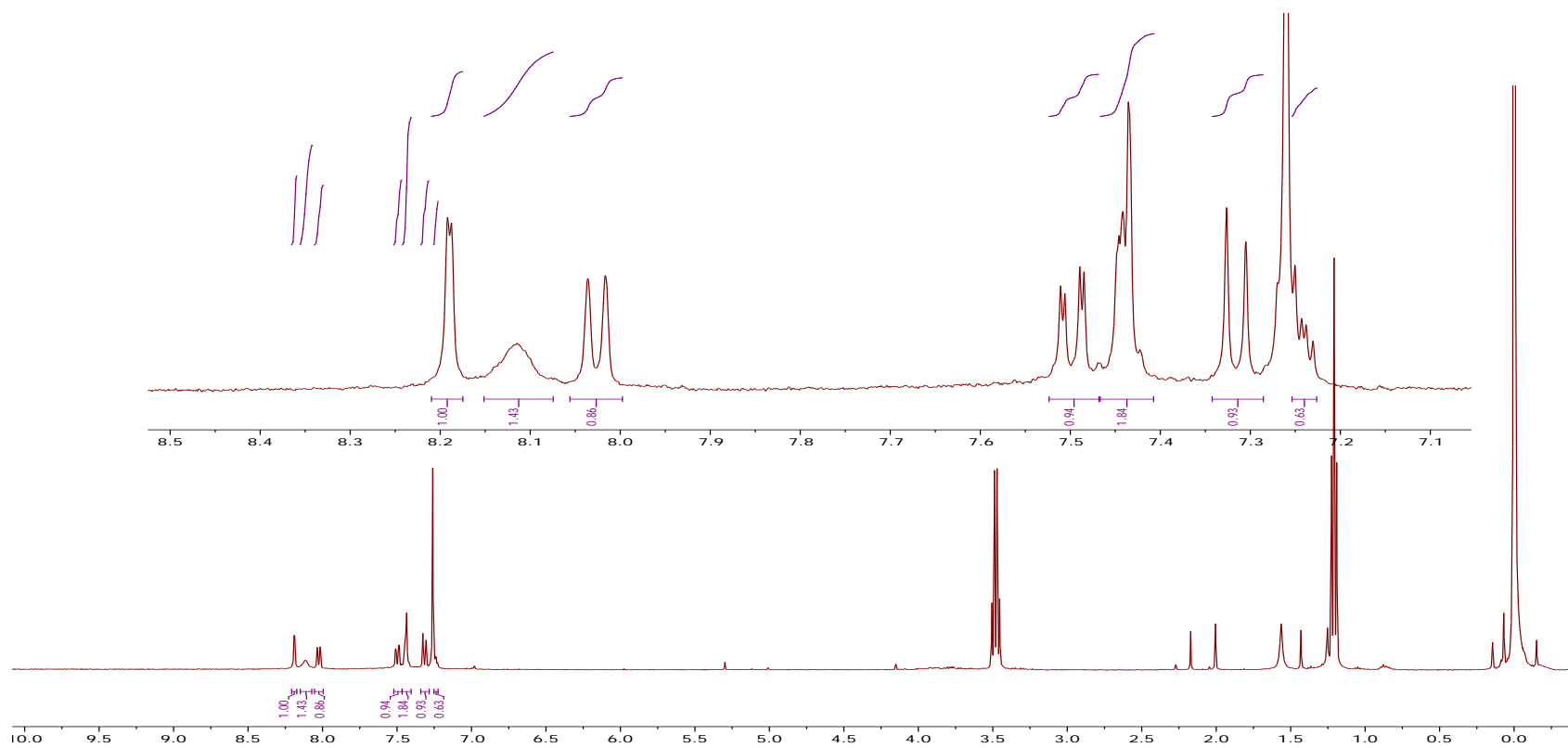
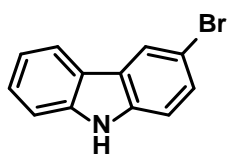


Figure A40 ^1H NMR of 45 in CDCl_3 at 20°C

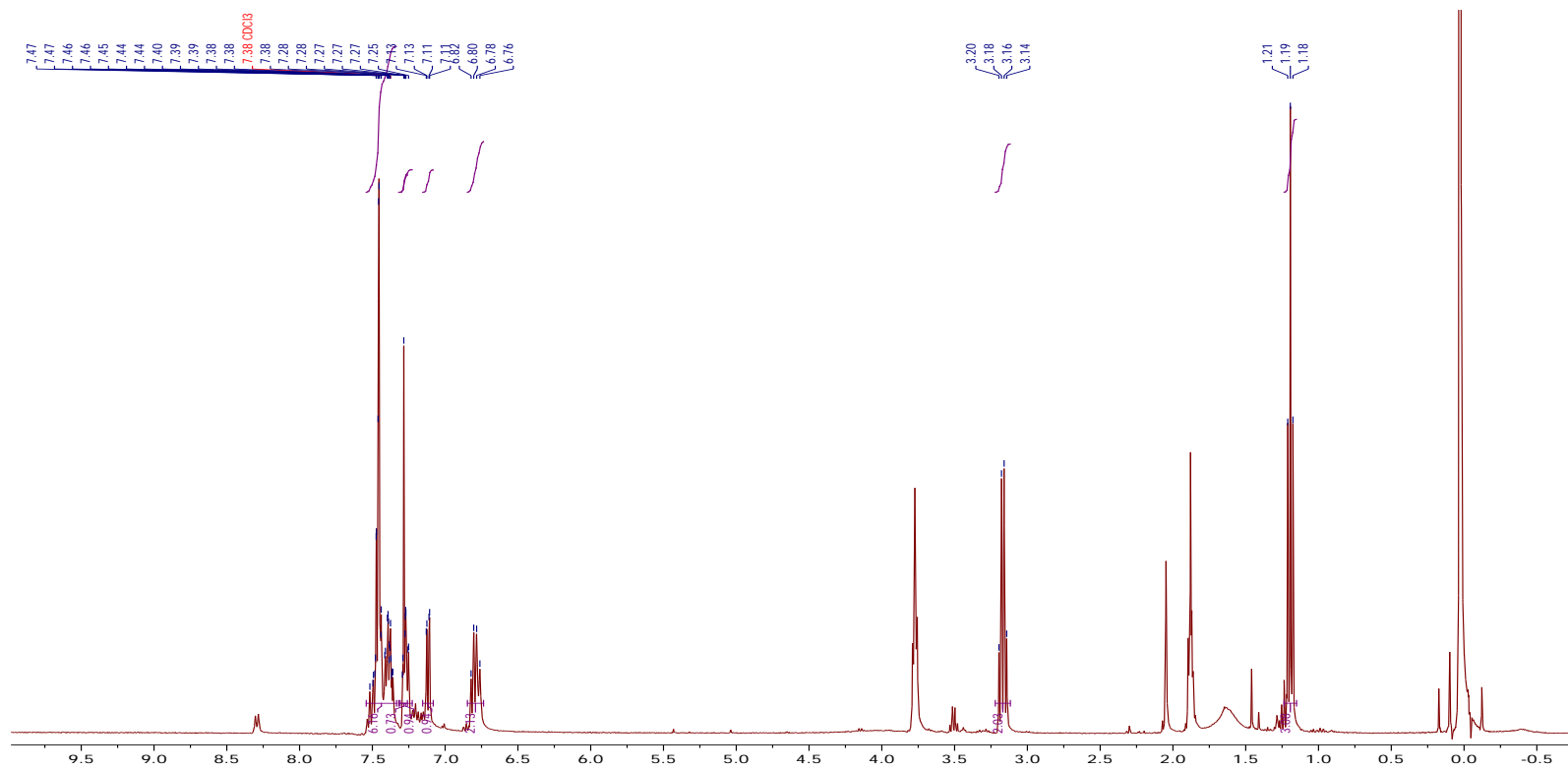
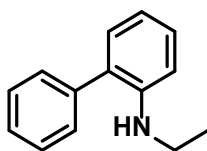


Figure A41 ¹H NMR of **29** in CDCl₃ at 22 °C

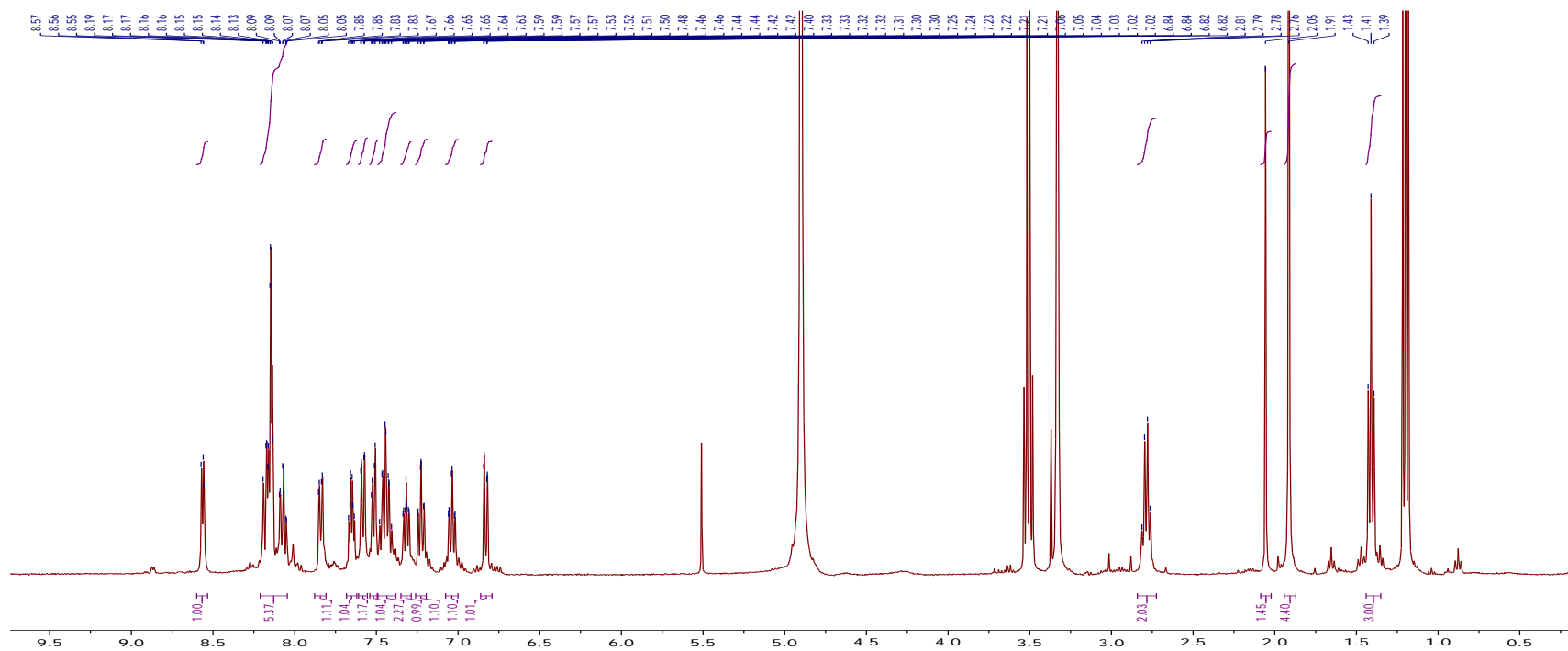
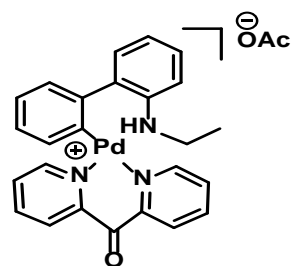


Figure A42 ¹H NMR of **33** in methanol-d₄ at 22 °C

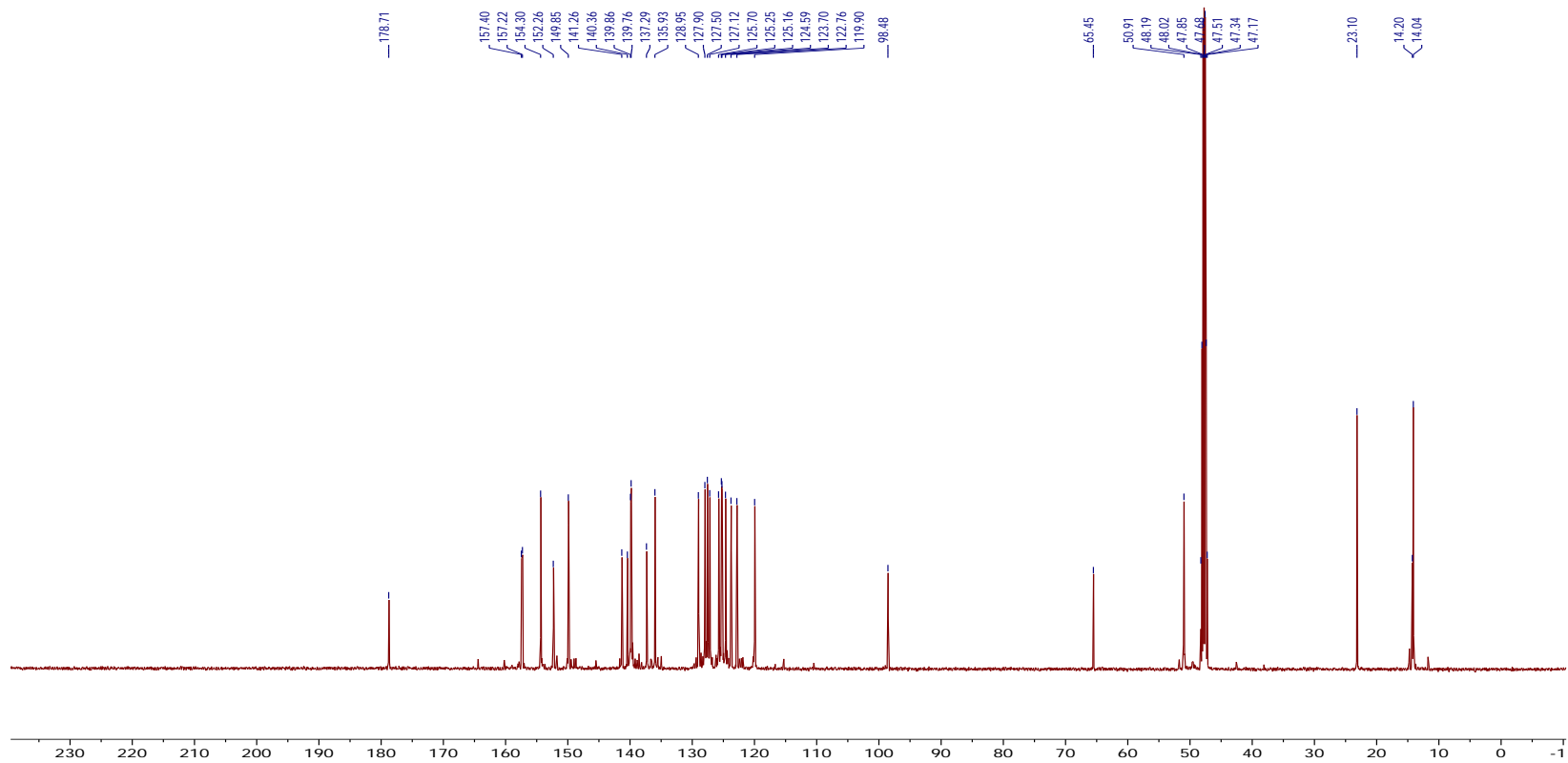
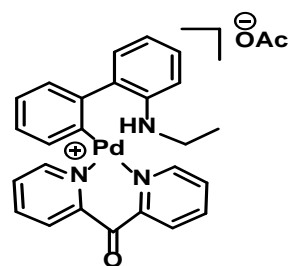


Figure A43 ^{13}C NMR of **33** in methanol- d_4 at 22 °C

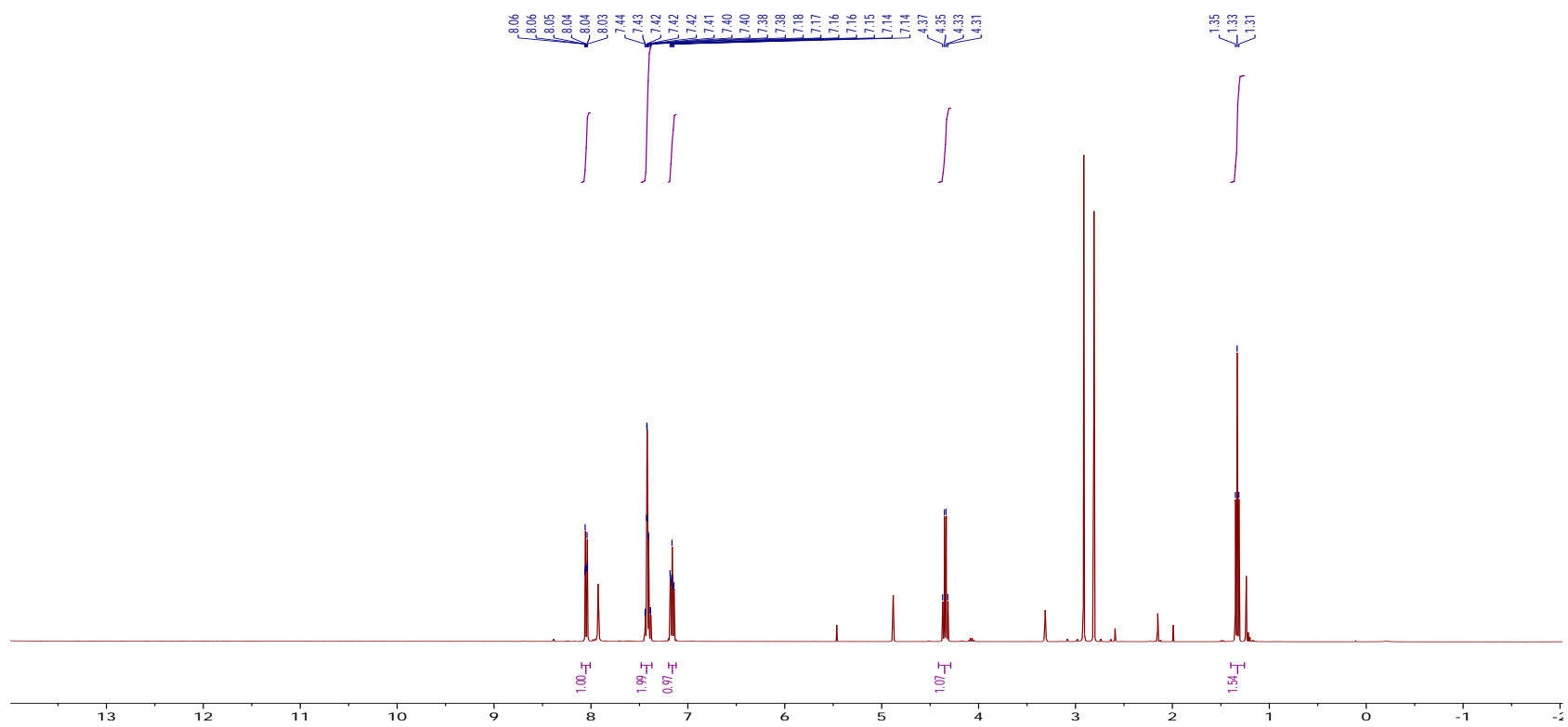
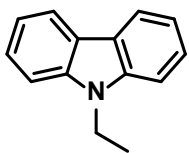


Figure A44 ^1H NMR of **43** in methanol- d_4 at 22 °C

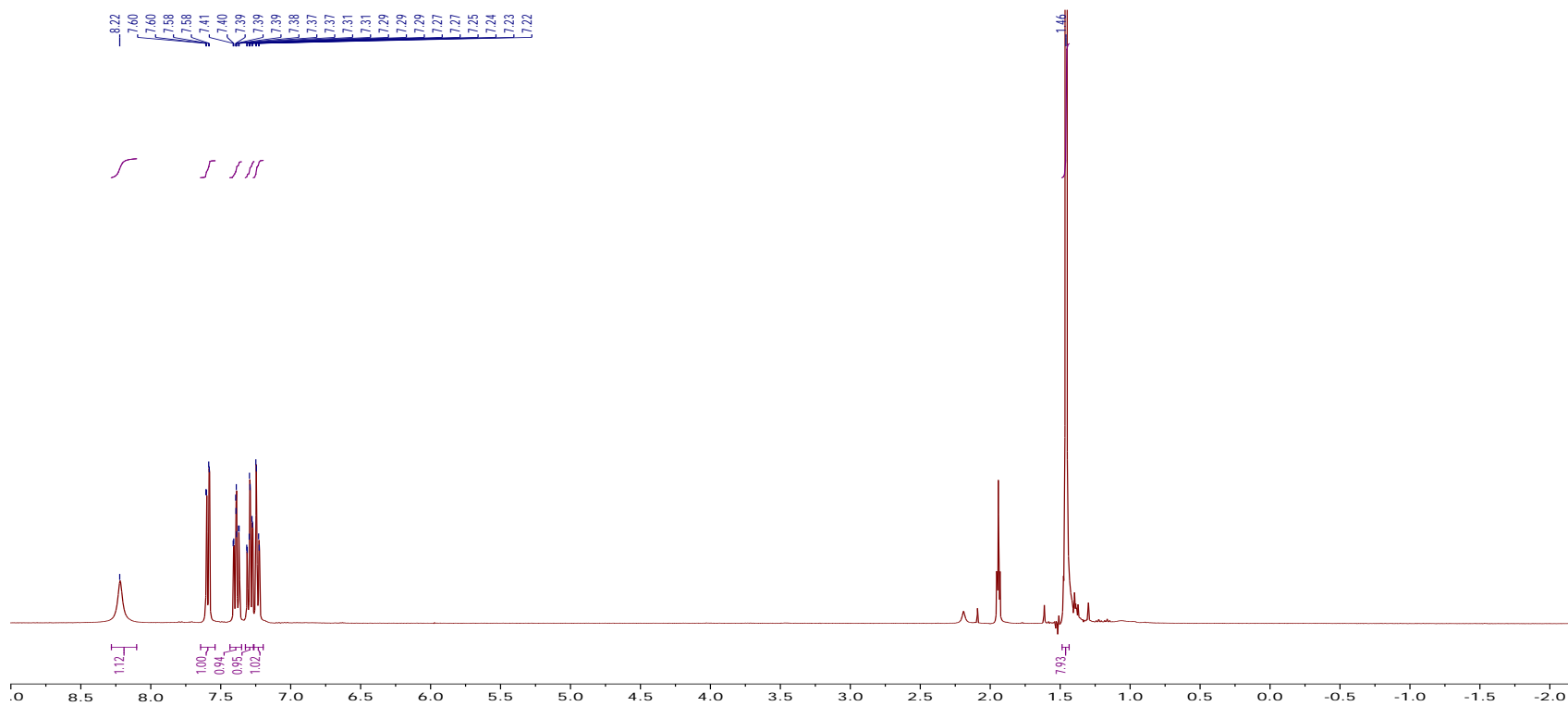
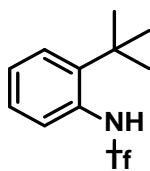


Figure A45 ¹H NMR of **78** in CD₃CN at 22 °C

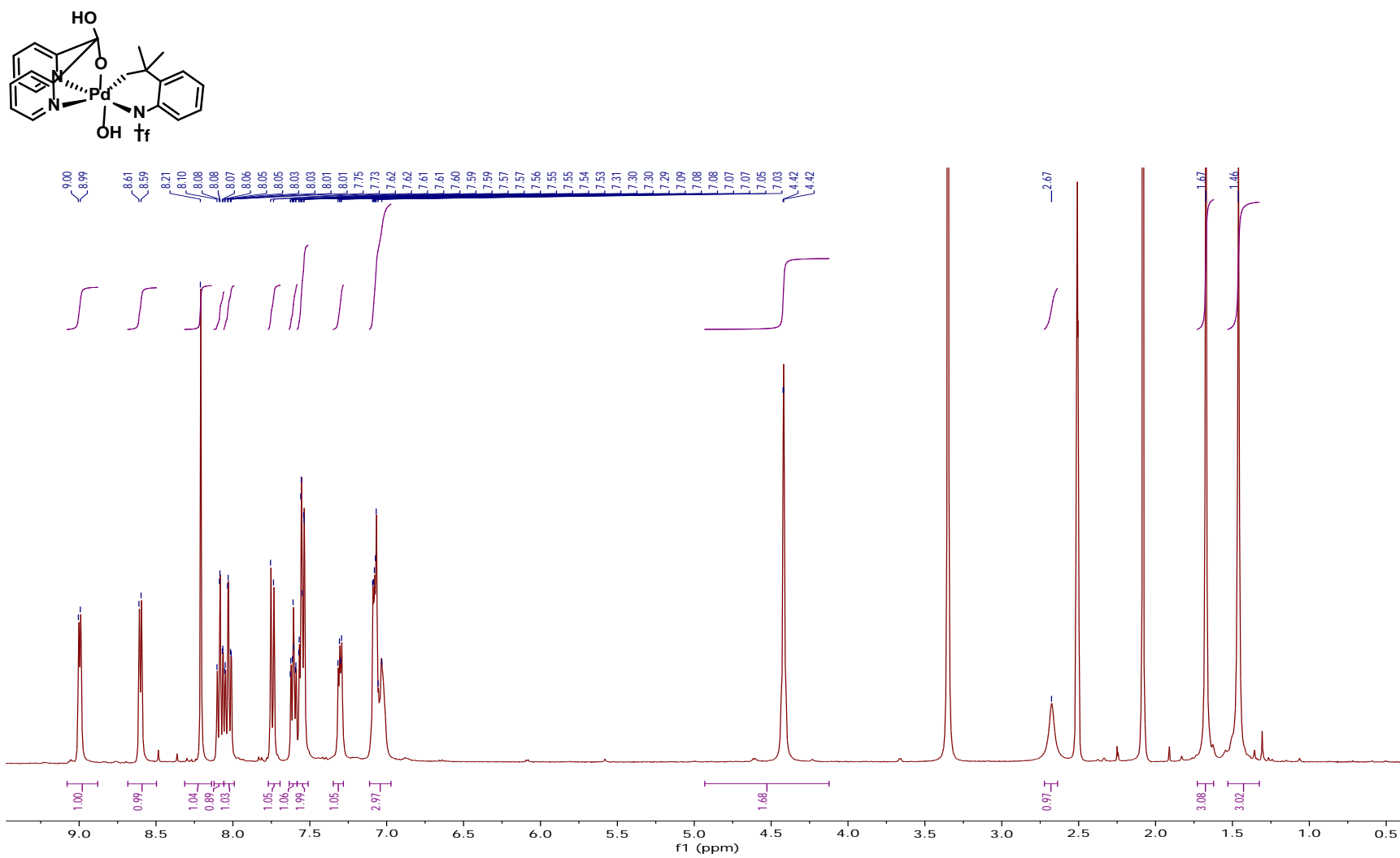


Figure A46 ^1H NMR of **84** in $\text{DMSO-}d_6$ at $22\text{ }^\circ\text{C}$

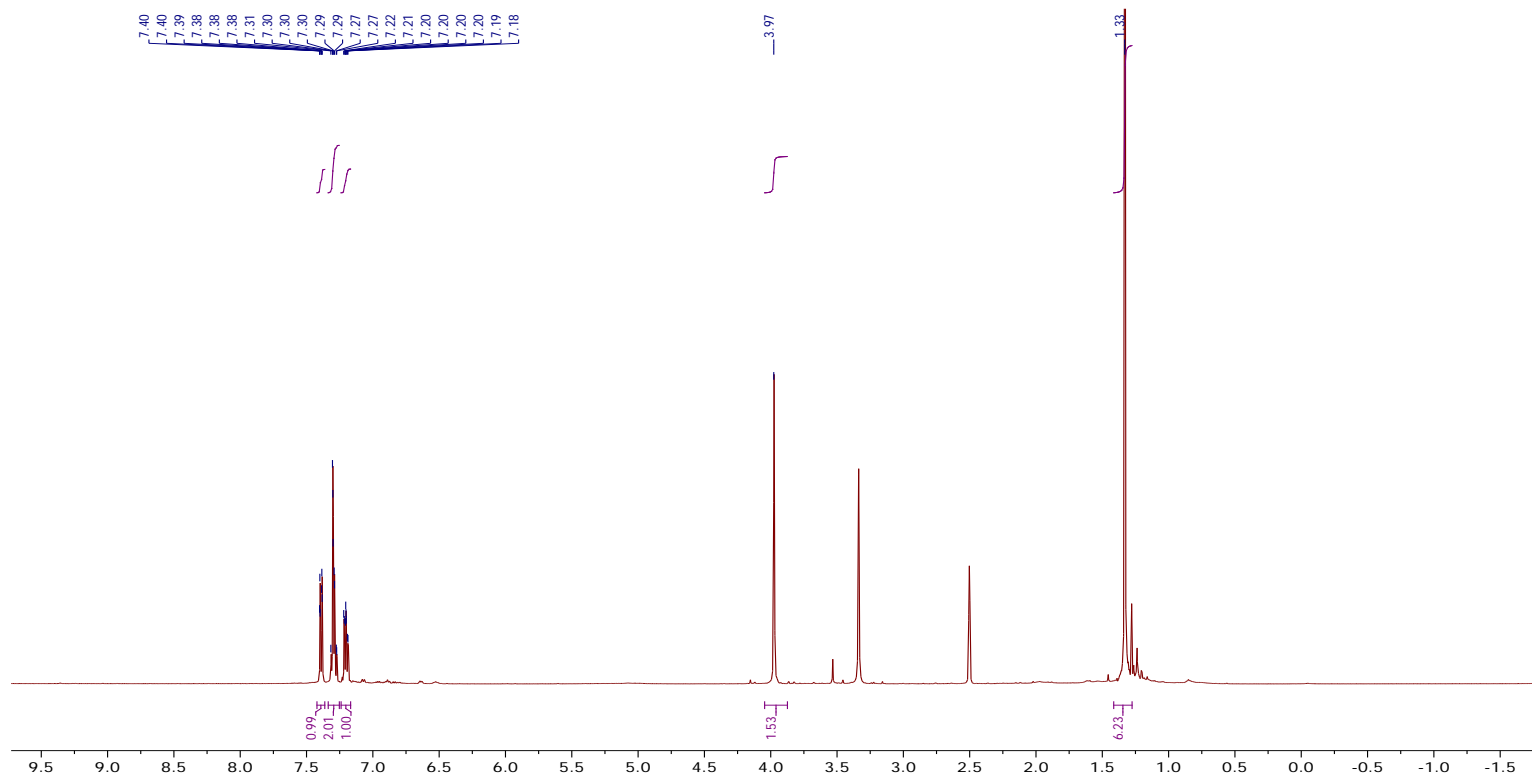
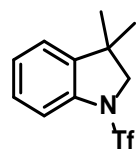


Figure A47 ¹H NMR of 86 in DMSO-*d*₆ at 22 °C

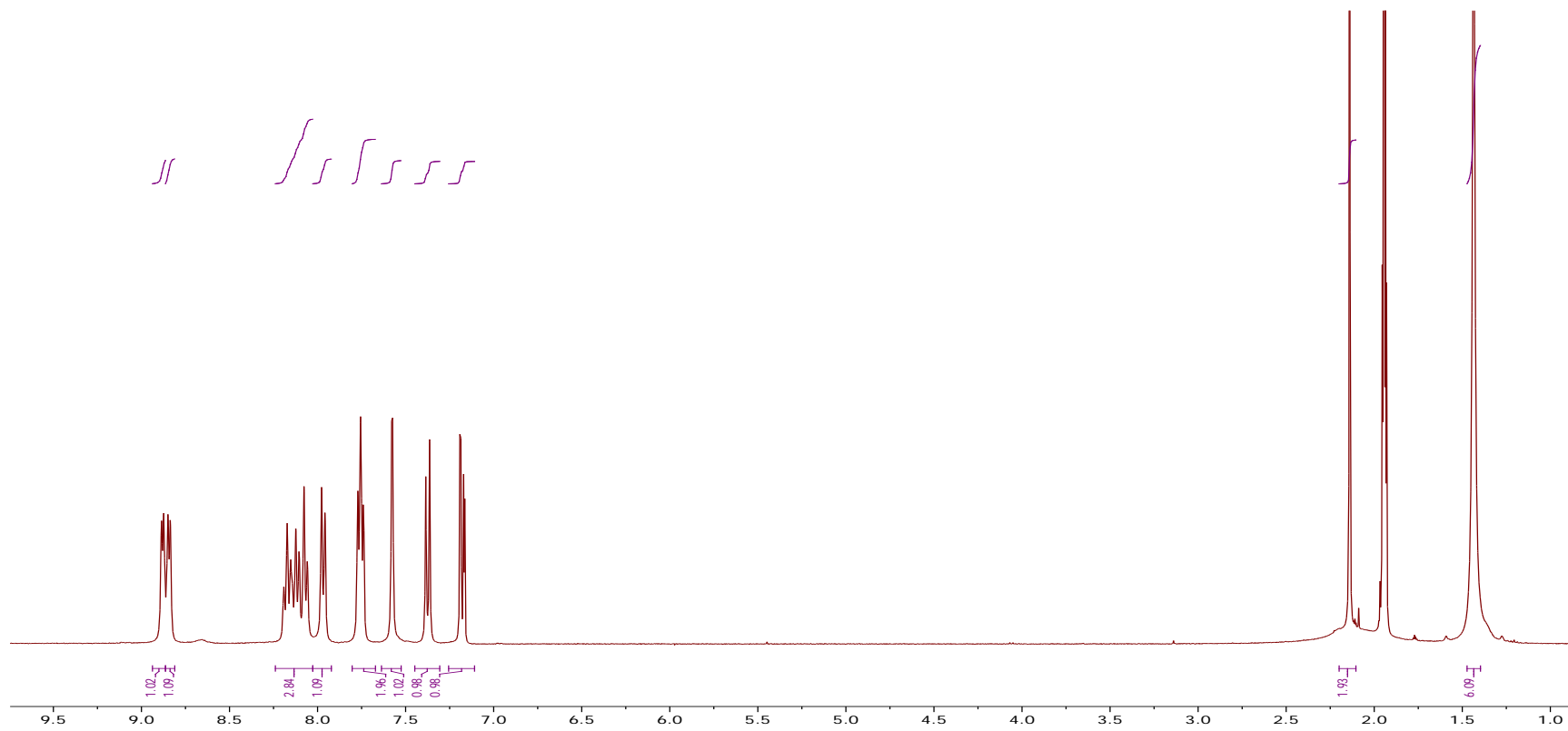
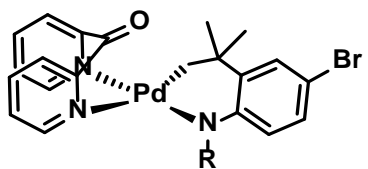


Figure A48 ^1H NMR of **82** in CD_3CN at 22 °C

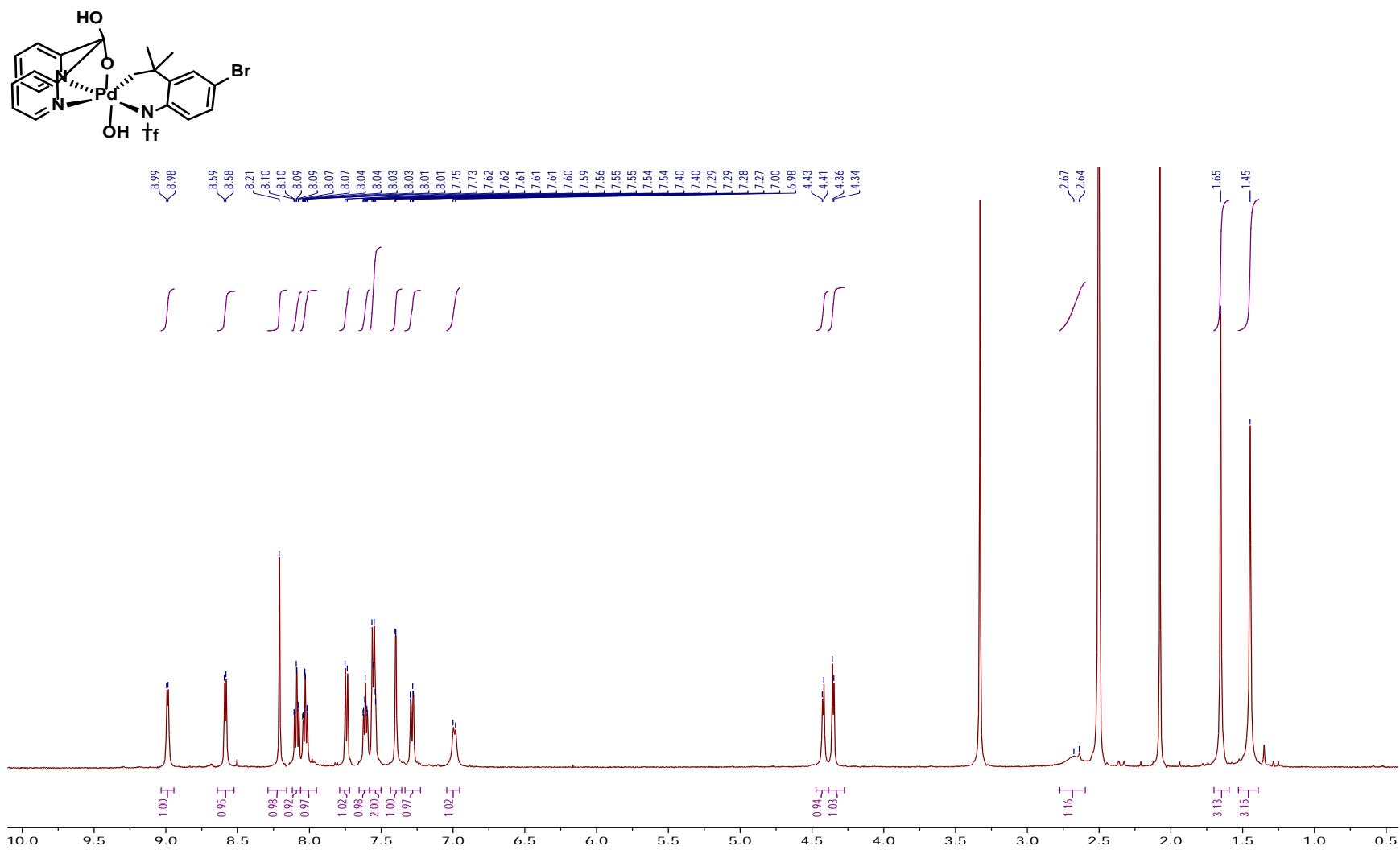


Figure A49 ^1H NMR of **91** in $\text{DMSO}-d_6$ at $22\text{ }^\circ\text{C}$

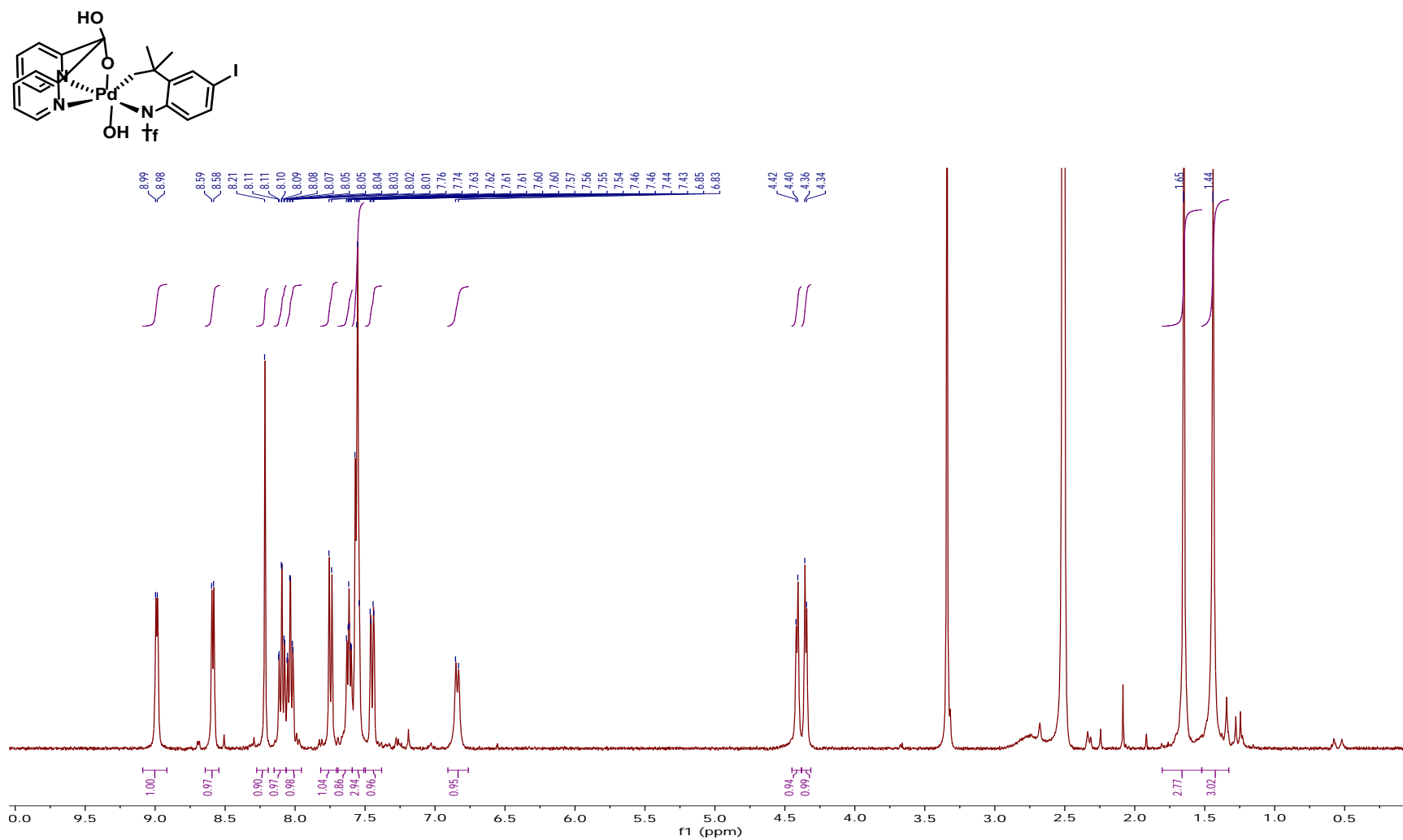


Figure A50 ^1H NMR of **92** in DMSO- d_6 at 22 °C

References

1. Hartwig, J. F. *J. Am. Chem. Soc.* **2016**, *138*, 2-24.
2. Hartwig, J. F., Palladium-Catalyzed Amination of Aryl Halides and Related Reactions. In *Handbook of Organopalladium Chemistry for Organic Synthesis*, John Wiley & Sons, Inc.: 2002; pp 1051-1096.
3. Nicolaou, K. C.; Bulger, P. G.; Sarlah, D. *Angew. Chem., Int. Ed.* **2005**, *44*, 4442-4489.
4. Lyons, T. W.; Sanford, M. S. *Tetrahedron* **2009**, *65*, 3211-3221.
5. Dick, A. R.; Sanford, M. S. *Tetrahedron* **2006**, *62*, 2439-2463.
6. Labinger, J. A.; Bercaw, J. E. *Nature* **2002**, *417*, 507-514.
7. Jones, W. D., Activation of C-H Bonds: Stoichiometric Reactions. In *Activation of Unreactive Bonds and Organic Synthesis*, Murai, S.; Alper, H.; Gossage, R. A.; Grushin, V. V.; Hidai, M.; Ito, Y.; Jones, W. D.; Kakiuchi, F.; van Koten, G.; Lin, Y. S.; Mizobe, Y.; Murai, S.; Murakami, M.; Richmond, T. G.; Sen, A.; Suginome, M.; Yamamoto, A., Eds. Springer Berlin Heidelberg: Berlin, Heidelberg, 1999; pp 9-46.
8. Jones, W. D.; Feher, F. J. *Acc. Chem. Res.* **1989**, *22*, 91-100.
9. Julia, F.; Gonzalez-Herrero, P. *J. Am. Chem. Soc.* **2016**, *138*, 5276-5282.
10. Lin, Z. *Coord. Chem. Rev.* **2007**, *251*, 2280-2291.
11. Ephritikhine, M. *Chem. Rev.* **1997**, *97*, 2193-2242.
12. Burger, B. J.; Thompson, M. E.; Cotter, W. D.; Bercaw, J. E. *J. Am. Chem. Soc.* **1990**, *112*, 1566-1577.
13. Barros, N.; Eisenstein, O.; Maron, L.; Tilley, T. D. *Organometallics* **2008**, *27*, 2252-2257.
14. Gorelsky, S. I.; Lapointe, D.; Fagnou, K. *J. Am. Chem. Soc.* **2008**, *130*, 10848-10849.

15. Lane, B. S.; Brown, M. A.; Sames, D. *J. Am. Chem. Soc.* **2005**, *127*, 8050-8057.
16. Lafrance, M.; Rowley, C. N.; Woo, T. K.; Fagnou, K. *J. Am. Chem. Soc.* **2006**, *128*, 8754-8756.
17. Lafrance, M.; Fagnou, K. *J. Am. Chem. Soc.* **2006**, *128*, 16496-16497.
18. Davies, D. L.; Donald, S. M. A.; Macgregor, S. A. *J. Am. Chem. Soc.* **2005**, *127*, 13754-13755.
19. Ryabov, A. D. *Chem. Rev.* **1990**, *90*, 403-424.
20. Topczewski, J. J.; Sanford, M. S. *Chem. Sci.* **2015**, *6*, 70-76.
21. Racowski, J. M.; Ball, N. D.; Sanford, M. S. *J. Am. Chem. Soc.* **2011**, *133*, 18022-18025.
22. Ball, N. D.; Gary, J. B.; Ye, Y.; Sanford, M. S. *J. Am. Chem. Soc.* **2011**, *133*, 7577-7584.
23. Maleckis, A.; Sanford, M. S. *Organometallics* **2011**, *30*, 6617-6627.
24. Maleckis, A.; Kampf, J. W.; Sanford, M. S. *J. Am. Chem. Soc.* **2013**, *135*, 6618-6625.
25. Lindley, J. *Tetrahedron* **1984**, *40*, 1433-1456.
26. Kosugi, M.; Kameyama, M.; Migita, T. *Chem. Lett.* **1983**, *12*, 927-928.
27. Miyaura, N.; Suzuki, A. *Chem. Rev.* **1995**, *95*, 2457-83.
28. Guram, A. S.; Buchwald, S. L. *J. Am. Chem. Soc.* **1994**, *116*, 7901-2.
29. Driver, M. S.; Hartwig, J. F. *J. Am. Chem. Soc.* **1997**, *119*, 8232-8245.
30. Hartwig, J. F. *Angew. Chem., Int. Ed.* **1998**, *37*, 2046-2067.
31. Wolfe, J. P.; Wagaw, S.; Marcoux, J.-F.; Buchwald, S. L. *Acc. Chem. Res.* **1998**, *31*, 805-818.
32. Hamann, B. C.; Hartwig, J. F. *J. Am. Chem. Soc.* **1998**, *120*, 3694-3703.
33. Fitton, P.; Rick, E. A. *J. Organomet. Chem.* **1971**, *28*, 287-291.
34. Amatore, C.; Pfluger, F. *Organometallics* **1990**, *9*, 2276-2282.
35. Driver, M. S.; Hartwig, J. F. *J. Am. Chem. Soc.* **1997**, *119*, 8232-8245.
36. Gillie, A.; Stille, J. K. *J. Am. Chem. Soc.* **1980**, *102*, 4933-4941.
37. Xu, L.-M.; Li, B.-J.; Yang, Z.; Shi, Z.-J. *Chem. Soc. Rev.* **2010**, *39*, 712-733.

38. Sehnal, P.; Taylor, R. J. K.; Fairlamb, I. J. S. *Chem. Rev.* **2010**, *110*, 824-889.
39. Uson, R.; Fornies, J.; Navarro, R. *J. Organomet. Chem.* **1975**, *96*, 307-12.
40. Moriarty, R. M.; Om, P., Oxidation of Carbonyl Compounds with Organohypervalent Iodine Reagents. In *Organic Reactions*, John Wiley & Sons, Inc.: 2004.
41. Yoneyama, T.; Crabtree, R. H. *J. Mol. Catal. A: Chem.* **1996**, *108*, 35-40.
42. Dick, A. R.; Hull, K. L.; Sanford, M. S. *J. Am. Chem. Soc.* **2004**, *126*, 2300-2301.
43. Dick, A. R.; Kampf, J. W.; Sanford, M. S. *J. Am. Chem. Soc.* **2005**, *127*, 12790-12791.
44. Racowski, J. M.; Dick, A. R.; Sanford, M. S. *J. Am. Chem. Soc.* **2009**, *131*, 10974-10983.
45. Byers, P. K.; Canty, A. J.; Crespo, M.; Puddephatt, R. J.; Scott, J. D. *Organometallics* **1988**, *7*, 1363-1367.
46. Whitfield, S. R.; Sanford, M. S. *J. Am. Chem. Soc.* **2007**, *129*, 15142-15143.
47. Desai, L. V.; Malik, H. A.; Sanford, M. S. *Org. Lett.* **2006**, *8*, 1141-1144.
48. Oloo, W.; Zavalij, P. Y.; Zhang, J.; Khaskin, E.; Vedernikov, A. N. *J. Am. Chem. Soc.* **2010**, *132*, 14400-14402.
49. Zhang, J.; Khaskin, E.; Anderson, N. P.; Zavalij, P. Y.; Vedernikov, A. N. *Chem. Comm.* **2008**, *44*, 3625-3627.
50. Qu, F.; Khusnutdinova, J. R.; Rath, N. P.; Mirica, L. M. *Chem. Comm.* **2014**, *50*, 3036-3039.
51. Racowski, J. M.; Gary, J. B.; Sanford, M. S. *Angew. Chem., Int. Ed.* **2012**, *51*, 3414-3417.
52. Furuya, T.; Kaiser, H. M.; Ritter, T. *Angew. Chem., Int. Ed.* **2008**, *47*, 5993-5996, S5993/1-S5993/78.
53. Camasso, N. M.; Perez-Temprano, M. H.; Sanford, M. S. *J. Am. Chem. Soc.* **2014**, *136*, 12771-12775.

54. Perez-Temprano, M. H.; Racowski, J. M.; Kampf, J. W.; Sanford, M. S *J. Am. Chem. Soc.* **2014**, *136*, 4097-4100.
55. Pendleton, I. M.; Perez-Temprano, M. H.; Sanford, M. S.; Zimmerman, P. M. *J. Am. Chem. Soc.* **2016**, *138*, 6049-60.
56. Powers, D. C.; Ritter, T. *Organometallics* **2013**, *32*, 2042-2045.
57. Powers, D. C.; Ritter, T. *Nat. Chem.* **2009**, *1*, 302-309.
58. Powers, D. C.; Lee, E.; Ariaferd, A.; Sanford, M. S.; Yates, B. F.; Canty, A. J.; Ritter, T. *J. Am. Chem. Soc.* **2012**, *134*, 12002-12009.
59. Oloo, W. N.; Zavalij, P. Y.; Vedernikov, A. N. *Organometallics* **2013**, *32*, 5601-5614.
60. Tsang, W. C. P.; Zheng, N.; Buchwald, S. L. *J. Am. Chem. Soc.* **2005**, *127*, 14560-14561.
61. Pawlikowski, A. V.; Getty, A. D.; Goldberg, K. I. *J. Am. Chem. Soc.* **2007**, *129*, 10382-10393.
62. Jordan-Hore, J. A.; Johansson, C. C. C.; Gulias, M.; Beck, E. M.; Gaunt, M. J. *J. Am. Chem. Soc.* **2008**, *130*, 16184-16186.
63. Hursthouse, M. B.; Sloan, O. D.; Thornton, P.; Walker, N. P. C. *Polyhedron* **1986**, *5*, 1475-1478.
64. Albert, J.; Granell, J.; Zafrilla, J.; Font-Bardia, M.; Solans, X. *J. Organomet. Chem.* **2005**, *690*, 422-429.
65. Klinkenberg, J. L.; Hartwig, J. F. *J. Am. Chem. Soc.*, **2012**, *134*, 5758-5761.
66. Arrechea, P. L.; Buchwald, S. L. *J. Am. Chem. Soc.* **2016**, *138*, 12486-12493.
67. Driver, M. S.; Hartwig, J. F. *J. Am. Chem. Soc.* **1995**, *117*, 4708-4709.
68. Hartwig, J. F. *Inorg. Chem.* **2007**, *46*, 1936-1947.
69. Abrahams, S. C.; Collin, R. L.; Lipscomb, W. N. *Acta Crystallographica* **1951**, *4*, 15-20.
70. Soper, A. K.; Benmore, C. J. *Phys. Rev. Lett.* **2008**, *101*, 065502.
71. Camasso, N. M.; Sanford, M. S. *Science* **2015**, *347*, 1218-1220.

72. Abada, E.; Zavalij, P. Y.; Vedernikov, A. N. *J. Am. Chem. Soc.* **2017**, *139*, 643-646.
73. Collet, F.; Lescot, C.; Dauban, P. *Chem. Soc. Rev.* **2011**, *40*, 1926-1936.
74. Ramirez, T. A.; Zhao, B.; Shi, Y. *Chem. Soc. Rev.* **2012**, *41*, 931-942.
75. Neumann, J. J.; Rakshit, S.; Dröge, T.; Glorius, F. *Angew. Chem., Int. Ed.* **2009**, *48*, 6892-6895.
76. Muniz, K. *Angew. Chem., Int. Ed.* **2009**, *48*, 9412-9423.
77. Iglesias, A.; Perez, E. G.; Muniz, K. *Angew. Chem., Int. Ed.* **2010**, *49*, 8109-8111.
78. Iglesias, A.; Alvarez, R.; de Lera, A. R.; Muniz, K. *Angew. Chem., Int. Ed.* **2012**, *51*, 2225-2228.
79. Mei, T.-S.; Wang, X.; Yu, J.-Q. *J. Am. Chem. Soc.* **2009**, *131*, 10806-10807.
80. Brookhart, M.; Grant, B.; Volpe, A. F. *Organometallics* **1992**, *11*, 3920-3922.
81. Pendleton, I. M.; Pérez-Temprano, M. H.; Sanford, M. S.; Zimmerman, P. M. *J. Am. Chem. Soc.* **2016**, *138*, 6049-6060.
82. Iskra, J.; Stavber, S.; Zupan, M. *Synthesis* **2004**, *2004*, 1869-1873.
83. Li, F.; Frett, B.; Li, H.-y. *Synlett* **2014**, *25*, 1403-1408.
84. Youn, S. W.; Bihn, J. H.; Kim, B. S. *Org. Lett.* **2011**, *13*, 3738-3741.
85. Antonchick, A. P.; Samanta, R.; Kulikov, K.; Lategahn, J. *Angew. Chem., Int. Ed.* **2011**, *50*, 8605-8608.
86. Thu, H.-Y.; Yu, W.-Y.; Che, C.-M. *J. Am. Chem. Soc.* **2006**, *128*, 9048-9049.
87. Davies, H. M. L.; Morton, D. *J. Org. Chem.* **2016**, *81*, 343-350.
88. Holland, P. L.; Andersen, R. A.; Bergman, R. G.; Huang, J.; Nolan, S. P. *J. Am. Chem. Soc.* **1997**, *119*, 12800-12814.
89. Riehl, J. F.; Jean, Y.; Eisenstein, O.; Pelissier, M. *Organometallics* **1992**, *11*, 729-737.

